Aus dem
Deutschen Zentrum für Neurodegenerative Erkrankungen
Direktor: Prof. Dr. Pierluigi Nicotera
Arbeitsgrupleiter: Prof. Dr. Donato A. Di Monte

INTERNEURONAL SPREADING OF ALPHA-SYNUCLEIN IN PARKINSON'S DISEASE

HABILITATIONSSCHRIFT

zur Erlangung der venia legendi
der Hohen Medizinischen Fakultät
der Rheinischen Friedrich-Wilhelms-Universität Bonn
für das Lehrgebiet "Neurowissenschaft".

Vorgelegt von

Ayşe Ulusoy, PhD

Wissenschaftlicher Mitarbeiterin am Deutschen Zentrum für Neurodegenerative Erkrankungen, Bonn 2023

Fachvertreter
Prof. Dr. Christian Steinhäuser
Institutes für Zelluläre Neurowissenschaften
des Universitätsklinikums Bonn

To my father Murat Gümrükçüoğlu

"The only thing that makes life possible is permanent, intolerable uncertainty: not knowing what comes next."
Ursula K. Le Guin, The Left Hand of Darkness

The following eight original papers are the basis for the cumulative thesis, which summarizes and discusses the main results of the publications.

ORIGINAL PAPERS AND MANUSCRIPTS

I. Ulusoy, A., Rusconi, R., Perez-Revuelta, B.I., Musgrove, R.E., Helwig, M., Winzen-Reichert, B., and Di Monte, D.A. (2013). Caudo-rostral brain spreading of α-synuclein through vagal connections. EMBO Mol Med 5, 1119-1127.

II. Ulusoy, A., Musgrove, R.E., Rusconi, R., Klinkenberg, M., Helwig, M., Schneider, A., and Di Monte, D.A. (2015). Neuron-to-neuron α-synuclein propagation in vivo is independent of neuronal injury. Acta Neuropathol Commun 3, 13.

III. Helwig, M., Klinkenberg, M., Rusconi, R., Musgrove, R.E., Majbour, N.K., El-Agnaf, O.M., Ulusoy, A., and Di Monte, D.A. (2016). Brain propagation of transduced α-synuclein involves non-fibrillar protein species and is enhanced in α-synuclein null mice. Brain 139, 856-870.

IV. Ulusoy, A., Phillips, R.J., Helwig, M., Klinkenberg, M., Powley, T.L., and Di Monte, D.A. (2017). Brain-to-stomach transfer of α-synuclein via vagal preganglionic projections. Acta Neuropathol 133, 381-393.

V. Rusconi, R., Ulusoy, A., Aboutalebi, H., and Di Monte, D.A. (2018). Long-lasting pathological consequences of overexpression-induced α-synuclein spreading in the rat brain. Aging Cell 17 :e12727.

VI. Musgrove, R.E., Helwig, M., Bae, E.J., Aboutalebi, H., Lee, S.J., Ulusoy, A., and Di Monte, D.A. (2019). Oxidative stress in vagal neurons promotes parkinsonian pathology and intercellular α-synuclein transfer. J Clin Invest 129, 3738-3753.

VII. Helwig, M*., Ulusoy, A*., Rollar, A., O'Sullivan, S.A., Lee, S.S.L., Aboutalebi, H., Pinto-Costa, R., Jevans, B., Klinkenberg, M., and Di Monte, D.A. (2022). Neuronal hyperactivity-induced oxidant stress promotes in vivo α-synuclein brain spreading. Sci Adv 8, eabn0356. * Equal contribution

VIII. Klinkenberg, M., Helwig, M., Pinto-Costa, R., Rollar, A., Rusconi, R., Di Monte, D.A., and Ulusoy, A. (2023). Interneuronal in vivo transfer of synaptic proteins. Cells 12, 569.

TABLE OF CONTENTS

ABBREVIATIONS

3-NT	3-nitrotyrosine
6-OHDA	6-hydroxydopamine
α-syn	α-synuclein
β-syn	β-synuclein
AAV	recombinant adeno-associated virus
ChAT	choline acetyltransferase
CNO	clozapine-N-oxide
CNS	central nervous system
DA	dopamine
DOPA	3,4-dihydroxyphenylalanine
DMX	dorsal motor nucleus of the vagus (X) nerve
DREADD	designer receptor exclusively activated by designer drugs
GFP	enhanced green fluorescent protein
hM3D	human M_3 muscarinic DREADD
hM4D	human M_3 muscarinic DREADD
ITR	inverted terminal repeat
LB	Lewy body
LC	locus coeruleus
MPTP	1-methyl-4-phenyl-1,2,3,6-tetrahydropyridine
NA	nucleus ambiguus
NTS	nucleus tractus solitarius
PD	Parkinson's disease

PLA	proximity ligation assay
PFF	pre-formed fibrils
ROS	reactive oxygen species
SNAP25	synaptosomal-associated protein of 25kDa
TH	tyrosine hydroxyalse
VAMP2	vesicle-associated membrane protein 2
WPRE	Woodchuck hepatitis virus post-transcriptional regulatory element

1. INTRODUCTION

Parkinson's disease (PD) is the most common neurodegenerative movement disorder (Mhyre et al., 2012). It is characterized by the degeneration of dopamine-producing neurons in the substantia nigra pars compacta, leading to the development of motor symptoms such as tremors, rigidity, bradykinesia, and postural instability. Additionally, non-motor symptoms, including cognitive impairment, depression, anxiety, sleep disorders, and autonomic dysfunction, typically accompany these motor symptoms. While these symptoms are not fatal, disease complications (i.e., frequent falls and aspiration pneumonia) can be severe and considerably impact the patients' and their caregivers' quality of life.

Current therapeutics used to treat PD patients target the symptoms of the disease. Currently there is no cure or treatment options that can reverse neurodegeneration or slow disease progression. Oral L-3,4 dihydroxyphenylalanine (L-DOPA) pharmacotherapy is currently the most effective and widely used standard medical treatment for patients, which provides symptomatic relief for mainly the dopamine-loss-associated motor impairments of PD. However, the benefits of this therapy are limited as every year, an additional 10% of the patients begin to suffer from multiple side effects, including disabling peak-dose dyskinesias (abnormal involuntary movements), wearing-off phenomena, and on-off swings as the disease progresses (Ahlskog and Muenter, 2001). Thus, within ten years from the onset of the disease, the majority of the patients will have severe complications from L-DOPA treatment, critically compromising the quality of their lives. PD disease affects 6.3 million people worldwide and 260,000 people in Germany, making it the second most common neurodegenerative disorder after Alzheimer's disease (https://www.braincouncil.eu). The socio-economic burden of PD on society is expected to rise even more in our aging society, underscoring the urgency to find therapeutic targets for disease-modifying treatments.

Progression of disease pathology in PD

The formation of the neuronal protein inclusion bodies, namely Lewy bodies and Lewy neurites, in the PD brain is the pathological hallmark of the disease (Lewy, 1912; Tretiakoff, 1919). The main component of the Lewy bodies is alphα-synuclein (α-syn) (Spillantini et al., 1997). α-syn is a natively unfolded protein enriched in the pre-synaptic nerve terminals. Specific localization of α-syn in the synapse is suggested to be mediated by its ability to bind lipids (i.e., synaptic membranes) and pre-synaptic proteins (Burre et al., 2018; Maroteaux et al., 1988). Changes in α-syn amino acid sequence as well as increased α-syn expression, for example, by missense mutations, multiplications, and polymorphisms in the α-syn gene, may trigger PD development (Chiba-Falek and Nussbaum, 2001; Ibanez et al., 2004; Kruger et al., 1998; Maraganore et al., 2006; Pasanen et al., 2014; Polymeropoulos et al., 1997; Proukakis et al., 2013; Singleton et al., 2003; Zarranz et al., 2004). Interestingly, these disease-causing modifications of α-syn are also associated with increased propensity to aggregate and alterations in synaptic vesicle binding that likely interfere with its synaptic localization, indicating that the structure and subcellular localization of α-syn may play an important role in PD pathogenesis (Burre et al., 2018; Fortin et al., 2004; Stockl et al., 2008).

Extensive studies of normal and diseased human brains have shown that α-syn pathology develops predictably in different parts of the brain, often distinguished as the "six Braak stages of α syn deposition" (Braak et al., 2003a). The Braak hypothesis proposes that α-syn pathology spreads throughout the brain in a specific pattern, following a sequence of brain regions based on their anatomical connections (Braak et al., 2003b). This progression is thought to occur through interneuronal transfer of misfolded α-syn from one neuron to another (Freundt et al., 2012). Braak et al. (2003b) have also postulated that α-syn pathology begins in the enteric nervous system before spreading to the brain, specifically to the dorsal motor nucleus of the vagus nerve (DMX). As the disease progresses, the pathology is then spread to higher brain regions such as the locus coeruleus (LC), amygdala, the substantia nigra pars compacta and neocortex. Importantly, these regions that are affected by Lewy pathology throughout the disease progression are synaptically connected to each other (Braak et al., 2003b; Van Den Berge and Ulusoy, 2022). The spread of these α-syn aggregates through synaptically coupled networks is likely a crucial pathogenic factor and may link pathology and clinical symptoms. Indeed, several neuropathological evidence have illustrated that Lewy pathology and neurodegeneration not only occurs in the central nervous system (CNS) but in multiple peripheral organs as well (Beach et al., 2010; Gelpi et al., 2014), including the gut (Chiang and Lin, 2019; Stokholm et al., 2016), heart (Orimo et al., 2008) and skin (Donadio et al., 2016). It is also plausible to postulate that some, if not all, non-motor autonomic symptoms such as constipation, orthostatic hypotension, and dry skin may be linked to peripheral α-syn pathologies (Borghammer, 2018; Cheon et al., 2008; Palma and Kaufmann, 2020).

A likely scenario that may explain the body-to-brain transfer of α-syn pathology is through the vagus nerve (Braak et al., 2003b). The vagus nerve is the tenth cranial nerve. It emerges from the medulla oblongata, extends through the neck, and reaches all the way down to the abdomen. It is the main component of the parasympathetic nervous system and controls several vital functions, including the function of the heart, lungs, and digestive tract. The nerve is also a primary conduit that relays inflammatory and metabolic signals between the body and the brain: it (i) modulates inflammation by cholinergic signaling through efferent vagal activity, also known as the cholinergic anti-inflammatory pathway and (ii) regulates metabolic homeostasis by neuronal and endocrine signaling to control gastrointestinal function, pancreatic secretion as well as hepatic glucose production (Pavlov and Tracey, 2012). Several lines of neuropathological and experimental evidence support that the vagus nerve is involved in PD pathology. First, the DMX is the initial brain region where α-syn pathology is detected at early phases of lewy body diseases and is heavily affected throughout the course of PD (Braak et al., 2003a). Moreover, α-syn aggregates are present in the vagus nerve of PD patients but not in healthy controls (Mu et al., 2013). Interestingly, patients who underwent vagotomy show decreased risk of PD, further supporting the critical role of the vagus nerve in disease pathogenesis (Svensson et al., 2015). Finally, injecting α-syn seeds into the upper gastrointestinal system in mice leads to the transport of the protein into the vagus nerve and, thereafter, to the DMX (Holmqvist et al., 2014). Taken together, these findings strongly implicate the role of the vagus nerve in PD pathology development and suggest that it may be involved in the transfer of PD pathology between the gut and the brain.

Bi-directional progression of PD pathology

Although widely accepted, the Braak hypothesis has been criticized partly because not all patients follow the proposed staging system. Several studies have reported that approximately one-third of PD patients do not follow the Braak staging scheme, and approximately 15% do not show pathology in the DMX (Attems and Jellinger, 2008; Parkkinen et al., 2008). Longitudinal neuropathological evaluation of the Sydney multicenter study also described a high degree of neuropathological clinical heterogeneity among PD patients, where 50% of cases were consistent with the Braak staging, showing a brainstem-predominant Lewy pathology with slow disease progression (Halliday et al., 2008). Nevertheless, the remaining cases showed either a fast-progressing PD course with dementia and severe neocortical disease, or a late-onset, shorter-survival PD with widespread limbic and neocortical PD pathology and additional pathologies in the brain, suggesting that the pathology is most likely initiated in the brain rather than the gut. In a more recent population-based neuropathological study of 124 elderly patients with Lewy pathology, Raunio et al. (2019) described that two-thirds of the samples represented a clear caudo-rostral pattern, similar to what Braak and colleagues (Braak et al., 2003a) have described, and the rest were characterized with an amygdala-based pattern with origin in the amygdala. These patients were defined with substantial α-syn accumulation in the amygdala or limbic area and milder caudal (brainstem, medulla, and spinal cord) and rostral neocortical pathologies. Taken together, it is essential to recognize the heterogenicity of PD and the existence of different populations that may have various sites of onsets (Alafuzoff et al., 2009; Titova et al., 2017). Nevertheless, despite the variability in disease progression, these disease subtypes will evolve to a similar advanced disease stage (e.g., motor and congitive dysfunctions) over time, where not only the brain but also several peripheral organs are affected (Horsager et al., 2020). This suggests that α-syn pathology spreading is a common pathogenetic factor in PD independent of the site of onset. However, how α-syn spreads from one brain region to another is yet to be identified.

α-Synuclein propagation

The prion field introduces one central hypothesis of this pathological spreading. It is long known from the field of prion diseases that protein pathology is not limited to one region and spreads trans-synaptically (Polymenidou and Cleveland, 2012; Prusiner, 2013). Initially, a presence of a pathogen such as a virus or a prion was proposed to explain the progressive nature of the protein pathology in neurodegenerative diseases (Braak et al., 2003b; Gajdusek et al., 1977; Prusiner, 1984). The hypothesis became even more accepted following post-mortem findings of PD patient brains transplanted with fetal stem cells. 11 and 16 years post-transplantation of fetal nigral tissue into the striatum of PD patients, pathological α-syn was detected in the surviving graft neurons (Kordower et al., 2008; Li et al., 2008). The presence of Lewy pathology in decade-old fetal neurons was indeed unexpected and raised questions on whether the host pathology could be transmitted in a prion-like manner into the grafted neurons (Kordower and Brundin, 2009).

These initial findings and following debates accelerated a new line of research leading to the development of α-syn seeding models of PD, where pathogenic 'seeds' in the form of preformed α-syn fibrils (PFFs) or human PD brain lysate or homogenate are injected. These pathogenic seeds elicit aggrega-

tion, hyperphosphorylation, and ubiquitination of endogenous α-syn (Aulic et al., 2014; Luk et al., 2009; Volpicelli-Daley et al., 2011). Injection of PFFs into the brain of rodents or primates triggers aggregation of endogenous α-syn, typically in brain regions that are connected to the injection site (Luk et al., 2012a; Luk et al., 2012b; Masuda-Suzukake et al., 2013; Patterson et al., 2019; Paumier et al., 2015; Shimozawa et al., 2017).

Mechanisms of interneuronal α-synuclein transfer

A sequence of events must occur between the first-order and second-order neurons for α-syn to propagate (**Figure 1**). Pathological α-syn first needs to be released from the first-order neuron either

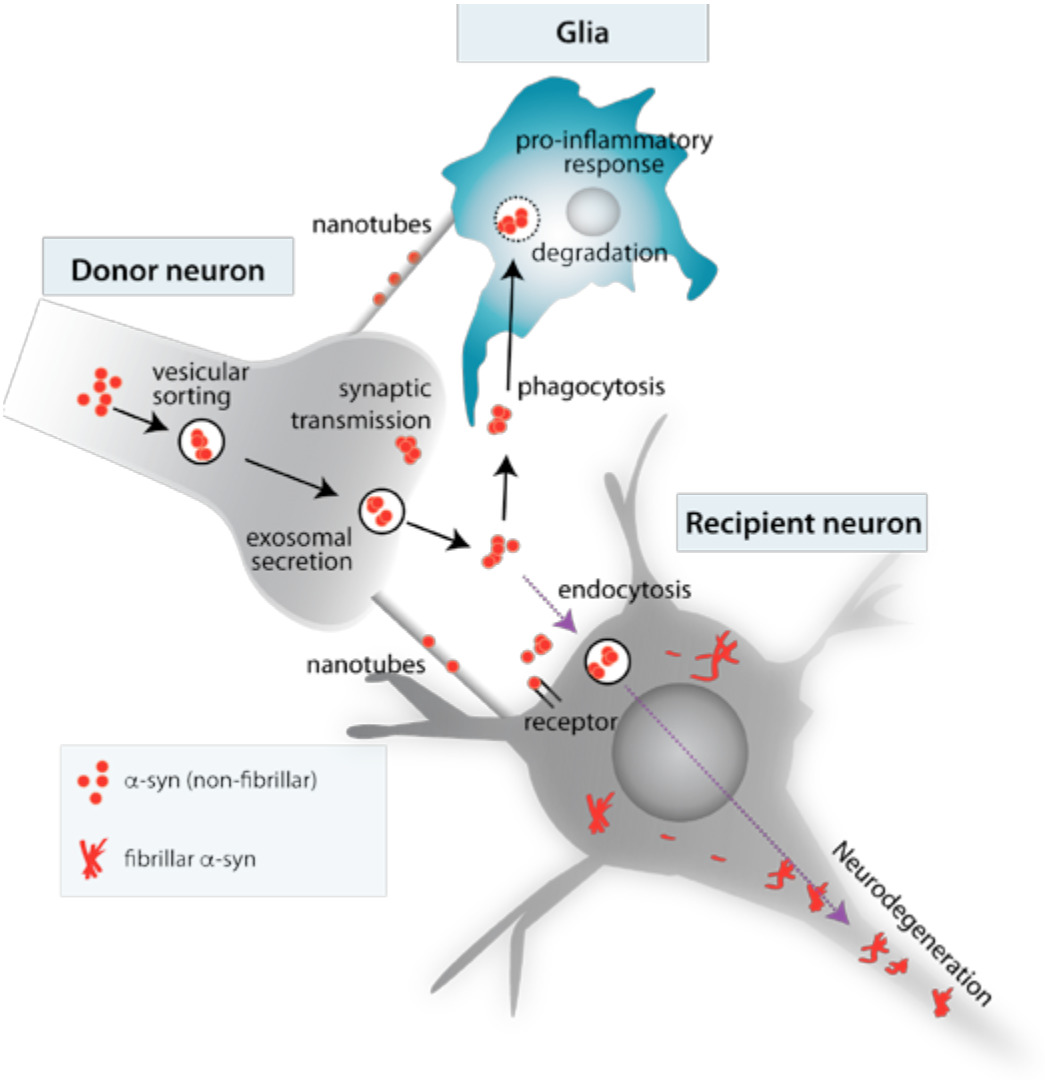

Figure1. Possible mechanisms of interneuronal α-synuclein transfer. α-syn spreading occurs by neuron-to-neuron α-syn transfer. More specifically, misfolded cytosolic α–syn is released by exosomal secretion, synaptic transmission or by being released freely (non-vesicular) into the extracellular space. In the healthy brain, extracellular α-syn likely is taken up into microglial cells by phagocytosis or tunneling nanotubes, and cleared by lysosomal degradation. However, in the diseased brain due to the chronic inflammatory state, microglial activity is altered. Consequently, extracellular α-syn is taken up by the recipient neurons and transferred to the other brain areas through axonal projections. When these vulnerable neuronal populations are affected by α-syn pathology they eventually degenerate.

passively following the death of the neuron or actively through a biological mechanism such as via exosomes (Jang et al., 2010) or through synapses (Ferreira et al., 2021; Van Den Berge et al., 2019; Yamada and Iwatsubo, 2018). In vivo, experimental evidence suggests that α-syn is likely transferred by an active mechanism rather than a passive one (Ulusoy et al., 2015). Although there is no consensus regarding the structure of the released α-syn, several lines of evidence suggest oligomeric species, in particular β-sheet rich oligomers, of α-syn are the likely species that are released (Danzer et al., 2007; Danzer et al., 2009; Delenclos et al.; Helwig et al., 2016; Kim et al., 2013; Kovacs et al., 2014). Once released into the extracellular space, the protein needs to be then taken up by the next-order cell. The identity of this cell can be a neuron (Danzer et al.; Danzer et al., 2009) or a glial cell (Lee et al., 2010; Scheiblich et al., 2021). Suggested mechanisms for α-syn specific uptake are through receptor-binding, i.e., lymphocyte-activation gene 3 or toll-like receptor-2 binding (Kim et al., 2013; Mao et al., 2016), endocytosis (Hansen et al., 2011) or via tunneling nanotubes (Abounit et al., 2016; Scheiblich et al., 2021). Once taken up by a new cell, α-syn aggregates can then induce neuronal dysfunction and further seed aggregation. These processes can be facilitated by various molecular mechanisms, which can promote the release, uptake, or conversion of α-syn to a pathological form. These mechanisms include oxidative stress, post-translational modifications of α-syn (such as nitration or aggregation), and neuronal activity (Helwig et al., 2016; Helwig et al., 2022; Musgrove et al., 2019; Schildknecht et al., 2013; Wu et al., 2020; Yamada and Iwatsubo, 2018).

In this habilitation thesis, I have accumulated the results obtained from several experiments and publications aiming to develop and characterize animal models to reproduce interneuronal α-syn spreading and tested hypotheses implicated in interneuronal α-syn spreading, such as cell death, seeding of endogenous α-syn, aggregation, oxidative stress, and neuronal activity.

2. AIMS OF THE THESIS

The overriding goal of this thesis work was to study the molecular mechanisms underlying the interneuronal spreading of α-syn. In particular, the following specific aims defined the basis of the projects:

1-To model interneuronal spreading of α-syn in vivo (Paper I-rats, III-mice and IV-bi-directional spread)

2-To test mechanisms implicated in the pathological spreading of α-syn.

- cell death (Paper II)
- seeding (Paper III) and aggregation (Papers III, VI, VII, and VIII)
- oxidative stress (Papers VI and VII)
- aberrant neuronal activity (Paper VII)

3- To test the bi-directionality of α-syn spreading (Paper IV)

4- To evaluate the long-term effects of interneuronal α-syn spreading (Paper V)

5- To assess the specificity of interneuronal spreading to α-syn (Paper VIII)

Box 1: In situ proximity ligation

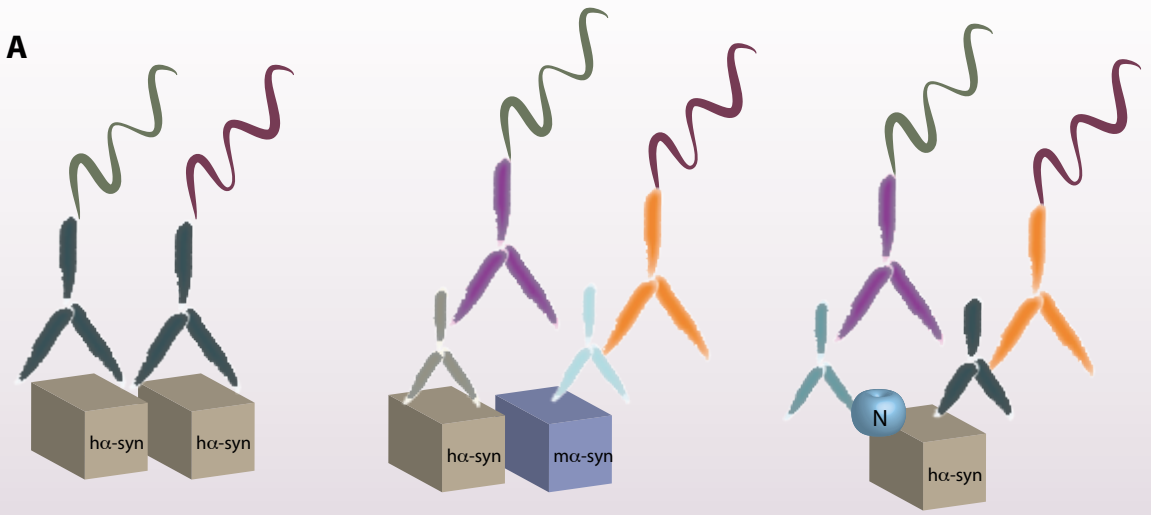

1) Protein self-interactions 2) Protein-protein interactions 3) Post-translational modifications

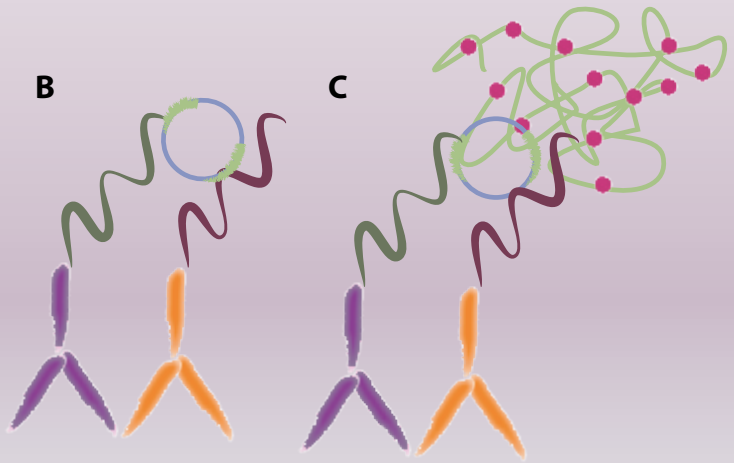

Ligation and rolling circle DNA synthesis

Amplification and detection

Proximity ligation assay (PLA) is a powerful tool for the specific and sensitive detection of protein-related events in tissue. (**A**) In this thesis, PLA was employed for several purposes: 1) detecting protein self-interactions, 2) detecting protein-protein interactions, and 3) detecting protein posttranslational modifications. PLA utilizes specific probes that are conjugated either to the primary antibody (direct PLA) or to the secondary antibody (indirect PLA). For instance, the direct PLA method was used to detect α-syn self-interactions. (**B**) Each PLA probe is equipped with a short, sequence-specific DNA strand. When the PLA probes are in close proximity (i.e., <40nm), the DNA strands can initiate rolling circle DNA synthesis. (**C**) The DNA synthesis reaction leads to the amplification of the DNA circle. The amplified DNA can then be detected using fluorescent-labeled complementary oligonucleotide probes or through an HRP-based enzymatic reaction for brightfield visualization.

3. RESULTS AND COMMENTS

Ulusoy, A., Rusconi, R., Perez-Revuelta, B.I., Musgrove, R.E., Helwig, M., Winzen-Reichert, B., and Di Monte, D.A. (2013). Caudo-rostral brain spreading of α-synuclein through vagal connections. EMBO Mol Med 5, 1119-1127.

Objective: To study the molecular mechanisms underlying the interneuronal spreading of α-syn in vivo, the first step of my post-doctoral studies was to establish a model of α-syn propagation. A specific goal was to model a spreading paradigm that mimics the caudo-rostral spreading seen in PD patients. For this purpose, we used viral vectors encoding for human α-syn to target the dorsal medulla oblongata via the vagus nerve.

At the time when we conducted these experiments, caudo-rostral spreading of α-syn in PD patient brains was well known, yet, experimental evidence showing caudo-rostral α-syn spreading was missing. Although several groups have reproduced seeding pathology in vivo by injecting α-syn PFFs into the brain parenchyma and successfully demonstrated that disease pathology can be replicated by seeding endogenous α-syn (Luk et al., 2012a; Luk et al., 2012b; Masuda-Suzukake et al., 2013), the PFF injection model was not free of drawbacks. First, the pathology was initiated from an artificial brain region, i.e., the striatum or the cortex, which is most likely not the site PD pathology begins. Moreover, the model used injections of high concentrations of PFFs (e.g., 5-10 µg total and 2-2.5µg/µl in concentration) into the parenchyma. Even though α-syn is present in the extracellular space in the brain, the concentrations are in the range of 0.5 ng/ml in α-syn overexpressing mice and 5 ng/ml in PD patient brains (Emmanouilidou et al., 2011), suggesting that the injected concentration of PFFs were more than 100 times higher than the pathological levels. Additionally, the model bypassed a crucial biological pathway from the sequence of events that takes place during interneuronal α-syn spreading: release of α-syn from the neuron. Therefore, we aimed to develop an animal model to reproduce α-syn spreading from the brainstem to more rostral brain regions following a stereotypical pattern in vivo by expressing human α-syn intraneuronally through the vagus nerve.

Methods and results: We conducted experiments in rats to show that the α-syn protein, once expressed in the DMX, can travel up to more frontal brain regions. The specific and sensitive detection of human α-syn was possible due to the presence of human specific α-syn antibodies that do not bind to the endogenous murine forms. In this model (**Figure 2**), exogenous human α-syn is expressed explicitly in the vagus nerve-connected nuclei in the medulla oblongata using adeno-associated viral vectors (AAV). These vagus nerve connected structures consist of the efferent vagal projections and their neuronal cell bodies in the DMX and nucleus ambiguus, and the afferent projections and terminals in the nucleus tractus solitarius. Altogether, they are called the vagal complex. Although not reported in the manuscript, the model also featured human α-syn accumulation in the vagal terminals in the stomach wall (**Figure 2**).

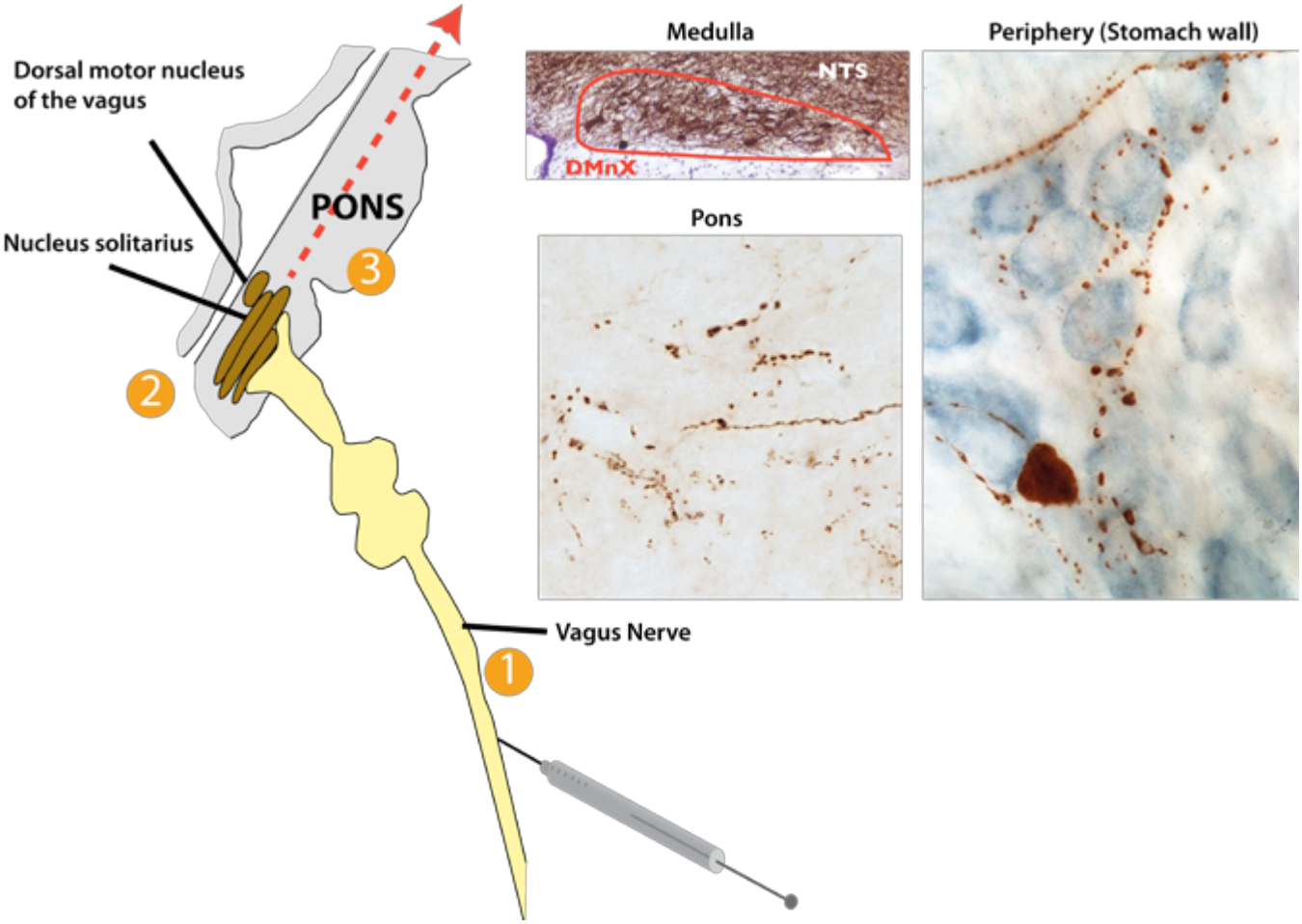

Figure 2. Model of caudo-rostral α-synuclein spreading. Injections of AAV vectors encoding for exogenous (human) α-syn into the vagus nerve (1) leads to a robust transgene expression in the vagal nuclei and terminals at 4 weeks post-injection (2). Protein expression (brown) at 4 weeks is limited to these regions, i.e., the dorsal motor nucleus of the vagus nerve (DMnX), nucleus tractus solitarius (NTS) and the vagal terminals in the periphery (e.g., in the stomach wall). (3) At later time points (e.g., 8 and 18 weeks) however, exogenous α-syn can be detected in more frontal regions (i.e. pons) and are defined as neuron-to-neuron transfer.

The rationale for this specific route is the involvement of the vagus nerve and the DMX in PD development. In the brain, the vagus nerve either terminates or stems from the nuclei in the medulla. Therefore, detecting exogenous protein in the more rostral brain regions indicates interneuronal α-syn transmission to the recipient neurons. AAV-induced expression of the exogenous proteins (i.e., α-syn and GFP) were detected explicitly within the neurons of the DMX and nucleus ambiguous and the terminals of the nucleus tractus solitarius (NTS) at 4 weeks after AAV injection. At 8 weeks post-surgery, human α-syn protein (but not the virus or the control GFP protein) was observed in the pons and over time in more rostral regions, following a stereotypical distribution of protein transfer, supporting that α-syn can indeed be transferred from the recipient neuron within the vagal nuclei to neurons from other brain regions in a time-dependent manner. Although AAV vectors are not known to pass transsynaptically, we performed control experiments to rule out the possibility of viral transduction in frontal brain regions **a)** by overex-

pressing another protein, i.e., GFP and **b)** by assessing viral transcripts (i.e., WPRE) within the frontal brain regions.

Conclusions: These experiments show that the presence of α-syn in frontal brain regions is not due to a spread of AAV vectors. We quantified the spreading by counting human α-syn containing axons or unbiased stereological analysis using a probe that assess length and density (i.e., space balls probe). In summary, these results provided direct evidence of α-syn transfer from the lower brainstem to the higher brain regions.

Research Article
Caudo-rostral α-synuclein spreading

TRANSPARENT PROCESS OPEN ACCESS EMBO Molecular Medicine

Caudo-rostral Brain Spreading of α-Synuclein through Vagal Connections

*Ayse Ulusoy, Raffaella Rusconi, Blanca I. Pérez-Revuelta, Ruth E. Musgrove, Michael Helwig, Bettina Winzen-Reichert, Donato A. Di Monte**

Keywords: Adeno-associated virus; Parkinson's disease; protein transport; rat; vagus nerve

DOI 10.1002/emmm.201302475

Received January 09, 2013
Revised April 08, 2013
Accepted April 10, 2013

α-Synuclein accumulation and pathology in Parkinson's disease typically display a caudo-rostral pattern of progression, involving neuronal nuclei in the medulla oblongata at the earliest stages. In this study, selective expression and accumulation of human α-synuclein within medullary neurons was achieved *via* retrograde transport of adeno-associated viral vectors unilaterally injected into the vagus nerve in the rat neck. The exogenous protein progressively spread toward more rostral brain regions where it could be detected within axonal projections. Propagation to the pons, midbrain and forebrain followed a stereotypical pattern of topographical distribution. It affected areas such as the coeruleus–subcoeruleus complex, dorsal raphae, hypothalamus and amygdala ipsilateral and, to a lesser extent, contralateral to the injection side. Spreading was accompanied by evidence of neuritic pathology in the form of axonal varicosities intensely immunoreactive for human α-synuclein and containing Thioflavin-S-positive fibrils. Thus, overexpression of human α-synuclein in the lower brainstem is sufficient to induce its long-distance caudo-rostral propagation, recapitulating features of Parkinson's disease and mechanisms of disease progression.

INTRODUCTION

Brain accumulation, aggregation and spreading of α-synuclein (α-syn) are hallmarks of Parkinson's (PD) and other neurodegenerative diseases (Spillantini et al, 1997). Although the exact mechanisms triggering this α-syn pathology are yet to be fully elucidated, both clinical and experimental evidence is consistent with a key role of increased α-syn expression as a causative or predisposing factor in disease pathogenesis. Indeed, a life-long elevation of α-syn expression due to multiplication mutations of its gene causes familial parkinsonism; other conditions, such as aging and neuronal injury, associated with more transient α-syn increases could also promote α-synuclein pathology and enhance disease risk (Ross et al, 2008; Simon-Sanchez et al, 2009; Ulusoy and Di Monte, 2013). A significant feature of α-syn pathology in PD is its pattern of ascending progression. Typically, early targets of α-syn accumulation are neurons in the medulla oblongata (MO), particularly in the dorsal motor nucleus of the vagus nerve (DMnX) and the reticular formation (Braak et al, 2003a; Braak et al, 2003b). During disease progression, α-syn pathology spreads upwardly toward the pons, mesencephalon and higher brain regions, following a stereotypical pattern that may reflect neuron-to-neuron transmission (Desplats et al, 2009; Hansen et al, 2011; Freundt et al, 2012) and propagation *via* interconnected brain pathways (Braak et al, 2003a; Luk et al, 2012a; Luk et al, 2012b). The reason(s) that underlie the involvement of MO neurons in the early stages of α-syn accumulation are not fully understood. It has been hypothesized, however, that pathogenic forms of the protein may initially reach the MO while being carried from peripheral sites (e.g., enteric plexi) to the CNS through the vagus nerve (Braak et al, 2003b; Pan-Montojo et al, 2012).

Caudo-rostral spreading of α-syn from the lower brainstem remains to be demonstrated experimentally, and no animal model is currently available that directly mimics this important PD feature. Furthermore, it is unclear whether increased expression of α-syn would itself be capable of causing long-distance upward transmission of the protein and its pathology. To address these unanswered questions, a new model of targeted elevation of neuronal α-syn in the rat MO was first developed. Using this model, we were then able to show progressive caudo-rostral α-syn propagation and pathological protein accumulation within dystrophic axons.

German Center for Neurodegenerative Diseases (DZNE), Bonn, Germany
***Corresponding author:** Tel: +49 228 43302650; Fax: +49 228 43302689
E-mail: donato.dimonte@dzne.de

RESULTS AND DISCUSSION

An experimental strategy was designed by which human α-syn (hα-syn) could be specifically overexpressed in the rat MO and then "traced forward" to assess its potential spreading. Recombinant adeno-associated viral vectors (AAV) expressing either wild-type hα-syn or green fluorescent protein (GFP) were injected into the left vagus nerve in the rat neck with the intent of transducing MO neurons through retrograde viral transport (Towne et al, 2010).

Robust staining of MO tissue with a specific hα-syn (Fig 1A and B) or GFP (Supporting Information Fig 1) antibody at 2 weeks post-injection indicated successful transduction via cranial nerve X. The pattern of immunoreactivity was consistent with targeted expression since it followed the predicted anatomical distribution of efferent and afferent fibers forming the vagus nerve. Efferent projections originate in the DMnX and the nucleus ambiguus. Consequently, retrograde viral transport through these fibers resulted in robust transgene (hα-syn or GFP) expression within somata and neurites of these nuclei (Fig 1A and B, Supporting Information Fig 1). Cholinergic DMnX cells could be double-stained with antibodies against the vesicular acetylcholine transporter and hα-syn, further confirming targeted transduction (Fig 1C–E). Transgene expression within neuronal cell bodies was only observed in the DMnX and nucleus ambiguus ipsilateral to AAV injection. This is consistent with the results of earlier anatomical studies showing unilateral labeling of DMnX perikarya after injections of tracers into the rat vagus nerve (Leslie et al, 1982).

Afferent vagal fibers projecting to the dorsal MO originate from sensory neurons in the inferior vagal ganglion from where they reach the nucleus of the tractus solitarius. Viral transduction of these cells was indicated by strong hα-syn staining of axonal bundles occupying an area dorsal to the DMnX (Fig 1A and F). Labeled fibers were mostly observed ipsilateral to the AAV injection. However, in agreement with previous reports demonstrating bilateral terminal fields of vagal sensory afferents (Leslie et al, 1982; Kalia & Sullivan, 1982; Odekunle & Bower, 1985), some of these axons crossed the midline and innervated the contralateral MO (Fig 1A and F). The pattern of distribution of efferent and afferent vagal fibers in the MO was virtually undistinguishable between animals injected with hα-syn- or GFP-carrying AAV vectors (Fig 1A and B, Supporting Information Fig 1).

The majority of rats (>60%) displayed evidence of strong transduction, with a significant number of stained cell bodies and high density of immunoreactive neurites (Fig 1A, B and F). qRT-PCR performed on DMnX-containing MO tissue from these high expressor animals revealed a 2.9-fold increase in total (rat plus human) α-syn mRNA; rat-only α-syn expression was unchanged (Fig 1G). The extent of neuronal immunoreactivity was less pronounced in a second group of animals (Supporting Information Fig 2), suggesting a less effective transduction with viral DNA. Total α-syn mRNA was 1.6 fold higher in the MO of these rats as compared to control tissue (Fig 1G). MO samples were also collected at 1 week and 3 weeks post-injection; qRT-PCR analyses demonstrated that maximal transduction was already reached at 1 week and remained unchanged at 2 and 3 weeks (Fig 1H).

Three sets of experiments were designed to further define the distribution of AAV transduction in high expressor rats. In the first set, total α-syn mRNA was quantified by qRT-PCR in DMnX-containing MO tissue from the side of the brain contralateral to viral injection; data showed levels not significantly different than control values (Fig 1G). Then, qRT-PCR analysis was performed on samples from different caudo-rostral portions of the MO and different quadrants of the pons. Total α-syn mRNA was enhanced in the MO, particularly its middle portion (Fig 1I). In contrast, no changes occurred in the pons, indicating absence of virus-encoded hα-syn mRNA (Fig 1I). The genome of our AAV vector also encoded for the woodchuck hepatitis virus post-transcriptional regulatory element (WPRE). Therefore, in the third set of experiments, MO and pontine tissue was analyzed for expression of this enhancer element using WPRE-hybridizing primers. RT-PCR results confirmed the occurrence of AAV transduction in the MO but found no evidence of WPRE mRNA in the dorso-medial and ventro-lateral (Fig 1J) as well as dorso-lateral and ventro-medial (not shown) pons.

The rat vagus nerve is comprised of axons that originate from or terminate in the MO and upper cervical spinal cord (Kalia & Sullivan, 1982). Thus, under our experimental conditions, presence of transduced protein in brain regions rostral to the MO would be consistent with interneuronal upward spreading. To test this possibility, we analyzed post-mortem histological sections throughout the brain of rats killed at 4, 8 or 18 weeks after vagal injection. Hα-syn or GFP immunoreactivity remained confined to the MO at the earliest time point. After longer post-injection intervals, however, evidence of ascending protein propagation characterized the brain of rats with high hα-syn expression. The exogenous protein was detected within discrete axonal projections that became immunoreactive for hα-syn. Labeled fibers were already seen in the pons and caudal midbrain at 8 weeks (Fig 2A). At 18 weeks, they were significantly more numerous and also occupied the rostral mesencephalon and prosencephalic areas (Fig 2B and C).

Progressive hα-syn spreading affected not only the left side of the brain (ipsilateral to viral injection) but also the contralateral pons, midbrain and forebrain; the count of immunoreactive axons was approximately 35% in the right as compared to the left hemisphere (Fig 2D). The most likely explanation for this intriguing finding relates to the bilateral distribution of axons that project from higher brain regions to nuclei in the MO (van der Kooy et al, 1984). Through these projections, the hα-syn released from neurons in the left MO could be taken up and transported to ipsilateral as well as contralateral sites.

Spreading followed a stereotypical pattern and sequence of topographical distribution (Fig 2E). Predilection loci included the pontine coeruleus–subcoeruleus complex (Fig 2F) where hα-syn-containing neurites could be double-labeled for tyrosine hydroxylase (Supporting Information Fig 3). In the midbrain, hα-syn-labeled fibers were observed in the dorsal raphae, periacqueductal gray and in the area of the peripeduncular nucleus dorsolateral to the substantia nigra (SN) pars reticulata (Fig 2G and H). Other typical sites were the hypothalamus in the

www.embomolmed.org

Research Article
Ayse Ulusoy et al.

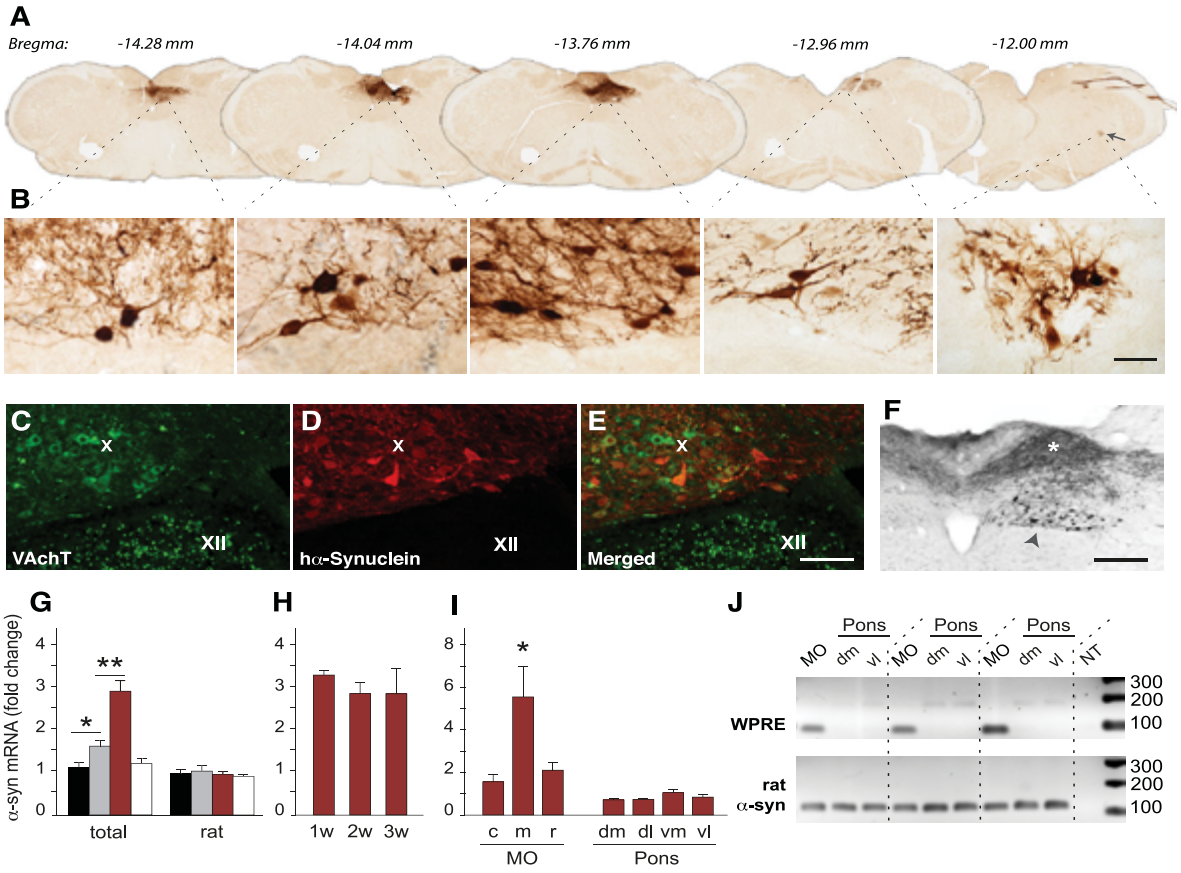

Figure 1. Vagal injections of hα-syn-carrying AAV induce region-specific transduction.

A,B. Representative MO sections from a high expressor rat killed at 2 weeks post viral injection were stained for hα-syn. Caudo-rostral sections at corresponding Bregma levels were visualized at lower (A) and higher (B) magnification. The nucleus ambiguus (arrow) is visible in the section at Bregma −12.00 mm. Higher-magnification images show neuronal bodies and neurites in the DMnX and nucleus ambiguus. Scale bar, 50 μm.

C-E. A representative section of the MO from a high expressor rat was double-stained with anti-vesicular acetylcholine transporter (VAchT) and anti-hα-syn antibodies. Confocal images show an area comprising neurons in the DMnX (X) and hypoglossal nucleus (XII). While VAchT immunoreactivity labeled neurons in both nuclei (green), hα-syn staining was only present in the DMnX (red) where it co-localized with the cholinergic marker (merged image). These observations are consistent with targeted transduction *via* vagus nerve projections. Scale bar, 200 μm.

F. A representative section of the MO from a high expressor rat was immunostained with an anti-hα-syn antibody. Arrowhead indicates cell bodies in the left (ipsilateral to viral injection) DMnX. The asterisk highlights neuronal projections immunoreactive for hα-syn at the level of the nucleus of the tractus solitarius. Some of these projections cross the mid-line and innervate the contralateral MO. Scale bar, 100 μm.

G. Analyses were made at 2 weeks post viral injection. For each rat, DMnX-containing samples from the caudal, middle and rostral MO were combined. qRT-PCR analyses measured total (rat + human) and rat-only α-syn mRNA levels. Data are shown from (i) the MO of control rats (black bars, n = 6), (ii) the left (AAV-injected side) MO of low expressor animals (gray bars, n = 4), (iii) the left (AAV-injected side) MO of high expressor rats (red bars, n = 10), and (iv) the right MO (contralateral to the AAV injection) of high expressors (empty bars, n = 4). ANOVA and *post hoc t* test with Bonferroni correction, $F_{3,20} = 17.80$. Mean ± SEM. $^{*}P < 0.05$ and $^{**}P < 0.01$.

H. Total (rat + human) α-syn mRNA levels were compared by qRT-PCR at 1, 2 and 3 weeks post injection in DMnX-containing samples from the left (AAV-injected side) MO of high expressor rats (n ≥ 3/group). Tissue was collected as described above in G. Mean ± SEM.

I. Total α-syn mRNA levels were measured by qRT-PCR in DMnX-containing samples from the left (AAV-injected side) caudal (c), middle (m) or rostral (r) MO of high expressor rats. ANOVA and Tukey *post hoc* test, $F_{2,14} = 6.409$. Analyses were also made in samples from the dorso-medial (dm), dorso-lateral (dl), ventro-medial (vm) and ventro-lateral (vl) pons. Mean ± SEM. $^{*}P < 0.05$.

J. WPRE and rat-only α-syn mRNA was amplified by RT-PCR in DMnX-containing samples from the left (AAV-injected side) MO of high expressor rats (n = 3). Analyses were also made in samples from the left dorso-medial (dm) and ventro-lateral (vl) pons. Specific bands were detected at 85 (WPRE) and 117 (rat α-syn) bp. NT labeling indicates non-template controls.

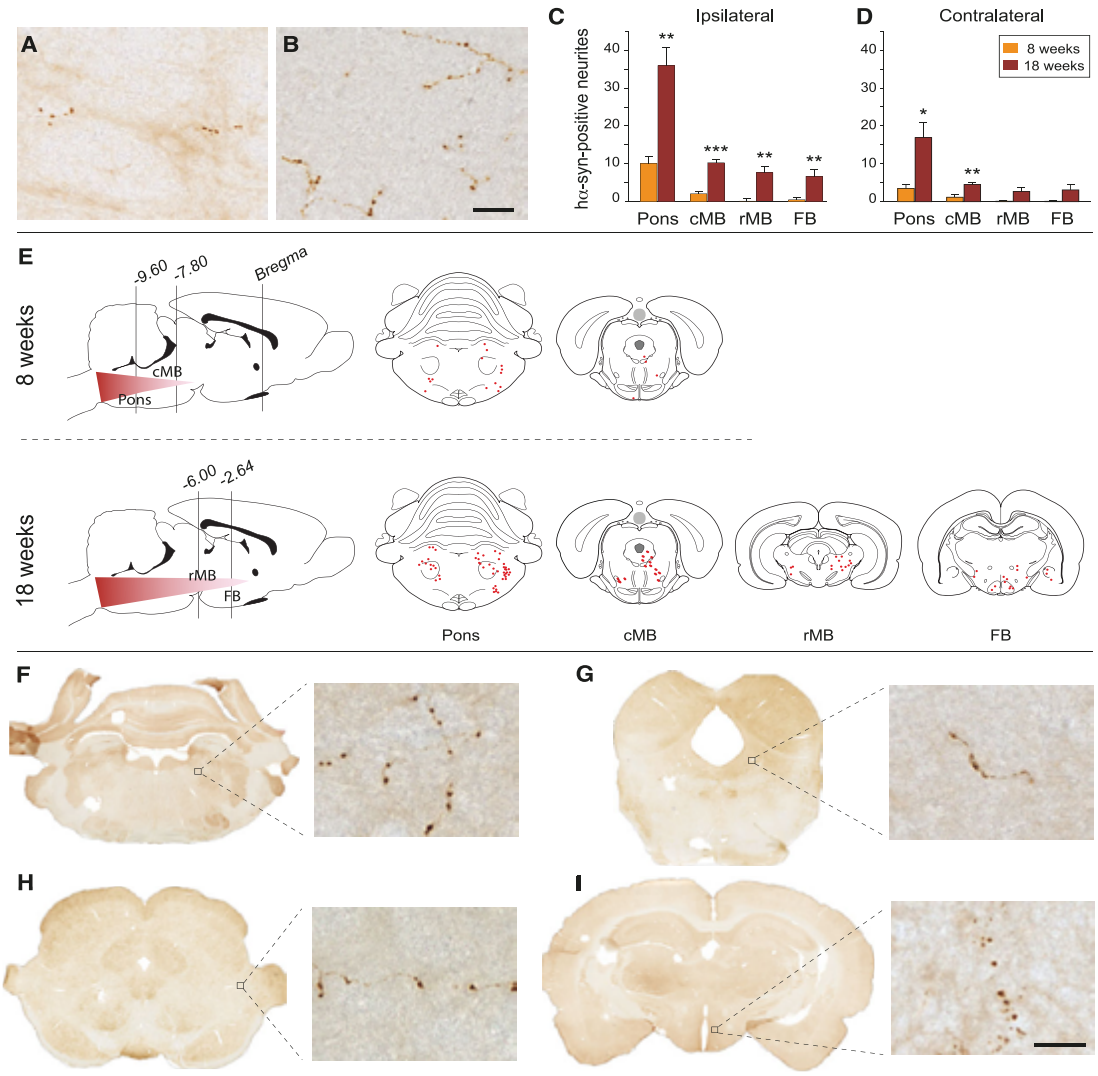

Figure 2. Hα-syn progressively spreads from the MO to more rostral brain regions.

A,B. Representative images of hα-syn-immunoreactive axons in tissue sections from the pons of high expressor rats sacrificed 8 (A) or 18 (B) weeks after vagal injection. Scale bar, 25 μm.

C,D. The number of neuritic projections immunostained with an anti-hα-syn antibody was counted in the pons, caudal midbrain (cMB), rostral midbrain (rMB) and forebrain (FB) at 8 and 18 weeks post injection. Counts are from the side of the brain ipsilateral (C) and contralateral (D) to viral injection. Mean (n = 5/group) ± SEM. $^{*}P < 0.05$, $^{**}P < 0.01$, $^{***}P < 0.001$ by two-tailed *t* test.

E. Topographical plot of the distribution and spreading of hα-syn-labeled neurites. Neuronal fibers from representative brain sections are shown as red dots. Bregma values indicate the caudo-rostral level.

F–I. Representative tissue sections from the pons (F), caudal midbrain (G), rostral midbrain (H) and forebrain (I) of high expressor rats sacrificed at 18 weeks post vagal injection. Higher magnification images from the coeruleus-subcoeruleus complex (F), periacqueductal gray (G), peripeduncular nucleus (H) and hypothalamus (I) show axonal projections stained with an anti-hα-syn antibody. Scale bar (higher magnification panels), 25 μm.

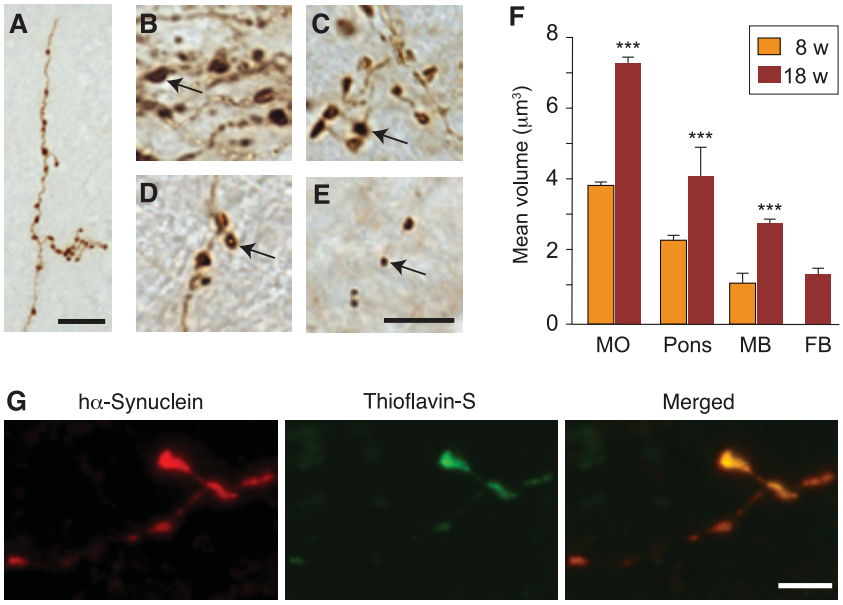

Figure 3. Spreading of hα-syn is associated with neuritic pathology.

A. Brain sections from a high expressor rat killed 18 weeks after vagal injection were stained with an anti-hα-syn antibody. The representative image shows a pontine axon with intensely stained swellings. Scale bar, 20 μm.

B–E. Hα-syn-immunoreactive neuritic varicosities in different brain regions at 18 weeks post injection. Arrows indicate swellings of different sizes in the MO (B, 7.3 μm^3), pons (C, 4.1 μm^3), midbrain (D, 2.8 μm^3) and forebrain (E, 1.4 μm^3). Scale bar, 10 μm.

F. The volume of hα-syn-immunoreactive neuritic swellings was measured in the MO (n = 1568 and 2406 swellings at 8 and 18 weeks, respectively), pons (n = 357 and 461 at 8 and 18 weeks), midbrain (n = 8 and 296 at 8 and 18 weeks) and forebrain (n = 34 at 18 weeks). Mean ± SEM. $^{***}P < 0.001$ by Wilcoxon Rank Sums test.

G. Confocal images of a pontine axon stained with an anti-hα-syn antibody (red) and Thioflavin-S (green). Merged images show co-localization. Scale bar, 5 μm.

diencephalon (Fig 2I) and the amygdala in the medial temporal lobe. All of these areas share a relevant feature, i.e. direct projections into the MO (Ter Horst et al, 1991; van der Kooy et al, 1984), supporting a mechanism of hα-syn transmission *via* anatomically interconnected pathways.

Results in high expressor rats, as described so far, contrasted with findings in animals with more moderate hα-syn expression and in rats injected with GFP-carrying AAV. The former displayed a few immunoreactive fibers only in the pons and only at the 18-week time point (Supporting Information Fig 4). The latter showed no significant GFP propagation.

Accumulation of hα-syn in the MO as well as extra-medullary sites was accompanied by morphological evidence of neuronal abnormalities. In particular, hα-syn-containing axons often appeared as sinuous threads with irregularly spaced, densely labeled varicosities (Fig 3A–E). The volume of these swellings augmented over time and was more pronounced in caudal *vs*. rostral brain regions, consistent with increasing hα-syn burden and progressive neuritic pathology (Fig 3F). Staining with Thioflavin-S and co-localization of Thioflavin-S with hα-syn immunoreactivity was used to assess neuronal content of hα-syn amyloid fibrils. In the pons, a small percentage of hα-syn-labeled neurites were stained with Thioflavin-S at 8 weeks. Co-localization characterized a higher proportion of pontine fibers at 18 weeks (Fig 3G), when rare Thioflavin-S-positive neurites were also seen in midbrain and forebrain sections. In all instances, staining with Thioflavin-S detected hα-syn fibrils primarily within neuritic swellings.

No evidence of hα-syn spreading and no overt sign of neuronal damage were found in the SN pars compacta (SNc). Stereological counting of dopaminergic neurons in rats killed 18 weeks after vagal injection confirmed that the cell number was unchanged in the left SNc of rats injected with hα-syn-carrying AAV (10,500 ± 452.6) as compared to values (i) in the right SNc (10,633 ± 427.3) from the same animals, and (ii) in the left and right SNc of control rats injected with GFP-carrying AAV (10,343 ± 449.5, left; 10.417 ± 435.8, right) (ANOVA, $F_{3,12} = 0.07968$, $P = 0.9698$).

The animal model described in this study provides experimental support in favor of the hypothesis that accumulation of α-syn in the MO can trigger further build-up and transmission of the protein toward more rostral CNS regions. Significant features of hα-syn spreading in rats include (i) the targeting of preferred anatomical sites, (ii) a consistent sequence of histological

progression, and (iii) bilateral but asymmetric brain burden. These observations are noteworthy since they resemble important aspects of α-syn pathology in PD.

Other findings of this study are apparently less consistent with the human disease. For example, while propagation of hα-syn proceeded through axonal projections, no evidence of accumulation of the exogenous protein was found within neuronal cell bodies. Furthermore, mapping of hα-syn throughout the rat brain revealed its absence in the SNc. These two results, which are at odds with the occurrence of α-syn-containing inclusions within neuronal somata and the vulnerability of nigral dopaminergic cells to α-syn pathology in PD, may underscore limitations of the animal model. It is also quite possible, however, that features described above recapitulate early events in the spreading of α-syn leading to its pathological accumulation. Indeed, previously published experimental work supports the notion that α-syn pathology affects first axonal projections and then neuronal cell bodies, mimicking a retrograde progression of degenerative changes that has also been proposed for PD (Decressac et al, 2012, Cheng et al, 2010). The absence of hα-syn in the SNc during its initial spreading from the MO could reflect the lack of direct anatomical connections between these two brain regions. Follow-up studies are warranted to determine if spreading of the exogenous protein would ultimately reach the SNc at later (>18 weeks post AAV injection) time points.

Results of this study bear significant implications concerning mechanisms and consequences of interneuronal α-syn transmission. Previous work *in vitro* and *in vivo* has shown cell-to-cell passage of soluble α-syn (Desplats et al, 2009; Hansen et al, 2011). Here, we document long-distance α-syn spreading that is triggered by overexpression of the protein in a concentration-, time- and connectivity-dependent fashion. As importantly, build-up and propagation of α-syn was accompanied by morphological evidence of neuritic injury and increasing formation of fibrillar deposits. Luk and colleagues (2012a,b) have recently reported that, once misfolded fibrillar forms of α-syn are inoculated directly into the rodent brain, they induce a prion-like spreading of α-syn pathology associated with frank neurodegeneration. This important observation together with our present findings raises the possibility of the following scenario. Enhanced concentration, interneuronal transmission and aggregation of α-syn could set up a self-perpetuating loop that, fueled by the generation of toxic protein fibrils, may ultimately underlie the progression of α-syn pathology and neurodegenerative cascade in PD.

MATERIALS AND METHODS

Vectors

Recombinant adeno-associated virus (serotype 2 genome and serotype 6 capsid, AAV) was used for transgene expression of human α-synuclein (hα-syn) or enhanced green fluorescent protein (GFP) under the control of the human Synapsin1 promoter. Gene expression was enhanced using a woodchuck hepatitis virus post-transcriptional regulatory element (WPRE) and a polyA signal (Ulusoy et al, 2012). AAV vector production, purification, concentration and titration were performed by Vector Biolabs (Philadelphia, PA). Vector preparations were stored in PBS with 5% glycerol at −80°C until use. Titration of the concentrated vectors was performed using quantitative PCR and primers against WPRE. Injected titers for AAV-hα-syn and AAV-GFP were 1.0×10^{13} and 1.8×10^{13} genome copies/ml, respectively.

Surgical procedure

Young adult female Sprague Dawley rats weighing 200–250 g were obtained from Charles River (Kisslegg, Germany). Animals were housed under a 12 h light/12-h dark cycle with free access to food and water. Experimental protocols were approved by the ethical committee of the State Agency for Nature, Environment and Consumer Protection in North Rhine Westphalia. Surgical procedures were performed on animals anesthetized with 2% isoflurane mixed with O_2 and N_2O. A 2 cm-incision was made at the midline of the rat neck, and the left vagus nerve was isolated from the surrounding tissue. A paraffin plate was placed underneath the nerve to provide support during injection and to prevent viral contamination of the surrounding tissue. Vector solution (2 μl) was injected at the rate of 0.5 μl/min using a glass capillary with a tip diameter of 60 μm fitted to a 5 μl Hamilton syringe. The capillary was kept in place for 3–4 minutes after injection.

Tissue preparation

Animals were killed under pentobarbital anesthesia and perfused through the ascending aorta with saline, followed by ice-cold 4% (w/v) paraformaldehyde. Brains were removed, immersion-fixed in 4% paraformaldehyde (for 24 h) and cryopreserved in 25% (w/v) sucrose solution. Forty-μm sections were cut on the coronal plane using a freezing microtome. Sections throughout the brain were stored at −20°C in phosphate buffer (pH 7.4) containing 30% glycerol and 30% ethylene glycol.

Histology

All immunohistochemical stainings were performed on free-floating sections. Brain sections were rinsed with Tris-buffered saline (TBS, pH 7.6). For brightfield microscopy, quenching of the endogenous peroxidase activity was achieved by incubation in a mixture of 3% H_2O_2 and 10% methanol in TBS. Non-specific binding sites were blocked by incubation in TBS with 0.25% Triton-X-100 (TBS-T) containing 5% normal serum. Samples were then incubated overnight at room temperature in primary antibody solution containing 1% normal serum in TBS-T. The following primary antibodies were used: mouse anti-hα-syn clone syn211 (36-008, Millipore; 1:10,000 dilution for color reaction or 1:3,000 for fluorescent detection), chicken anti-GFP (ab13970, abcam; 1:10,000), rabbit anti-tyrosine hydroxylase (for double-staining in the pons, AB152, Millipore; 1:1,000), mouse anti-tyrosine hydroxylase (for stereological cell counting, MAB318, Millipore; 1:2,000) and guinea pig anti-vesicular acetylcholine transporter (AB1588, Millipore; 1:500). Sections were rinsed, incubated (for 1 h at room temperature) in appropriate biotinylated secondary antibody solution (Vector Laboratories; 1:200) and then treated with avidin-biotin-peroxidase complex (ABC Elite kit, Vector Laboratories). Color reaction was developed using 3,3′-diaminobenzidine kit (Vector Laboratories). Sections were mounted on coated slides and coverslipped with Depex (Sigma).

For double-labeling immunofluorescence, primary antibodies were used as described above. Hα-syn was detected using biotinylated horse-anti-mouse (BA2001, Vector Laboratories) and a streptavidin-conjugated Dylight fluorophore (Dylight 488 or Dylight 594, Vector

The paper explained

PROBLEM:

α-Synuclein accumulation is a cardinal feature of Parkinson's disease (PD), so much so that a pathological staging of disease severity, first proposed by Braak and colleagues, is based on the spreading of α-synuclein lesions throughout the brain. Interestingly, initial sites of protein accumulation are nuclei in the lower brainstem; from there, α-synuclein pathology propagates upwardly in a progressive fashion. No animal model of α-synuclein caudo-rostral spreading is currently available, limiting our ability to study and elucidate mechanisms involved in the accumulation and propagation of α-synuclein and ultimately in disease development.

RESULTS:

We were able to reproduce PD-like α-synuclein spreading from the lower brainstem toward more rostral regions in the rat brain. The new model involved injection of viral vectors carrying human α-synuclein DNA into the vagus nerve in the rat neck, retrograde transport of the vectors, transduction of neurons and overexpression of α-synuclein within neuronal cell bodies and neurites in the medulla oblongata. Results provided important insight into mechanisms of α-synuclein accumulation, propagation and pathology. α-Synuclein overexpression was sufficient to trigger its interneuronal transfer into axonal projections innervating the medulla oblongata and connecting it to rostral sites in the pons, midbrain and forebrain. This effect was time- and concentration-dependent and was accompanied by evidence of protein fibrillation and neuritic pathology.

IMPACT:

Our findings provide direct evidence of long-distance α-synuclein propagation that could explain, at least in part, the caudo-rostral pattern of disease progression in PD. Data also demonstrate a relationship between increased α-synuclein expression, ascendant protein spreading and neuronal abnormalities, recapitulating mechanisms of likely relevance to PD pathogenesis. Future investigations using this new rat model will likely further our understanding of α-synuclein pathophysiology and contribute to the development of therapeutic strategies targeting α-synuclein accumulation and propagation.

Laboratories; 1:400). Tyrosine hydroxylase and vesicular acetylcholine transporter were detected directly with Dylight 594. Thioflavin-S treatment was performed on hα-syn-stained sections mounted on glass slides; it consisted of 8-min incubations in 0,05% Thioflavin-S (dissolved in water) followed by sequential differentiation in 80-95-95% ethanol (3 minutes each). Fluorescent-labeled slides were all coated with PVA-DABCO (Sigma). Observations were made under a Zeiss LSM 710 NLO confocal microscope using 488 and 561 nm lasers with sequential acquisition.

Histological quantifications

All evaluations were made by investigators blinded to treatment/experimental group. To determine the number of hα-syn-positive neurites, counts were made using sections at pre-defined Bregma coordinates (Paxinos & Watson, 2009): Bregma −9.60 mm in pons, −7.80 mm in caudal midbrain, −6.00 mm in rostral midbrain and −2.64 mm in forebrain.

The volume of hα-syn-immunoreactive swellings was measured in MO, pons, midbrain and forebrain at 8 and 18 weeks post vagal injection. For each region and time point, data were obtained and pooled from 5 animals. Tissue sections were visualized with a 63x oil immersion objective (Numerical aperture = 1.4) on either a Nikon Eclipse 90i (Nikon) or an Olympus IX2 UCB microscope equipped with Stereo Investigator software version 9 (MBF Biosciences). A guard zone thickness of 1 μm was set at the top and bottom of each section. For MO, measurements were carried out on a section at the level of the obex. After delineating the dorso-medial region of the left hemisphere, sampling parameters were set to count 4% of the area. For the pons (section taken at Bregma −9.60 mm), 68% of the entire left hemisphere was sampled. For the midbrain (Bregma −6.0 mm) and forebrain (Bregma −2.64 mm), 100% of the left hemisphere was analyzed. The stereological isotropic nucleator probe (Stereo Investigator) was used as previously described (Gundersen et al, 1988). To estimate volumes, the nucleator probe was set to generate 4 random isotropic linear rays emerging from a user-defined center point within each varicosity. The points at which the 4 rays touched the perimeter of the swelling were also manually defined. Varicosities with a volume greater than 0.5 μm^3 were included in data analysis.

The total number of tyrosine hydroxylase-positive neurons was estimated using an unbiased stereological quantification method and employing the optical fractionator principle (Stereo Investigator) (Ulusoy et al, 2010). The SN was delineated at low magnification in every sixth section throughout the entire region. Counting was performed using a 63× Plan-Apo oil objective on an Olympus IX2 UCB microscope equipped with a MBF Mac6000 System stage (Microbrightfield) and a high precision encoder. The coefficient of error was calculated according to Gundersen and Jensen (1987), and values were <0.10.

Reverse Transcription PCR (RT-PCR)

Samples for RT-PCR and quantitative RT-PCR (qRT-PCR) analyses were obtained from 40-μm fixed tissue sections. The dorso-medial quadrant of the left MO containing the DMnX was dissected and pooled from caudo-rostral, equally spaced (2 sections every 160 μm) sections at Bregma −14.76 to −12.48 mm. These samples were used to generate data in Fig 1G and H. MO data in Fig 1I were obtained using DMnX-contained samples dissected from equally spaced (3 sections every 120 μm) sections at caudal (Bregma −14.76 to −14.00 mm), middle (Bregma −14.00 mm to −13.36 mm) or rostral (Bregma −13.36 mm

to −12.48 mm) levels. In Fig 1I and J, samples from the dorso-medial, dorso-lateral, ventro-medial and ventro-lateral pons were dissected from equally spaced (2 sections every 160 μm) sections between Bregma −10.32 and −9.00 mm. Control tissue and reference samples were generated using the same dissection procedures, and control brains were obtained from sham-operated rats.

Total RNA was extracted using the "RecoverAll Total Nucleic Acid Kit" (Ambion), according to manufacturer's instructions. RNA yield was measured by absorbance reading. cDNA was synthesized using 150 ng of total RNA (SuperScript VILO Master Mix, Invitrogen). The following primer sequences were used: total (human plus rat) α-syn: 5′ tggttttgtcaaaaaggaccag forward and 5′ ccttcctcagaaggcatttc reverse; rat-only α-syn: 5′ gagttctgcggaagcctagagagc forward (aligning on the 5′ UTR region of rat α-syn mRNA) and 5′ gttttctcagcagcagccacaactcc reverse; WPRE: 5′ ccgttgtcaggcaacgtg forward and 5′ agctgacaggtggtggcaat reverse; hypoxantine phosphoribosyltransferase 1 (housekeeping gene): 5'gaccggttctgtcatgtcg forward and 5'acctggttcatcatcactaatcac reverse.

In some instances (Fig 1J), RT-PCR products were run on a 1.5% agarose gel. For qRT-PCR (Fig 1G–I), analyses were performed in triplicates, using 1 μl of cDNA and Power SYBR Green Master Mix (Applied Biosystems). Relative quantities (fold changes) were obtained after normalization to the expression of the housekeeping gene and calibration to the corresponding reference sample.

Statistical analyses

Statistical analyses were carried out with JMP Pro Statistical software (version 10.0.0; SAS Institute). For normally distributed data, means between two groups were compared with two-tailed *t*-test and comparisons of means from multiple groups were analyzed with one-way ANOVA followed by Tukey *post hoc* test or *t* test with Bonferroni correction. Non-normally distributed data were analyzed with non-parametric Wilcoxon rank sum test. Statistical significance was set at $P < 0.05$.

Author contributions

AU designed experiments, performed surgeries and carried out histological analyses and counts; RR set up and performed qRT-PCR; BIPR carried out analyses for protein aggregation; REM and MH set up and performed image analysis and quantification of neuritic pathology; BWR assisted with surgeries and histological preparations; DADM designed experiments, analyzed data and wrote the paper with input from the other authors.

Acknowledgements

The authors wish to thank H. Braak, K. Del Tredici, S. Jewell, D. Bano and M. Lotti for valuable comments on the data and manuscript, F. Hesse for assistance with histological preparations and C. Moehl for assistance with image analysis. AAV backbone plasmids were a kind gift from D. Kirik. This work was supported by the Blanche A. Paul Foundation and the Centres of Excellence in Neurodegeneration Research (CoEN).

Supporting Information is available at EMBO Molecular Medicine Online.

The authors declare that they have no conflict of interest.

References

Braak H, Del Tredici K, Rub U, de Vos RA, Jansen Steur EN, Braak E (2003a) Staging of brain pathology related to sporadic Parkinson's disease. Neurobiol Aging 24: 197-211

Braak H, Rub U, Gai WP, Del Tredici K (2003b) Idiopathic Parkinson's disease: possible routes by which vulnerable neuronal types may be subject to neuroinvasion by an unknown pathogen. J Neural Transm 110: 517-536

Cheng HC, Ulane CM, Burke RE (2010) Clinical progression in Parkinson disease and the neurobiology of axons. Ann Neurol 67: 715-725

Decressac M, Mattsson B, Lundblad M, Weikop P, Björklund A (2012) Progressive neurodegenerative and behavioural changes induced by AAV-mediated overexpression of α-synuclein in midbrain dopamine neurons. Neurobiol Dis 45: 939-953

Desplats P, Lee HJ, Bae EJ, Patrick C, Rockenstein E, Crews L, Spencer B, Masliah E, Lee SJ (2009) Inclusion formation and neuronal cell death through neuron-to-neuron transmission of α-synuclein. Proc Natl Acad Sci U S A 106: 13010-13015

Freundt EC, Maynard N, Clancy EK, Roy S, Bousset L, Sourigues Y, Covert M, Melki R, Kirkegaard K, Brahic M (2012) Neuron-to-neuron transmission of α-synuclein fibrils through axonal transport. Ann Neurol 72: 517-524

Gundersen HJ, Bagger P, Bendtsen TF, Evans SM, Korbo L, Marcussen N, Moller A, Nielsen K, Nyengaard JR, Pakkenberg B *et al*, (1988) The new stereological tools: disector, fractionator, nucleator and point sampled intercepts and their use in pathological research and diagnosis. APMIS 96: 857-881

Gundersen HJ, Jensen EB (1987) The efficiency of systematic sampling in stereology and its prediction. J Microsc 147: 229-263

Hansen C, Angot E, Bergstrom AL, Steiner JA, Pieri L, Paul G, Outeiro TF, Melki R, Kallunki P, Fog K *et al*, (2011) α-Synuclein propagates from mouse brain to grafted dopaminergic neurons and seeds aggregation in cultured human cells. J Clin Invest 121: 715-725

Kalia M, Sullivan JM (1982) Brainstem projections of sensory and motor components of the vagus nerve in the rat. J Comp Neurol 211: 248-265

Leslie RA, Gwyn DG, Hopkins DA (1982) The central distribution of the cervical vagus nerve and gastric afferent and efferent projections in the rat. Brain Res Bull 8: 37-43

Luk KC, Kehm V, Carroll J, Zhang B, O'Brien P, Trojanowski JQ, Lee VM (2012a) Pathological α-synuclein transmission initiates Parkinson-like neurodegeneration in nontransgenic mice. Science 338: 949-953

Luk KC, Kehm VM, Zhang B, O'Brien P, Trojanowski JQ, Lee VM (2012b) Intracerebral inoculation of pathological α-synuclein initiates a rapidly progressive neurodegenerative α-synucleinopathy in mice. J Exp Med 209: 975-986

Odekunle A, Bower AJ (1985) Brainstem connections of vagal afferent nerves in the ferret: an autoradiographic study. J Anat 140: 461-469

Pan-Montojo F, Schwarz M, Winkler C, Arnhold M, O'Sullivan GA, Pal A, Said J, Marsico G, Verbavatz JM, Rodrigo-Angulo M *et al*, (2012) Environmental toxins trigger PD-like progression via increased α-synuclein release from enteric neurons in mice. Sci Rep 2: 898

Paxinos G, Watson C (2009) The rat brain in stereotaxic coordinates, London: Academic Press

Ross OA, Braithwaite AT, Skipper LM, Kachergus J, Hulihan MM, Middleton FA, Nishioka K, Fuchs J, Gasser T, Maraganore DM *et al*, (2008) Genomic investigation of α-synuclein multiplication and parkinsonism. Ann Neurol 63: 743-750

Simon-Sanchez J, Schulte C, Bras JM, Sharma M, Gibbs JR, Berg D, Paisan-Ruiz C, Lichtner P, Scholz SW, Hernandez DG *et al*, (2009) Genome-wide association study reveals genetic risk underlying Parkinson's disease. Nat Genet 41: 1308-1312

Spillantini MG, Schmidt ML, Lee VM, Trojanowski JQ, Jakes R, Goedert M (1997) α-Synuclein in Lewy bodies. Nature 388: 839-840

Ter Horst GJ, Toes GJ, Van Willigen JD (1991) Locus coeruleus projections to the dorsal motor vagus nucleus in the rat. Neuroscience 45: 153-160

Towne C, Schneider BL, Kieran D, Redmond DE, Jr., Aebischer P (2010) Efficient transduction of non-human primate motor neurons after intramuscular delivery of recombinant AAV serotype 6. Gene Ther 17: 141-146

Ulusoy A, Bjorklund T, Buck K, Kirik D (2012) Dysregulated dopamine storage increases the vulnerability to α-synuclein in nigral neurons. Neurobiol Dis 47: 367-377

Ulusoy A, Di Monte DA (2013) α-Synuclein Elevation in Human Neurodegenerative Diseases: Experimental, Pathogenetic, and Therapeutic Implications. Mol Neurobiol 47: 484-494

Ulusoy A, Febbraro F, Jensen PH, Kirik D, Romero-Ramos M (2010) Co-expression of C-terminal truncated α-synuclein enhances full-length α-synuclein-induced pathology. Eur J Neurosci 32: 409-422

van der Kooy D, Koda LY, McGinty JF, Gerfen CR, Bloom FE (1984) The organization of projections from the cortex, amygdala, and hypothalamus to the nucleus of the solitary tract in rat. J Comp Neurol 224: 1-24

Supporting Information Figure 1

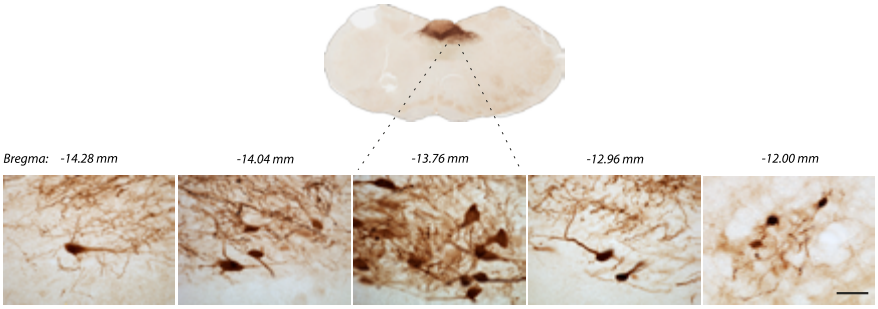

Supporting Information Figure 1. Vagal injections of GFP-carrying AAV induce robust transduction of DMnX neurons. Representative MO sections from a rat killed at 2 weeks post viral injection were stained with an anti-GFP antibody. Caudo-rostral sections at corresponding Bregma levels show robustly stained neuronal bodies and neurites in the DMnX and nucleus ambiguous (Bregma -12.00 mm). Scale bar, 50 µm. A lower magnification section is shown at Bregma -13.76 mm.

Supporting Information Figure 2

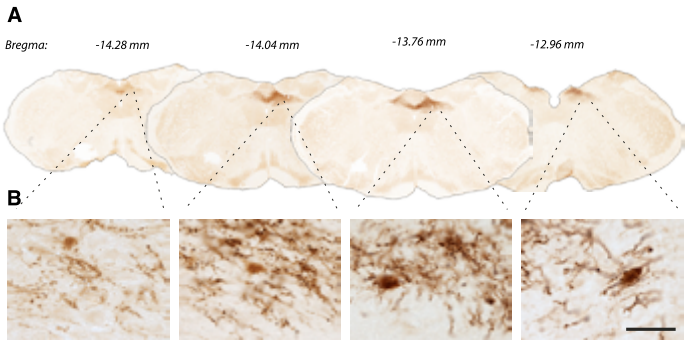

Supporting Information Figure 2. Hα-syn expression in the MO of a rat with suboptimal AAV transduction. MO sections from a rat killed at 2 weeks after injection with hα-syn-carrying AAV were stained for hα-syn. Caudo-rostral sections at corresponding Bregma levels were visualized at lower (A) and higher (B) magnification. Higher-magnification images show neuronal bodies and neurites in the DMnX. The extent and intensity of immunoreactivity is evidently less pronounced in these images as compared to images in Figure 1 obtained from a high expressor animal. Scale bar, 50 μm.

Supporting Information Figure 3

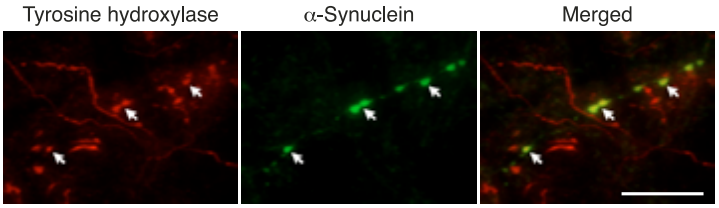

Supporting Information Figure 3. Hα-syn spreads from the MO to catecholaminergic neurons in the pons. Tissue was collected from a high expressor rat killed 18 weeks after AAV injection. Confocal images show a pontine (coeruleus-subcoeruleus area) axon (arrows) co-labeled for tyrosine hydroxylase and hα-syn. The merged panel illustrates co-localization. Scale bar, 20 μm.

Supporting Information Figure 4

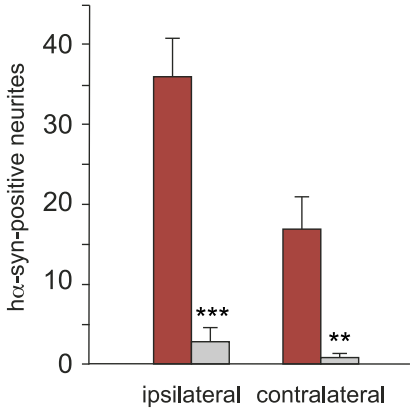

Supporting Information Figure 4. Hα-syn spreads from the MO to pons in rats with suboptimal AAV transduction. The number of neuritic projections immunostained with an anti-hα-syn antibody was counted in the pons of rats sacrificed at 18 weeks post vagal injection. Counts in low expressors (gray bars, n=6) are compared with values in high expressor animals (red bars, n=5). Counts are shown from the side of the brain ipsilateral and contralateral to viral injection. Data from high expressors are the same as those reported in Figure 2C,D. Mean ± SEM. **P<0.01, ***P<0.001 by two-tailed t test.

Ulusoy, A., Musgrove, R.E., Rusconi, R., Klinkenberg, M., Helwig, M., Schneider, A., and Di Monte, D.A. (2015). Neuron-to-neuron α-synuclein propagation in vivo is independent of neuronal injury. Acta Neuropathol Commun 3, 13.

Objective: After establishing a model of caudo-rostral α-syn spreading, we set out to test the involvement of neurodegeneration in disease propagation. These sets of experiments in Paper II were designed to unravel the role of neuronal death in interneuronal α-syn transfer, as the passive release of α-syn from damaged neurons could be a phenomenon of particular relevance during neurodegenerative processes. Indeed, it is plausible to suggest that pathological forms of α-syn can be released upon cell death. Extracellular α-syn could then be internalized into nearby neurons, causing further seeding and propagation of the pathology.

Methods and results: α-Syn spreading was induced using AAV-mediated overexpression of α-syn in the vagal complex, as described in Paper I. Two separate viral vector batches were used to induce exogenous α-syn expression. Although injection of these two batches generated similar levels of α-syn transduction, one batch led to neuronal death, whereas the other did not result in toxicity. If the hypothesis suggesting that α-syn propagation is caused by neuronal damage holds true, one would expect increased spreading following the administration of the batch that induced neurodegeneration. However, results did not support the hypothesis since α-syn spreading was significantly reduced as a consequence of cell injury, suggesting that maintenance of cellular integrity is required for effective neuron-to-neuron transfer of α-syn.

Conclusions: Our experiments aiming to investigate the role of neurodegeneration in the propagation of caudo-rostral α-syn revealed, contrary to the initial hypothesis, that neuronal death reduced α-syn spreading, challenging the notion that passive release of α-syn from damaged cells contributes to pathology propagation. These results suggest that maintaining cellular integrity is crucial for efficient neuron-to-neuron transfer of α-syn. Our findings shed light on the complex mechanisms underlying α-syn propagation and highlight the importance of understanding the role of neurodegeneration in disease progression.

Ulusoy et al. Acta Neuropathologica Communications (2015) 3:13
DOI 10.1186/s40478-015-0198-y

ACTA NEUROPATHOLOGICA COMMUNICATIONS

RESEARCH Open Access

Neuron-to-neuron α-synuclein propagation *in vivo* is independent of neuronal injury

Ayse Ulusoy[1], Ruth E Musgrove[1], Raffaella Rusconi[1], Michael Klinkenberg[1], Michael Helwig[1], Anja Schneider[2,3] and Donato A Di Monte[1*]

Abstract

Introduction: Interneuronal propagation of α-synuclein has been demonstrated in a variety of experimental models and may be involved in disease progression during the course of human synucleinopathies. The aim of this study was to assess the role that neuronal injury or, *vice versa*, cell integrity could have in facilitating interneuronal α-synuclein transfer and consequent protein spreading in an *in vivo* animal model.

Results: Viral vectors carrying the DNA for human α-synuclein were injected into the rat vagus nerve to trigger protein overexpression in the medulla oblongata and consequent spreading of human α-synuclein toward pons, midbrain and forebrain. Two vector preparations sharing the same viral construct were manufactured using identical procedures with the exception of methods for their purification. They were also injected at concentrations that induced comparable levels of α-synuclein transduction/overexpression in the medulla oblongata. α-Synuclein load was associated with damage (at 6 weeks post injection) and death (at 12 weeks) of medullary neurons after treatment with only one of the two vector preparations. Of note, neuronal injury and degeneration was accompanied by a substantial reduction of caudo-rostral propagation of human α-synuclein.

Conclusions: Interneuronal α-synuclein transfer, which underlies protein spreading from the medulla oblongata to more rostral brain regions in this rat model, is not a mere consequence of passive release from damaged or dead neurons. Neuronal injury and degeneration did not exacerbate α-synuclein propagation. In fact, data suggest that cell-to-cell passage of α-synuclein may be particularly efficient between intact, relatively healthy neurons.

Keywords: Adeno-associated viral vector, Neurodegeneration, Parkinson's disease, Rat, Vagus nerve

Introduction

Neuron-to-neuron propagation of pathological forms of α-synuclein (α-syn) is a phenomenon of likely relevance for the development and progression of human α-synucleinopathies such as Parkinson's disease (PD). Several lines of evidence support this assertion. Observations in post-mortem PD brain reveal a stereotypical accumulation of α-syn-containing Lewy bodies and Lewy neurites. Compatible with a mechanism of interneuronal α-syn spreading, these pathological lesions progressively affect interconnected brain regions, starting from the caudal brainstem and moving toward mesocortical and neocortical areas [1,2]. From the experimental standpoint, neuron-to-neuron α-syn transmission has been demonstrated *in vitro* in a variety of cell culture systems as well as *in vivo* in animal models [3-10]. Results of *in vivo* studies also support a relationship between α-syn propagation and neurodegenerative processes. When mice were injected intrastriatally with fibrillar α-syn, protein spreading not only reached neuronal populations distant from the injection site but also caused dopaminergic cell death in the substantia nigra [11]. In a separate model mimicking the spreading pattern of PD, interneuronal transmission of α-syn could be initiated by its overexpression in the rat medulla oblongata (MO); caudo-rostral spreading toward pons, midbrain and forebrain was accompanied by accumulation and aggregation of α-syn into swollen dystrophic axons [12].

Elucidation of the mechanisms involved in the transfer of α-syn (and/or pathological forms of it) from donor to recipient cells bears significant pathogenetic implications and could provide clues for therapeutic intervention

* Correspondence: donato.dimonte@dzne.de
[1]German Center for Neurodegenerative Diseases (DZNE), Ludwig-Erhard-Allee 2, 53175 Bonn, Germany
Full list of author information is available at the end of the article

targeting protein spreading. Experimental evidence suggests that α-syn could initially be secreted *via* membrane-bound vesicles, such as exosomes, and then taken up *via* endocytotic pathways, such as adsorptive endocytosis and dynamin-dependent endocytosis [3,4,13-16]. While these mechanisms would involve intact healthy cells, a critical unaddressed question remains the role that neuronal injury/death may play in facilitating α-syn access into the extracellular space. Passive release of α-syn from damaged neurons would be of particular relevance during neurodegenerative processes. Indeed, a vicious cycle could be envisioned by which pathological α-syn accumulation causes neuronal damage, neurodegeneration results in α-syn release, and extracellular α-syn becomes available for internalization into nearby neurons. Injury of these neurons would ultimately perpetuate the cycle and cause further propagation of α-syn pathology.

Experiments in this study were designed to determine the role of neuronal damage or, *vice versa*, cell integrity in α-syn propagation *in vivo*. α-Syn spreading from the caudal brainstem toward more rostral brain regions was triggered by protein overexpression in the rat MO and compared under experimental conditions characterized by absence of neurodegeneration *vs.* a loss of α-syn-containing neurons. Results demonstrated that passive release from injured neurons is not essential for triggering α-syn transmission, nor does it exacerbate protein spreading. In fact, α-syn propagation was more pronounced in the absence than in the presence of neurodegeneration, underscoring the importance of neuron-to-neuron α-syn transfer between intact, relatively healthy cells.

Materials and methods

Vectors

Recombinant adeno-associated virus (serotype 2 genome and serotype 6 capsid, AAV) was used for transgene expression of human wild-type α-synuclein (hα-syn) or enhanced green fluorescent protein (GFP) under the control of the human Synapsin1 promoter. Gene expression was enhanced using a woodchuck hepatitis virus post-transcriptional regulatory element (WPRE) and a polyadenylation signal sequence (polyA) [12,17]. Experiments compared the effects of two AAV preparations: AAV prep 1 (Vector Biolabs, Philadelphia, PA, USA) and AAV prep 2 (Sirion Biotech, Martinsried, Germany). For both preparations, 293 HEK cells were transfected with the same reporter plasmid (Additional file 1: Figure S1). Crude cell lysates containing the viral particles were then purified by either (i) two consecutive CsCl gradient centrifugations (AAV prep 1), or (ii) centrifugation through a discontinuous iodixanol gradient followed by heparin affinity chromatography (AAV prep 2). AAV preparations were concentrated and resuspended in phosphate buffered saline. Titration of the concentrated vectors was performed using quantitative PCR with primers against WPRE. Injected titers were 1×10^{13} genome copies/ml for hα-syn-AAV prep 1 and between 5×10^{12} and 1×10^{13} genome copies/ml for hα-syn-AAV prep 2. In experiments in which the effects of GFP overexpression were compared, GFP-AAV prep 1 or GFP-AAV prep 2 were injected at a titer of 1×10^{13} genome copies/ml.

Animals and surgical procedure

Young adult female Sprague Dawley rats weighing 200–250 g were obtained from Charles River (Kisslegg, Germany). They were housed under a 12-h light/12-h dark cycle with free access to food and water. Experimental design and procedures were approved by the ethical committee of the State Agency for Nature, Environment and Consumer Protection in North Rhine Westphalia. Following anesthetization with 2% isoflurane mixed with O_2 and N_2O, a 2 cm-incision was made at the midline of the rat neck. The left vagus nerve was isolated from the surrounding tissue, and the vector solution (2 μl) was injected at a flow rate of 0.5 μl/min using a glass capillary (tip diameter = 60 μm) fitted onto a 5 μl Hamilton syringe. Control animals were injected with vehicle using the same volume and at the same flow rate. After injection, the capillary was kept in place for 3–4 minutes.

Tissue preparation

Animals were killed under pentobarbital anesthesia and perfused through the ascending aorta with saline, followed by ice-cold 4% (w/v) paraformaldehyde. Brains were removed, immersion-fixed in 4% paraformaldehyde (for 24 h) and cryopreserved in 25% (w/v) sucrose solution. Coronal sections (40 μm) throughout the brain were cut using a freezing microtome and stored at −20° C in phosphate buffer (pH 7.4) containing 30% glycerol and 30% ethylene glycol.

3,3′-Diaminobenzidine staining

Free-floating brain sections were rinsed with Tris-buffered saline (TBS, pH 7.6). Endogenous peroxidase activity was quenched by incubation in a mixture of 3% H_2O_2 and 10% methanol in TBS. Non-specific binding sites were blocked using 5% normal serum in TBS containing 0.25% Triton-X-100 (TBS-T). Samples were then incubated overnight at room temperature in TBS-T containing 1% bovine serum albumin and primary antibodies: mouse anti-hα-syn clone syn211 (36–008, Merck Millipore, Darmstadt, Germany; 1:10,000 dilution), chicken anti-GFP (ab13970, Abcam; 1:10,000 dilution), and goat anti-choline acetyltransferase (AB144P, Millipore; 1:200 dilution). Sections were rinsed and incubated (for 1 h at room temperature) in biotinylated secondary

antibody solution (horse anti-mouse BA2001 or rabbit anti-goat BA5000; Vector Laboratories, Burlingame, CA, USA; 1:200 dilution). Following treatment with avidin-biotin-peroxidase (ABC Elite kit, Vector Laboratories), color reaction was developed using 3,3′-diaminobenzidine kit (Vector Laboratories). Sections were mounted on coated slides, dried, stained (if appropriate) with cresyl violet (FD Neurotechnologies, Columbia, MD, USA) and coverslipped with Depex (Sigma-Aldrich, St. Louis, MO, USA).

Brightfield microscopy images were obtained using an IX2 UCB microscope from Olympus (Hamburg, Germany) equipped with a motorized stage (MBF Mac6000 System stage, MBF Biosciences). For z-stacking analysis, stacks were collected at 1 μm intervals, and a single image was generated by deep focus post-processing. Low magnification images of entire brain sections were generated using an Axioscan Z1 (Carl Zeiss, Göttingen, Germany) slide scanner.

Fluorescence staining

Following blocking procedures (see above), tissue sections were incubated overnight with the following primary antibodies: mouse anti-hα-syn clone syn211 (36–008, Merck Millipore; 1:3,000 dilution), rabbit anti-poly ADP ribose polymerase (PARP) p85 fragment (G7341, Promega; 1:100 dilution), and mouse anti-hα-syn 5G4 (847–0102004001, Analytic Jena; 1:1000 dilution). Reactions with primary antibodies raised in mice were followed by incubations with biotinylated horse anti-mouse (BA2001, Vector Laboratories) secondary antibody. Streptavidin-conjugated DyLight fluorophore (DyLight 488, Vector Laboratories; 1:400 dilution) was then used for detection. Reactions with primary antibodies raised in rabbit were followed by incubations in the presence of DyLight 594-conjugated horse anti-rabbit secondary antibody (Vector Laboratories; 1:400 dilution). Sections were mounted on coated slides and coverslipped with PVA-DABCO (Sigma). Confocal fluorescence images were collected using a Zeiss LSM700 inverted laser scanning microscope.

Histological quantifications

All histological evaluations were performed by investigators blinded to sample treatment. The total number of Nissl-positive and hα-syn-immunoreactive neurons was estimated in the dorsal motor nucleus of the vagus nerve (DMnX) using unbiased stereology [18]. Every sixth section throughout the entire DMnX was sampled. After delineation of the DMnX under a 10x objective (Additional file 2: Figure S2), counting was performed using a 60x Plan-Apo oil objective (Numerical aperture = 1.4). A guard zone thickness of 1 μm was set at the top and bottom of each section. Neurons were counted using the optical fractionator technique (Stereo Investigator software version 9, MBF Biosciences, Williston, VT, USA). The sampling interval in the X-Y coordinate axis was adjusted so that at least 100 cells were counted for each DMnX (sampling grid size: 125 × 125 mm; counting frame: 60 × 60 mm). Coefficient of error was calculated according to Gundersen and Jensen [19]; values <0.10 were accepted.

Every sixth section throughout the entire DMnX was used for volume estimates of DMnX neurons immunoreactive for hα-syn or choline acetyltransferase (ChAT). Measurements were made on (i) all hα-syn-labeled cells present in these sections, or (ii) a population of ChAT-positive neurons selected *via* stereological sampling. Volumes were calculated according to the isotropic nucleator method [20]. For each neuron, a nucleator probe was set to generate 6 random isotropic linear rays that emerged from a user-defined center point. The points at which the 6 rays touched the profile of the neuron were manually defined and used for volumetric estimates. Analyses were carried out using the Stereo Investigator software version 9 (MBF Biosciences).

Fluorescence intensity measurements were carried out on all α-syn-positive neurons present in three MO sections at the level of obex (Bregma: −13.8, −13.56 and −13.32 mm). For each neuron, confocal images were collected using a 60x objective at a single focal plane where the nucleus was clearly visible. All image settings including laser power, exposure time, gain, offset and scanning speed were kept constant throughout the measurements. For each neuron, background readings were obtained on empty areas at the same focal depth. Image analyses were carried out using the Fiji software (version 2.0) [21]. Corrected total cell fluorescence (CTCF) was calculated by the following formula: Integrated Density - (Area occupied by the selected cell x Mean fluorescence of background readings). CTCF values were averaged for each animal.

Quantification of hα-syn positive axons was made using sections at pre-defined Bregma coordinates [22]: −9.48 mm in pons, −7.80 mm in caudal midbrain, −6.00 mm in rostral midbrain and −2.40 mm in forebrain. At each section, all immunostained axons were counted using an Axioscope microscope (Carl Zeiss) under a 20x Plan-Apo objective.

The length of hα-syn-containing axons was estimated using the Space Balls stereological probe (Stereo Investigator software version 9, MBF Biosciences) [23]. Measurements were made on serial sections of the pons (Bregma: −9.7 to −9.22 mm) where an area encompassing the locus coeruleus and the parabrachialis nucleus was delineated. A virtual hemisphere (12 μm radius) was placed randomly within this area, and systematic sampling was performed at intervals of 100 μm in both X and Y axes. A guard zone of 1 μm was set at the top and bottom of each tissue section. While the microscope stage moved through the Z-axis, the circle diameter of the Space Balls hemisphere decreased concentrically at

each 1 μm focal plane. The number of intersections between fibers and circles was counted and used to estimate a mean total fiber length. Volume of the reference region was estimated by the Cavalieri point-counting method applying a step length size of 200 μm [24]. Fiber density was calculated by the ratio total fiber length/volume of reference region.

Reverse transcription PCR (RT-PCR)

Fixed tissue sections (40 μm) from rats injected with hα-syn-AAV preparations or vehicle were used for conventional or quantitative RT-PCR (qRT-PCR) analysis. Dorso-medial quadrants of the left (injected side) MO, which contained the DMnX, were dissected and pooled from equally spaced (2 sections every 160 μm) sections at Bregma −14.76 to −12.48 mm. Total RNA was extracted using the "RecoverAll Total Nucleic Acid Kit" (Ambion, Austin, TX, USA), and cDNA was synthesized by reverse transcription (SuperScript VILO Master Mix, Invitrogen, Carlsbad, CA, USA) using 100 ng of total RNA. The following primer sequences were used: (i) total (rat plus human) α-synuclein: 5'tggttttgtcaaaaaggaccag forward and 5'ccttcctcagaaggcatttc reverse; (ii) hypoxantine phosphoribosyltransferase 1 (housekeeping gene): 5'gaccggttctgtcatgtcg forward and 5'acctggttcatcatcactaatcac reverse, (iii) rat-only α-synuclein: 5'gagttctg cggaagcctagagagc forward and 5'gttttctcagcagcagccaca actcc reverse; and (iv) WPRE: 5'caattccgtggtgttgtcgg forward and 5'caaagggagatccgactcgt reverse. Analyses were performed in triplicates, using 1 μl of cDNA and Power SYBR Green Master Mix (Applied Biosystems Warrington, UK). For conventional RT-PCR the product was run on 1.5% agarose gel and visualized by EtBr staining. For qRT-PCR, measurements were performed using a StepOne plus real time PCR instrument with built-in software (Applied Biosystems). Relative quantities (fold changes) were calculated after normalization to housekeeping gene expression and calibration to a reference sample from vehicle-injected animals.

Statistical analyses

Analyses were performed using JMP Pro Statistical software (version 10.0.0; SAS Institute, Cary, NC, USA). Means between two groups were compared with two-tailed *t*-test. Comparisons between multiple groups were carried out with one-way ANOVA followed by Tukey *post hoc* test. Statistical significance was set at $P < 0.05$.

Results

Viral vector-mediated α-syn transduction

Two separate preparations of hα-syn-carrying AAV, hα-syn-AAV prep 1 and hα-syn-AAV prep 2, were used for these experiments. Vector construct was identical for both preparations that only differed in regard to protocols employed for their purification (Additional file 1: Figure S1). Using an experimental paradigm previously described [12], AAV vectors were injected into the left vagus nerve in the rat neck. Animals were killed at 6 weeks post AAV treatment, and brain tissue was initially collected for RT-PCR measurements. To ascertain targeted transduction, amplification reactions evaluated the presence of WPRE, an enhancer element incorporated into the genome of the AAV vectors, in tissue specimens from the MO and pons. RT-PCR using WPRE-hybridizing primers confirmed hα-syn-AAV prep 1- and prep 2-mediated transfection in samples from the dorso-medial quadrant of the left (ipsilateral to vagal injections) MO containing the DMnX; in contrast, no WPRE mRNA was detected in pontine tissue (Figure 1a). Levels of transgene expression were then assessed by qRT-PCR measurements of total (rat plus human) α-syn mRNA in DMnX-containing specimens of the left MO. At the vector dilutions used for these studies, vagal injections with hα-syn-AAV prep 1 or prep 2 yielded samples with similar levels of α-syn overexpression. In these samples, total α-syn mRNA was increased by 3.7 (prep 1) and 3.6 (prep 2) folds (Figure 1b).

The extent of AAV-mediated transduction was also estimated histologically by calculating the percentages of hα-syn-containing neurons over the total number of neurons in the DMnX. Brains were collected postmortem at 6 weeks after vagal injections. The DMnX was delineated on tissue slices throughout the entire MO (Additional file 2: Figure S2), and stereological cell counting was performed after immunostaining with a specific hα-syn antibody and counterstaining with cresyl violet (Figure 2a and b). The percentage of transduced neurons was calculated by the formula: [number of cells that were both Nissl-stained and immunoreactive for hα-syn] / [total number of Nissl-positive neurons] x 100. Confirming previous results [12], no neurons immunoreactive for hα-syn were found in the right DMnX contralateral to the vagal injection side. In contrast, hα-syn-overexpressing cells were present in the left MO of AAV-treated rats and accounted for approximately 30% of the total DMnX neurons after injections with either hα-syn-AAV prep 1 or prep 2 (Figure 2c).

To further evaluate hα-syn transduction at the protein level, tissue sections of the left MO were stained for immunofluorescence with an anti-hα-syn antibody, and optical densitometry was used to measure the intensity of immunoreactivity within DMnX neurons. This semiquantitative analysis revealed no significant differences between samples from rats killed at 6 weeks after treatment with either hα-syn-AAV prep 1 or prep 2 (Figure 2d-f).

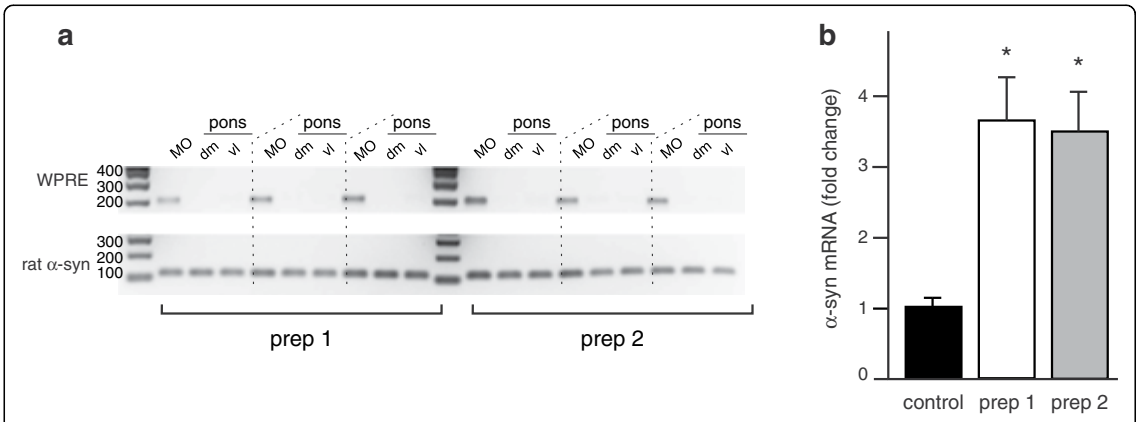

Figure 1 Assessment of transduction efficiency at the mRNA level. Analyses were performed at 6 weeks post treatment. **(a)** Rats received a single injection of hα-syn-AAV prep 1 (n = 3) or prep 2 (n = 3) into the vagus nerve. RT-PCR was performed to detect WPRE or, as a control, rat α-syn mRNA in DMnX-containing samples from the left (injected side) MO as well as in samples from the left dorso-medial (dm) and ventro-lateral (vl) pons. Specific bands were detected at 204 (WPRE) and 117 (rat a-syn) bp. **(b)** Animals received a single injection of vehicle (controls, n = 4), hα-syn-AAV prep 1 (n = 7) or hα-syn-AAV prep 2 (n = 7). Total (rat + human) α-syn mRNA levels were assayed by qRT-PCR in DMnX-containing samples from the left (injected side) MO. Values are means ± SEM. *P <0.05 *vs.* the control group (one-way ANOVA followed by Tukey's post hoc test, $F_{2,17} = 5.26$).

Early pathological changes caused by AAV transduction

Pathological changes were first evaluated in rats killed at 6 weeks post vagal injections. To determine whether AAV-mediated hα-syn transduction was associated with neurodegeneration, the number of Nissl-stained neurons was estimated by stereological cell counting in the DMnX of control untreated animals as well as in the right (contralateral to vagal injections) and left (ipsilateral) DMnX of AAV-injected rats. No cell death was observed as a consequence of transduction with either hα-syn-AAV prep 1 or prep 2. Indeed, the counts of DMnX neurons were not significantly different in control tissue as compared to samples from the right and left MO of AAV-treated animals (Figure 3a).

A second set of analyses assessed the possibility that, even in the absence of frank neurodegeneration, morphological (cell shrinkage) and/or biological (cleavage of PARP) signs of neuronal injury may be triggered by AAV transfection. Upon microscopic observation, the size of hα-syn-immunoreactive neurons appeared to be reduced in the DMnX of rats treated with hα-syn-AAV prep 1 as compared to hα-syn-AAV prep 2 (Figure 3b,c). Measurements using the stereological nucleator tool confirmed these observations; single cell volume was measured for several hundreds of unbiasedly selected neurons and averaged to obtain a mean cell volume. The mean volume of normal cholinergic DMnX neurons was estimated in tissue from control rats stained with an antibody against ChAT. No difference in cell volume was measured between these control neurons and neurons positive for hα-syn after transduction with hα-syn-AAV prep 2. Treatment with hα-syn-AAV prep 1 resulted instead in a >25% decrease in mean volume of hα-syn-overexpressing neurons (Figure 3d). Immunostaining with an antibody against the 85 kDa (p85) fragment of cleaved PARP (cPARP) was performed to assess caspase-dependent PARP cleavage as a marker of apoptotic processes. Rare neurons immunoreactive for both hα-syn and cPARP were seen in the left DMnX of rats injected with hα-syn-AAV prep 1, whereas no cPARP-positive cells could be detected in DMnX tissue from hα-syn-AAV prep 2-treated animals (Figure 3e).

Evidence of neuronal injury triggered by treatment with hα-syn-AAV prep 1 but not prep 2 prompted us to assess the possibility that differences in toxicity between the two preparations may be associated with changes in formation and accumulation of aggregated α-syn forms. Coronal sections of the left MO from prep 1- or prep 2-injected rats were immunostained with an antibody that has been shown to possess much higher reactivity toward aggregated as compared to monomeric α-syn [25]. While labeling was detected within DMnX neurons in all injected animals (Figure 3f and g), a comparison of fluorescence intensity by densitometric analysis did not reveal significant differences between the two treatment groups (Figure 3h).

Later neurodegenerative changes induced by AAV transduction

To determine whether early cell injury at 6 weeks post transduction was ultimately followed by neurodegeneration, neuronal survival was evaluated in rats killed at 12 weeks after vagal injection. At this later time point, stereological cell count of DMnX neurons in the left

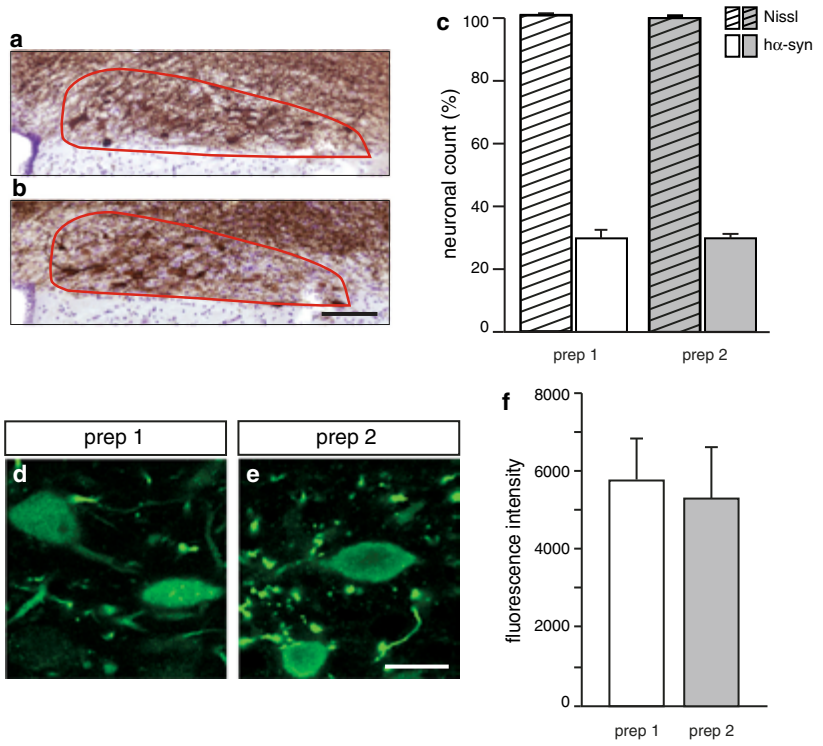

Figure 2 Comparison of intraneuronal hα-syn expression after transduction with hα-syn-AAV prep 1 *vs.* prep 2. Analyses were performed at 6 weeks post treatment. **(a, b)** Representative sections of the MO (Bregma: −13.68 mm) were obtained from rats treated with **(a)** hα-syn-AAV prep 1 or **(b)** prep 2. Tissues were immunostained with anti-hα-syn and counterstained with cresyl violet. The DMnX is delineated in red. Scale bar in **(b)** = 100 μm. **(c)** Nissl-stained neurons (striped bars) and hα-syn-immunoreactive cells (solid bars) were counted in the left (injected side) DMnX of animals treated with hα-syn-AAV prep 1 (n = 7) or prep 2 (n = 7). Values (means ± SEM) are expressed as percent of the total number of Nissl-stained neurons. **(d, e)** Representative images of DMnX neurons immunostained with an anti-hα-syn antibody from rats treated with **(d)** hα-syn-AAV prep 1 or **(e)** prep 2. Scale bar in **(e)** = 20 μm. **(f)** Fluorescence intensity of hα-syn-immunoreactive DMnX neurons was measured by optical densitometry in rats treated with hα-syn-AAV prep 1 (n = 4) or prep 2 (n = 4). Values (pixels) are means ± SEM.

MO revealed a reduction of total Nissl-stained cells of approximately 15% in animals injected with hα-syn-AAV prep 1; in contrast, no cell loss was triggered as a consequence of transduction with hα-syn-AAV prep 2 (Figure 4a). The number of DMnX neurons that were both Nissl-stained and immunoreactive for hα-syn was also significantly decreased at 12 weeks after AAV prep 1 treatment. This reduction was evident relative to (i) the number of hα-syn-transduced cells in rats injected with hα-syn-AAV prep 1 and killed at the 6-week time point, as well as (ii) the count of hα-syn-immunoreactive neurons in animals treated with hα-syn-AAV prep 2 and analyzed at either 6 or 12 weeks post transduction (Figure 4b).

The toxic properties of AAV prep 1 *vs.* prep 2 were further evaluated in a separate set of experiments in which rats received vagal injections of GFP- rather than hα-syn-carrying viral vectors. The number of Nissl-stained neurons was counted in the left DMnX at 12 weeks after treatment with either GFP-AAV prep 1 or GFP-AAV prep 2. Results showed a 10% reduction of cells in animals injected with GFP-AAV prep 1; no cell loss was instead observed after transduction with GFP-AAV prep 2 (Additional file 3: Figure S3). The decrease in neuronal count caused by treatment with GFP-AAV prep 1 was slightly less pronounced than the cell loss induced by hα-syn-AAV prep 1; this difference did not reach statistical significance, however.

Propagation of hα-syn from the MO to pons

Enhanced expression of hα-syn in the rat MO has been shown to trigger its interneuronal propagation toward more rostral brain regions [12]. Protein spreading was first assessed in coronal sections of the pons where axonal projections immunoreactive for hα-syn were counted at 6 and 12 weeks post-treatment. At both time points, the number of axons containing the exogenous protein was significantly higher in animals transduced with hα-syn-AAV prep 2 as compared to hα-syn-AAV

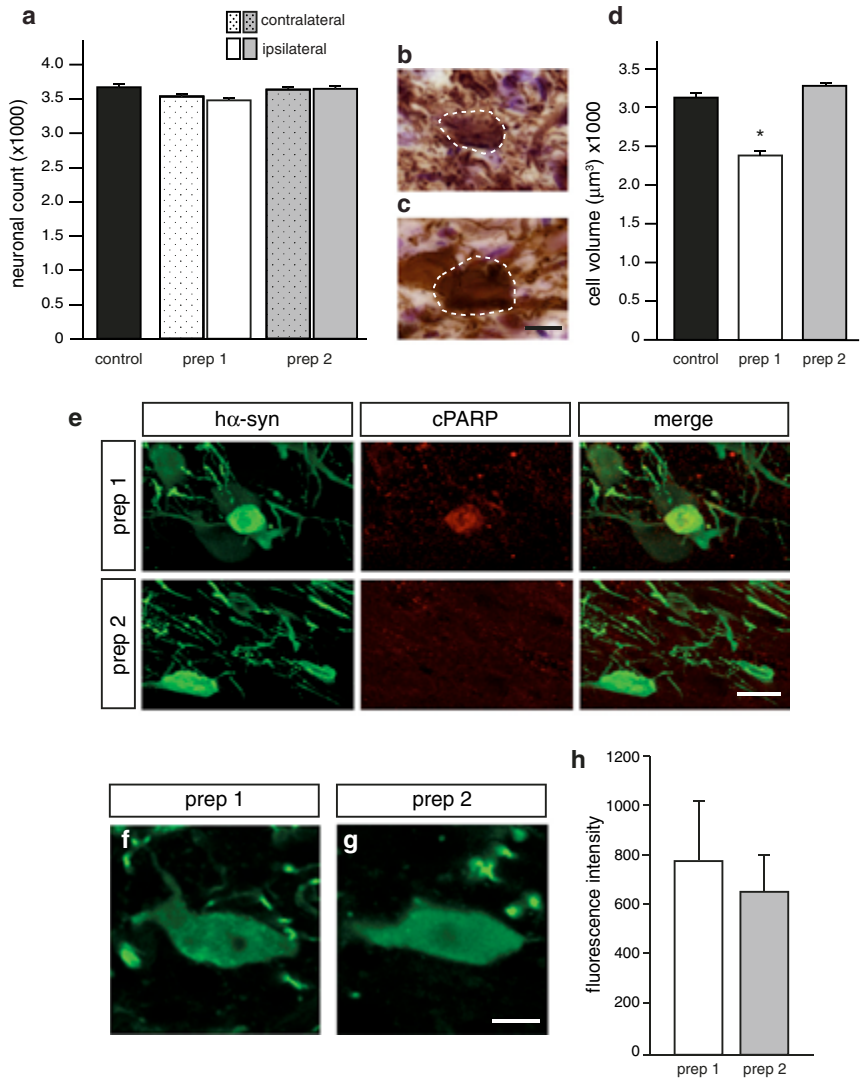

Figure 3 Early (6 weeks post treatment) toxic effects of hα-syn-carrying AAV vectors. (a-d) Rats received a single injection of vehicle (control animals, n = 3), hα-syn-AAV prep 1 (n = 7) or hα-syn-AAV prep 2 (n = 7) into the vagus nerve. **(a)** Stereological counts of Nissl-stained DMnX neurons were performed on tissue from the left (ipsilateral to AAV injections, solid bars) and right (contralateral to AAV injections, dotted bars) MO. Values are means ± SEM. **(b,c)** Representative sections of the MO (Bregma: −13.68 mm) were obtained from rats treated with **(b)** hα-syn-AAV prep 1 or **(c)** prep 2. Tissues were immunostained with an anti-hα-syn antibody. Images generated by z-stacking of two representative DMnX neurons are compared, showing an apparent decrease in cell size after transduction with hα-syn-AAV prep 1 **(b)**. Scale bar in **(c)** = 10 µm. **(d)** MO tissue sections were stained with either an antibody against ChAT (control tissue) or an anti-hα-syn antibody (rats injected with hα-syn-AAV prep 1 or prep 2). The volume (μm^3) of ChAT-positive or hα-syn-immunoreactive neurons was estimated using a six-ray isotropic nucleator probe [20]. Measurements were made on 695 cells from control animals, 671 cells from prep 1-treated rats and 878 cells from prep 2-injected animals. For each group, single cell values were averaged. Values are means ± SEM. *P <0.0001 *vs.* the control or prep 2 groups (one-way ANOVA followed by Tukey's post hoc test, $F_{2,2244} = 51.15$). **(e)** MO tissue sections from rats injected with hα-syn-AAV prep 1 or prep 2 were double-stained with antibodies against hα-syn and cleaved PARP (cPARP). Rare neurons (one of these neurons is shown in the upper panels) immunoreactive for both cPARP and hα-syn could be detected in hα-syn-AAV prep 1-treated animals. Scale bar = 20 µm. **(f-h)** DMnX-containing sections of the MO were immunostained with an antibody that preferentially reacts with aggregated forms of α-syn [25]. **(f,g)** Representative images of DMnX neurons from rats treated with **(f)** hα-syn-AAV prep 1 or **(g)** prep 2. Scale bar in **(g)** = 10 µm. **(h)** Fluorescence intensity of immunostained DMnX neurons was measured by optical densitometry in animals treated with hα-syn-AAV prep 1 (n = 4) or prep 2 (n = 4). Values (pixels) are means ± SEM.

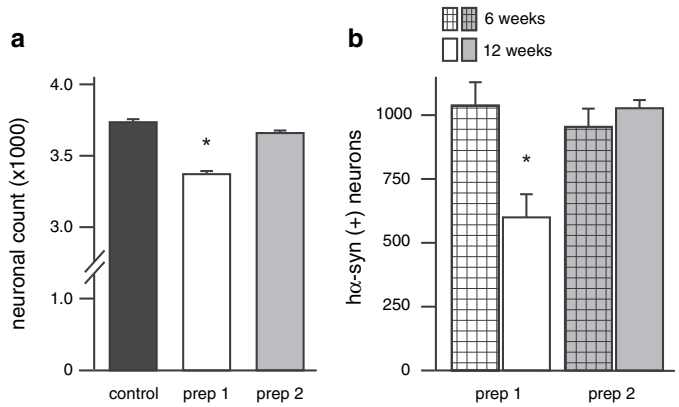

Figure 4 Neurodegenerative changes caused by hα-syn-AAV prep 1 transduction. (a) Rats received a single injection of vehicle (control animals, n = 3), hα-syn-AAV prep 1 (n = 5) or hα-syn-AAV prep 2 (n = 5) into the vagus nerve. Stereological counts of Nissl-stained DMnX neurons were performed at 12 weeks post treatment on tissue sections from the left (injected side) MO. Values are means ± SEM. *P <0.0001 *vs.* the control or prep 2 group (one-way ANOVA followed by Tukey's post hoc test, $F_{2,12} = 73.4$). **(b)** The number of neurons immunoreactive for hα-syn was counted stereologically in the left (AAV-injected side) DMnX of rats injected with either hα-syn-AAV prep 1 or prep 2. Analyses were performed at 6 (bars with pattern, n = 7/group) or 12 weeks (solid bars, n = 5/group) post treatment. Values are means ± SEM. *P <0.005 *vs.* each of the other three groups (one-way ANOVA followed by Tukey's post hoc test, $F_{3,23} = 10.82$).

prep 1 (Figure 5a). At 12 weeks, analyses of tissue sections by microscopic examination revealed that, in rats transduced with hα-syn-AAV prep 1, spreading from the MO affected only sparse axons in specific pontine regions, such as the coeruleus–subcoeruleus complex (Figure 5b). In these same regions of animals treated with hα-syn-AAV prep 2, propagation of the exogenous protein was indicated by the presence of numerous immunoreactive axons (Figure 5c). Pathological fibers loaded with hα-syn appeared as tortuous threads with intensely labeled varicosities; the presence of these swellings often produced an image of punctuated immunoreactivity on single-plane microscopy.

To confirm unbiased neuritic quantifications, the mean total length and density of fibers immunoreactive for hα-syn were estimated using the Space Balls stereological tool [23]. Measurements were carried out in pontine sections at 12 weeks post AAV injections. Random and systematic sampling was performed on an anatomically defined area encompassing the locus coeruleus and the parabrachialis nucleus (Figure 5d); this area was chosen because it represents a preferential spreading site within the pons. Results of these measurements confirmed a significant difference in protein propagation between the two treatment groups. The mean total length of hα-syn-containing axons was 72,973 ± 7,243 mm and 251,597 ± 50,341 mm after transduction with hα-syn-AAV prep 1 and prep 2, respectively. Fiber density was also more than three times greater in pontine sections from prep 2-injected rats (Figure 5e).

Caudo-rostral spreading of hα-syn beyond the pons

A final set of analyses involved counting the number of hα-syn-immunoreactive axons in coronal sections frontal to the pons. At 6 weeks, spreading of hα-syn triggered by AAV prep 1 reached the midbrain as its most rostral outpost. Progression of the spreading at 12 weeks was indicated by the occurrence of sparse fibers containing hα-syn in selected forebrain regions (e.g., hypothalamus and amygdala, Bregma: −2.40 mm) (Figure 6a). Treatment of rats with AAV prep 2 yielded counts of hα-syn-immunoreactive axons that were consistently higher than values seen with AAV prep 1 (Figure 6a). Labeled fibers were already present in forebrain sections at 6 weeks and became relatively abundant in the hypothalamus and amygdala at 12 weeks (Figure 6b-d). At this later time point following injections with AAV prep 2, a few axons were also detected in forebrain areas rostral to the anterior commissure (Bregma: +0.48 mm), such as the bed nucleus of the stria terminalis (Figure 6e and f).

Discussion

Results of an earlier study demonstrated that propagation of hα-syn from the MO to more rostral regions of the rat brain could be triggered by AAV-mediated hα-syn transduction and was dependent on the levels of mRNA and protein overexpression. Very little spreading was observed when AAV transduction produced less than a one-fold increase in α-syn mRNA and a weak hα-syn immunostaining of MO neurons; this modest effect contrasted with the pronounced caudo-rostral propagation seen when mRNA levels were approximately three-fold

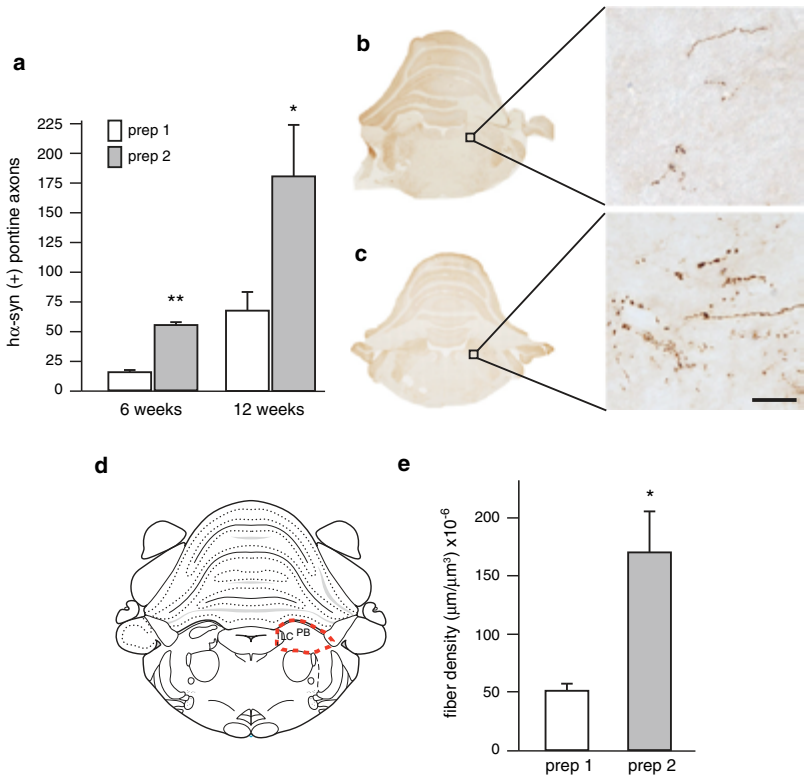

Figure 5 Spreading of hα-syn to the pons after AAV-mediated transduction of MO neurons. (a) Rats received a single injection of hα-syn-AAV prep 1 (open bars) or hα-syn-AAV prep 2 (filled bars) into the vagus nerve. The number of axonal projections immunostained with an anti-hα-syn antibody was counted in the left (injected side) pons at 6 (n = 7/group) and 12 (n = 5/group) weeks post injection. Values are means ± SEM. ***P* <0.0001 *vs.* the prep 1 group at 6 weeks (*t* test, $F_{1,13} = 120.99$). **P* <0.05 *vs.* the prep 1 group at 12 weeks (*t* test, $F_{1,9} = 6.01$). **(b, c)** Representative pontine sections (Bregma: −9.48 mm) were obtained from rats injected with **(b)** hα-syn-AAV prep 1 or **(c)** prep 2 and sacrificed at 12 weeks post treatment. Higher magnification images from the coeruleus-subcoeruleus complex were obtained by z-stacking. They show axonal projections immunostained with an anti-hα-syn antibody. Scale bar = 30 µm. **(d, e)** Rats received a single injection of hα-syn-AAV prep 1 (n = 5) or prep 2 (n = 5) and were killed at 12 weeks post treatment. **(d)** An area encompassing the locus coeruleus (LC) and the parabrachialis nucleus (PB) was delineated on serial sections throughout the pons (a schematic representation of one of these sections at Bregma −9.6 mm is shown), and **(e)** the density of fibers immunoreactive for hα-syn was estimated using the Space Balls stereological tool [23]. Values are means ± SEM. **P* <0.05 *vs.* the prep 1 group (*T* test: $F_{1,9} = 10.96$).

higher than control values and labeling of histological MO sections revealed robust hα-syn immunoreactivity [12]. The purpose of this present investigation was to determine if other factors, besides intraneuronal expression levels, affected hα-syn spreading in this model. In particular, we aimed at assessing the relationship between neuronal injury and inter-neuronal α-syn propagation.

The two hα-syn-AAV preparations used in this study were injected into the rat vagus nerve at concentrations capable of inducing comparable levels of hα-syn overexpression in the MO. Despite this similarity, hα-syn-AAV prep 1 and prep 2 differed significantly with regard to their toxic effects, with neuronal damage being evident only after treatment with hα-syn-AAV prep 1. Contamination with impurities (e.g., empty capsids) and/or reagents used for their preparation (e.g., CsCl) is known to underlie the toxic potential of viral vectors [26-28]. Production of AAV prep 1 and prep 2 involved different purification procedures, which can result in various degrees of contamination. It is quite likely therefore that greater injury caused by hα-syn-AAV prep 1 arose from a relatively less thorough purification and a higher concentration of toxic byproducts.

Stereological cell counting of DMnX neurons revealed a reduction of total Nissl-stained cells at 12 weeks after treatment with hα-syn-AAV prep 1 as well as GFP-AAV prep 1. These data are consistent with non-specific toxic effects due to AAV prep 1 contamination. It is noteworthy that in rats injected with hα-syn-AAV prep 1 (i) the count of DMnX neurons immunoreactive for hα-syn was also decreased at the 12-week time point, and (ii) this decrease in hα-syn-positive cells (−437 ± 59 cells as compared to values at 6 weeks) fully accounted for the

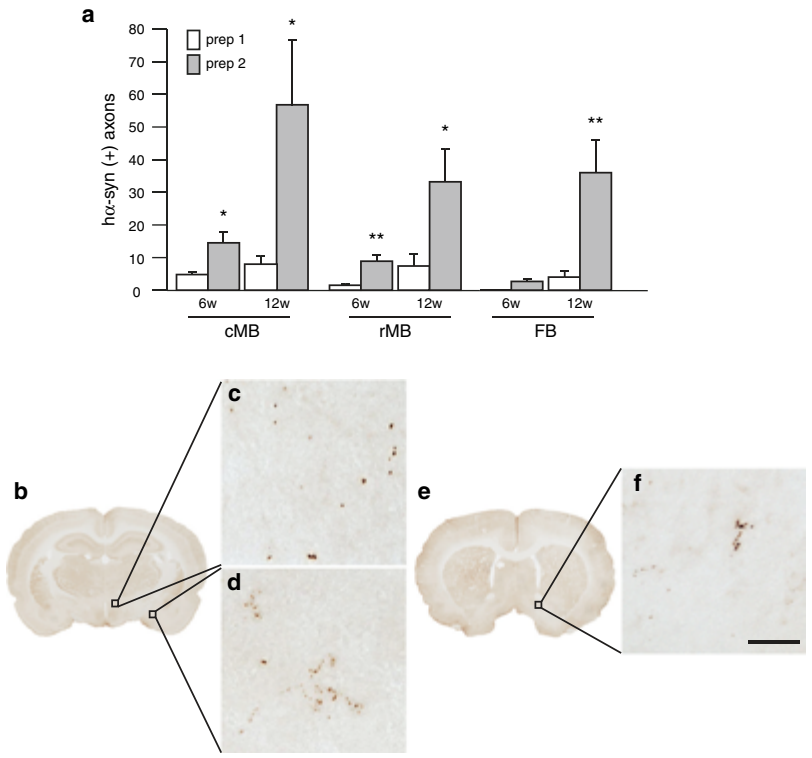

Figure 6 Caudo-rostral spreading of hα-syn reaches midbrain and forebrain regions. (a) Rats received a single injection of hα-syn-AAV prep 1 (open bars) or prep 2 (filled bars) into the vagus nerve. The number of axonal projections immunoreactive for hα-syn was counted in the left (injected side) caudal midbrain (cMB), rostral midbrain (rMB) and forebrain (FB) at 6 (n = 7/group) and 12 (n = 5/group) weeks post treatment. Values are means ± SEM. $^{**}P < 0.01$ and $^{*}P < 0.05$. *T* test: $F_{1,13} = 7.88$ and $F_{1,9} = 5.88$ in the cMB at 6 and 12 weeks, respectively; $F_{1,13} = 10.10$ and $F_{1,9} = 5.86$ in the rMB at 6 and 12 weeks, respectively; $F_{1,9} = 9.94$ in the FB at 12 weeks. **(b,e)** Representative sections of the forebrain at **(b)** Bregma: −2.40 mm and **(e)** Bregma: +0.48 mm were obtained from rats injected with AAV prep 2 and sacrificed at 12 weeks post treatment. **(c, d, f)** Higher magnification images from the **(c)** hypothalamus, **(d)** amygdala and **(f)** bed nucleus of the stria terminalis were generated by z-stacking. They show axonal projections immunostained with an anti-hα-syn antibody. Scale bar (for **c**, **d** and **f**) in **(f)** = 30 μm.

reduction in total Nissl-stained neurons (−438 ± 23 cells). Thus, despite the involvement of non-specific factors in AAV prep 1 toxicity, neuronal damage caused by hα-syn-AAV prep 1 still targeted DMnX neurons containing hα-syn. It is quite likely that protein overexpression made these cells particularly vulnerable to injury; if so, neurodegeneration might have arisen from the combined effects of hα-syn burden and AAV prep 1 toxicity.

Taken together, findings on neuronal transduction and cell damage in animals injected with hα-syn-AAV prep 1 *vs.* prep 2 revealed: (i) induction of comparable hα-syn overexpression, (ii) neuronal injury caused by one but not the other AAV preparation, and (iii) selectivity of this injury that targeted hα-syn-containing neurons. These features justified the following two assumptions concerning protein transmission after AAV prep 1- or prep 2-induced hα-syn overexpression. First, any potential difference in propagation would be unlikely to reflect changes in hα-syn levels at the site of initial protein transfer, i.e. MO neurons. Second, a comparison of spreading triggered by hα-syn-AAV prep 1 *vs.* prep 2 would be expected to yield different results should hα-syn transmission be significantly affected by damage/death of neurons.

Spreading was assessed by counting the number of axonal projections immunoreactive for hα-syn in brain regions rostral to the MO. Axons forming the rat vagus nerve originate from or terminate in the MO [29]; intravagal injections of hα-syn-carrying AAV vectors cause neuronal transduction and protein overexpression that are also confined to the MO [12]. Therefore, presence of hα-syn within axons that project from the pons, midbrain or forebrain to the MO [30-34] is indicative of caudo-rostral propagation *via* interneuronal protein transfer. Several lines of evidence from the present as well as earlier investigations support these assertions. Specific transduction is indicated by the pattern of AAV-induced overexpression that reproduces the anatomical

brain distribution of efferent and afferent fibers forming the vagus nerve [12,29]. For example, because efferent vagal fibers originate from the DMnX and nucleus ambiguus [29], these two MO nuclei represent the only sites where, following AAV transduction, neuronal cell bodies immunoreactive for hα-syn are observed [12]. When markers of AAV transduction, such as hα-syn and WPRE mRNAs, were measured in the MO and pons, they could only be detected in specimens of the MO ipsilateral to vagal injections [12]. It would be highly unlikely for the serotype of AVV used in our experiments, i.e. AAV6, to be transferred intact across cells *via* mechanisms such as transcytosis [35]. Lack of cell bodies immunoreactive for hα-syn and lack of transcriptional AAV markers in brain regions rostral to the MO not only indicate specific transduction but also rule out the possibility that translocation of viral vectors rather than neuron-to-neuron transfer of hα-syn may underlie caudo-rostral spreading of the exogenous protein. Strong evidence supporting lack of transmission of viral particles also came from experiments in which rats received vagal injections of GFP- rather than hα-syn-AAV; in contrast to results in animals transduced with hα-syn, protein spreading was not observed in GFP-AAV-treated rats [12].

Overexpression of hα-syn caused by injections with either hα-syn-AAV prep 1 or prep 2 triggered caudo-rostral propagation as indicated by the finding that hα-syn-positive axons became progressively evident in the pons, midbrain and forebrain. Spreading after treatment with hα-syn-AAV prep 1 or prep 2 was consistently observed within areas such as the coeruleus–subcoeruleus complex (pons), dorsal raphae (midbrain) and amygdala (forebrain). Of note, the substantia nigra pars compacta (SNc) was not one of these predilection targets for hα-syn propagation. A likely explanation for these findings relates to anatomical brain connections since hα-syn-immunoreactive axons were primarily seen in regions with direct projections into the MO [30-34,36]. At the two time points considered in this study (6 and 12 weeks post treatment), spreading and accumulation of hα-syn beyond the MO affected neuritic projections while apparently sparing neuronal cell bodies; pathological changes were also evident in the form of enlarged dystrophic axons. Interestingly, a preferential axonal burden, as seen in this model of protein spreading, appears to be a feature common to a variety of experimental paradigms involving α-syn toxicity [9,37,38]. Greater vulnerability to neuritic accumulation/pathology could result, at least in part, from impaired degradation of axonal α-syn together with α-syn-induced disruption of axonal transport motor proteins [38,39]. Lack of cell body pathology and lack of hα-syn spreading to the SNc may be perceived as limitations of this experimental paradigm to reproduce PD features. On the other hand, findings are also consistent with the interpretation that this model of α-syn propagation triggered by protein overexpression in the MO mimics pathogenetic events that occur early in the disease process; early lesions may target axonal projections, involve a single trans-synaptic passage of α-syn and temporarily spare SNc neurons.

Conclusions

Our present finding that spreading of hα-syn occurred after transduction with either hα-syn-AAV prep 1 or prep 2, i.e. in the presence or absence of neuronal injury/death, bears significant implications. Similarly, it is noteworthy that (i) the count of hα-syn-positive axons was much lower in the pons, midbrain and forebrain of rats injected with hα-syn-AAV prep 1 as compared to prep 2, and (ii) propagation of the exogenous protein toward regions rostral to the MO was less advanced when, as a consequence of hα-syn-AAV prep 1 administration, protein overexpression was associated with enhanced toxicity. Taken together, these results support the conclusion that release from damaged cells is not essential for, neither it enhances interneuronal hα-syn propagation. Data in our model are also consistent with an inverse correlation between neuronal injury and hα-syn spreading. Mechanisms underlying this effect are unclear. It is conceivable that an enhanced stress response within dying cells (e.g., changes in protein degradation) may negatively modulate hα-syn transmission. An alternative and possibly complementary explanation is that neuron-to-neuron α-syn passage involves active mechanisms between relatively healthy cells and is therefore most efficient when neuronal integrity is maintained. Important corollaries to this latter interpretation include the facts that (i) neuronal activity in the form, for example, of synaptic transmission may modulate α-syn propagation [6,40], (ii) specific mechanisms, such as exocytosis, could play a role in protein release and subsequent α-syn transmission [14-16], and (iii) future work aimed at elucidating these mechanisms has the potential to identify new targets for therapeutic intervention against protein spreading in human synucleinopathies.

Additional files

Additional file 1: Figure S1. Steps involved in the production of the two AAV preps used in this study. The reporter plasmid contained DNA coding for human Synapsin1 (promoter), hα-syn, WPRE (enhancer) and polyA (enhancer). This plasmid was used for transfection of 293 HEK cells. Crude cell lysates were then purified by either (i) two consecutive CsCl gradient centrifugations (AAV prep 1), or (ii) centrifugation through a discontinuous iodixanol gradient followed by heparin affinity chromatography (AAV prep 2).

Additional file 2: Figure S2. Delineation of the rat DMnX for stereological cell counting. Every sixth section throughout the entire DMnX was used for

stereological counting, yielding 8–9 sections/rat. Representative images of four of these sections at Bregma **(a)** -14.04, **(b)** -13.76, **(c)** -13.68 and **(d)** -13.36 were stained with cresyl violet. The DMnX is delineated in red. Scale bar = 100 μm.

Additional file 3: Figure S3. Rats received a single injection of vehicle (control animals, n=3), GFP-AAV prep 1 (n=7) or GFP-AAV prep 2 (n=4) into the vagus nerve. Stereological counts of Nissl-stained DMnX neurons were performed at 12 weeks post treatment on tissue sections from the left (injected side) MO. Values (means ± SEM) represent: [number of neurons in the DMnX ipsilateral to the injection side] / [number of neurons in the DMnX contralateral to the injection side] x 100. * P <0.0001 *vs.* the control or prep 2 group (one-way ANOVA followed by Tukey's post hoc test, $F_{2,13} = 22.62$).

Abbreviations

α-syn: Alpha-synuclein; AAV: Recombinant adeno-associated virus; ChAT: Choline acetyltransferase; CTCF: Corrected total cell fluorescence; DMnX: Dorsal motor nucleus of the vagus nerve; GFP: Enhanced green fluorescent protein; hα-syn: Human wild-type alpha-synuclein; MO: Medulla oblongata; PARP: Poly ADP ribose polymerase; PD: Parkinson's disease; PolyA: Polyadenylation signal sequence; RT-PCR: Reverse transcription polymerase chain reaction; SNc: Substantia nigra pars compacta; TBS: Tris-buffered saline; TBS-T: TBS containing Triton-X-100; WRPE: Woodchuck hepatitis virus post-transcriptional regulatory element.

Competing interests

The authors declare that they have no competing interests.

Authors' contributions

AU designed experiments, performed surgeries and carried out histological analyses and axonal counts; REM and MH set up and performed other quantitative histological analyses (e.g., stereological cell counting and measurements of cell volume); RR and MK set up and performed molecular biology analyses; AS assisted with AAV preparations; DADM designed experiments, analyzed data and wrote the paper with input from the other authors. All authors read and approved the final manuscript.

Acknowledgements

The authors wish to thank Dr. Sarah A. Jewell for her valuable comments on the data and manuscript, Ms. Franziska Hesse and Dr. Bettina Winzen-Reichert for assistance with histological preparations and Dr. Hans Fried and Mr. Kevin Keppler for assistance with image analysis. This work was supported by the Paul Foundation, the Backus Foundation and the Centres of Excellence in Neurodegeneration Research (CoEN).

Author details

[1]German Center for Neurodegenerative Diseases (DZNE), Ludwig-Erhard-Allee 2, 53175 Bonn, Germany. [2]German Center for Neurodegenerative Diseases (DZNE), Göttingen, Germany. [3]Department of Psychiatry and Psychotherapy, University Medicine Göttingen, Göttingen, Germany.

Received: 26 January 2015 Accepted: 24 February 2015
Published online: 24 March 2015

References

1. Braak H, Del Tredici K, Rub U, de Vos RA, Jansen Steur EN, Braak E (2003) Staging of brain pathology related to sporadic Parkinson's disease. Neurobiol Aging 24:197–211, doi: S0197458002000659
2. Braak H, Rub U, Gai WP, Del Tredici K (2003) Idiopathic Parkinson's disease: possible routes by which vulnerable neuronal types may be subject to neuroinvasion by an unknown pathogen. J Neural Transm 110:517–536, doi: 10.1007/s00702-002-0808-2
3. Desplats P, Lee HJ, Bae EJ, Patrick C, Rockenstein E, Crews L, Spencer B, Masliah E, Lee SJ (2009) Inclusion formation and neuronal cell death through neuron-to-neuron transmission of α-synuclein. Proc Natl Acad Sci U S A 106:13010–13015, doi:0903691106 10.1073/pnas.0903691106
4. Hansen C, Angot E, Bergstrom AL, Steiner JA, Pieri L, Paul G, Outeiro TF, Melki R, Kallunki P, Fog K, Li JY, Brundin P (2011) α-Synuclein propagates from mouse brain to grafted dopaminergic neurons and seeds aggregation in cultured human cells. J Clin Invest 121:715–725, doi: 10.1172/JCI43366
5. Luk KC, Kehm VM, Zhang B, O'Brien P, Trojanowski JQ, Lee VM (2012) Intracerebral inoculation of pathological α-synuclein initiates a rapidly progressive neurodegenerative α-synucleinopathy in mice. J Exp Med 209:975–986, doi: 10.1084/jem.20112457
6. Freundt EC, Maynard N, Clancy EK, Roy S, Bousset L, Sourigues Y, Covert M, Melki R, Kirkegaard K, Brahic M (2012) Neuron-to-neuron transmission of α-synuclein fibrils through axonal transport. Ann Neurol 72:517–524, doi: 10.1002/ana.23747
7. Masuda-Suzukake M, Nonaka T, Hosokawa M, Oikawa T, Arai T, Akiyama H, Mann DM, Hasegawa M (2013) Prion-like spreading of pathological α-synuclein in brain. Brain 136:1128–1138, doi:awt037 10.1093/brain/awt037
8. Rey NL, Petit GH, Bousset L, Melki R, Brundin P (2013) Transfer of human α-synuclein from the olfactory bulb to interconnected brain regions in mice. Acta Neuropathol 126:555–573, doi: 10.1007/s00401-013-1160-3
9. Recasens A, Dehay B, Bove J, Carballo-Carbajal I, Dovero S, Perez-Villalba A, Fernagut PO, Blesa J, Parent A, Perier C, Farinas I, Obeso JA, Bezard E, Vila M (2014) Lewy body extracts from Parkinson disease brains trigger α-synuclein pathology and neurodegeneration in mice and monkeys. Ann Neurol 75:351–362, doi: 10.1002/ana.24066
10. Sacino AN, Brooks M, McKinney AB, Thomas MA, Shaw G, Golde TE, Giasson BI (2014) Brain Injection of α-Synuclein Induces Multiple Proteinopathies, Gliosis, and a Neuronal Injury Marker. J Neurosci 34:12368–12378, doi: 10.1523/JNEUROSCI. 2102-14.2014
11. Luk KC, Kehm V, Carroll J, Zhang B, O'Brien P, Trojanowski JQ, Lee VM (2012) Pathological α-synuclein transmission initiates Parkinson-like neurodegeneration in nontransgenic mice. Science 338:949–953, doi: 10.1126/science.1227157
12. Ulusoy A, Rusconi R, Perez-Revuelta BI, Musgrove RE, Helwig M, Winzen-Reichert B, Di Monte DA (2013) Caudo-rostral brain spreading of α-synuclein through vagal connections. EMBO Mol Med 5:1051–1059. doi:10.1002/emmm.201302475
13. Volpicelli-Daley LA, Luk KC, Patel TP, Tanik SA, Riddle DM, Stieber A, Meaney DF, Trojanowski JQ, Lee VM (2011) Exogenous α-synuclein fibrils induce Lewy body pathology leading to synaptic dysfunction and neuron death. Neuron 72(1):57–71, doi: 10.1016/j.neuron.2011.08.033
14. Danzer KM, Kranich LR, Ruf WP, Cagsal-Getkin O, Winslow AR, Zhu L, Vanderburg CR, McLean PJ (2012) Exosomal cell-to-cell transmission of α synuclein oligomers. Mol Neurodegener 7:42, doi: 10.1186/1750-1326-7-42
15. Schneider A, Simons M (2013) Exosomes: vesicular carriers for intercellular communication in neurodegenerative disorders. Cell Tissue Res 352:33–47, doi: 10.1007/s00441-012-1428-2
16. Bae EJ, Yang NY, Song M, Lee CS, Lee JS, Jung BC, Lee HJ, Kim S, Masliah E, Sardi SP, Lee SJ (2014) Glucocerebrosidase depletion enhances cell-to-cell transmission of α-synuclein. Nat Commun 5:4755, doi: 10.1038/ncomms5755
17. Loeb JE, Cordier WS, Harris ME, Weitzman MD, Hope TJ (1999) Enhanced expression of transgenes from adeno-associated virus vectors with the woodchuck hepatitis virus posttranscriptional regulatory element: implications for gene therapy. Hum Gene Ther 10:2295–2305, doi: 10.1089/10430349950016942
18. West MJ (1999) Stereological methods for estimating the total number of neurons and synapses: issues of precision and bias. Trends Neurosci 22:51–61
19. Gundersen HJ, Jensen EB (1987) The efficiency of systematic sampling in stereology and its prediction. J Microsc 147:229–263
20. Gundersen HJ, Bagger P, Bendtsen TF, Evans SM, Korbo L, Marcussen N, Moller A, Nielsen K, Nyengaard JR, Pakkenberg B, Sorensen FB, Vesterby A, West MJ (1988) The new stereological tools: disector, fractionator, nucleator and point sampled intercepts and their use in pathological research and diagnosis. APMIS 96:857–881
21. Schindelin J, Arganda-Carreras I, Frise E, Kaynig V, Longair M, Pietzsch T, Preibisch S, Rueden C, Saalfeld S, Schmid B, Tinevez JY, White DJ, Hartenstein V, Eliceiri K, Tomancak P, Cardona A (2012) Fiji: an open-source platform for biological-image analysis. Nat Methods 9:676–682, doi: 10.1038/nmeth.2019
22. Paxinos G, Watson C (2009) The rat brain in stereotaxic coordinates, 2nd edn. Academic Press, London
23. Mouton PR, Gokhale AM, Ward NL, West MJ (2002) Stereological length estimation using spherical probes. J Microsc 206:54–64
24. Gundersen HJ, Jensen EB, Kieu K, Nielsen J (1999) The efficiency of systematic sampling in stereology–reconsidered. J Microsc 193:199–211
25. Kovacs GG, Wagner U, Dumont B, Pikkarainen M, Osman AA, Streichenberger N, Leisser I, Verchere J, Baron T, Alafuzoff I, Budka H, Perret-Liaudet A, Lachmann I (2012) An antibody with high reactivity for disease-associated α-synuclein reveals extensive brain pathology. Acta Neuropathol 124:37–50, doi: 10.1007/s00401-012-0964-x

26. Summerford C, Samulski RJ (1999) Viral receptors and vector purification: new approaches for generating clinical-grade reagents. Nat Med 5:587–588, doi: 10.1038/8470
27. Ulusoy A, Bjorklund T, Hermening S, Kirik D (2008) In vivo gene delivery for development of mammalian models for Parkinson's disease. Exp Neurol 209:89–100, doi: 10.1016/j.expneurol.2007.09.011
28. Lock M, Alvira M, Vandenberghe LH, Samanta A, Toelen J, Debyser Z, Wilson JM (2010) Rapid, simple, and versatile manufacturing of recombinant adeno-associated viral vectors at scale. Hum Gene Ther 21:1259–1271, doi: 10.1089/hum.2010.055
29. Kalia M, Sullivan JM (1982) Brainstem projections of sensory and motor components of the vagus nerve in the rat. J Comp Neurol 211:248–265, doi: 10.1002/cne.902110304
30. Schwaber JS, Kapp BS, Higgins GA, Rapp PR (1982) Amygdaloid and basal forebrain direct connections with the nucleus of the solitary tract and the dorsal motor nucleus. J Neurosci 2:1424–1438
31. ter Horst GJ, Luiten PG, Kuipers F (1984) Descending pathways from hypothalamus to dorsal motor vagus and ambiguus nuclei in the rat. J Auton Nerv Syst 11:59–75
32. van der Kooy D, Koda LY, McGinty JF, Gerfen CR, Bloom FE (1984) The organization of projections from the cortex, amygdala, and hypothalamus to the nucleus of the solitary tract in rat. J Comp Neurol 224:1–24, doi: 10.1002/cne.902240102
33. Chiba T, Murata Y (1985) Afferent and efferent connections of the medial preoptic area in the rat: a WGA-HRP study. Brain Res Bull 14:261–272
34. Blessing WW, Li YW, Wesselingh SL (1991) Transneuronal transport of herpes simplex virus from the cervical vagus to brain neurons with axonal inputs to central vagal sensory nuclei in the rat. Neuroscience 42:261–274
35. Di Pasquale G, Chiorini JA (2006) AAV transcytosis through barrier epithelia and endothelium. Mol Ther 13:506–516, doi: 10.1016/j.ymthe.2005.11.007
36. Albanese A, Altavista MC, Rossi P (1986) Organization of central nervous system dopaminergic pathways. J Neural Transm Suppl 22:3–17
37. Decressac M, Mattsson B, Lundblad M, Weikop P, Bjorklund A (2012) Progressive neurodegenerative and behavioural changes induced by AAV-mediated overexpression of α-synuclein in midbrain dopamine neurons. Neurobiol Dis 45:939–953, doi: 10.1016/j.nbd.2011.12.013
38. Chu Y, Morfini GA, Langhamer LB, He Y, Brady ST, Kordower JH (2012) Alterations in axonal transport motor proteins in sporadic and experimental Parkinson's disease. Brain 135:2058–2073, doi: 10.1093/brain/aws133
39. Prots I, Veber V, Brey S, Campioni S, Buder K, Riek R, Bohm KJ, Winner B (2013) α-Synuclein oligomers impair neuronal microtubule-kinesin interplay. J Biol Chem 288:21742–21754, doi: 10.1074/jbc.M113.451815
40. Guo JL, Lee VM (2014) Cell-to-cell transmission of pathogenic proteins in neurodegenerative diseases. Nat Med 20:130–138, doi: 10.1038/nm.3457

Figure S1

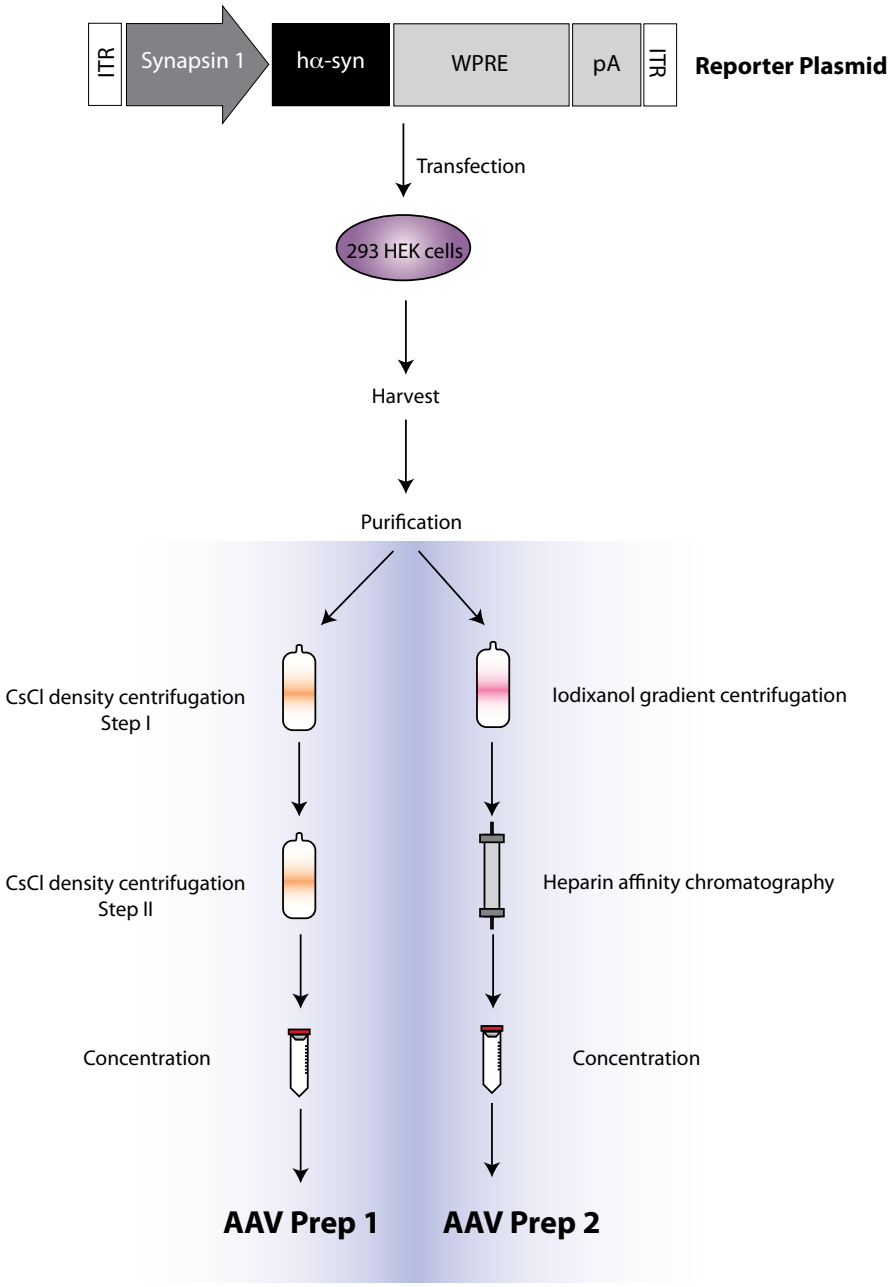

Figure S1. Steps involved in the production of the two AAV preps used in this study. The reporter plasmid contained DNA coding for human Synapsin1 (promoter), hα-syn, WPRE (enhancer) and polyA (enhancer). This plasmid was used for transfection of 293 HEK cells. Crude cell lysates were then purified by either (i) two consecutive CsCl gradient centrifugations (AAV prep 1), or (ii) centrifugation through a discontinuous iodixanol gradient followed by heparin affinity chromatography (AAV prep 2).

Figure S2

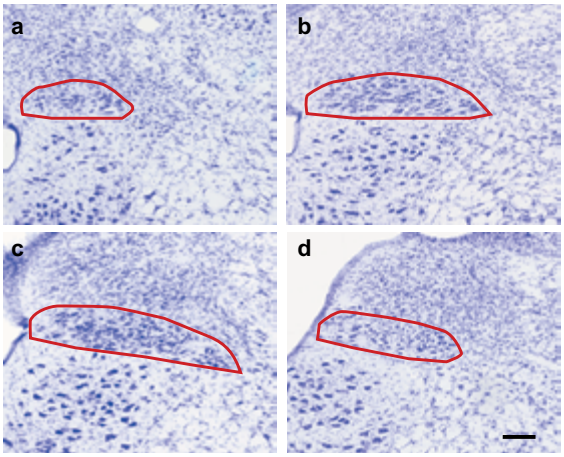

Figure S2. Delineation of the rat DMnX for stereological cell counting. Every sixth section throughout the entire DMnX was used for stereological counting, yielding 8-9 sections/rat. Representative images of four of these sections at Bregma (**a**) -14.04, (b) -13.76, (**c**) -13.68 and (**d**) -13.36 were stained with cresyl violet. The DMnX is delineated in red. Scale bar = 100 μm.

Figure S3

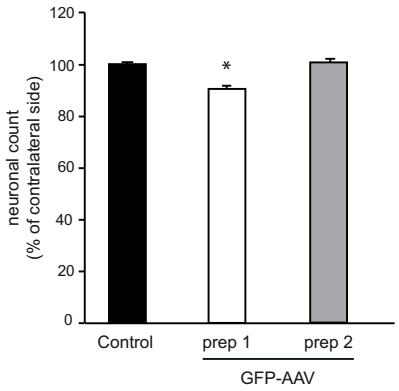

Figure S3. Rats received a single injection of vehicle (control animals, n=3), GFP-AAV prep 1 (n=7) or GFP-AAV prep 2 (n=4) into the vagus nerve. Stereological counts of Nissl-stained DMnX neurons were performed at 12 weeks post treatment on tissue sections from the left (injected side) MO. Values (means ± SEM) represent: [number of neurons in the DMnX ipsilateral to the injection side] / [number of neurons in the DMnX contralateral to the injection side] x 100. * $P < 0.0001$ vs. the control or prep 2 group (one-way ANOVA followed by Tukey's post hoc test, $F_{2,13} = 22.62$).

Helwig, M., Klinkenberg, M., Rusconi, R., Musgrove, R.E., Majbour, N.K., El-Agnaf, O.M., **Ulusoy, A.**, and Di Monte, D.A. (2016). Brain propagation of transduced α-synuclein involves non-fibrillar protein species and is enhanced in α-synuclein null mice. Brain 139, 856-870.

Objective: Here, we asked if interneuronal spreading of α-syn required fibrillar forms or if this transfer could be carried out via other lower molecular weight species (i.e., monomeric and oligomeric). One of the best tools for addressing this question is the use of knockout mice that lacks endogenous α-syn expression.

Methods and results: Execution of these experiments faced two technical challenges. The first challenge concerns the species of the experimental model. Although several lines of knockout rats have been developed, the cost and time for developing an α-syn knockout rat were not optimal. In contrast several commercial α-syn mice are available via various resources. We, therefore, adopted the vagus AAV injection model to mice, and used two different α-syn knockout mouse lines for these experiments. This study's second challenge was the difficulties in detecting different species of α-syn on the tissue in a spatial manner. Detection of fibrillar forms of the protein technically can be achieved through several

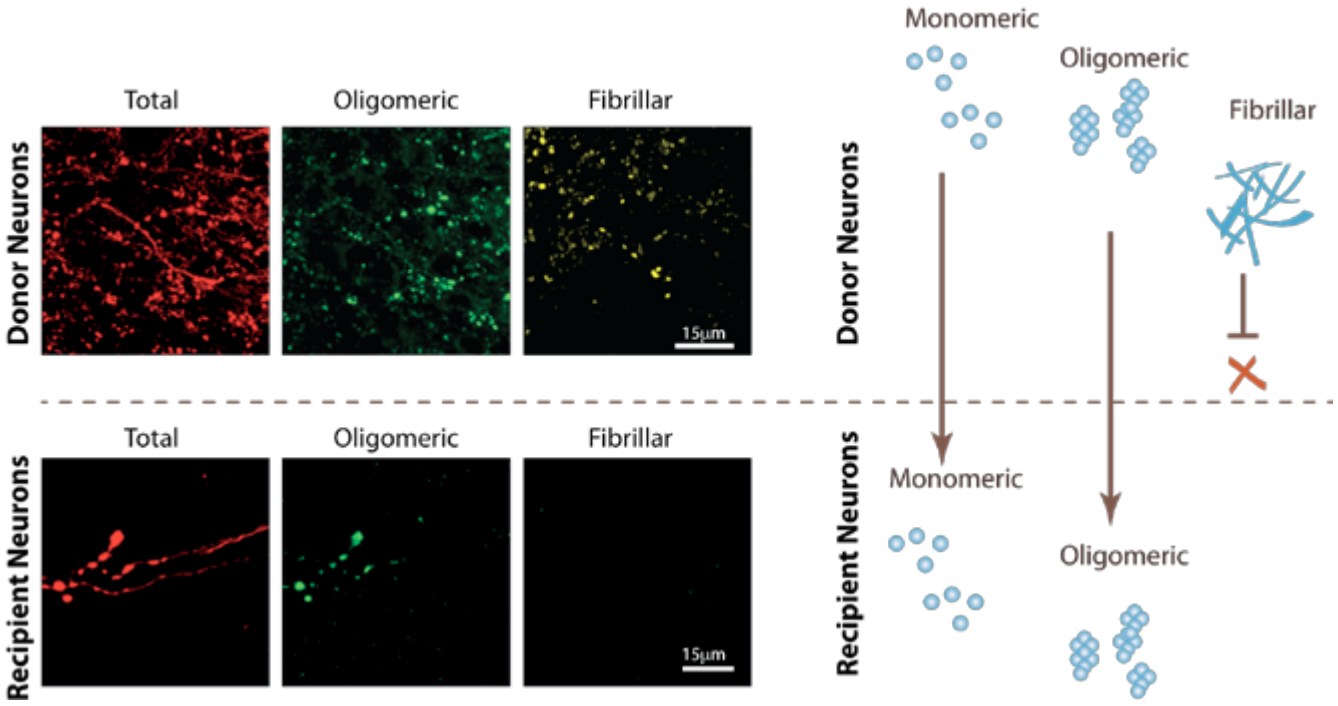

Figure 3. Illustration of different α-synuclein species involved in neuron-to-neuron transfer. Donor neurons in the dorsal medulla oblongata and recipeint neurons in the pons were stained using three different α-syn antibodies: an antibody detecting the total human α-syn (red), an antibody that did not recognize monomeric species (green) and an antibody that recognize only fibrillar species (yellow). Data suggest that although all three species of α-syn is present in the DMX, fibrillar α-syn cannot be trasnferred to the recipient neurons.

biochemical techniques that require large amounts of tissue. To give an example, the weight of a mouse brain hemisphere is around 200 mg (Manglani et al., 2019). In comparison, dissection of the DMX yields less than 5 mg of tissue. Furthermore, the amount of exogenous α-syn in the pons, midbrain, or basal forebrain is limited to a handful of axons, making it almost impossible to isolate/detect/analyze the structure of the exogenous protein in this model with conventional detection methods, in particular in the recipient neurons. To overcome this issue, in this manuscript, we established two methods for detecting oligomeric and fibrillar forms of α-syn in situ: proximity ligation assay and conformation-specific antibody staining for oligomeric and fibrillar forms of α-syn.

Targeted expression of human α-syn in the vagal system was induced by injecting AAV vectors into the vagus nerve of wild-type α-syn knockout mice. In line with the observations from the rat model, α-syn overexpression in the vagal complex induced spreading of α-syn from the donor vagal neurons to the recipient neurons in more rostral brain areas and affected nuclei such as the LC, dorsal raphae and amygdala in the pons, midbrain, and forebrain. Interneuronal transfer of exogenous α-syn was assessed using two separate lines of α-syn knockout mice. Results demonstrated that the lack of endogenous α-syn did not interfere with the interneuronal transfer but resulted in a more pronounced and advanced propagation.

Aggregation of human α-syn was detected using a proximity ligation assay, Thioflavin-S staining, and with different confirmation-specific antibodies recognizing oligomeric, fibrillar, and/or total (monomeric and aggregated) α-syn. Following viral vector transduction, all kind of α-syn species (i.e., monomeric, oligomeric, and fibrillar) were detected within donor neurons in the medulla oblongata. In contrast, recipient axons in the pons were devoid of immunoreactivity for fibrillar α-syn, indicating that non-fibrillar forms of α-syn were primarily transferred from one neuron to the other and diffused within the brain (**Figure 3**).

Conclusions: This study elucidates that long-distance spreading and accumulation of monomeric and oligomeric α-syn do not necessarily involve pathological seeding. However, these smaller molecular weight species of mobile α-syn may mediate early pathological processes during disease development and contribute to neuronal burden during the pathogenesis of neurodegenerative diseases.

Brain Advance Access published December 30, 2015

doi:10.1093/brain/awv376 BRAIN 2015: Page 1 of 15 | 1

BRAIN
A JOURNAL OF NEUROLOGY

Brain propagation of transduced α-synuclein involves non-fibrillar protein species and is enhanced in α-synuclein null mice

Michael Helwig,[1] Michael Klinkenberg,[1] Raffaella Rusconi,[1] Ruth E. Musgrove,[1] Nour K. Majbour,[2] Omar M. A. El-Agnaf,[3] Ayse Ulusoy[1] and Donato A. Di Monte[1]

Aggregation and neuron-to-neuron transmission are attributes of α-synuclein relevant to its pathogenetic role in human synucleinopathies such as Parkinson's disease. Intraparenchymal injections of fibrillar α-synuclein trigger widespread propagation of amyloidogenic protein species via mechanisms that require expression of endogenous α-synuclein and, possibly, its structural corruption by misfolded conformers acting as pathological seeds. Here we describe another paradigm of long-distance brain diffusion of α-synuclein that involves inter-neuronal transfer of monomeric and/or oligomeric species and is independent of recruitment of the endogenous protein. Targeted expression of human α-synuclein was induced in the mouse medulla oblongata through an injection of viral vectors into the vagus nerve. Enhanced levels of intra-neuronal α-synuclein were sufficient to initiate its caudo-rostral diffusion that likely involved at least one synaptic transfer and progressively reached specific brain regions such as the locus coeruleus, dorsal raphae and amygdala in the pons, midbrain and forebrain. Transfer of human α-synuclein was compared in two separate lines of α-synuclein-deficient mice versus their respective wild-type controls and, interestingly, lack of endogenous α-synuclein expression did not counteract diffusion but actually resulted in a more pronounced and advanced propagation of exogenous α-synuclein. Self-interaction of adjacent molecules of human α-synuclein was detected in both wild-type and mutant mice. In the former, interaction of human α-synuclein with mouse α-synuclein was also observed and might have contributed to differences in protein transmission. In wild-type and α-synuclein-deficient mice, accumulation of human α-synuclein within recipient axons in the pons, midbrain and forebrain caused morphological evidence of neuritic pathology. Tissue sections from the medulla oblongata and pons were stained with different antibodies recognizing oligomeric, fibrillar and/or total (monomeric and aggregated) α-synuclein. Following viral vector transduction, monomeric, oligomeric and fibrillar protein was detected within donor neurons in the medulla oblongata. In contrast, recipient axons in the pons were devoid of immunoreactivity for fibrillar α-synuclein, indicating that non-fibrillar forms of α-synuclein were primarily transferred from one neuron to the other, diffused within the brain and led to initial neuronal injury. This study elucidates a paradigm of α-synuclein propagation that may play a particularly important role under pathophysiological conditions associated with enhanced α-synuclein expression. Rapid long-distance diffusion and accumulation of monomeric and oligomeric α-synuclein does not necessarily involve pathological seeding but could still result in a significant neuronal burden during the pathogenesis of neurodegenerative diseases.

1 German Centre for Neurodegenerative Diseases (DZNE), Ludwig-Erhard-Allee 2, 53175 Bonn, Germany
2 Department of Biochemistry, College of Medicine and Health Sciences, United Arab Emirates University, Tawam Medical Campus, Khalifa Ibn Zayed street, Al-Ain, United Arab Emirates
3 College of Science and Engineering, Hamad Bin Khalifa University, Qatar Foundation, Education City, P.O. Box 5825 Doha, Qatar

Correspondence to: Donato A. Di Monte,
German Centre for Neurodegenerative Diseases (DZNE),
Ludwig-Erhard-Allee 2, 53175 Bonn,

Received June 26, 2015. Revised October 15, 2015. Accepted October 29, 2015.

Germany
E-mail: donato.dimonte@dzne.de

Keywords: adeno-associated virus; fibrils; oligomers; Parkinson's disease; vagus nerve

Abbreviations: α-syn = α-synuclein; AAV = adeno-associated viral vector; DMnX = dorsal motor nucleus of the vagus nerve; GFP = green fluorescent protein; PLA = proximity ligation assay; WPRE = woodchuck hepatitis virus post-transcriptional regulatory element

Introduction

The protein α-synuclein (α-syn, encoded by *SNCA*) is implicated in the pathogenesis of several neurodegenerative diseases that include Parkinson's disease and are collectively referred to as synucleinopathies (Halliday *et al.*, 2011). While the precise mechanisms underlying α-syn pathology in these diseases have yet to be fully defined, the tendency of α-syn to assemble into oligomeric and fibrillar aggregates and its ability to pass from donor to recipient neurons are likely to play important pathogenetic roles (Desplats *et al.*, 2009; Uversky and Eliezer, 2009; Guo and Lee, 2014). Protein aggregation may ultimately lead to the formation of intracellular α-syn-containing inclusions, such as Lewy bodies and Lewy neurites, which are characteristic of human synucleinopathies (Spillantini *et al.*, 1997; Tu *et al.*, 1998). Neuron-to-neuron protein transmission could contribute to the spreading of α-syn pathology and explain, at least in part, the caudo-rostral pattern of α-syn accumulation first described in Parkinson's disease brain by Braak and colleagues (Braak *et al.*, 2003*a*, *b*); α-syn lesions are initially seen in the lower brainstem and subsequently diffuse toward mesocortical and neocortical areas via anatomically interconnected pathways.

Animal models have been developed in an attempt to mimic Parkinson's disease-like α-syn spreading, to assess its relationship with protein aggregation and unravel mechanisms of progressive pathology. At least two experimental strategies have succeeded in triggering long-distance α-syn propagation in rodents. The first approach involves direct injections of α-syn-containing preparations into the mouse brain (e.g. into the striatum or substantia nigra). More precisely, inoculations consisted of: (i) tissue homogenates containing insoluble α-syn from the brains of synucleinopathy patients; (ii) pathological brain lysates from α-syn transgenic mice; or (iii) solutions of α-syn fibrils generated from recombinant protein (Luk *et al.*, 2012*a*, *b*; Mougenot *et al.*, 2012; Masuda-Suzukake *el al.*, 2013; Sacino *et al.*, 2013; Recasens *et al.*, 2014; Peelaerts *et al.*, 2015). A second paradigm to induce progressive α-syn build-up is based on injections of adeno-associated viral vectors (AAVs) carrying human α-syn DNA into the rat vagus (X) nerve. This treatment resulted in targeted transduction in the medulla oblongata and overexpression of human α-syn within medulla oblongata neurons connected to the rat vagus nerve. Interestingly, enhanced levels of intra-neuronal human α-syn were sufficient to trigger its trans-synaptic passage and caudo-rostral diffusion that, in a time-dependent fashion, reached pontine, midbrain and finally forebrain regions (Ulusoy *et al.*, 2013, 2015).

Similarities and differences between models of protein transmission bear important pathogenetic implications as they could elucidate toxic properties of α-syn relevant to human synucleinopathies. Two intriguing features characterize α-syn diffusion in mice receiving intraparenchymal α-syn injections. Following brain inoculations, the ensuing pathology was characterized by accumulation and propagation of insoluble forms of the protein (Luk *et al.*, 2012*a*, *b*; Masuda-Suzukake *el al.*, 2013; Sacino *et al.*, 2013; Recasens *et al.*, 2014; Peelaerts *et al.*, 2015). Secondly, α-syn spreading in this model appeared to be contingent upon expression of endogenous α-syn and interactions between endogenous α-syn and deleterious forms of the protein present in the inoculates. A prion-like mechanism of aggregation and propagation has been suggested to underlie such interactions; indeed, similar to observations in prion models, no diffusion of pathology was observed if α-syn-containing preparations were injected into the brain of α-syn-deficient mice (Blättler *et al.*, 1997; Angot *et al.*, 2010; Luk *et al.*, 2012*a*; Mougenot *et al.*, 2012; Recasens *et al.*, 2014).

The role played by non-fibrillar versus fibrillar α-syn remains unclear in animals in which protein transmission is triggered by its increased intraneuronal expression. Similarly, it is unknown whether the presence of endogenous α-syn affects protein aggregation and propagation under this latter experimental paradigm. The current study was designed to address these important questions. Following up on earlier work in rats (Ulusoy *et al.*, 2013, 2015), a mouse model of AAV-mediated human α-syn transduction and caudo-rostral protein diffusion was developed and used to compare pathology in wild-type versus α-syn-deficient animals. Conformation-specific antibodies were used for immunohistochemical analyses correlating protein transmission with the accumulation of non-fibrillar and/or fibrillar α-syn species. Data revealed intriguing features of this model that apparently differ from observations in paradigms of prion-like α-syn spreading. In particular, we found that propagation of transduced α-syn throughout the mouse brain involved transfer and build-up of monomeric and oligomeric species, and was enhanced rather than counteracted by ablation of the endogenous protein.

Germany
E-mail: donato.dimonte@dzne.de

Keywords: adeno-associated virus; fibrils; oligomers; Parkinson's disease; vagus nerve

Abbreviations: α-syn = α-synuclein; AAV = adeno-associated viral vector; DMnX = dorsal motor nucleus of the vagus nerve; GFP = green fluorescent protein; PLA = proximity ligation assay; WPRE = woodchuck hepatitis virus post-transcriptional regulatory element

Introduction

The protein α-synuclein (α-syn, encoded by *SNCA*) is implicated in the pathogenesis of several neurodegenerative diseases that include Parkinson's disease and are collectively referred to as synucleinopathies (Halliday *et al.*, 2011). While the precise mechanisms underlying α-syn pathology in these diseases have yet to be fully defined, the tendency of α-syn to assemble into oligomeric and fibrillar aggregates and its ability to pass from donor to recipient neurons are likely to play important pathogenetic roles (Desplats *et al.*, 2009; Uversky and Eliezer, 2009; Guo and Lee, 2014). Protein aggregation may ultimately lead to the formation of intracellular α-syn-containing inclusions, such as Lewy bodies and Lewy neurites, which are characteristic of human synucleinopathies (Spillantini *et al.*, 1997; Tu *et al.*, 1998). Neuron-to-neuron protein transmission could contribute to the spreading of α-syn pathology and explain, at least in part, the caudo-rostral pattern of α-syn accumulation first described in Parkinson's disease brain by Braak and colleagues (Braak *et al.*, 2003*a*, *b*); α-syn lesions are initially seen in the lower brainstem and subsequently diffuse toward mesocortical and neocortical areas via anatomically interconnected pathways.

Animal models have been developed in an attempt to mimic Parkinson's disease-like α-syn spreading, to assess its relationship with protein aggregation and unravel mechanisms of progressive pathology. At least two experimental strategies have succeeded in triggering long-distance α-syn propagation in rodents. The first approach involves direct injections of α-syn-containing preparations into the mouse brain (e.g. into the striatum or substantia nigra). More precisely, inoculations consisted of: (i) tissue homogenates containing insoluble α-syn from the brains of synucleinopathy patients; (ii) pathological brain lysates from α-syn transgenic mice; or (iii) solutions of α-syn fibrils generated from recombinant protein (Luk *et al.*, 2012*a*, *b*; Mougenot *et al.*, 2012; Masuda-Suzukake *el al.*, 2013; Sacino *et al.*, 2013; Recasens *et al.*, 2014; Peelaerts *et al.*, 2015). A second paradigm to induce progressive α-syn build-up is based on injections of adeno-associated viral vectors (AAVs) carrying human α-syn DNA into the rat vagus (X) nerve. This treatment resulted in targeted transduction in the medulla oblongata and overexpression of human α-syn within medulla oblongata neurons connected to the rat vagus nerve. Interestingly, enhanced levels of intra-neuronal human α-syn were sufficient to trigger its trans-synaptic passage and caudo-rostral diffusion that, in a time-dependent fashion, reached pontine, midbrain and finally forebrain regions (Ulusoy *et al.*, 2013, 2015).

Similarities and differences between models of protein transmission bear important pathogenetic implications as they could elucidate toxic properties of α-syn relevant to human synucleinopathies. Two intriguing features characterize α-syn diffusion in mice receiving intraparenchymal α-syn injections. Following brain inoculations, the ensuing pathology was characterized by accumulation and propagation of insoluble forms of the protein (Luk *et al.*, 2012*a*, *b*; Masuda-Suzukake *el al.*, 2013; Sacino *et al.*, 2013; Recasens *et al.*, 2014; Peelaerts *et al.*, 2015). Secondly, α-syn spreading in this model appeared to be contingent upon expression of endogenous α-syn and interactions between endogenous α-syn and deleterious forms of the protein present in the inoculates. A prion-like mechanism of aggregation and propagation has been suggested to underlie such interactions; indeed, similar to observations in prion models, no diffusion of pathology was observed if α-syn-containing preparations were injected into the brain of α-syn-deficient mice (Blättler *et al.*, 1997; Angot *et al.*, 2010; Luk *et al.*, 2012*a*; Mougenot *et al.*, 2012; Recasens *et al.*, 2014).

The role played by non-fibrillar versus fibrillar α-syn remains unclear in animals in which protein transmission is triggered by its increased intraneuronal expression. Similarly, it is unknown whether the presence of endogenous α-syn affects protein aggregation and propagation under this latter experimental paradigm. The current study was designed to address these important questions. Following up on earlier work in rats (Ulusoy *et al.*, 2013, 2015), a mouse model of AAV-mediated human α-syn transduction and caudo-rostral protein diffusion was developed and used to compare pathology in wild-type versus α-syn-deficient animals. Conformation-specific antibodies were used for immunohistochemical analyses correlating protein transmission with the accumulation of non-fibrillar and/or fibrillar α-syn species. Data revealed intriguing features of this model that apparently differ from observations in paradigms of prion-like α-syn spreading. In particular, we found that propagation of transduced α-syn throughout the mouse brain involved transfer and build-up of monomeric and oligomeric species, and was enhanced rather than counteracted by ablation of the endogenous protein.

Materials and methods

Vectors

Transgene expression of human α-syn or enhanced green fluorescent protein (GFP) was induced using recombinant AAVs (AAV 2/6; Vector Biolabs). Gene expression was under the control of the human *SYN1* promoter and enhanced using a woodchuck hepatitis virus post-transcriptional regulatory element (WPRE) and a polyadenylation signal sequence (Loeb *et al.*, 1999; Ulusoy *et al.*, 2013). Stock preparations were diluted to generate injection titres of 0.75 and 1.5×10^{13} genome copies (gc)/ml for human α-syn-AAV, and 1.0×10^{13} gc/ml for GFP-AAV.

Animals, surgical procedure and tissue preparation

Experiments were carried out in 8-week-old female mice. Mice harbouring a spontaneous *Snca* deletion (C57BL/6JOlaHsd) and corresponding wild-type controls (C57BL/6JRj) were obtained from Harlan and Janvier Labs, respectively. Animals with a targeted *Snca* deletion at exons 1–2 (B6;129X1-*Snca*^{tm1Rosl}/J) and wild-type controls (B6;129F2) were from Jackson Laboratory. Mice were housed with *ad libitum* access to food and water under a 12-h light/12-h dark cycle. Experimental protocols were approved by the State Agency for Nature, Environment and Consumer Protection in North Rhine Westphalia.

Following anaesthesia, a 1-cm incision was made at the midline of the neck. The left vagus nerve was isolated from the carotid artery, and vector solution (750 nl) was injected at a flow rate of 160 nl/min using a 36-gauge blunt steel needle fitted onto a 10 µl NanoFil syringe. The syringe was connected to an UltraMicroPump with control unit (World Precision Instruments). After injection, the needle was kept in place for two to three additional minutes.

Animals were killed under pentobarbital anaesthesia. Unless differently specified, they were perfused through the ascending aorta first with saline containing heparin and then with ice-cold 4% (w/v) paraformaldehyde. Brains were removed, immersion-fixed in 4% paraformaldehyde and cryopreserved in 30% (w/v) sucrose solution. Coronal sections (35 µm) throughout the brain were cut using a freezing microtome and stored at −20°C in phosphate buffer (pH 7.4) containing 30% glycerol and 30% ethylene glycol.

Western blot analysis and enzyme-linked immunosorbent assay

A list of antibodies used for these measurements is provided in Supplementary Table 1. Fresh tissue was used for these analyses. Brains were removed, and coronal brain blocks encompassing the entire medulla oblongata or pons were cut and used for dissection of the dorsal left (AAV injected side) and right (contralateral side) quadrants. Tissue was first homogenized and then sonicated in phosphate-buffered saline (pH 7.4) containing protease inhibitors (Roche) and 1% Triton™ X-100 (Roth). Samples were centrifuged at 18 000*g* for 30 min, protein content was determined, and the supernatants (30 or 50 µg protein) were separated on a 12% acrylamide/bis-acrylamide gel. The gel was blotted on a polyvinylidene difluoride membrane (Millipore). Post-transfer membranes were treated with 0.4% paraformaldehyde as described by Lee *et al.* (2011) and blocked with 5% fat-free milk. Overnight incubations in mouse anti-human (h) α-syn (4B12, Genetex; 1:500), mouse anti-α-tubulin (DM1A, Sigma-Aldrich; 1:20 000) or rabbit anti-β-synuclein (ab6165, Abcam; 1:500) were followed by 1-h treatment with alkaline phosphate-conjugated anti-mouse or anti-rabbit IgG (Promega; 1:1000 or 1:10 000). Signal was detected by enhanced chemiluminescence (Applied Biosystems) and a ChemiDoc MP imaging system (Bio-Rad). Signal intensity was quantified by densitometry with Fiji software (Schindelin *et al.*, 2012).

For quantification of human α-syn and total (mouse plus human) α-syn by enzyme-linked immunosorbent assay (ELISA), 384-well microplates were coated and incubated overnight at 4°C with 0.1 µg/ml sheep anti-α-syn (Syn-140) in 200 mM $NaHCO_3$, pH 9.6 (50 µl/well). After washing and blocking, 50 µl of mouse brain lysate (30 µg/ml of protein concentration) were added to each well in duplicates. Tissue was dissected as described above, and homogenized in lysis buffer (CelLytic™ M; Sigma) containing protease/phosphatase inhibitors (Pierce) and EDTA. After centrifugation (3000*g* for 30 min), supernatants were collected and used for analyses. For detection of total α-syn, samples were incubated at 37°C for 2 h with rabbit anti-α-syn (FL-140, Santa Cruz Biotechnology; 1:5000); for measurements of human α-syn, incubations were carried out with mouse anti-hα-syn (11D12; 1:1000). Plates were washed and then incubated for 2 h at 37°C with horseradish peroxidase-conjugated donkey anti-mouse IgG or goat anti-rabbit IgG (Jackson ImmunoResearch). Following a final wash, 50 µl/well of an enhanced chemiluminescent substrate (Pierce Biotechnology) was added. Chemiluminescence was measured with VICTOR™ X3 plate reader (PerkinElmer). A standard curve was generated using serial dilutions of recombinant human α-syn.

Reverse transcription polymerase chain reaction

The four quadrants of paraformaldehyde-fixed coronal sections of medulla oblongata (Bregma: −7.08 to −7.64 mm) or rostral pons (Bregma: −5.68 to −5.02 mm) were dissected (Paxinos and Franklin, 2001). Total RNA was extracted using Nucleic Acid Isolation Kit (Ambion). cDNA was synthesized from 100 ng template RNA using SuperScript® VILO Master Mix (Life Technologies) (20 µl final volume). WPRE, mouse α-syn and hypoxanthine guanine phosphoribosyl transferase (*Hprt*) were assayed by conventional reverse trancription polymerase chain reaction (RT-PCR). The following primer combinations were used: (i) 5'caattccgtggtgttgtcgg forward and 5'caaagggagatccgactcgt reverse (WPRE); (ii) 5'agtggagggagctgggaatatag forward and 5'ccaggattccttcctgtgggtac reverse (mouse α-syn); and (iii) 5'tcctcctcagaccgctttt forward and 5'cctggttcatcatcgctaatc reverse (*Hprt*). RT-PCR products obtained from 30 cycles were separated on 1.5% agarose gels. For quantitative RT-PCR, triplicate measurements were made using a StepOnePlus™ real-time PCR system (Applied Biosystems). The reaction mix (20 µl) contained 1 µl cDNA, Power SYBR® Green (Applied Biosystems) and

human α-syn-specific primers: 5'aatgaagaaggagccccacag forward and 5'aaggcatttcataagcctcattgtc reverse. Relative quantities (fold changes) were obtained after calibration to a reference sample consisting of 0.9 ng RNA extracted from human brain (Agilent Technologies).

Brightfield microscopy and quantitative analyses

Free-floating brain sections were processed for brightfield microscopy as previously described (Ulusoy *et al.*, 2013). Primary antibodies were mouse anti-hα-syn (syn211, Merck Millipore; 1:50 000), chicken anti-GFP (ab13970, Abcam; 1:50 000) and mouse anti-hα-syn (5G4, Analytic Jena; 1:500) (Supplementary Table 1). Images were obtained using an Observer.Z1 microscope (Carl Zeiss) equipped with a motorized stage. When specified, stacks were collected at 2-µm intervals with a 63 × Plan-Apochromat objective, and a single image was generated by deep focus post-processing. Low magnification photographs of entire brain sections were obtained by computerized image stitching (ZEN 2012 Blue edition, Carl Zeiss).

Human α-syn- or GFP-immunoreactive axons were counted in sections at predefined Bregma coordinates using an Axioscope microscope (Carl Zeiss) under a 63 × Plan-Apochromat objective. Analyses were performed by investigators blinded to treatment/experimental group. Length and density of human α-syn-containing axons were estimated using the Space Balls stereological probe (Stereo Investigator version 9, MBF Biosciences). A previously described method was adapted (Ulusoy *et al.*, 2015). Measurements were made on three sections of the pons (Bregma: −5.68, −5.51 and −5.34 mm) where an area encompassing the locus coeruleus and the nucleus parabrachialis was delineated. A virtual hemisphere (10-µm radius) was placed randomly within this area, and systematic sampling was done at intervals of 60 µm in both *x*- and *y*-axes.

Fluorescence microscopy

To retrieve antigen-binding sites, free-floating medulla oblongata and pontine sections were treated with 2 µg/ml proteinase K (Sigma-Aldrich) for 10 min at room temperature. Six primary antibodies were used (Supplementary Table 1). Two of these antibodies recognize both monomeric and aggregated forms of the protein (AB5038P, Millipore; 1:400, and C-20, Santa Cruz Biotechnology; 1:1000). The other four antibodies, Syn-F1, Syn-F2, Syn-O1 and Syn-O2, are non-commercial and have been previously characterized (Vaikath *et al.*, 2015). They recognize only mature amyloid α-syn fibrils (Syn-F1 and Syn-F2; 1:1000 and 1:500), or both α-syn fibrils and α-syn oligomers (Syn-O1 and Syn-O2; 1:1000 and 1:2000). AB5038P and C-20 dilutions were adjusted to visualize highly expressed protein avoiding detection of basal α-syn. Sections were incubated overnight with pairs of these antibodies. Immunoreactivity was then visualized with secondary antibodies conjugated with DyLight® 488 and DyLight® 594 (Vector Laboratories). Double-stained sections were analysed using a LSM700 Zeiss confocal microscope equipped with 488 and 555 nm excitation lasers. Stack images (1-µm intervals) were collected by sequential scanning using a 63 × Plan-Apochromat objective.

A separate set of free-floating medulla oblongata and pontine sections were not subjected to antigen retrieval. They were sequentially incubated with syn211 (1:6000), biotinylated horse anti-mouse secondary and a streptavidine-conjugated fluorophore (Dylight® 594, Vector Laboratories; 1:200). Thioflavin S staining was performed on mounted syn211-immunolabeled sections. Sections were incubated for 8 min in 0.05% Thioflavin S dissolved in water, rinsed and then washed (3 min/wash) in 80, 95 and 95% ethanol. Slides were coverslipped with PVA-DABCO (Sigma), and tissue was analysed under a Zeiss LSM 710 NLO confocal microscope using 488 and 561 nm lasers with sequential acquisition.

Proximity ligation assay

The method originally described by Roberts *et al.* (2015) was used with modifications. To detect human–human α-syn interactions, syn211 antibody (Millipore) was conjugated with Plus or Minus oligonucleotide probes (Duolink® Probemaker kit, Olink). To detect mouse–human α-syn interactions, a murine-specific α-syn antibody (D37A6, Cell Signaling) was conjugated with Plus and syn211 antibody was conjugated with Minus probes (Supplementary Table 1). Antigen retrieval was achieved by incubation of free-floating sections with citrate buffer (pH 6.0) for 15 min at 95°C. After quenching, a proximity ligation assay (PLA) was performed using Duolink® Brightfield detection kit (Olink). Sections were blocked with Duolink blocking solution and then incubated overnight with PLA® Plus and Minus probes (1:100 dilution for human–human α-syn interactions; 1:40 and 1:200 for mouse–human α-syn interactions). Sections treated without the Minus probe served as negative controls. On the following day, ligation, amplification and detection were carried out according to manufacturer's specifications, and the signal was developed with novaRED™ substrates. Sections were mounted on coated slides and, in some instances, counterstained with haematoxylin prior to coverslipping with Duolink® *in situ* brightfield mounting medium.

Statistical analyses

Unpaired *t*-test was used for comparisons of means between two groups. Analyses were performed using JMP Pro Statistical software (version 10.0.0; SAS Institute). Statistical significance was set at $P < 0.05$.

Results

Targeted expression of transgenic human α-syn in the mouse medulla oblongata

Experiments were carried out in control mice as well as mice lacking α-syn due to a spontaneous deletion of the α-syn gene (Specht and Schoepfer, 2001). In these mutant mice, absence of α-syn was not compensated by any significant increase in β-syn protein, a close homologue of α-syn (data not shown). AAVs carrying human α-syn DNA (*SNCA*) were injected into the left vagus nerve in

the mouse neck to induce targeted human α-syn overexpression in the medulla oblongata. Successful transduction was already evident at 2 weeks post-AAV injection and could be demonstrated histologically as well as by western blot and PCR analyses. Immunostaining of medulla oblongata sections with a specific anti-hα-syn antibody (syn211) revealed localization of the exogenous protein that matched the anatomical distribution of efferent and afferent fibres forming the vagus (X) nerve. Efferent fibres are strictly ipsilateral and stem from cell bodies within the dorsal motor nucleus of the X nerve (DMnX) and nucleus ambiguus (Leslie *et al.*, 1982). Viral vectors injected into the vagus nerve reached these two nuclei that contained cell bodies and neuronal projections robustly labelled for human α-syn; staining of DMnX and nucleus ambiguus neurons was only seen on the left (ipsilateral to the injection side) side of the brain (Fig. 1). Afferent fibres of the vagus nerve originate from neuronal cell bodies in the inferior and superior vagal ganglia. They convey sensory information mostly to the ipsilateral nucleus of the tractus solitarius, but also innervate the contralateral medulla oblongata (Kalia and Sullivan, 1982; Leslie *et al.*, 1982; Odekunle and Bower, 1985). Consistent with this bilateral pattern of distribution, human α-syn-stained axons occupied the left nucleus of the tractus solitarius but also crossed the midline to reach the dorsal medulla oblongata on the right side of the brain (Fig. 1A). The dense arborization of labelled fibres contrasted with the absence of human α-syn-containing cell bodies in the nucleus of the tractus solitarius and other terminal fields of vagal afferents. Of note, pattern and intensity of human α-syn immunoreactivity were similar in medulla oblongata sections from either control or mutant mice (Fig. 1).

Western blot analyses carried out at 2 weeks post-AAV injection showed robust bands immunoreactive for human α-syn in specimens from the dorsal left (injected side) medulla oblongata; human α-syn protein was also detected, albeit in the form of weaker bands, in the dorsal right medulla oblongata contralateral to vagal injections (Fig. 2A). Semi-quantitative densitometric measurements revealed no significant differences in levels of the transduced protein between wild-type controls and mice lacking α-syn (Fig. 2B). In contrast to findings in the medulla oblongata, samples from the pons were devoid of human α-syn at this 2-week time point (Fig. 2A). Human α-syn protein was also assayed by ELISA in the dorsal left and right medulla oblongata. Data confirmed that expression of the transduced protein was similar in wild-type and mutant mice; in both groups of animals, values were ~4 times higher in the left as compared to the right medulla oblongata (Fig. 2C). ELISA measurements were then carried out to compare levels of total (mouse plus human) α-syn in the dorsal left medulla oblongata of untreated versus AAV-injected wild-type mice. Total α-syn was increased by ~50% as a consequence of AAV administration (Fig. 2D). This increase was found in whole tissue specimens that, in injected mice, contained both transduced and non-transduced neurons. It is noteworthy, therefore, that levels of α-syn overexpression in these treated animals are likely to be significantly greater within cells targeted by AAV transduction.

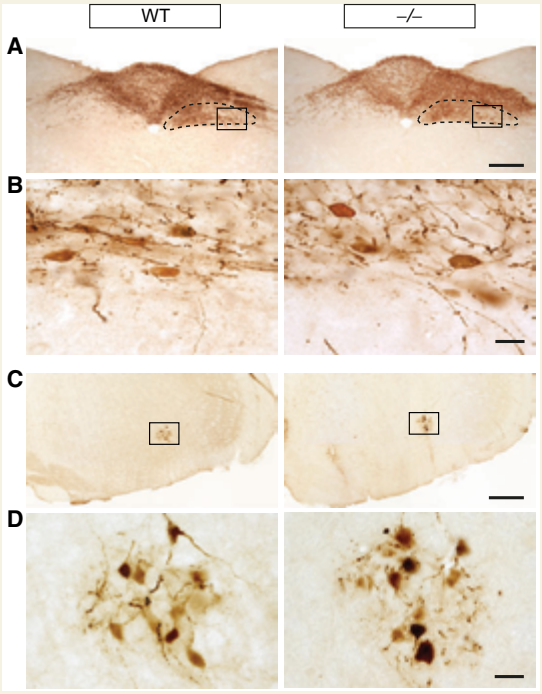

Figure 1 Targeted overexpression of human α-syn in the mouse medulla oblongata. Mice were killed at 2 weeks after a single injection of human α-syn-carrying AAVs (1.5×10^{13} gc/ml) into the left vagus nerve. (**A**) Representative sections of the dorsal medulla oblongata (Bregma: −7.48 mm) were obtained from wild-type (WT) and α-syn-deficient (−/−) mice. Tissue was immunostained with a specific anti-hα-syn antibody. The DMnX is delineated by dashed lines, and the square box indicates the area shown in (**B**) at higher magnification. Scale bars: **A** = 200 μm; **B** = 25 μm. (**C**) Representative sections of the left (injected side) ventral medulla oblongata (Bregma: −6.84 mm) immunostained for human α-syn. The square box encompasses the nucleus ambiguus that is shown in (**D**) at higher magnification. Scale bars: **C** = 200 μm; **D** = 25 μm.

Transgene expression at the mRNA level was assessed by quantitative RT-PCR after amplification with human α-syn (*SNCA*) specific primers. To compare expression in control versus α-syn-deficient mice, *SNCA* mRNA levels were quantified relative to RNA extracted from human brain. At 2 weeks post-AAV treatment, *SNCA* mRNA was detected in tissue from the dorsal left but not the dorsal right medulla oblongata (Fig. 2E); this finding is consistent with the presence of transduced neuronal cell bodies in the DMnX on the side of the brain ipsilateral but not contralateral to vagal injections. Levels of human α-syn expression in left DMnX-containing tissue were comparable between control animals and mice lacking α-syn (Fig. 2E).

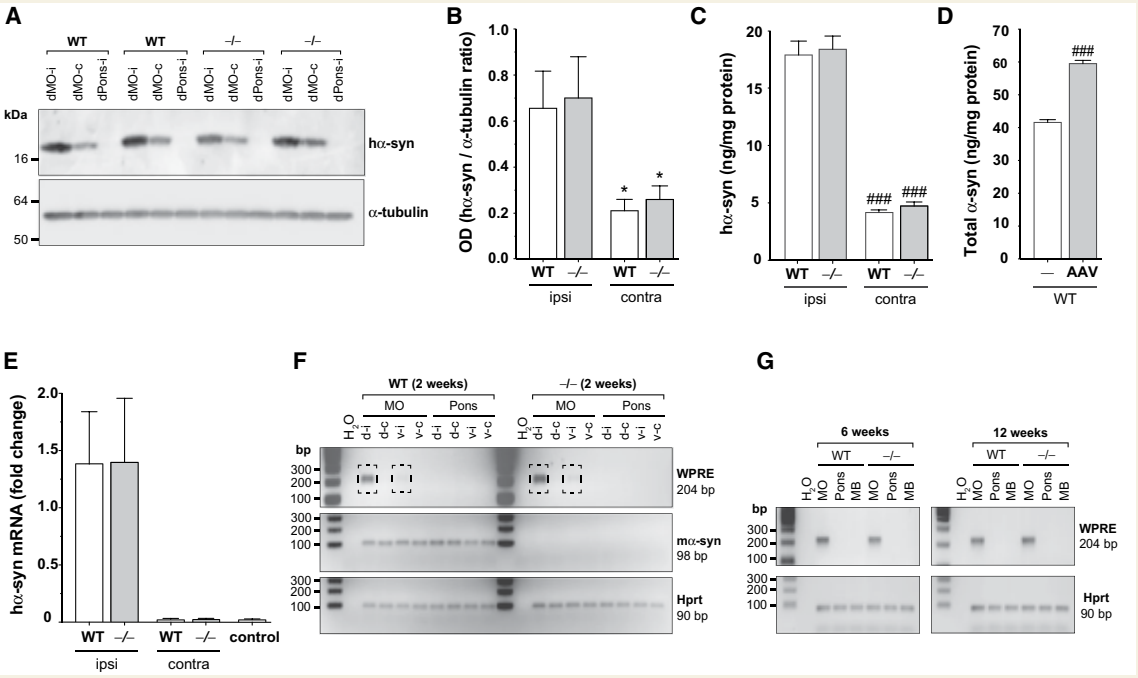

Figure 2 Transgene expression after vagal AAV injections. (**A** and **B**) Mice received a single injection of human α-syn-carrying AAVs (1.5×10^{13} gc/ml) into the left vagus nerve, and analyses were performed at 2 weeks post-treatment. (**A**) Tissue was collected from: the dorsal quadrant of the medulla oblongata ipsilateral (dMO-i) and contralateral (dMO-c) to AAV injections, and the dorsal quadrant of the pons ipsilateral (dPons-i) to AAV injections. Representative western blots from two wild-type (WT) and two α-syn-deficient (−/−) mice show immunoreactivity specific for human α-syn and α-tubulin. (**B**) Semi-quantitative analysis of band intensity (expressed as human α-syn/α-tubulin ratio) of western blots from the dorsal quadrant of the medulla oblongata ipsilateral (ipsi) and contralateral (contra) to AAV injections. Error bars are + SEM. Unpaired *t*-test comparing data in contralateral samples versus the corresponding values in tissues ipsilateral to AAV injections. $F(1,13) = 12.43$ for wild-type groups and $F(1,13) = 8.034$ for −/− groups. $^{*}P < 0.05$. (**C**) The dorsal quadrants of the medulla oblongata ipsilateral (ipsi) and contralateral (contra) to AAV injections (1.5×10^{13} gc/ml) were collected from wild-type (WT) and α-syn-deficient (−/−) mice and assayed for human α-syn by ELISA. Error bars are + SEM. Unpaired *t*-test comparing data in contralateral samples versus the corresponding values in tissues ipsilateral to AAV injections. $F(1,12) = 141.1$ for wild-type groups and $F(1,14) = 120.5$ for −/− groups. $^{\#\#\#\#}P < 0.0001$. (**D**) Levels of total (mouse plus human) α-syn were compared in samples from untreated wild-type mice versus wild-type animals in which 1.5×10^{13} gc/ml AAV was injected into the left vagus nerve. Error bars are + SEM. Unpaired *t*-test comparing data in AAV-injected mice versus values in untreated control animals. $F(1,15) = 193.9$. $^{\#\#\#\#}P < 0.0001$. (**E**) Analyses were performed at 2 weeks after a single injection of human α-syn-carrying AAVs (1.5×10^{13} gc/ml) into the left vagus nerve. Levels of human α-syn (*SNCA*) mRNA were measured by quantitative RT-PCR in samples from the dorsal quadrant of the medulla oblongata ipsilateral to AAV injections in wild-type and −/− mice ($n = 10$/group). Human α-syn (*SNCA*) mRNA was also assessed in tissue samples from the medulla oblongata contralateral to AAV injections ($n \geqslant 9$/group) and in control medulla oblongata samples devoid of human α-syn that were obtained from untreated mice ($n = 8$). The medulla oblongata contralateral values were comparable to control values, indicating background measurements and lack of specific human α-syn expression. Data are expressed as fold changes relative to reference samples containing 0.9 ng RNA extracted from human brain. Error bars are + SEM. (**F**) RT-PCR was performed to detect WPRE, mouse α-syn (mα-syn) or, as a loading control, Hprt in medulla oblongata and pontine samples from: dorsal quadrant tissues ipsilateral (**d–i**) and contralateral (**d–c**) to AAV injections, and ventral quadrant specimens ipsilateral (**v–i**) and contralateral (**v–c**) to injections (1.5×10^{13} gc/ml). Tissues were collected at 2 weeks post-treatment. Specific bands were detected at 204 (WPRE), 98 (mouse α-syn) and 90 (Hprt) bp. Dashed boxes indicate WPRE amplification signals in specimens from the **d–i** and **v–i** medulla oblongata. (**G**) WPRE and Hprt were assayed by RT-PCR at 6 and 12 weeks post-AAV treatment in dorsal quadrant tissues of the left medulla oblongata, pons and midbrain (MB) ipsilateral to AAV injections.

To further demonstrate confinement of AAVs within targeted areas of the medulla oblongata, measurements of WPRE (an enhancer element incorporated into the AAV genome) mRNA were used as markers of AAV transduction. Assays were initially carried out in mice sacrificed 2 weeks after AAV injection. After amplification using WPRE-hybridizing primers, RT-PCR analysis showed a pattern of tissue-specific expression characterized by strong and faint bands in samples from the dorsal left and ventral left medulla oblongata, respectively (Fig. 2F). This pattern, evident in both control and mutant mice, reflects transduction of DMnX (dorsal medulla oblongata) and nucleus ambiguus (ventral medulla oblongata) neurons ipsilateral (left) to AAV injections. No evidence of AAV-

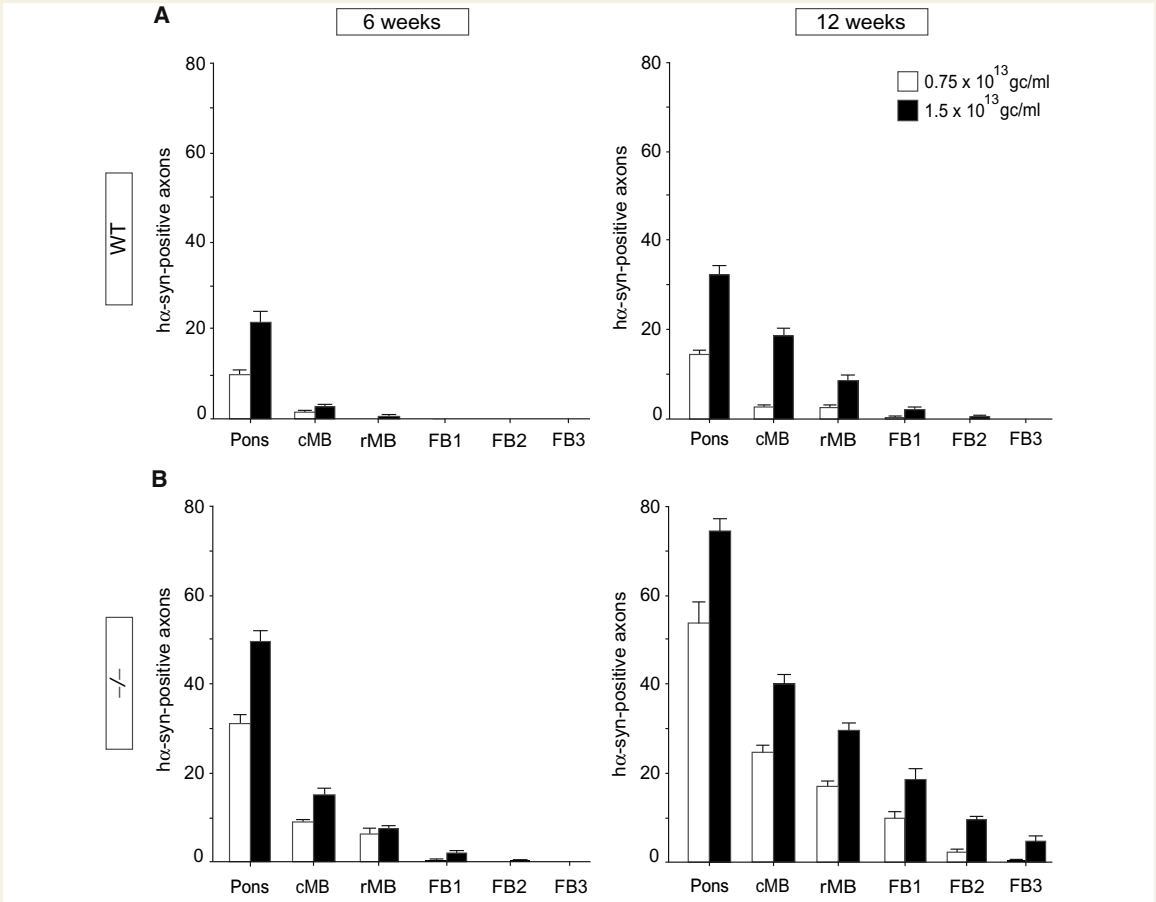

Figure 3 Counts of human α-syn-immunoreactive axons in AAV-injected mice. Wild-type (WT, **A**) and α-syn-deficient (−/−, **B**) mice received a single injection of human α-syn-carrying AAVs (0.75 or 1.5 × 10^{13} gc/ml) into the left vagus nerve. Analyses were performed at 6 and 12 weeks post-treatment. Tissues were immunostained with an anti-hα-syn antibody, and human α-syn-positive axons were counted in the left (injected side) hemisphere of coronal sections from the: pons (Bregma: −5.40 mm), caudal midbrain (cMB; Bregma: −4.60 mm), rostral midbrain (rMB, Bregma: −3.40 mm) and forebrain (FB; FB1, Bregma: −2.18 mm; FB2, Bregma: −0.94 mm; FB3, Bregma: + 0.14 mm). Error bars are + SEM. Statistical comparisons are reported in Supplementary Table 2.

derived mRNA was found in the right medulla oblongata as well as in the left or right pons (Fig. 2F). Similar measurements were then performed in medulla oblongata, pontine and midbrain specimens collected at 6 and 12 weeks post-AAV injection. Even at these later time points, specific WPRE bands were detected in the medulla oblongata but not in other brain regions rostral to it (Fig. 2G).

Caudo-rostral propagation of human α-syn in wild-type mice

Tissue sections from mice killed at different time points post-AAV injection were immunostained with syn211 antibody. While no immunoreactivity was detected in the pons, midbrain and forebrain at 2 weeks, neuronal projections positive for human α-syn were observed in brain regions rostral to the medulla oblongata at later time points. In wild-type mice injected with 0.75 × 10^{13} gc/ml AAV, a few human α-syn-containing axons occupied the pons (Bregma −5.4 mm) and caudal midbrain (Bregma −4.6 mm) at 6 weeks post-treatment (Fig. 3A and Supplementary Fig. 1A). A titre-dependent effect was indicated by data showing a greater number of human α-syn-positive fibres in the pons and caudal midbrain of animals injected with 1.5 × 10^{13} gc/ml AAV (Fig. 3A and Supplementary Fig. 1A). In 2 of 11 of these mice, immunoreactive axons were also seen in the rostral portion of the midbrain (Bregma −3.4 mm). Findings at 6 weeks were then compared to fibre counts in tissue sections from animals killed at 12 weeks after AAV transduction. The number of stained axons was significantly increased in mice treated with either of the two AAV titres at this later time point (Fig. 3A and Supplementary Fig. 1A).

Furthermore, consistent with progressive caudo-rostral propagation, neuritic projections immunoreactive for the exogenous protein were found in sections of the forebrain; most rostral outposts were at Bregma −2.18 and −0.94 mm after injections with the lower and higher AAV titre, respectively.

To further rule out the possibility that neuron-to-neuron translocation of viral vectors rather than inter-neuronal protein transfer was responsible for human α-syn transmission, a group of mice received vagal injections of GFP- rather than human α-syn-carrying AAVs. Results of these experiments showed that, even in the presence of robust transgene expression in the medulla oblongata, GFP-containing neurons were virtually absent in tissue sections from the pons, midbrain and forebrain of mice killed at either 6 or 12 weeks after GFP-AAV treatment (Supplementary Fig. 2).

Human α-syn propagation in α-syn-deficient mice

Counts of neuronal projections immunoreactive for human α-syn were carried out in brain tissue from α-syn-deficient mice injected with human α-syn-AAVs. Regardless of whether animals were treated with the lower or higher AAV titre and whether analyses were performed at the 6- or 12-week time point, the number of human α-syn-positive axons was at least two times greater in brain regions rostral to the medulla oblongata of mutant mice as compared to wild-type controls (Fig. 3B, Supplementary Fig. 1B and Supplementary Table 2). In the former group of animals, the advancing protein also reached areas that were considerably more anterior; in particular, when animals lacking α-syn were killed at 12 weeks after treatment with the higher AAV titre, human α-syn-immunoreactive fibres could be seen in forebrain sections as rostral as Bregma + 0.14 mm.

Caudo-rostral brain propagation of human α-syn followed a stereotypical pattern of topographical distribution and affected predilection sites that were alike between control and mutant mice. They included the coeruleus-subcoeruleus complex and parabrachial area in the pons (Fig. 4A and B), the dorsal raphae and periaqueductal grey in the midbrain (Supplementary Fig. 3A and B), the hypothalamus in the diencephalon and the amygdala in the medial temporal lobe (Supplementary Fig. 3C and D). Axons loaded with human α-syn appeared as beaded winding threads, and immunoreactivity was typically more robust within the irregularly spaced varicosities (Fig. 4B and Supplementary Fig. 3B and D).

Differences in human α-syn diffusion between wild-type and α-syn-deficient mice were confirmed by measurements of the length and density of human α-syn-labelled fibres using the Space Balls stereological tool. A region encompassing the coeruleus and parabrachial complexes (CPC) was delineated throughout serial pontine sections from animals injected with 1.5×10^{13} gc/ml AAV and killed at 6 and 12 weeks post-treatment. Data obtained by unbiased CPC sampling revealed that both the mean total length and density of human α-syn-immunoreactive axons were significantly greater in mutant as compared to control mice; ~4- and 2-fold differences were seen at 6 and 12 weeks post-treatment, respectively (Fig. 4C and D).

A separate set of experiments was carried out in a different line of α-syn-deficient mice generated by targeted disruption of exons 1 and 2 of the α-syn gene (Abeliovich *et al.*, 2000). Knockout mice and genetically matched controls received vagal human α-syn-AAV injections (1.5×10^{13} gc/ml) and were sacrificed at 5 weeks post-treatment. Counts of human α-syn-positive axons showed higher numbers in the pons and caudal midbrain of animals lacking endogenous α-syn (Fig. 5A). Most rostral areas occupied by labelled fibres were in the caudal and rostral midbrain in control and knockout mice, respectively. Enhanced propagation in the absence of endogenous α-syn was confirmed by Space Balls measurements of human α-syn-immunoreactive axons in the CPC; data revealed 2-fold increases in fibre length and density in α-syn-deficient as compared to α-syn-expressing animals (Fig. 5B and C).

Relationship between protein overexpression, aggregation and propagation

Immunohistochemical analyses were carried out on tissue sections from the medulla oblongata and pons using a variety of anti-α-syn antibodies. Two of these antibodies (AB5038P and C-20) recognize both monomeric and aggregated forms of the protein. The other antibodies display conformation-specific reactivity towards aggregated α-syn and have been shown to detect (i) mature amyloid α-syn fibrils (Syn-F1 and Syn-F2); or (ii) α-syn fibrils as well as α-syn oligomers (Syn-O1, Syn-O2 and 5G4) (Kovacs *et al.*, 2012; Vaikath *et al.*, 2015). All antibodies stained transduced medulla oblongata tissue containing the DMnX, nucleus ambiguus and nucleus of the tractus solitarius and, with all antibodies, no significant differences in labelling distribution and intensity were observed between wild-type and α-syn-deficient mice (Fig. 6 and Supplementary Fig. 4). Representative images in Fig. 6 show α-syn-containing neuronal projections in the DMnX stained with AB5038P, Syn-F1 and Syn-O2. Immunoreactivity for AB5038P revealed a dense fibre pattern that likely reflected the presence of both monomeric and aggregated α-syn. Of the two aggregate-specific antibodies, Syn-O2 revealed a denser network of immunoreactive neuronal processes than Syn-F1 (Fig. 6C and D versus Fig. 6A and B), consistent with its ability to detect oligomeric as well as fibrillar forms of the protein. A progressive burden of aggregate pathology is suggested by the observation that, with both Syn-F1 and Syn-O2, a more pronounced pattern of immunoreactivity was seen at 12 weeks as compared to 6 weeks

Furthermore, consistent with progressive caudo-rostral propagation, neuritic projections immunoreactive for the exogenous protein were found in sections of the forebrain; most rostral outposts were at Bregma −2.18 and −0.94 mm after injections with the lower and higher AAV titre, respectively.

To further rule out the possibility that neuron-to-neuron translocation of viral vectors rather than inter-neuronal protein transfer was responsible for human α-syn transmission, a group of mice received vagal injections of GFP- rather than human α-syn-carrying AAVs. Results of these experiments showed that, even in the presence of robust transgene expression in the medulla oblongata, GFP-containing neurons were virtually absent in tissue sections from the pons, midbrain and forebrain of mice killed at either 6 or 12 weeks after GFP-AAV treatment (Supplementary Fig. 2).

Human α-syn propagation in α-syn-deficient mice

Counts of neuronal projections immunoreactive for human α-syn were carried out in brain tissue from α-syn-deficient mice injected with human α-syn-AAVs. Regardless of whether animals were treated with the lower or higher AAV titre and whether analyses were performed at the 6- or 12-week time point, the number of human α-syn-positive axons was at least two times greater in brain regions rostral to the medulla oblongata of mutant mice as compared to wild-type controls (Fig. 3B, Supplementary Fig. 1B and Supplementary Table 2). In the former group of animals, the advancing protein also reached areas that were considerably more anterior; in particular, when animals lacking α-syn were killed at 12 weeks after treatment with the higher AAV titre, human α-syn-immunoreactive fibres could be seen in forebrain sections as rostral as Bregma + 0.14 mm.

Caudo-rostral brain propagation of human α-syn followed a stereotypical pattern of topographical distribution and affected predilection sites that were alike between control and mutant mice. They included the coeruleus-subcoeruleus complex and parabrachial area in the pons (Fig. 4A and B), the dorsal raphae and periaqueductal grey in the midbrain (Supplementary Fig. 3A and B), the hypothalamus in the diencephalon and the amygdala in the medial temporal lobe (Supplementary Fig. 3C and D). Axons loaded with human α-syn appeared as beaded winding threads, and immunoreactivity was typically more robust within the irregularly spaced varicosities (Fig. 4B and Supplementary Fig. 3B and D).

Differences in human α-syn diffusion between wild-type and α-syn-deficient mice were confirmed by measurements of the length and density of human α-syn-labelled fibres using the Space Balls stereological tool. A region encompassing the coeruleus and parabrachial complexes (CPC) was delineated throughout serial pontine sections from animals injected with 1.5×10^{13} gc/ml AAV and killed at 6 and 12 weeks post-treatment. Data obtained by unbiased CPC sampling revealed that both the mean total length and density of human α-syn-immunoreactive axons were significantly greater in mutant as compared to control mice; ~4- and 2-fold differences were seen at 6 and 12 weeks post-treatment, respectively (Fig. 4C and D).

A separate set of experiments was carried out in a different line of α-syn-deficient mice generated by targeted disruption of exons 1 and 2 of the α-syn gene (Abeliovich *et al.*, 2000). Knockout mice and genetically matched controls received vagal human α-syn-AAV injections (1.5×10^{13} gc/ml) and were sacrificed at 5 weeks post-treatment. Counts of human α-syn-positive axons showed higher numbers in the pons and caudal midbrain of animals lacking endogenous α-syn (Fig. 5A). Most rostral areas occupied by labelled fibres were in the caudal and rostral midbrain in control and knockout mice, respectively. Enhanced propagation in the absence of endogenous α-syn was confirmed by Space Balls measurements of human α-syn-immunoreactive axons in the CPC; data revealed 2-fold increases in fibre length and density in α-syn-deficient as compared to α-syn-expressing animals (Fig. 5B and C).

Relationship between protein overexpression, aggregation and propagation

Immunohistochemical analyses were carried out on tissue sections from the medulla oblongata and pons using a variety of anti-α-syn antibodies. Two of these antibodies (AB5038P and C-20) recognize both monomeric and aggregated forms of the protein. The other antibodies display conformation-specific reactivity towards aggregated α-syn and have been shown to detect (i) mature amyloid α-syn fibrils (Syn-F1 and Syn-F2); or (ii) α-syn fibrils as well as α-syn oligomers (Syn-O1, Syn-O2 and 5G4) (Kovacs *et al.*, 2012; Vaikath *et al.*, 2015). All antibodies stained transduced medulla oblongata tissue containing the DMnX, nucleus ambiguus and nucleus of the tractus solitarius and, with all antibodies, no significant differences in labelling distribution and intensity were observed between wild-type and α-syn-deficient mice (Fig. 6 and Supplementary Fig. 4). Representative images in Fig. 6 show α-syn-containing neuronal projections in the DMnX stained with AB5038P, Syn-F1 and Syn-O2. Immunoreactivity for AB5038P revealed a dense fibre pattern that likely reflected the presence of both monomeric and aggregated α-syn. Of the two aggregate-specific antibodies, Syn-O2 revealed a denser network of immunoreactive neuronal processes than Syn-F1 (Fig. 6C and D versus Fig. 6A and B), consistent with its ability to detect oligomeric as well as fibrillar forms of the protein. A progressive burden of aggregate pathology is suggested by the observation that, with both Syn-F1 and Syn-O2, a more pronounced pattern of immunoreactivity was seen at 12 weeks as compared to 6 weeks

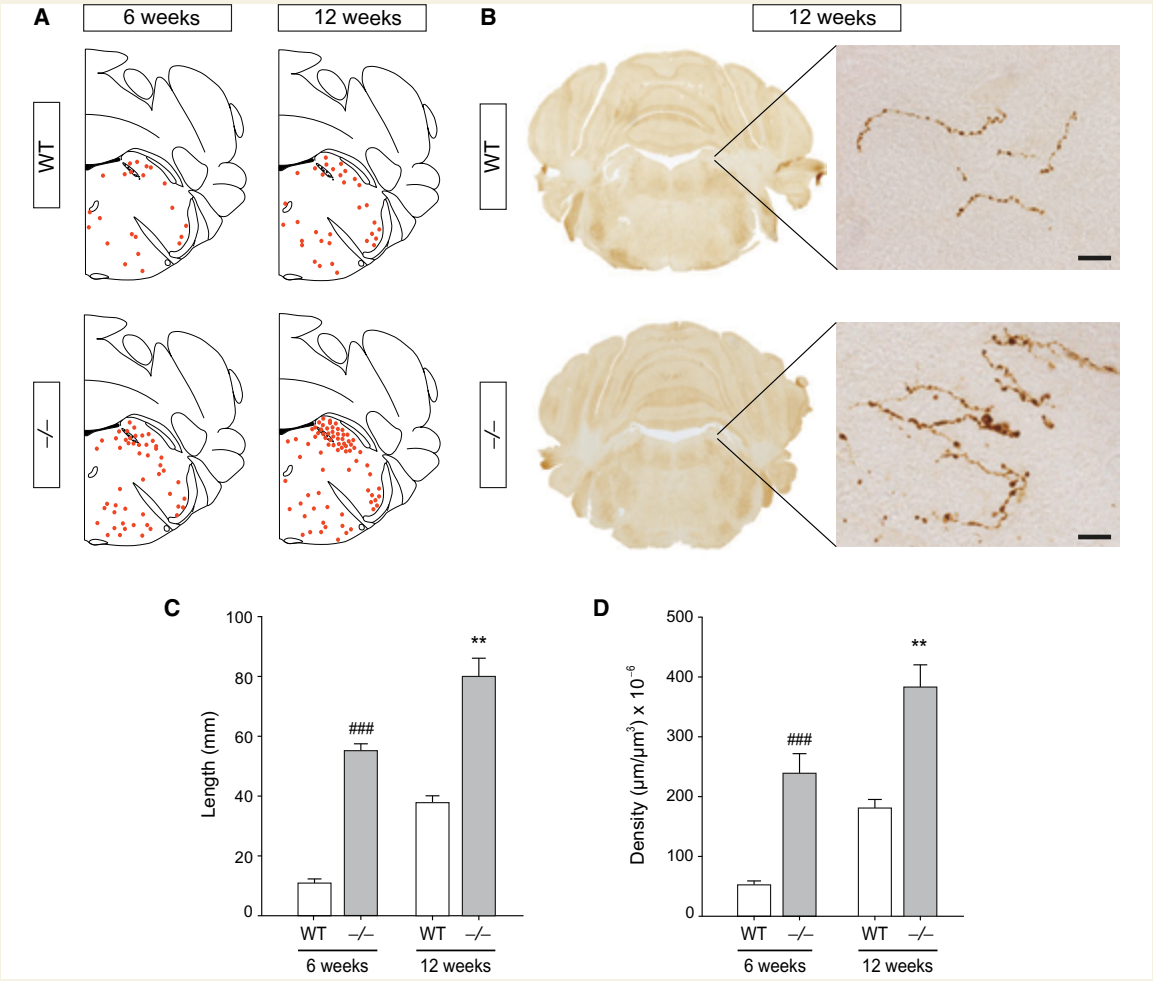

Figure 4 Number, distribution, length and density of human α-syn-immunoreactive axons in wild-type versus α-syn-deficient mice. Wild-type (WT) and α-syn-deficient (−/−) mice received a single injection of human α-syn-carrying AAVs (1.5×10^{13} gc/ml) into the left vagus nerve. (**A**) Schematic plots of the distribution of human α-syn-labelled axons in the left (injected side) pons at 6 and 12 weeks post-AAV injection. (**B**) Representative pontine sections (Bregma: −5.40 mm) were obtained from mice sacrificed at 12 weeks post-treatment. Higher magnification images were obtained by z-stacking and show axonal projections in the nucleus parabrachialis immunostained with an anti-hα-syn antibody. Scale bars = 25 µm. (**C** and **D**) Length (**C**) and density (**D**) of human α-syn-immunoreactive axons were estimated in a pontine area encompassing the locus coeruleus and the nucleus parabrachialis using the Space Balls stereological tool. Measurements were made in the left (injected side) pons in specimens collected at 6 and 12 weeks post-AAV injection. Error bars are + SEM. Unpaired *t*-test comparing data in α-syn-deficient mice versus the corresponding values in wild-type animals. $F(1,10) = 12.35$ for length comparison at 6 weeks; $F(1,9) = 5.547$ for length comparison at 12 weeks; $F(1,10) = 7.641$ for density comparison at 6 weeks; $F(1,9) = 11.44$ for density comparison at 12 weeks. $^{**}P < 0.005$; $^{\#\#\#}P < 0.0001$.

post-vagal injection (Fig. 6). Results obtained with AB5038P, Syn-F1 and Syn-O2 matched the pattern of immunoreactivity seen in medulla oblongata tissue stained with C-20, Syn-F2 and Syn-O1, respectively (Supplementary Fig. 4). Moreover, labelling with 5G4 revealed close similarities with the staining produced by Syn-O1 or Syn-O2 (data not shown).

To further assess the formation of amyloid fibrils, sections of the medulla oblongata were immunolabelled with anti-hα-syn and then stained with Thioflavin S. In these sections, a number of neurons (mostly neuronal projections) immunoreactive for human α-syn were also stained with Thioflavin S (Fig. 7A and B). To confirm protein oligomerization, samples were processed by PLA. This technique allows labelling of adjacent α-syn molecules and has recently been used to detect non-fibrillar, most likely oligomeric α-syn in histological brain specimens from patients with Parkinson's disease (Roberts *et al.*, 2015). Two

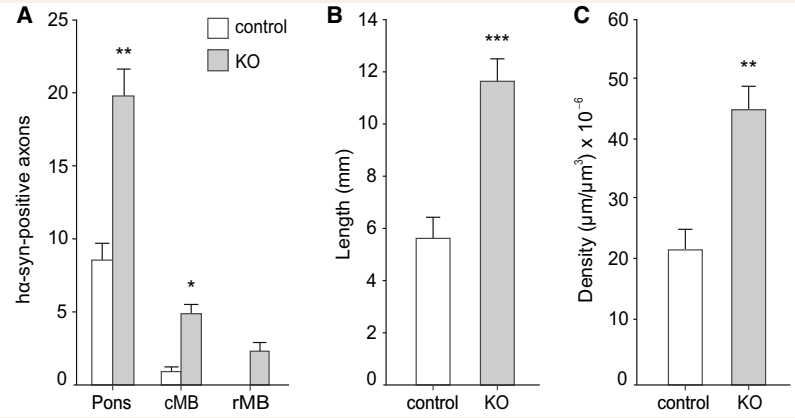

Figure 5 Count, length and density of human α-syn-positive axons in control versus α-syn-knockout mice. Control and α-syn-knockout (KO) mice received a single injection of human α-syn-carrying AAVs (1.5×10^{13} gc/ml) into the left vagus nerve. Analyses were performed at 5 weeks post-treatment when brain tissue sections were immunostained with an anti-hα-syn antibody. (**A**) Human α-syn-positive axons were counted in the left (injected side) hemisphere of coronal sections from the: pons (Bregma: −5.40 mm), caudal midbrain (cMB; Bregma: −4.60 mm) and rostral midbrain (rMB, Bregma: −3.40 mm). Error bars are + SEM. Unpaired *t*-test comparing data in knockout mice versus the corresponding values in control animals. $F(1,8) = 3.569$ in the pons, and $F(1,8) = 8.143$ in the caudal midbrain. $^{*}P < 0.05$; $^{**}P < 0.005$. (**B** and **C**) Length (**B**) and density (**C**) of human α-syn-immunoreactive axons were estimated in a pontine area encompassing the locus coeruleus and the nucleus parabrachialis. Error bars are + SEM. Unpaired *t*-test comparing data in knockout mice versus the corresponding values in control animals. $F(1,8) = 4.830$ for length comparison; $F(1,8) = 1.175$ for density comparison. $^{**}P < 0.005$; $^{***}P < 0.0005$.

separate sets of PLA probes were designed to recognize self-interaction between human α-syn molecules or to label human α-syn in close proximity to mouse α-syn. Specific human–human α-syn signal was present in medulla oblongata tissue from either wild-type or α-syn-deficient mice injected with AAV (Fig. 7C). Immunoreactivity for human–mouse α-syn was also detected, but only in sections from AAV-injected wild-type animals; in these mice, *in situ* amplification revealed a stronger signal for human–human α-syn than human–mouse α-syn interactions (Fig. 7C versus Fig. 7D).

A final set of analyses was carried out in pontine tissue from AAV-transduced wild-type and α-syn-deficient mice. Sections were double-stained with either AB5038P plus Syn-F1 or AB5038P plus Syn-O2. Labelling with the first pair of antibodies showed no evidence of Syn-F1 immunoreactivity within axons positive for total α-syn at either 6 (Supplementary Fig. 5A and B) or 12 weeks (Fig. 8A and B) post-treatment. In contrast, staining with AB5038P and Syn-O2 revealed co-localization of immunoreactivity at both time points (Supplementary Fig. 5C and D, and Fig. 8C and D). Thioflavin S staining and human–human α-syn PLA were used to gain further evidence consistent with absence of α-syn amyloid fibrils and presence of α-syn oligomers, respectively. No reactivity for Thioflavin S was detected within pontine axons affected by human α-syn propagation (data not shown). On the other hand, when pontine tissue was processed for human–human α-syn PLA, specific labelling was observed only in sections from AAV-injected mice; reactivity was particularly intense within axonal swellings, conferring an image of punctate fibre profiles on single-plane microscopy (Fig. 8E).

Discussion

Inter-neuronal transfer and brain spreading of proteins implicated in human neurodegenerative diseases may be facilitated by interactions between pathological forms of the proteins generated within donor cells and the corresponding normal protein expressed within recipient neurons (Guo and Lee, 2014). Extending earlier work in rats (Ulusoy *et al.*, 2013, 2015), we generated a mouse model in which protein propagation was triggered by overexpression of human α-syn within donor neurons in the medulla oblongata. Spreading was then compared between wild-type mice and α-syn-deficient animals, i.e. in the presence and absence of endogenous α-syn expression within recipient cells. We found that intravagal injections of viral vectors carrying human α-syn DNA were indeed capable of inducing targeted overexpression of human α-syn in the mouse medulla oblongata, which was followed by caudo-rostral protein diffusion. The rate and extent of this propagation were dependent upon the transduction titre and progressed over time following a stereotypical pattern of anatomical distribution. Starting at 6 weeks post-vagal injection, immunoreactivity for human α-syn could be detected within axons first in the pons, then in the midbrain and finally in the forebrain. Human α-syn reached areas such as the coeruleus–subcoeruleus complex (pons),

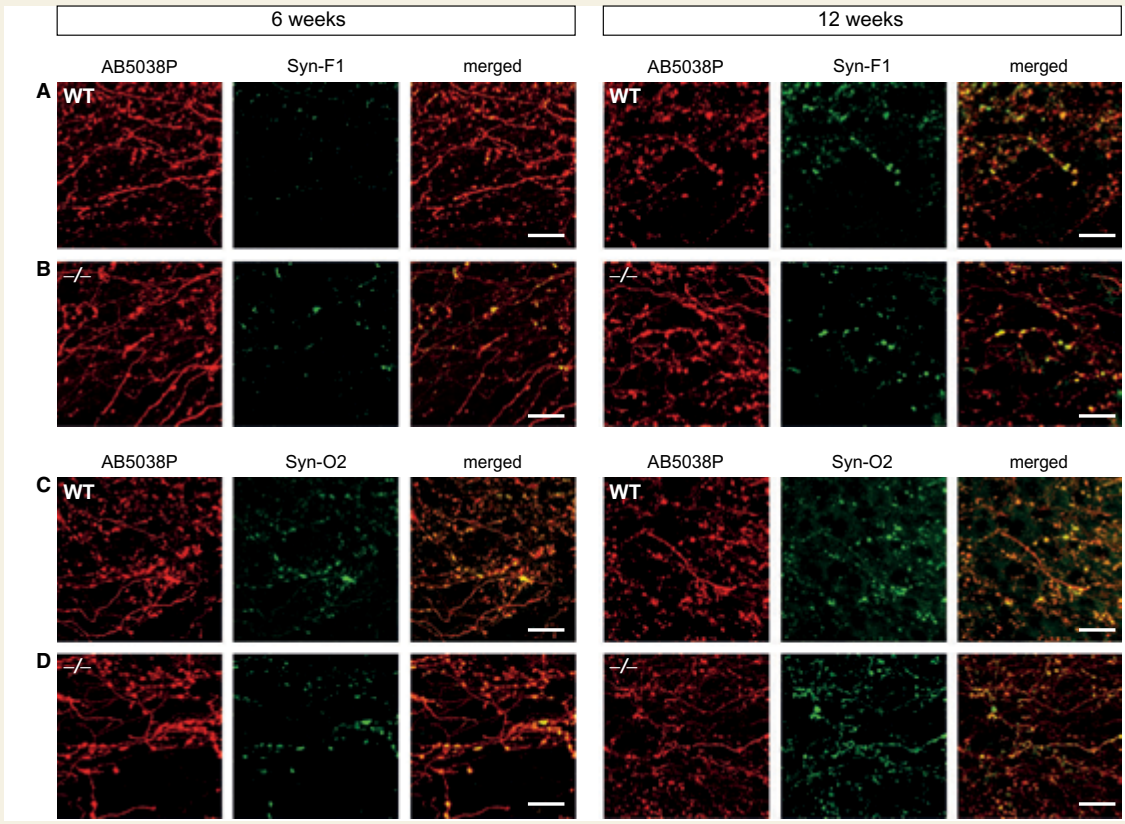

Figure 6 Immunohistochemical characterization of aggregated α-syn in the DMnX. Wild-type (WT, **A** and **C**) and α-syn-deficient (–/–, **B** and **D**) mice received a single injection of human α-syn-carrying AAVs (1.5×10^{13} gc/ml) into the left vagus nerve. Analyses were performed at 6 and 12 weeks post-treatment. Representative sections of the medulla oblongata (Bregma: −7.32 mm) were double-immunostained with either (i) an antibody against total (monomeric and aggregated) α-syn (AB5038P) plus an antibody that specifically recognizes α-syn fibrils (Syn-F1) (**A** and **B**); or (ii) AB5038P plus an antibody that recognizes oligomeric and fibrillar forms of the protein (Syn-O2) (**C** and **D**). Images of the left (injected side) DMnX are shown. Scale bars = 15 μm.

dorsal raphae (midbrain) and amygdala (medial temporal lobe) that have no direct anatomical connections with the vagus (X) nerve; data are therefore consistent with trans-synaptic passage of the protein from donor medulla oblongata neurons to recipient axons projecting into the medulla oblongata from higher brain regions. To assess potential differences in protein transfer due to expression of endogenous α-syn, human α-syn-positive axons were counted in wild-type versus α-syn-deficient mice. This comparative analysis yielded intriguing results. Protein propagation was not enhanced by α-syn expression within recipient cells. On the contrary, it was significantly more pronounced in animals lacking endogenous protein. In this group of mice, counts of human α-syn-positive axons were consistently greater in the pons, midbrain and forebrain, and human α-syn diffusion toward regions rostral to the medulla oblongata was also more advanced.

Extensive efforts were focused on elucidating mechanisms of differential protein transmission in the presence and absence of endogenous α-syn. Increased propagation in α-syn-deficient mice was not a mere consequence of enhanced human α-syn expression as AAV-induced transduction, assessed at both the mRNA and protein levels, was comparable in control mice and mice lacking α-syn. Quite importantly, more pronounced diffusion in the absence of endogenous α-syn was observed in two separate lines of α-syn-deficient animals, one carrying a spontaneous deletion of the α-syn (*Snca*) gene and the other generated through genetic engineering techniques (Abeliovich *et al.*, 2000; Specht and Schoepfer, 2001). This observation makes it unlikely that differences in protein transmission seen in this study may arise from factors (e.g. the genetic background of mice with spontaneous α-syn loss) unrelated to α-syn deficiency. Lack of α-syn may be compensated by enhanced expression of its homologue β-syn (encoded by *Sncb*) that could in turn modify pathological features triggered by human α-syn transduction in mutant mice (Hashimoto *et al.*, 2004). A role of β-syn in modulating

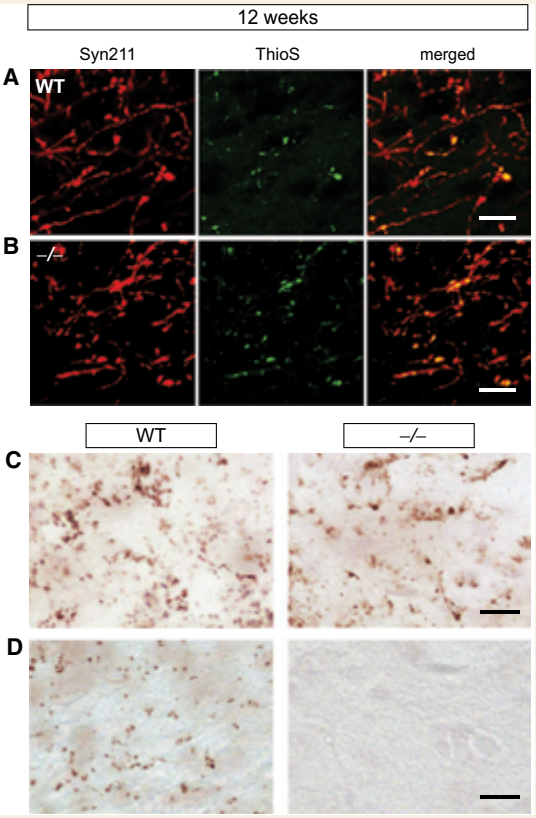

Figure 7 Fibrillar and oligomeric α-syn in the medulla oblongata of AAV-injected mice. Wild-type (WT) and α-syn-deficient (–/–) mice received a single injection of human α-syn-carrying AAVs (1.5×10^{13} gc/ml) into the left vagus nerve. Analyses were performed at 12 weeks post-treatment. (**A** and **B**) Representative sections of the medulla oblongata (Bregma: –7.32 mm) were double-stained with an antibody specific for human α-syn (Syn211) and Thioflavin S (ThioS). Images of the left (injected side) DMnX are shown. Scale bars = 10 μm. (**C**) Representative images of the left DMnX showing specific signal for human α-syn self-interaction detected by PLA. Scale bars = 15 μm. (**D**) Representative images of the left DMnX showing specific signal for human–mouse α-syn interactions detected by PLA. Scale bars = 15 μm.

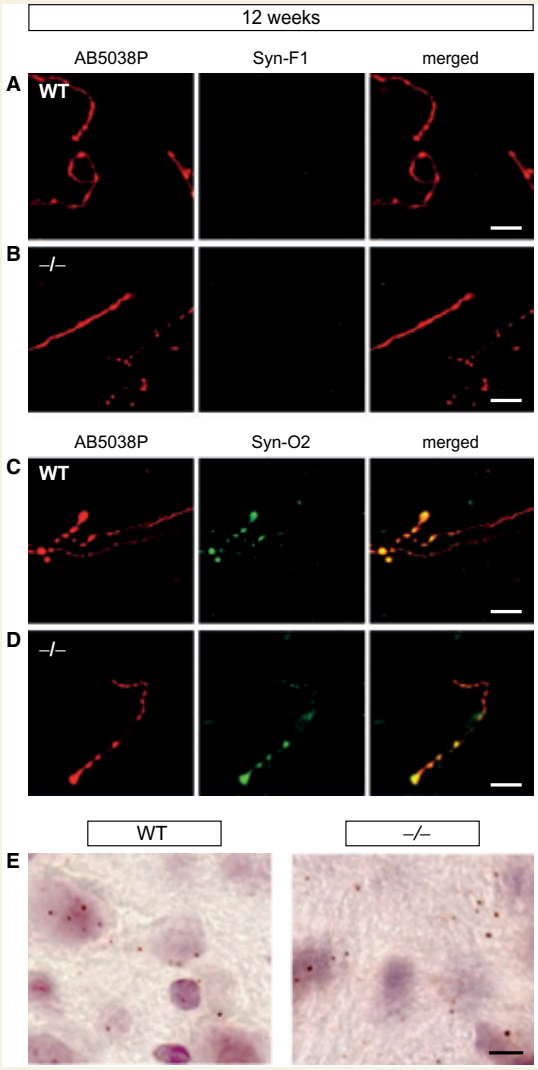

Figure 8 Immunohistochemical characterization of aggregated α-syn within pontine axons. Wild-type (WT) and α-syn-deficient (–/–) mice received a single injection of human α-syn-carrying AAVs (1.5×10^{13} gc/ml) into the left vagus nerve. Analyses were performed at 12 weeks post-treatment. (**A–D**) Representative sections of the pons (Bregma: –5.40 mm) were double-immunostained with either (i) an antibody against total (monomeric and aggregated) α-syn (AB5038P) plus an antibody that specifically recognizes α-syn fibrils (Syn-F1) (**A** and **B**); or (ii) AB5038P plus an antibody that recognizes oligomeric and fibrillar forms of the protein (Syn-O2) (**C** and **D**). Labelled axons in the left (injected side) pons are shown. Scale bars = 5 μm. (**E**) Representative pontine sections labelled with human–human α-syn PLA and counterstained with haematoxylin. The punctate brown staining likely represents accumulation of oligomeric human α-syn within axonal varicosities. Scale bars = 5 μm.

human α-syn propagation was ruled out, however, by findings showing that its levels were similar in the brain of wild-type and α-syn-deficient animals. Changes in protein conformation and aggregation have been suggested to affect α-syn's tendency to pass from one neuron to another and could therefore explain variations in protein spreading (Lee *et al.*, 2005, 2008; Angot and Brundin, 2009; Freundt *et al.*, 2012). Immunohistochemical analyses carried out as part of this study did not detect overt differences in monomeric, oligomeric and fibrillar α-syn in the medulla oblongata of control versus α-syn-deficient mice. Nonetheless, it is still conceivable that generation and accumulation of

discrete α-syn species (e.g. specific oligomeric forms of the protein) characterize these two groups of animals, contributing to enhancement or suppression of human α-syn diffusion (Danzer *et al.*, 2007). Different aggregate species with greater or lower tendency to propagate could be generated, for example, by distinct interactions of endogenous and/or exogenous α-syn with lipid surfaces in wild-type versus α-syn null animals (Barceló-Coblijn *et al.*, 2007; Galvagnion *et al.*, 2015).

Results of this study support the interpretation that decreased or enhanced protein transmission could be a consequence of human α-syn expression on a normal versus null α-syn background since, depending on this background, important differences in protein–protein interactions were found. Self-interaction of adjacent molecules of human α-syn was detected in mutant mice, whereas both human–human α-syn and human–mouse α-syn interactions were observed in AAV-injected wild-type animals. A variety of mechanisms influenced by α-syn interactions could ultimately modify protein propagation. One of these mechanisms may be the formation of distinct α-syn aggregates (see above), as *in vitro* evidence indicates that both rates and pathways of protein assembly were dramatically different in incubations of human α-syn alone, mouse α-syn alone or human and mouse α-syn together (Rochet *et al.*, 2000). Furthermore, changes in protein–protein interactions in wild-type versus null α-syn mice, as identified in the present study, could diversely affect neuronal functions relevant to intercellular transfer and brain propagation of the protein, such as synaptic vesicle exo- and endocytosis and axonal transport (Cabin *et al.*, 2005; Nemani *et al.*, 2010; Prasad *et al.*, 2011; Prots *et al.*, 2013; Vargas *et al.*, 2014).

Another important aim of this study was to assess the relationship between α-syn aggregation and propagation and, in particular, to determine if protein transmission was associated with the accumulation of oligomeric and/or fibrillar α-syn. Using several antibodies with distinct affinities toward aggregated forms of the protein (Kovacs *et al.*, 2012; Vaikath *et al.*, 2015), data revealed that both oligomeric and fibrillar aggregates were formed within donor neurons in the mouse medulla oblongata. In contrast, when recipient pontine axons were stained with either antibodies that recognize oligomeric and fibrillar α-syn or antibodies specific for α-syn amyloid fibrils, immunoreactivity was only observed with the former reagents. Taken together, these findings are consistent with the conclusion that, in this model, fibrillar α-syn is not transferred from donor to recipient neurons, nor is it required for caudo-rostral propagation and axonal accumulation of α-syn. On the other hand, the presence of oligomeric α-syn aggregates within these axons is compatible with two non-mutually exclusive interpretations. First, small α-syn aggregates may be capable of passing from one neuron to another and diffusing along axonal projections. The second possibility is that inter-neuronal transfer primarily involves monomeric α-syn that, once crowded within recipient axons, undergoes aggregation into oligomeric species. Axonal build-up of oligomeric α-syn aggregates was confirmed by analysis of tissue sections processed for α-syn PLA and was accompanied by evidence of pathological changes (e.g. thread-like axonal swelling). Experimental data linking α-syn transmission and oligomerization to axonal pathology bears significant implications. They support a primary role of non-fibrillar α-syn in early axonal injury. They also underscore the potential relevance of our experimental model to pathogenetic processes in Parkinson's disease since, in a recent report, neuritic accumulation of PLA-positive oligomeric α-syn was suggested to be an early pathological feature of Parkinson's disease brain (Roberts *et al.*, 2015).

The readiness of monomeric and/or oligomeric human α-syn to pass from one neuron to another and propagate within the mouse brain, as indicated by our present findings, is in line with results of an earlier work by Rey *et al.* (2013). In this previous study, different molecular species of human α-syn, i.e. monomeric, oligomeric or fibrillar, were directly injected into the mouse olfactory bulb; monomeric and oligomeric, but not fibrillar α-syn were shown to rapidly and efficiently diffuse along olfactory bulb-connected neuronal pathways. Important differences can instead be noted between results of this current study and features that characterize other models of α-syn propagation in which pathological forms of the protein are directly inoculated into the brain (Luk *et al.*, 2012*a*, *b*; Masuda-Suzukake *el al.*, 2013; Sacino *et al.*, 2013; Recasens *et al.*, 2014). Taking these differences into consideration, one could conclude that long-distance diffusion of α-syn occurs through at least two mechanisms. One of these mechanisms involves inter-neuronal transfer of non-fibrillar protein that diffuses via axonal projections and directly damages these recipient neurons; trans-synaptic passage, axonal propagation and pathology are seemingly lessened when interactions between human and mouse α-syn occur. The second paradigm of protein spreading is triggered by exposure to insoluble α-syn and characterized by pathological accumulation of Thioflavin S-positive fibrillar aggregates. Under these experimental conditions, propagation appears to require expression of endogenous α-syn that may change conformation and become aggregated due to the seeding properties of a pathological form of the protein (Guo and Lee, 2014).

It could be speculated that different mechanisms of α-syn diffusion may play distinct roles under varying pathophysiological conditions. On the other hand, they may not necessarily represent diverging pathological pathways but act in sequence or synergistically during neurodegenerative processes. For example, highly mobile oligomeric forms of the protein, which may be predominantly accumulated at early pathological stages, could later acquire seeding properties that would fuel aggregation reactions, promote fibrillation and give rise to the deposition of intra-neuronal inclusions. Fibril formation may also signify progression toward a more aggressive neurotoxicity

(Peelaerts *et al.*, 2015). Alternatively or in addition, it is conceivable that initial build-up of oligomeric α-syn may predispose to secondary toxic 'hits' (e.g. oxidative stress and impairment of protein degradation pathways) that would induce seeding-competent conformational changes and trigger more advanced aggregate pathology.

Acknowledgements

We thank Dr Sarah A. Jewell for her valuable comments on the data and manuscript, Dr Bettina Winzen-Reichert, Ms. Franziska Hesse and Ms. Laura Jakobi for assistance with tissue preparations, and Dr Ireen Koenig (DZNE Light Microscope Facility) for assistance with image analysis.

Funding

This work was supported by the Paul Foundation, the Backus Foundation and the Centres of Excellence in Neurodegeneration Research (CoEN).

Supplementary material

Supplementary material is available at *Brain* online.

References

Abeliovich A, Schmitz Y, Fariñas I, Choi-Lundberg D, Ho WH, Castillo PE, et al. Mice lacking α-synuclein display functional deficits in the nigrostriatal dopamine system. Neuron 2000; 25: 239–52.

Angot E, Brundin P. Dissecting the potential molecular mechanisms underlying α-synuclein cell-to-cell transfer in Parkinson's disease. [Review]. Parkinsonism Relat Disord 2009; 15: 143–7.

Angot E, Steiner JA, Hansen C, Li JY, Brundin P. Are synucleinopathies prion-like disorders? [Review]. Lancet Neurol 2010; 9: 1128–38.

Barceló-Coblijn G, Golovko MY, Weinhofer I, Berger J, Murphy EJ. Brain neutral lipids mass is increased in α-synuclein gene-ablated mice. J Neurochem 2007; 101: 132–41.

Blättler T, Brandner S, Raeber AJ, Klein MA, Voigtländer T, Weissmann C, et al. PrP-expressing tissue required for transfer of scrapie infectivity from spleen to brain. Nature 1997; 389: 69–73.

Braak H, Del Tredici K, Rüb U, de Vos RA, Jansen Steur EN, Braak E. Staging of brain pathology related to sporadic Parkinson's disease. Neurobiol Aging 2003a; 24: 197–211.

Braak H, Rüb U, Gai WP, Del Tredici K. Idiopathic Parkinson's disease: possible routes by which vulnerable neuronal types may be subject to neuroinvasion by an unknown pathogen. J Neural Transm 2003b; 110: 517–36.

Cabin DE, Gispert-Sanchez S, Murphy D, Auburger G, Myers RR, Nussbaum RL. Exacerbated synucleinopathy in mice expressing A53T SNCA on a Snca null background. Neurobiol Aging 2005; 26: 25–35.

Danzer KM, Haasen D, Karow AR, Moussaud S, Habeck M, Giese A, et al. Different species of α-synuclein oligomers induce calcium influx and seeding. J Neurosci 2007; 27: 9220–32.

Desplats P, Lee HJ, Bae EJ, Patrick C, Rockenstein E, Crews L, et al. Inclusion formation and neuronal cell death through neuron-to-neuron transmission of α-synuclein. Proc Natl Acad Sci USA 2009; 106: 13010–5.

Freundt EC, Maynard N, Clancy EK, Roy S, Bousset L, Sourigues Y, et al. Neuron-to-neuron transmission of α-synuclein fibrils through axonal transport. Ann Neurol 2012; 72: 517–24.

Galvagnion C, Buell AK, Meisl G, Michaels TC, Vendruscolo M, Knowles TP, et al. Lipid vesicles trigger α-synuclein aggregation by stimulating primary nucleation. Nat Chem Biol 2015; 11: 229–34.

Guo JL, Lee VM. Cell-to-cell transmission of pathogenic proteins in neurodegenerative diseases. [Review]. Nat Med 2014; 20: 130–8.

Halliday G, Lees A, Stern M. Milestones in Parkinson's disease–clinical and pathologic features. [Review]. Mov Disord 2011; 26: 1015–21.

Hashimoto M, Rockenstein E, Mante M, Crews L, Bar-On P, Gage FH, et al. An antiaggregation gene therapy strategy for Lewy body disease utilizing beta-synuclein lentivirus in a transgenic model. Gene Ther 2004; 11: 1713–23.

Kalia M, Sullivan JM. Brainstem projections of sensory and motor components of the vagus nerve in the rat. J Comp Neurol 1982; 211: 248–65.

Kovacs GG, Wagner U, Dumont B, Pikkarainen M, Osman AA, Streichenberger N, et al. An antibody with high reactivity for disease-associated α-synuclein reveals extensive brain pathology. Acta Neuropathol 2012; 124: 37–50.

Lee BR, Kamitani T. Improved immunodetection of endogenous α-synuclein. PLoS One 2011; 6: 23939.

Lee HJ, Patel S, Lee SJ. Intravesicular localization and exocytosis of α-synuclein and its aggregates. J Neurosci 2005; 25: 6016–24.

Lee HJ, Suk JE, Bae EJ, Lee JH, Paik SR, Lee SJ. Assembly-dependent endocytosis and clearance of extracellular α-synuclein. Int J Biochem Cell Biol 2008; 40: 1835–49.

Leslie RA, Gwyn DG, Hopkins DA. The central distribution of the cervical vagus nerve and gastric afferent and efferent projections in the rat. Brain Res Bull 1982; 8: 37–43.

Loeb JE, Cordier WS, Harris ME, Weitzman MD, Hope TJ. Enhanced expression of transgenes from adeno-associated virus vectors with the woodchuck hepatitis virus posttranscriptional regulatory element: implications for gene therapy. Hum Gene Ther 1999; 10: 2295–305.

Luk KC, Kehm VM, Zhang B, O'Brien P, Trojanowski JQ, Lee VM. Intracerebral inoculation of pathological α-synuclein initiates a rapidly progressive neurodegenerative α-synucleinopathy in mice. J Exp Med 2012a; 209: 975–86.

Luk KC, Kehm V, Carroll J, Zhang B, O'Brien P, Trojanowski JQ, et al. Pathological α-synuclein transmission initiates Parkinson-like neurodegeneration in nontransgenic mice. Science 2012b; 338: 949–53.

Masuda-Suzukake M, Nonaka T, Hosokawa M, Oikawa T, Arai T, Akiyama H, et al. Prion-like spreading of pathological α-synuclein in brain. Brain 2013; 136: 1128–38.

Mougenot AL, Nicot S, Bencsik A, Morignat E, Verchère J, Lakhdar L, et al. Prion-like acceleration of a synucleinopathy in a transgenic mouse model. Neurobiol Aging 2012; 33: 2225–8.

Nemani VM, Lu W, Berge V, Nakamura K, Onoa B, Lee MK, et al. Increased expression of α-synuclein reduces neurotransmitter release by inhibiting synaptic vesicle reclustering after endocytosis. Neuron 2010; 65: 66–79.

Odekunle A, Bower AJ. Brainstem connections of vagal afferent nerves in the ferret: an autoradiographic study. J Anat 1985; 140: 461–9.

Paxinos G, Franklin KBJ. The mouse brain in stereotaxic coordinates. London: Academic Press; 2001.

Peelaerts W, Bousset L, Van der Perren A, Moskalyuk A, Pulizzi R, Giugliano M, et al. α-Synuclein strains cause distinct synucleinopathies after local and systemic administration. Nature 2015; 522: 340–4.

Prasad K, Tarasewicz E, Strickland PA, O'Neill M, Mitchell SN, Merchant K, et al. Biochemical and morphological consequences

of human α-synuclein expression in a mouse α-synuclein null background. Eur J Neurosci 2011; 33: 642–56.

Prots I, Veber V, Brey S, Campioni S, Buder K, Riek R, et al. α-Synuclein oligomers impair neuronal microtubule-kinesin interplay. J Biol Chem 2013; 288: 21742–54.

Recasens A, Dehay B, Bové J, Carballo-Carbajal I, Dovero S, Pérez-Villalba A, et al. Lewy body extracts from Parkinson disease brains trigger α-synuclein pathology and neurodegeneration in mice and monkeys. Ann Neurol 2014; 75: 351–62.

Rey NL, Petit GH, Bousset L, Melki R, Brundin P. Transfer of human α-synuclein from the olfactory bulb to interconnected brain regions in mice. Acta Neuropathol 2013; 126: 555–73.

Roberts RF, Wade-Martins R, Alegre-Abarrategui J. Direct visualization of α-synuclein oligomers reveals previously undetected pathology in Parkinson's disease brain. Brain 2015; 138: 1642–57.

Rochet JC, Conway KA, Lansbury PT. Inhibition of fibrillation and accumulation of prefibrillar oligomers in mixtures of human and mouse α-synuclein. Biochemistry 2000; 39: 10619–26.

Sacino AN, Brooks M, McGarvey NH, McKinney AB, Thomas MA, Levites Y, et al. Induction of CNS α-synuclein pathology by fibrillar and non-amyloidogenic recombinant α-synuclein. Acta Neuropathol Commun 2013; 1: 38.

Schindelin J, Arganda-Carreras I, Frise E, Kaynig V, Longair M, Pietzsch T, et al. Fiji: an open-source platform for biological-image analysis. Nat Methods 2012; 9: 676–82.

Specht CG, Schoepfer R. Deletion of the α-synuclein locus in a subpopulation of C57BL/6J inbred mice. BMC Neurosci 2001; 2:11.

Spillantini MG, Schmidt ML, Lee VM, Trojanowski JQ, Jakes R, Goedert M. α-Synuclein in Lewy bodies. Nature 1997; 388: 839–40.

Tu PH, Galvin JE, Baba M, Giasson B, Tomita T, Leight S, et al. Glial cytoplasmic inclusions in white matter oligodendrocytes of multiple system atrophy brains contain insoluble α-synuclein. Ann Neurol 1998; 44: 415–22.

Ulusoy A, Rusconi R, Pérez-Revuelta BI, Musgrove RE, Helwig M, Winzen-Reichert B, et al. Caudo-rostral brain spreading of α-synuclein through vagal connections. EMBO Mol Med 2013; 5: 1051–9.

Ulusoy A, Musgrove RE, Rusconi R, Klinkenberg M, Helwig M, Schneider A, et al. Neuron-to-neuron α-synuclein propagation in vivo is independent of neuronal injury. Acta Neuropathol Commun 2015; 3: 13.

Uversky VN, Eliezer D. Biophysics of Parkinson's disease: structure and aggregation of α-synuclein. [Review]. Curr Protein Pept Sci 2009; 10: 483–99.

Vaikath NN, Majbour NK, Paleologou KE, Ardah MT, van Dam E, van de Berg WD, et al. Generation and characterization of novel conformation-specific monoclonal antibodies for α-synuclein pathology. Neurobiol Dis 2015; 79: 81–99.

Vargas KJ, Makani S, Davis T, Westphal CH, Castillo PE, Chandra SS. Synucleins regulate the kinetics of synaptic vesicle endocytosis. J Neurosci 2014; 34: 9364–76.

Supplementary Table 1 List of primary antibodies used in this study

Antibody	Reactivity	Host	Use	Source	Dilution
syn211	human α-syn	mouse	histology, PLA	Merck Millipore	IF: 1:6,000[1] BM: 1:50,000[1]
4B12	human α-syn	mouse	western blot	GeneTex	1:500
11D12	human α-syn	mouse	ELISA	in house	1:1,000
D37A6	mouse α-syn	rabbit	PLA	Cell Signaling	–
Syn-140	α-syn (human + mouse)	sheep	ELISA	in house	0.1 µl/ml
FL-140	α-syn (human + mouse)	rabbit	ELISA	Santa Cruz	1:5,000
AB5038P	α-syn (human + mouse)	rabbit	histology	Merck Millipore	1:400
C-20	α-syn (human + mouse)	rabbit	histology	Santa Cruz	1:1,000
Syn-F1	fibrillar α-syn	mouse	histology	in house	1:1,000
Syn-F2	fibrillar α-syn	mouse	histology	in house	1:500
Syn-O1	oligomeric + fibrillar α-syn	mouse	histology	in house	1:1,000
Syn-O2	oligomeric + fibrillar α-syn	mouse	histology	in house	1:2,000
5G4	oligomeric + fibrillar α-syn	mouse	histology	Analytik Jena	1:500
ab6165	β-syn	rabbit	western blot	Abcam	1:500
DM1A	α-tubulin	mouse	western blot	Sigma	1:20,000
ab13970	GFP	chicken	histology	Abcam	1:50,000

[1]IF = immunofluorescence; BM = brightfield microscopy

Supplementary Table 2 Statistical analyses of the counts of hα-syn-positive axons

		0.75 x 10^{13} *vs.* 1.5 x 10^{13} gc/ml					
WT		Pons	cMB	rMB	FB1	FB2	FB3
	6 weeks	F(1,21) = 4.989 *P* = 0.0001	F(1,21) = 3.254 *P* = 0.0160	----	----	----	----
	12 weeks	F(1,23) = 4.834 *P* < 0.0001	F(1,23) = 8.044 *P* < 0.0001	F(1,23) = 11.96 *P* = 0.0002	F(1,23) = 22.32 *P* = 0.0183	----	----
−/−		Pons	cMB	rMB	FB1	FB2	FB3
	6 weeks	F(1,20) = 1.586 *P* < 0.0001	F(1,20) = 2.592 *P* = 0.0026	F(1,20) = 1.709 *P* = 0.3307	F(1,20) = 16.83 *P* = 0.0232	----	----
	12 weeks	F(1,17) = 2.668 *P* = 0.0033	F(1,17) = 1.520 *P* < 0.0001	F(1,17) = 2.27 *P* < 0.0001	F(1,17) = 2.657 *P* = 0.0042	F(1,17) = 1.441 *P* < 0.0001	F(1,17) = 24.53 *P* = 0.0010

		6 *vs.* 12 weeks					
0.75 x 10^{13}		Pons	cMB	rMB	FB1	FB2	FB3
	WT	F(1,22) = 0.97 *P* = 0.0047	F(1,22) = 13.20 *P* < 0.0001	----	----	----	----
	−/−	F(1,17) = 5.341 *P* = 0.0007	F(1,17) = 3.154 *P* < 0.0001	F(1,17) = 1.054 *P* < 0.0001	F(1,17) = 94.84 *P* < 0.0001	----	----
1.5 x 10^{13}		Pons	cMB	rMB	FB1	FB2	FB3
	WT	F(1,22) = 1.009 *P* = 0.0039	F(1,22) = 32.64 *P* < 0.0001	F(1,22) = 112.4 *P* < 0.0001	----	----	----
	−/−	F(1,20) = 1.262 *P* < 0.0001	F(1,20) = 1.849 *P* < 0.0001	F(1,20 = 4.088 *P* < 0.0001	F(1,20) = 14.87 *P* < 0.0001	F(1,20) = 33.50 *P* < 0.0001	----

		WT *vs.* −/−					
6 weeks		Pons	cMB	rMB	FB1	FB2	FB3
	0.75x10^{13}	F(1,20) = 3.655 *P* < 0.0001	F(1,20) = 21.11 *P* < 0.0001	----	----	----	----
	1.5 x 10^{13}	F(1,21) = 1.162 *P* < 0.0001	F(1,21) = 16.81 *P* < 0.0001	F(1,21) = 57.22 *P* < 0.0001	----	----	----
12 weeks		Pons	cMB	rMB	FB1	FB2	FB3
	0.75x10^{13}	F(1,19) = 37.37 *P* < 0.0001	F(1,19) = 5.957 *P* < 0.0001	F(1,19) = 12.83 *P* < 0.0001	F(1,19) = 94.83 *P* < 0.0001	----	----
	1.5 x 10^{13}	F(1,21) = 1.479 *P* < 0.0001	F(1,21) = 1.050 *P* < 0.0001	F(1,21) = 2.081 *P* < 0.0001	F(1,21) = 8.225 *P* < 0.0001	F(1,21) = 18.93 *P* < 0.0001	----

These comparisons of the effects of AAV titers, time points post AAV injection and presence (WT mice) *vs.* absence (−/− mice) of endogenous α-syn relate to data illustrated in Fig. 3.

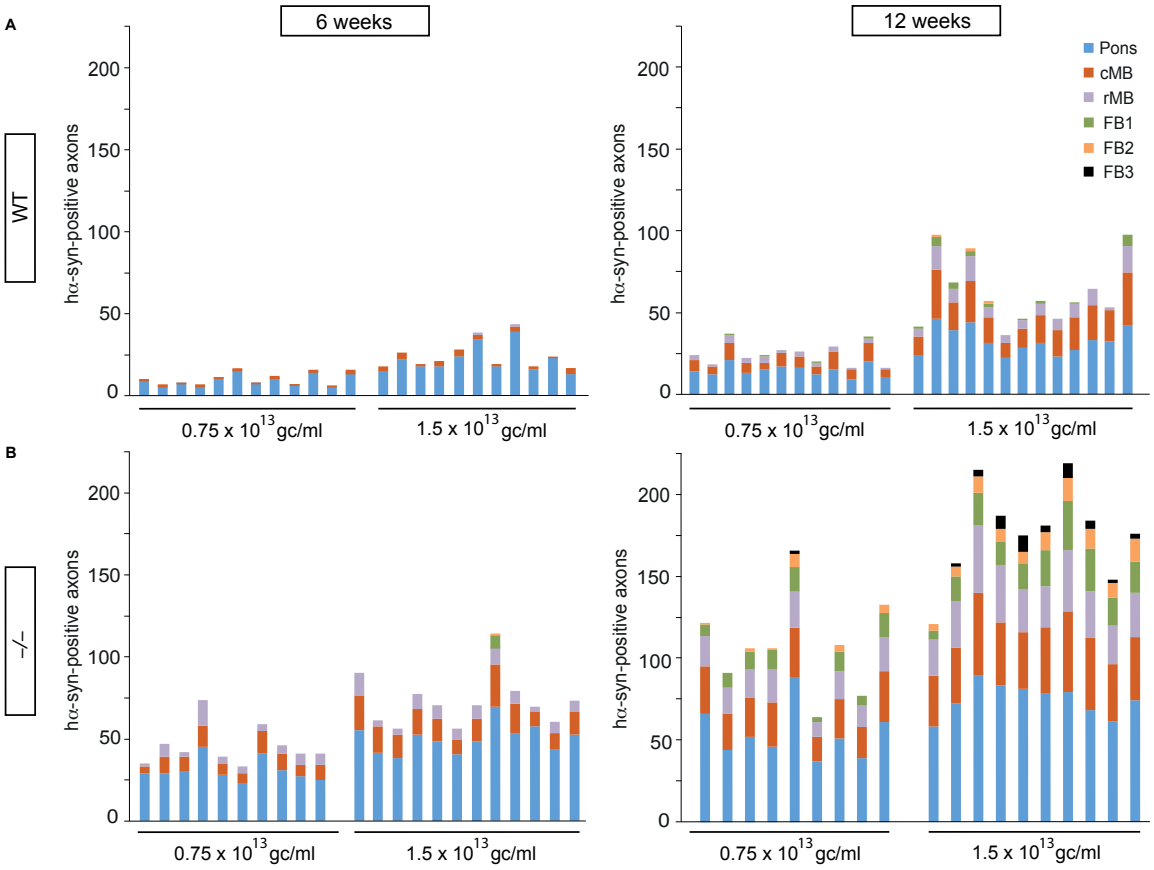

Supplementary figure 1. Counts of hα-syn-positive axons in individual mice injected with AAVs. Wild-type (WT, **A**) and α-syn-deficient (–/–, **B**) mice received a single injection of hα-syn-carrying AAVs (0.75 or 1.5 x 10^{13} gc/ml) into the left vagus nerve. Analyses were performed at 6 and 12 weeks post treatment. Tissue was immunostained with an anti-hα-syn antibody, and hα-syn-immunoreactive axons were counted in the left (injected side) hemisphere. Each column represents an individual animal. Stacked values were obtained in the pons (blue), caudal midbrain (brown), rostral midbrain (purple), caudal forebrain (green), middle forebrain (yellow) and rostral forebrain (black).

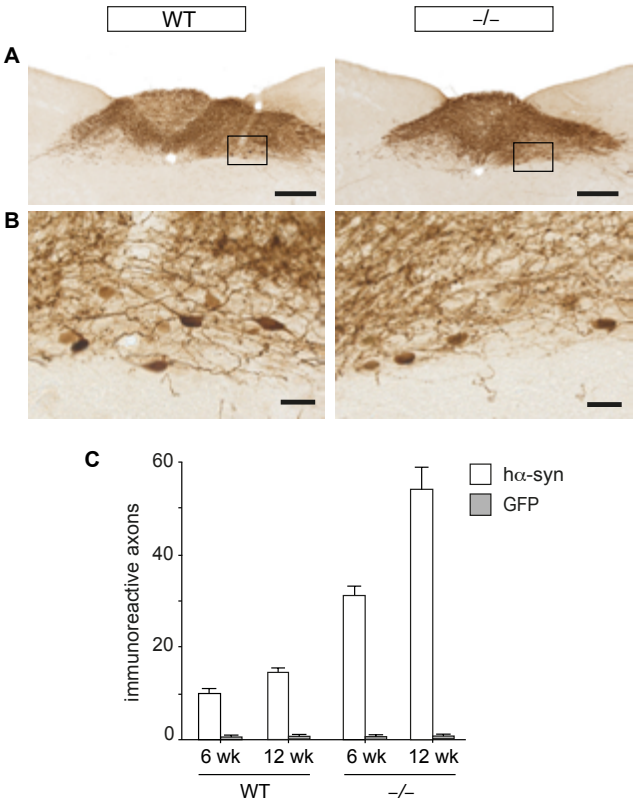

Supplementary figure 2. AAV-induced GFP expression in the mouse MO. (**A**) Mice were killed at 2 weeks after a single injection of GFP-carrying AAVs (1.0 x 10^{13} gc/ml) into the left vagus nerve. Representative sections of the dorsal MO (Bregma: –7.48 mm) were obtained from wild-type (WT) and α-syn-deficient (–/–) mice. Tissue was immunostained with a specific anti-GFP antibody. The square box indicates an area shown in (**B**) at higher magnification. Scale bars in (A) = 200 μm, and in (B) = 25 μm. (**C**) Wild-type (WT) and α-syn-deficient (–/–) mice were killed at 6 and 12 weeks (wk) after a single injection of either hα-syn-carrying (0.75 x 10^{13} gc/ml) or GFP-carrying (1.0 x 10^{13} gc/ml) AAVs into the left vagus nerve. Tissue was immunostained with either an anti-hα-syn or a GFP antibody, and immunoreactive axons were counted in the left (injected side) pons. Data from hα-syn-overexpressing mice are the same as those reported in Figure 3 and are shown here for comparative purposes. Error bars are + SEM.

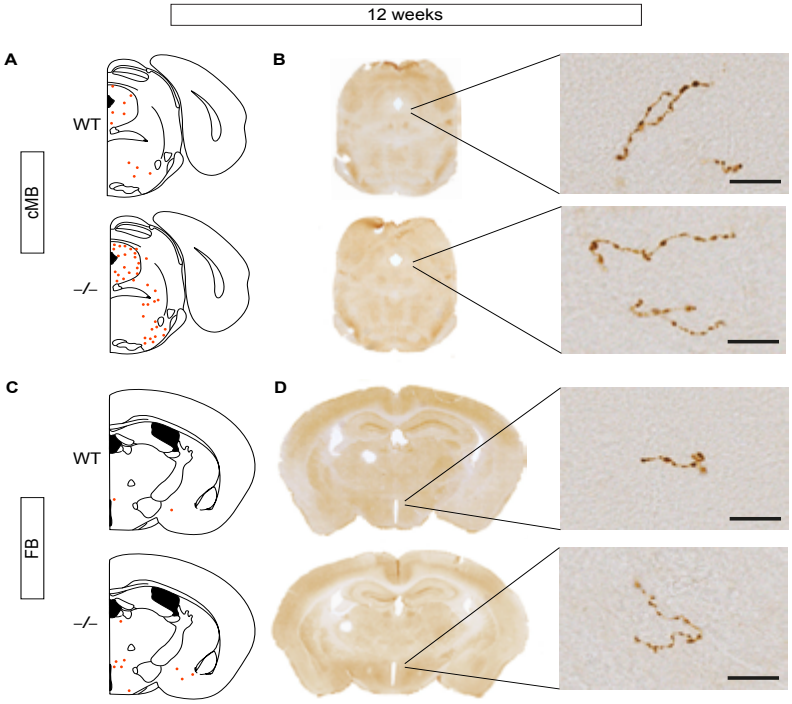

Supplementary figure 3. Hα-syn-immunoreactive axons in the mouse midbrain and forebrain. Wild-type (WT) and α-syn-deficient (–/–) mice received a single injection of hα-syn-carrying AAVs (1.5 x 10^{13} gc/ml) into the left vagus nerve. (**A** and **C**) Schematic plots of the distribution hα-syn-labeled axons in the left (injected side) caudal midbrain (cMB; Bregma: –4.6 mm, A) and forebrain (FB; Bregma: –0.94 mm, **C**) at 12 weeks post AAV injection. (**B** and **D**) Representative sections of the left cMB and FB were obtained from mice sacrificed at 12 weeks post treatment. Higher magnification images were obtained by z-stacking and show axonal projections in the periaqueductal gray (**B**) and hypothalamus (**D**) immunostained with an anti-hα-syn antibody. Scale bars = 25 μm.

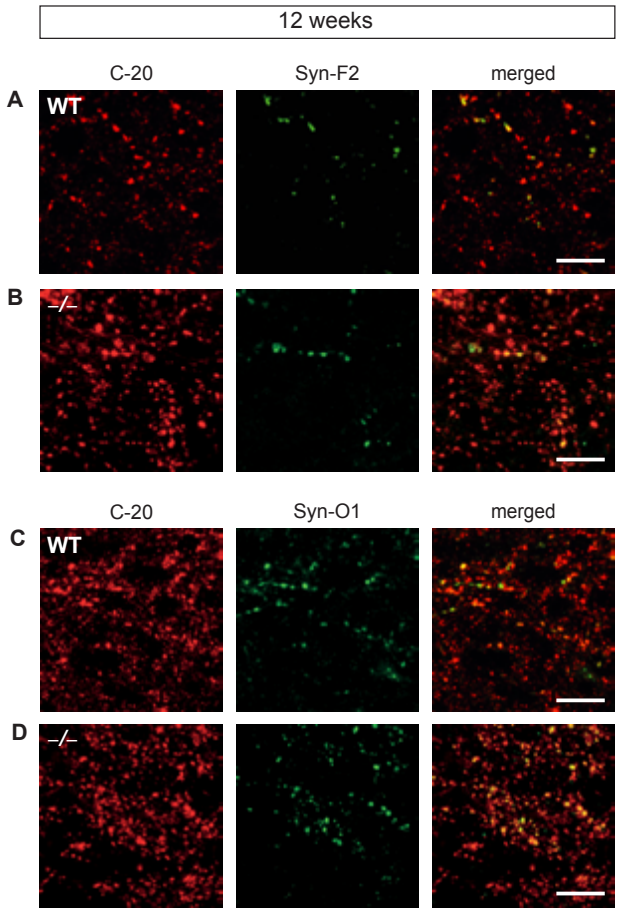

Supplementary figure 4. Immunohistochemical characterization of aggregated α-syn in the DMnX. Wild-type (WT, **A** and **C**) and α-syn-deficient (–/–, **B** and **D**) mice received a single injection of hα-syn-carrying AAVs (1.5 x 10^{13} gc/ml) into the left vagus nerve. Analyses were performed at 12 weeks post treatment. Representative sections of the MO were double-immunostained with either (i) an antibody against total (monomeric and aggregated) α-syn (C-20) plus an antibody that specifically recognizes α-syn fibrils (Syn-F2) (**A** and **B**), or (ii) C-20 plus an antibody that recognizes oligomeric and fibrillar forms of the protein (Syn-O1) (**C** and **D**). Images of the left (injected side) DMnX are shown. Scale bars = 20 μm.

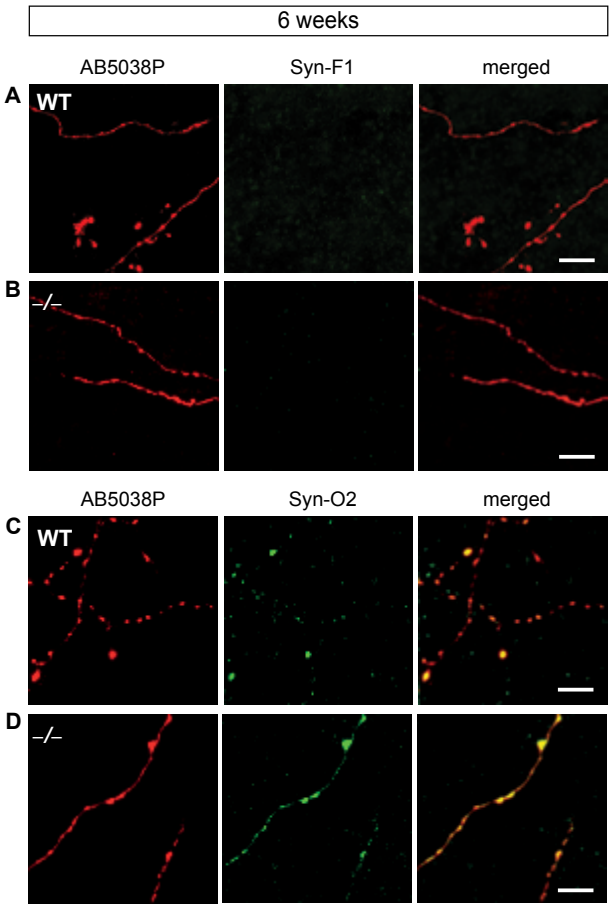

Supplementary figure 5 Immunohistochemical characterization of aggregated α-syn within pontine axons. Wild-type (WT) and α-syn-deficient (–/–) mice received a single injection of hα-syn-carrying AAVs (1.5 x 10^{13} gc/ml) into the left vagus nerve. Analyses were performed at 6 weeks post treatment. (**A**-**D**) Representative sections of the pons were double-immunostained with either (i) an antibody against total (monomeric and aggregated) α-syn (AB5038P) plus an antibody that specifically recognizes α-syn fibrils (Syn-F1) (**A** and **B**), or (ii) AB5038P plus an antibody that recognizes oligomeric and fibrillar forms of the protein (Syn-O2) (**C** and **D**). Labeled axons in the left pons are shown. Scale bars = 10 μm.

Ulusoy, A., Phillips, R.J., Helwig, M., Klinkenberg, M., Powley, T.L., and Di Monte, D.A. (2017). Brain-to-stomach transfer of α-synuclein via vagal preganglionic projections. Acta Neuropathol 133, 381-393.

Objective: PD pathology starts before the manifestation of symptoms, and evidence suggests that the pathology is initiated in the periphery (Braak et al., 2003b). Nevertheless, not all cases likely show the same site of onset and spreading direction (Horsager et al., 2020; Van Den Berge and Ulusoy, 2022). Therefore, we asked if α-syn, once expressed in the central nervous system, can travel to the periphery via interneuronal transfer.

Methods and results: AAV vectors encoding for human α-syn, or GFP were injected into the ventral midbrain of rats to target dopaminergic neurons in the substantia nigra pars compacta. Expression of the exogenous proteins was then evaluated at 2, 6, and 12 months. At every time point, human α-syn was detected in brain sections rostral and caudal to the initial site of overexpression. Due to the robust and widespread transduction, it was impossible to evaluate whether the exogenous protein's presence was due to initial vector transduction or an interneuronal transfer of the exogenous protein. However, caudally, human α-syn was detected within the cholinergic neurons of the DMX. Note that the cholinergic neurons of the DMX do not project to the frontal brain regions but only to the periphery. Therefore, this accumulation cannot be attributed to viral transduction but is due to interneuronal protein transfer. Indeed, in situ hybridization probes designed to detect viral transduction illustrated the lack of viral transduction within the DMX neurons. At later time points (6 and 12 months), human α-syn was found within fibers of the vagus nerve exiting the medulla oblongata, within the vagus nerve itself in the rat neck, and within vagal nerve endings in the stomach wall.

An interesting observation from these experiments was the accumulation of α-syn specifically within vagal efferents projecting to the myenteric plexus but not the afferent neurons, suggesting that there might be vulnerable neuronal populations (e.g., DMX) to take up α-syn and contribute to its spreading.

Conclusions: Our data supported that α-syn can be transferred bi-directionally: from the gut to the brain as well as from the brain to the gut. It appears that the DMX and its efferent projections are central to α-syn long-distance spreading. These studies, therefore, provided experimental evidence that the hypothesis suggesting that the pattern of α-syn pathology progression vary from patient to patient and may be either initiated in the gut or in the brain (Horsager et al., 2020).

Acta Neuropathol
DOI 10.1007/s00401-016-1661-y

ORIGINAL PAPER

Brain-to-stomach transfer of α-synuclein via vagal preganglionic projections

Ayse Ulusoy[1] · Robert J. Phillips[2] · Michael Helwig[1] · Michael Klinkenberg[1] · Terry L. Powley[2] · Donato A. Di Monte[1]

Received: 27 October 2016 / Revised: 16 December 2016 / Accepted: 16 December 2016

Abstract Detection of α-synuclein lesions in peripheral tissues is a feature of human synucleinopathies of likely pathogenetic relevance and bearing important clinical implications. Experiments were carried out to elucidate the relationship between α-synuclein accumulation in the brain and in peripheral organs, and to identify potential pathways involved in long-distance protein transfer. Results of this in vivo study revealed a route-specific transmission of α-synuclein from the rat brain to the stomach. Following targeted midbrain overexpression of human α-synuclein, the exogenous protein was capable of reaching the gastric wall where it was accumulated into preganglionic vagal terminals. This brain-to-stomach connection likely involved intra- and inter-neuronal transfer of non-fibrillar α-synuclein that first reached the medulla oblongata, then gained access into cholinergic neurons of the dorsal motor nucleus of the vagus nerve and finally traveled via efferent fibers of these neurons contained within the vagus nerve. Data also showed a particular propensity of vagal motor neurons and efferents to accrue α-synuclein and deliver it to peripheral tissues; indeed, following its midbrain overexpression, human α-synuclein was detected within gastric nerve endings of visceromotor but not viscerosensory vagal projections. Thus, the dorsal motor nucleus of the vagus nerve represents a key relay center for central-to-peripheral α-synuclein transmission, and efferent vagal fibers may act as unique conduits for protein transfer. The presence of α-synuclein in peripheral tissues could reflect, at least in some synucleinopathy patients, an ongoing pathological process that originates within the brain and, from there, reaches distant organs innervated by motor vagal projections.

Keywords Adeno-associated virus · Enteric nervous system · Parkinson's disease · Rat · Synucleinopathies · Vagus nerve

Introduction

Intraneuronal inclusions containing α-synuclein are hallmarks of Parkinson's disease and other neurological disorders such as dementia with Lewy bodies and multiple system atrophy [11, 22]. In typical Parkinson's disease, α-synuclein pathology is characterized by a progressive caudo-rostral advancement; initial lesions are observed in the lower brainstem and, in particular, the dorsal motor nucleus of the vagus nerve (DMnX) from where α-synuclein pathology spreads toward mesencephalic and ultimately cortical brain regions [6]. An important role of the DMnX and vagal connections in Parkinson's disease pathogenesis is further suggested by findings showing accumulation of α-synuclein deposits in the gut; this accumulation followed a pattern that matched the distribution of preganglionic terminals of DMnX-derived vagal efferents [2]. It has been hypothesized that the pathological process of Parkinson's disease, perhaps mediated by toxic α-synuclein species, may proceed from distant nerve endings in the gut toward the brain or, vice versa, from the

Electronic supplementary material The online version of this article (doi:10.1007/s00401-016-1661-y) contains supplementary material, which is available to authorized users.

✉ Donato A. Di Monte
donato.dimonte@dzne.de

[1] German Center for Neurodegenerative Diseases (DZNE), Sigmund-Freud-Strasse 27, 53127 Bonn, Germany

[2] Department of Psychological Sciences, Purdue University, 703 Third Street, West Lafayette, IN 47907-2081, USA

Published online: 23 December 2016

DMnX to the enteric nervous system following the course of the vagus nerve [11]. It has also been proposed that long, unmyelinated axons, such as those originating from DMnX neurons, may be particularly vulnerable to α-synuclein transfer and its pathological accumulation [6].

Several experimental studies in animal models support the ability of α-synuclein to move efficiently throughout the brain via intra- and inter-neuronal protein transmission [9, 23]. Some of these investigations have shown that α-synuclein can advance caudo-rostrally from the gastrointestinal tract to the brain and from lower to higher brain regions [12, 13, 15, 25]. No direct evidence to date, however, supports the ability of α-synuclein to travel long-distance in the opposite direction, from the brain parenchyma to peripheral nerve endings. Similarly, the hypothesis that distinct neuronal populations and, in particular, visceromotor vagal neurons, may contribute to a greater degree to the progression of α-synuclein pathology remains unsubstantiated from the experimental standpoint. Results of the present study provide important new clues on the central-to-peripheral and route-specific transmission of α-synuclein. Data reveal that viral vector-mediated overexpression of human α-synuclein (hα-synuclein) in the rat midbrain triggers its advancement via the vagus nerve and results in its pathological accumulation in the stomach wall. Interestingly, this accumulation targeted preganglionic vagal terminals while it did not occur within viscerosensory gastric afferents, pointing to a preferential route of protein transmission via neurons, namely DMnX cells and their projections, that are particularly able to accrue and deliver α-synuclein.

Materials and methods

Viral vectors

Recombinant adeno-associated viral vectors (AAVs; serotype 2 genome and serotype 6 capsid) were used for transgene expression of hα-synuclein or green fluorescent protein (GFP; Vector Biolabs). Expression, driven by the human *SYN1* promoter, was enhanced using woodchuck hepatitis virus post-transcriptional regulatory element (WPRE) and a polyadenylation signal sequence.

Animals and surgical procedure

Experimental procedures involving animals were approved by the State Agency for Nature, Environment and Consumer Protection in North Rhine Westphalia. Experiments were performed in female Sprague-Dawley rats (200–225 g; Charles River) housed under a 12-h light/12-h dark cycle with free access to food and water. During surgical procedures, rats were anesthetized with 2% isoflurane mixed with O_2 and N_2O. Each animal received a single unilateral injection of AAV solution (1.0×10^{13} genome copies/ml) either (1) into the left vagus nerve in the neck (2 µl), or (2) intraparenchymally, into the right ventral mesencephalon immediately dorsal to the substantia nigra pars compacta (1 µl). Vagal injections were made according to previously described protocols [25]. To target the substantia nigra, the following stereotaxic coordinates were used with a tooth bar setting of −2.3: 5.0 mm posterior and 2.0 mm lateral to bregma, and 7.1 mm ventral to dura mater. The injection was made at a rate of 0.4 µl/min using a Hamilton syringe fitted to a glass capillary. The capillary was left in position for 5 min before being withdrawn.

Tissue preparation

Animals were killed with pentobarbital. Brains used for in situ hybridization were snap frozen on dry ice and stored at −80 °C. At the time of analysis, they were cryosectioned (14 µm) and then mounted on polysine object slides. For histological analyses, rats were perfused through the ascending aorta first with physiological saline solution. At this time, a cannula was inserted via oral gavage to inflate the stomach with 10 ml saline. The perfusion continued using 4% ice-cold paraformaldehyde in 0.1 M phosphate buffer. The following organs/tissues were collected: brain, vagus nerve (including the nodose ganglion) in the rat neck and stomach. Brains and vagus nerves were post-fixed in 4% paraformaldehyde solution for 24 h and cryopreserved in 25% (w/v) sucrose solution. Coronal sections (40 µm) throughout the brain were cut using a freezing microtome, while each vagus nerve was sectioned (16 µm) longitudinally using a cryostat. Stomachs were post-fixed but not cryopreserved. They were divided into dorsal and ventral whole mounts by cutting along the greater and lesser curvatures.

Assays

All analyses, as described in the next paragraphs, were performed by investigators blinded to treatment/experimental group.

Brightfield microscopy

Medulla oblongata

Free-floating sections were quenched by incubations in a mixture of 3% H_2O_2 and 10% methanol in Tris-buffered saline (pH 7.6). Non-specific binding sites were blocked by incubations in Tris-buffered saline with 0.25% Triton X-100 containing 5% normal serum. Samples were

kept overnight at room temperature in a solution (Tris-buffered saline with 1% BSA and 0.25% Triton X-100) containing the primary antibody, i.e., mouse anti-hα-synuclein clone syn211 (36-008, Merck Millipore; 1:10 000). Sections were rinsed and incubated (for 1 h at room temperature) in biotinylated secondary antibody solution (Vector Laboratories; 1:200). Following treatment with avidin-biotin-horseradish peroxidase complex (PK 6100; ABC Elite kit, Vector Laboratories), color reaction was developed using a 3,3′-diaminobenzidine (DAB) kit (Vector Laboratories). Sections were mounted on coated slides, dried and coverslipped with Depex (Sigma-Aldrich). Stacked or tiled images collected with 40× or 10× Plan-Apochromat, respectively, were obtained using an IX2 UCB microscope from Olympus equipped with a motorized stage and camera (MBF Biosciences). Stacks were collected at 1 µm intervals, and a single image was generated by deep focus post-processing using Stereo Investigator software (version 9, MBF Biosciences). In a set of analyses, the percent of DMnX neurons overexpressing hα-synuclein was calculated after hα-synuclein-AAV injections into the rat vagus nerve. For these analyses, both the total number of Nissl-stained cells and the number of hα-synuclein-positive neurons was estimated using unbiased stereology [24].

Vagus nerve and nodose ganglion

Sections on slides were quenched and blocked as described above. They were incubated for 48 h at 4 °C in mouse anti-hα-synuclein (syn211; 1:2000) or chicken anti-GFP (ab13970, Abcam; 1:5000) and for 1 h at room temperature in ImmPRESS secondary antibody (Vector Laboratories). Color reaction was developed using a DAB kit. Images were collected using an Axiocam 503 color camera fitted to an Axioscope microscope (Zeiss).

Stomach

The mucosa and submucosa were removed by fine dissection, and the resulting smooth muscle whole mounts were rinsed in PBS followed by a 30-min soak in an endogenous peroxidase block (methanol:3% H_2O_2; 4:1). After additional rinses in PBS, the neuronal population of the myenteric plexus was counterstained with the pan-neuronal marker Cuprolinic Blue (quinolinic phthalocyanine; Polysciences). Whole mounts were then soaked for 5 days in normal serum block (0.5% Triton X-100, 5% normal serum, 2% BSA, and 0.08% Na Azide in PBS) followed by a 24 h soak in antiserum raised against hα-synuclein (syn211; 1:5000) or GFP (ab13970; 1:10 000) in primary diluent (0.3% Triton X-100, 2% normal serum, 2% BSA, and 0.08% Na Azide in PBS). Next, whole mounts were rinsed in PBS and incubated for 2 h in diluent (0.3% Triton X-100, 2% normal serum, and 2% BSA in PBS) with appropriate biotinylated secondary antibody (Vector Laboratories; 1:500). After several more PBS rinses, tissues were incubated for 1 h in avidin-biotin-horseradish peroxidase complex (Vector Laboratories) in PBS. Horseradish peroxidase was reacted with DAB and H_2O_2 in Tris-buffered saline for 3 min to yield a permanent deposit. Finally, stained whole mounts were mounted on gelatin-coated slides, air-dried overnight, dehydrated in an ascending series of alcohols, cleared in two xylene steps, and coverslipped with Cytoseal XYL (Richard-Allen Scientific). Brightfield photomicrographs were acquired using a Leica microscope fitted with a Spot Flex camera that was controlled using Spot Software (V4.7 Advanced Plus; Diagnostic Instruments).

Fluorescent microscopy

Free-floating sections were blocked in 5% horse serum and incubated in 1% BSA with the following primary antibodies raised against: hα-synuclein (syn211; 1:3000), GFP (ab13970; 1:5000), choline acetyltransferase (ChAT) (AB144, Merck Millipore; 1:100), Syn-O2 (1:2000) or Syn-F1 (1:1000). The latter two antibodies, gifts from Dr. O. El-Agnaf, have been previously characterized [26]. Appropriate fluorophore-conjugated secondary antibodies (DyLight 488 and DyLight 594, from Vector Laboratories; Alexa 488 and Alexa 594, from Abcam) (1:400) were used for detection, and samples were mounted and coverslipped using Vectashield mounting medium (Vector Laboratories). Sequential scans were performed with 10× and 63× Plan-Apochromat objectives using either (1) a LSM710NLO confocal laser scanning microscope (Carl Zeiss) with tunable lasers set at 490 and 595 nm, or (2) an IX2 UCB microscope (Olympus) with a DSU spinning disk unit (Olympus), a motorized stage (MBF Biosciences) and an EM-CCD camera (Hamamatsu). As negative controls, tissue sections were processed as described above with the only exception that the primary antibody (e.g., anti-ChAT) was omitted from the initial incubations (Supplementary Figure 1).

Fluorescent in situ hybridization

Samples were processed following a protocol modified from Raj et al. [19]. Twenty-six individual probes (18 bp each) were designed against WPRE and generated with 3′-amino modifications (BioSearch Technologies) coupled to a Quasar 570 fluorophore. Sections were first equilibrated to room temperature, fixed with 4% paraformaldehyde, washed with PBS and stored overnight in 70% ethanol. On the next day, after washing, they were incubated overnight at 37 °C in hybridization buffer containing labeled probes (125 nM) and, when needed, primary

antibodies. The following antibodies were used: anti-hα-synuclein (syn211; 1:1000) and anti-ChAT (AB144; 1:100). After washing, sections for in situ hybridization/immunofluorescence were incubated for 2 h at room temperature in PBS with DyLight 488 and DyLight 649 secondary antibodies (Vector Laboratories; 1:200). Samples were labeled with 4′,6-diamidino-2-phenylindole (5 ng/ml), washed and finally mounted with Vectashield mounting medium (Vector Laboratories). Images were obtained using a Zeiss Observer.Z1 Microscope (Carl Zeiss) equipped with a motorized stage and AxioCam MRm camera (Carl Zeiss). Figures were generated with 20× Plan-Apochromat (NA 0.8) and 63× Plan-Apochomat (NA 1.4) objectives followed by computerized image stitching with ZEN 2 software (Carl Zeiss).

RT-PCR

Samples were obtained from 40-μm fixed tissue sections. The right (injection side) ventral mesencephalon or dorsomedial portion of the medulla oblongata were dissected and pooled from equally spaced sections at Bregma: −4.56 to −6.48 mm or Bregma: −13.68 to −14.64 mm. RNA was extracted using Nucleic Acid Isolation Kit (Ambion). cDNA was synthesized using 100 ng of total RNA (SuperScript® VILO Master Mix, Life Technologies). cDNA was amplified (30 cycles) using Power SYBR® Green (Applied Biosystems) and 0.25 μM primers (Sigma-Aldrich) in a StepOnePlus Real-Time PCR System (Applied Biosystems). Primer pairs matching DNA sequences were: (1) 5′caattccgtggtgttgtcgg forward and 5′caaagggagatccgactcgt reverse (WPRE); (2) 5′aatgaagaaggagccccacag forward and 5′aaggcatttcataagcctcattgtc reverse (hα-synuclein); (3) 5′acgacggcaactacaagacc forward and 5′tcctccttgaagtcgatgcc reverse (GFP); (4) 5′gaccggttctgtcatgtcg forward and 5′acctggttcatcatcactaatcac reverse (hypoxanthine phosphoribosyltransferase 1). RT-PCR products were separated on agarose gels. DNA signals were visualized with Gel Red Nucleic Acid Gel Stain (Biotium) and imaged with InGenius imaging system and GeneSnap software (Syngene).

Results

Efferent and afferent vagal terminals in the gastric wall

The first set of experiments was designed to assess the distribution of hα-synuclein and its accumulation within gastric nerve endings following its overexpression directly in the vagal system. AAVs carrying the DNA for hα-synuclein or GFP were injected into the left vagus nerve in the rat neck with the intent of transducing DMnX cells in the medulla oblongata as well as neuronal cell bodies within vagal ganglia, in particular the nodose ganglion (Fig. 1a, c). In agreement with previously published results [24], approximately 30% of the total DMnX neurons showed robust overexpression of hα-synuclein after vagal injections of hα-synuclein-AAVs (Fig. 1b). Accumulation of the exogenous protein within gastric nerve endings was then assessed in animals killed several months (>6 months) after AAV treatment. Stomach whole mounts consisting of the longitudinal and circular smooth muscle layers encompassing the myenteric plexus were stained with a specific antibody that recognizes human but not rodent α-synuclein [10]. Robust immunoreactivity characterized fibers and nerve endings that, because of their morphology, could be identified as afferent vagal projections originating from neurons of the nodose ganglion [16, 28]. In particular, hα-synuclein was accumulated within intramuscular arrays (IMAs) of rectilinear terminals paralleling smooth muscle fibers and within highly arborizing intraganglionic laminar endings (IGLEs), the two main types of afferent vagal terminals (Fig. 1d, e). Earlier work has also elucidated the morphological features of efferent vagal fibers and nerve endings arising from cell bodies in the DMnX and terminating in the gastric wall [16, 27]. Immunoreactivity for hα-synuclein labeled preganglionic axons that, consistent with these features, formed varicosity-rich telodendria looping around a single neuron or multiple ganglionic cells (Fig. 1f). Similar to treatment with hα-synuclein-carrying AAVs, vagal injections of GFP-AAVs resulted in accumulation of the transduced protein within both viscerosensory and visceromotor projections in the rat stomach wall (data not shown).

Long-distance transmission of human α-synuclein from the brain to the stomach

To determine if α-synuclein was capable of traveling long-distance from the brain to peripheral tissues, hα-synuclein-carrying AAVs were unilaterally (right side) injected into the rat ventral mesencephalon immediately dorsal to the substantia nigra pars compacta. Animals were killed at 2, 6 or 12 months, and the distribution of hα-synuclein throughout the brain was evaluated in tissue sections rostral and caudal to the midbrain. Immunoreactivity for hα-synuclein was observed in sections spanning from the forebrain to the medulla oblongata on the right (AAV-injected) and, to a much smaller extent, the left side of the brain (Fig. 2a). Robust staining characterized regions anatomically connected to the transduced midbrain areas that included the striatum and hypothalamus rostrally, and the locus coeruleus caudally (Fig. 2b, c) [14, 29]. This pattern of protein distribution was already observed at 2 months and persisted at 6 and 12 months post-injection.

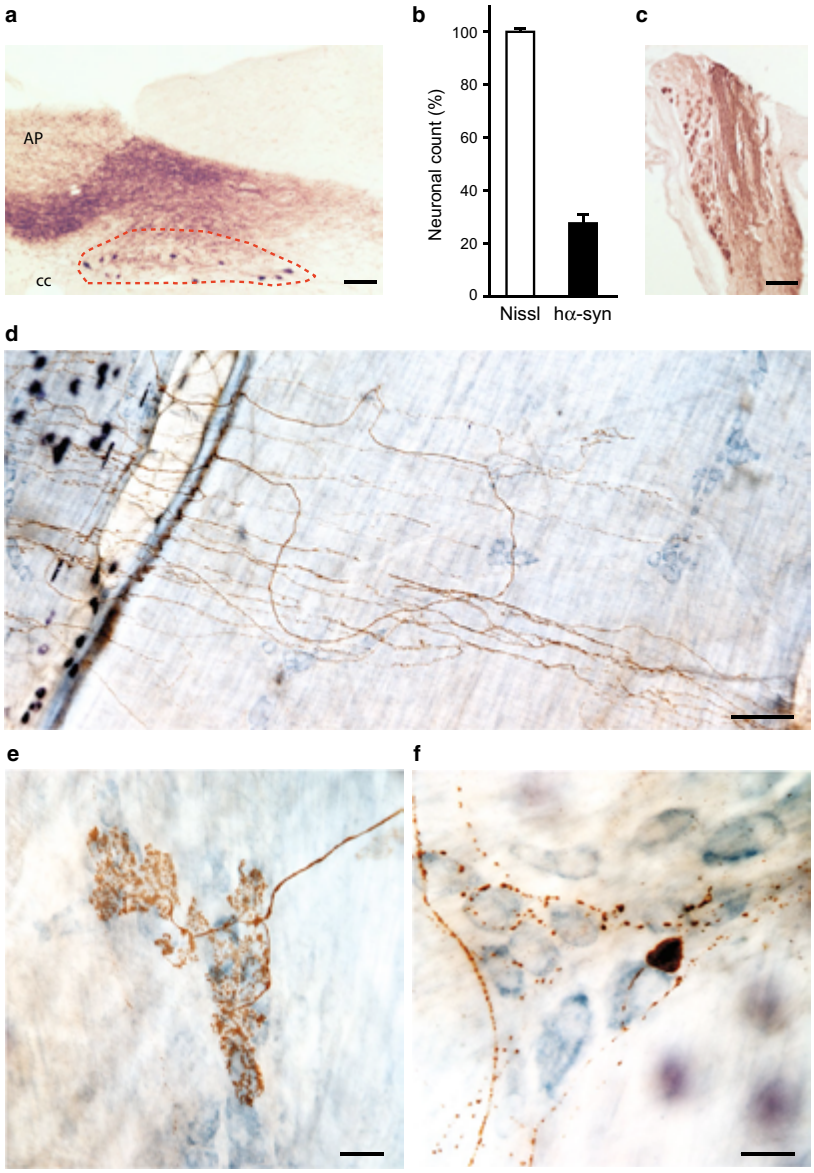

Fig. 1 Accumulation of hα-synuclein in the DMnX, nodose ganglion and gastric wall after injections of hα-synuclein-AAVs into the vagus nerve. **a–c** Rats ($n = 5$) received a single injection of hα-synuclein-carrying AAVs into the left vagus nerve. Analyses were performed at 2–3 weeks post-treatment. **a** A representative image shows a section of the medulla oblongata immunostained with anti-hα-synuclein; the left DMnX is delineated by *dashed lines*, and the area postrema (AP) and central canal (cc) are indicated. *Scale bar* 100 μm. **b** Medulla oblongata sections were used for stereological counting of Nissl-stained neurons (*empty bar*) and hα-synuclein-immunoreactive cells (*solid bar*) in the left DMnX. Values (mean ± SEM) are expressed as percent of the total number of Nissl-stained neurons. **c** The representative image shows neurons robustly labeled with anti-hα-synuclein in a section of the left nodose ganglion. *Scale bar* 100 μm. **d–f** Rats ($n = 5$) were killed 6–12 months after a single injection of hα-synuclein-carrying AAVs into the left vagus nerve. Stomach whole mounts were stained with anti-hα-synuclein and counter-stained with Cuprolinic Blue. Representative images show immuno-reactive fibers and nerve terminals: long intramuscular arrays (IMAs) of rectilinear terminals (**d**), a single vagal afferent terminating as highly arborizing intraganglionic laminar endings (IGLEs) (**e**), and varicosity-rich fibers with morphological features of preganglionic vagal efferents (**f**). *Scale bars* 100 μm in **d**, 25 μm in **e** and 20 μm in **f**

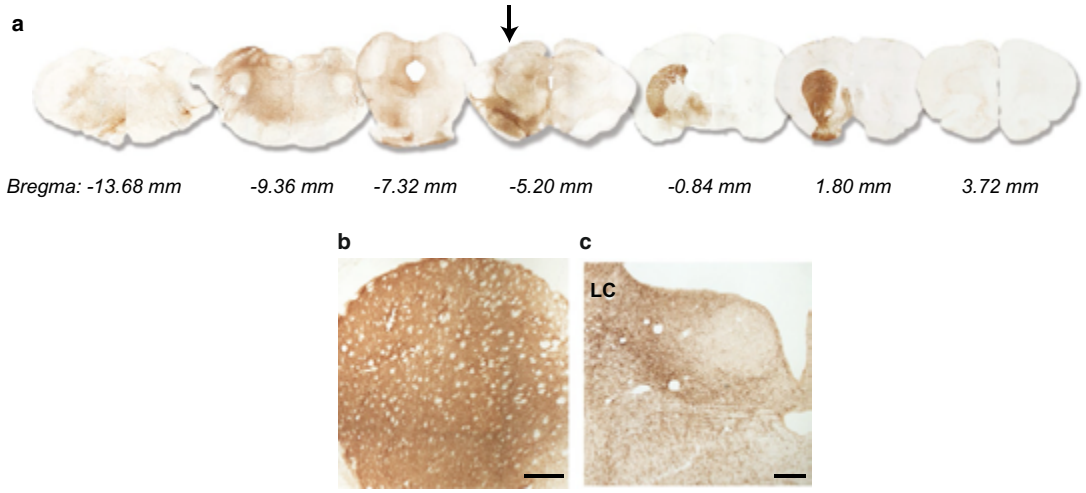

Fig. 2 Widespread brain distribution of hα-synuclein after midbrain AAV injections. Rats received a single intraparenchymal injection of hα-synuclein-AAVs into the right midbrain. **a** Analyses were made in 6 rats killed at 2 months. Representative images show brain sections at different Bregma levels stained with anti-hα-synuclein. A midbrain section containing the substantia nigra is at Bregma −5.20 mm (*arrow*). For illustration purposes, different scale factors were used to resize each section. **b**, **c** Rats ($n \geq 5$/time point) were killed at 2, 6 and 12 months post-treatment. Sections of the forebrain and pons containing the striatum (**b**) and locus coeruleus (LC) (**c**), respectively, were stained with anti-hα-synuclein. Representative images are from an animal killed at 2 months. *Scale bars* 250 μm

Stomach whole mounts of these AAV-injected rats were then assessed for immunohistochemical evidence of the exogenous protein. No immunoreactivity for hα-synuclein was observed in 6 rats killed at 2 months post-AAV injection; in contrast, hα-synuclein-positive axons and terminal varicosities were detected in the myenteric plexus of 5 out of 6 rats and 6 out of 10 animals killed at 6 and 12 months, respectively. Analysis of labeled tissues revealed the presence of markedly swollen axons (Fig. 3a). Clusters of nerve endings containing hα-synuclein encircled individual neurons (Fig. 3b, c, f) or small groups of neurons (Fig. 3d, e) within the ganglia of the plexus. The morphology and distribution of these varicosity-rich fibers were strikingly similar to previous descriptions of anterogradely labeled vagal motor nerve endings immunoreactive for endogenous α-synuclein [16, 27]. Consistent with progressive protein transfer and accumulation, myenteric ganglia with the highest density of robustly labeled terminals were found at the 12-month survival time (Fig. 3d–f). Of note, careful examination of gastric specimens for the presence of hα-synuclein-immunoreactive vagal afferents and viscerosensory terminals yielded negative results at both early and later time points post-AAV injections.

Human α-synuclein reaches nerve terminals in the stomach traveling via the vagus nerve

Accumulation of hα-synuclein within preganglionic vagal terminals of the myenteric plexus strongly suggests that, following its midbrain expression, the exogenous protein may reach peripheral tissues using the vagus nerve as a conduit. To substantiate this conclusion, a portion of the right (ipsilateral to the AAV injections) vagus nerve was collected from the neck of rats killed at 2, 6 and 12 months post-treatment. Examination of longitudinal sections of the Xth nerve stained for hα-synuclein revealed the presence of labeled fibers. Immunoreactive vagal projections were relatively rare and, for this reason, might have remained undetected even after careful evaluation of serial tissue sections. With this caveat in mind, results of our analysis indicated that hα-synuclein was absent in the vagus nerve of rats killed at 2 months ($n = 6$); labeled fibers were instead detected in >50% of nerves collected at either 6 ($n = 6$) or 12 ($n = 7$) months post-treatment (Fig. 4).

Detection of human α-synuclein protein within DMnX neurons in the medulla oblongata

Preganglionic terminals in the stomach wall originate in the DMnX, underscoring the importance that this medullary nucleus may have as a relay center for α-synuclein central-to-peripheral transmission. Experiments were therefore carried out to examine DMnX-containing medullary tissue for the presence of hα-synuclein mRNA and/or protein. Using RT-PCR, amplification reactions with hα-synuclein-hybridizing primers yielded no specific band at 3 weeks nor at 2, 6 and 12 months post-AAV treatment (Fig. 5a shows

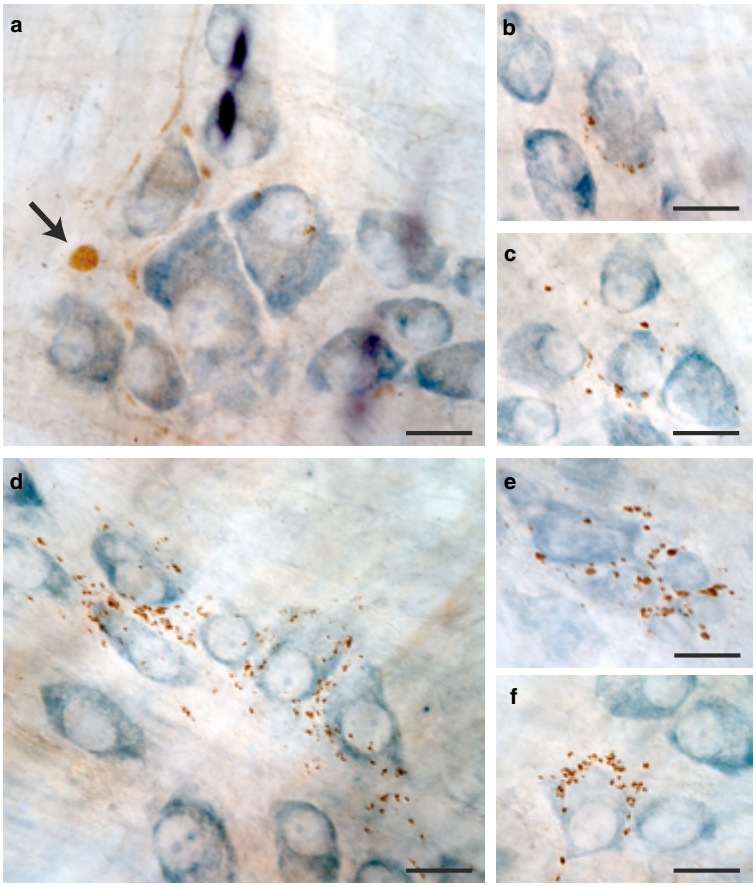

Fig. 3 Human α-synuclein immunoreactivity in the gastric wall after midbrain AAV injections. Rats received a single intraparenchymal injection of hα-synuclein-AAVs into the right midbrain. Stomach whole mounts from animals killed at 6 (**a**–**c**, $n = 6$) or 12 (**d**–**f**, $n = 10$) months post-treatment were stained with anti-hα-synuclein and counterstained with Cuprolinic Blue. Images from 5 of these animals (3 at 6 and 2 at 12 months) show a labeled swollen axon (*arrow* in **a**) and immunoreactive nerve endings around ganglionic cells (**b, c, f**) or groups of cells (**d**, **e**) of the myenteric plexus. *Scale bars* 20 μm

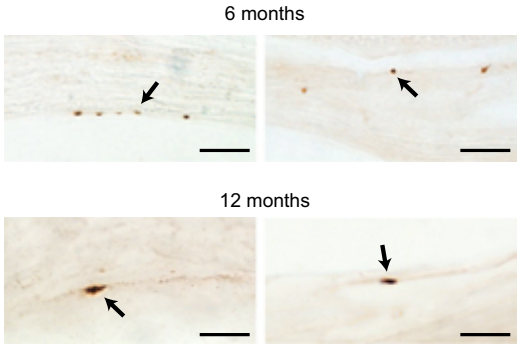

Fig. 4 Fibers of the vagus nerve containing hα-synuclein. Longitudinal sections of right vagus nerves collected from the rat neck at 6 ($n = 6$) or 12 ($n = 7$) months post-AAV-injection were stained with anti-hα-synuclein. Images from 4 of these animals, 2 at 6 and 2 at 12 months, show labeled portions of vagal fibers (*arrows*). *Scale bars* 10 μm

data at the 2-month time point). Samples were also analyzed for evidence of other AAV-derived products and, in particular, WPRE (an enhancer element incorporated into the AAV genome) mRNA. RT-PCR measurements showed lack of WPRE expression in specimens from the dorsal medulla oblongata (Fig. 5a). Similarly, WPRE mRNA was not detectable within cholinergic DMnX neurons using a highly sensitive fluorescent in situ hybridization technique coupled with immunohistochemistry [19]. Medullary tissue sections were probed with multiple WPRE-targeting oligonucleotides, yet no hybridization signal was present at either early or later time points (images at 2 months are shown in Fig. 5b, c). In situ hybridization was also carried out on tissue sections from the higher (Bregma −4.92 and −5.64 mm) and lower (Bregma −8.16 mm) midbrain and from the pons (Bregma −9.00 mm). In high-midbrain sections, neuronal cell bodies containing WPRE mRNA occupied the entire substantia nigra pars compacta (Fig. 5d), and transduced neurons were also scattered within areas

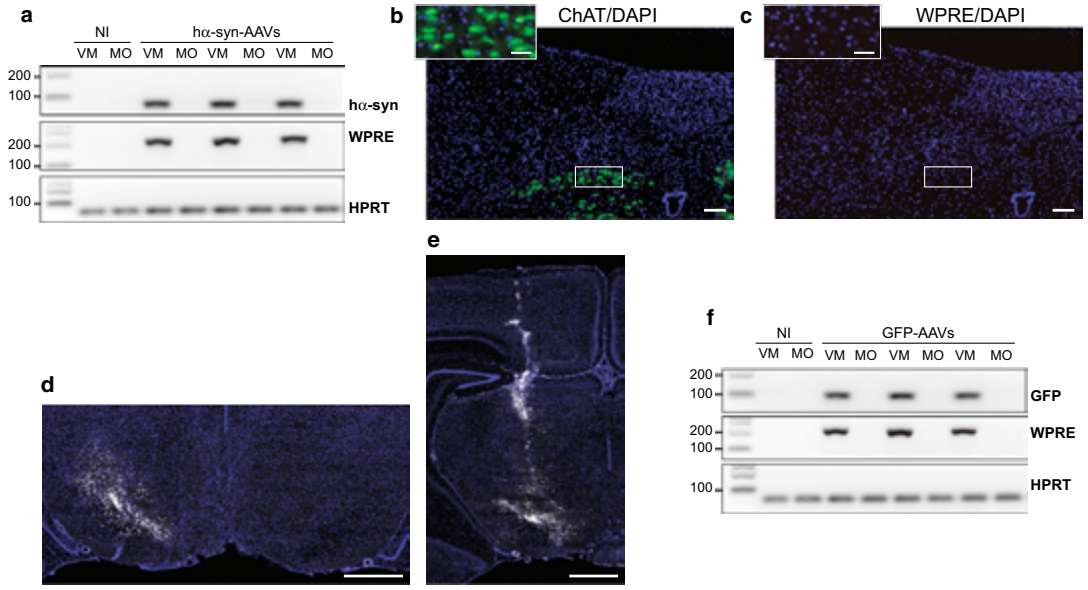

Fig. 5 Markers of transduction in the medulla oblongata and midbrain of AAV-injected rats. **a** Rats ($n = 6$) received midbrain injections of hα-synuclein-AAVs and were killed after 2 months. Non-injected (NI) animals provided control samples. Hα-synuclein (hα-syn), WPRE or hypoxanthine phosphoribosyltransferase 1 (HPRT) mRNA was assayed by RT-PCR in samples of the right (AAV-injected) ventral mesencephalon (VM) or dorso-medial medulla oblongata (MO). Specific bands were at 79 (hα-syn), 204 (WPRE), and 61 (HPRT) bp. **b, c** Medulla oblongata sections from rats injected with hα-synuclein-AAVs and killed at 2 months ($n = 4$) were processed for fluorescent in situ hybridization coupled with immunofluorescence to detect WPRE mRNA (*white*), ChAT (*green*) and DAPI (*blue*). Representative images show ChAT-positive cells (**b**) in the absence (no white signal) of WPRE hybridization (**c**). *Insets* show higher magnification images of the right DMnX. *Scale bars* 100 μm (*large panels*) and 50 μm (*insets*). **d, e** mRNA expression of WPRE (*white*) was evaluated in 4 rats killed 3 weeks after a single midbrain AAV injection. Midbrain sections were processed for fluorescent in situ hybridization and DAPI (*blue*). Representative images show right (AAV-injected) and left hemispheres (**d** Bregma = −5.64 mm) or only the right hemisphere (**e** Bregma = −4.92 mm). *Scale bars* 1 mm. **f** Rats ($n = 5$) received midbrain injections of GFP-AAVs and were killed after 2 months. Non-injected (NI) animals provided control samples. GFP, WPRE, or hypoxanthine phosphoribosyltransferase 1 (HPRT) mRNA was assayed by RT-PCR in samples of the right ventral mesencephalon (VM) or dorso-medial medulla oblongata (MO). Specific bands were at 94 (GFP), 204 (WPRE), and 61 (HPRT) bp

near the AAV injection site and needle track (Fig. 5e). No hybridization signal was instead detected in low-midbrain and pontine sections, further indicating lack of transmission/diffusion of viral particles toward brain regions distant to the mesencephalic target of AAV injections (Supplementary Figure 2).

Despite the absence of hα-synuclein mRNA and markers of AAV transduction in the lower brainstem, immunoreactivity for the exogenous protein was detected in the medulla oblongata and the DMnX; progressive burden was indicated by a time-dependent increase in axons loaded with hα-synuclein at 2, 6 and 12 months (Fig. 6a, b). Sections of the medulla oblongata containing the DMnX were also double-stained for ChAT and hα-synuclein (Fig. 6c–f). The presence of co-labeled DMnX projections supported accumulation of hα-synuclein within cholinergic vagal efferents (Fig. 6e; Supplementary Figure 3). Other DMnX axons were immunoreactive for hα-synuclein but not ChAT and likely represented neuronal projections passing through or reaching the DMnX from higher brain regions (Fig. 6f; Supplementary Figure 3). In caudal section of the medulla oblongata (e.g., Bregma –14.04 mm), ChAT-positive axons crossed the reticular formation and converged ventrolaterally to form the vagus nerve (Fig. 7a, b). Interestingly, at 6 and 12 but not 2 months post-AAV injection, a few of these intramedullary vagal fibers showed co-immunoreactivity for hα-synuclein (Fig. 7a, b).

Medullary tissue from AAV-injected rats was also stained with two conformation-specific antibodies, one that reacts with mature α-synuclein fibrils (Syn-F1) and the other recognizing both late (fibrils) and earlier (oligomers) forms of aggregated α-synuclein (Syn-O2) [12, 26]. Co-staining with Syn-F1 and ChAT very rarely identified Syn-F1-immunoreactive punctae within cholinergic vagal

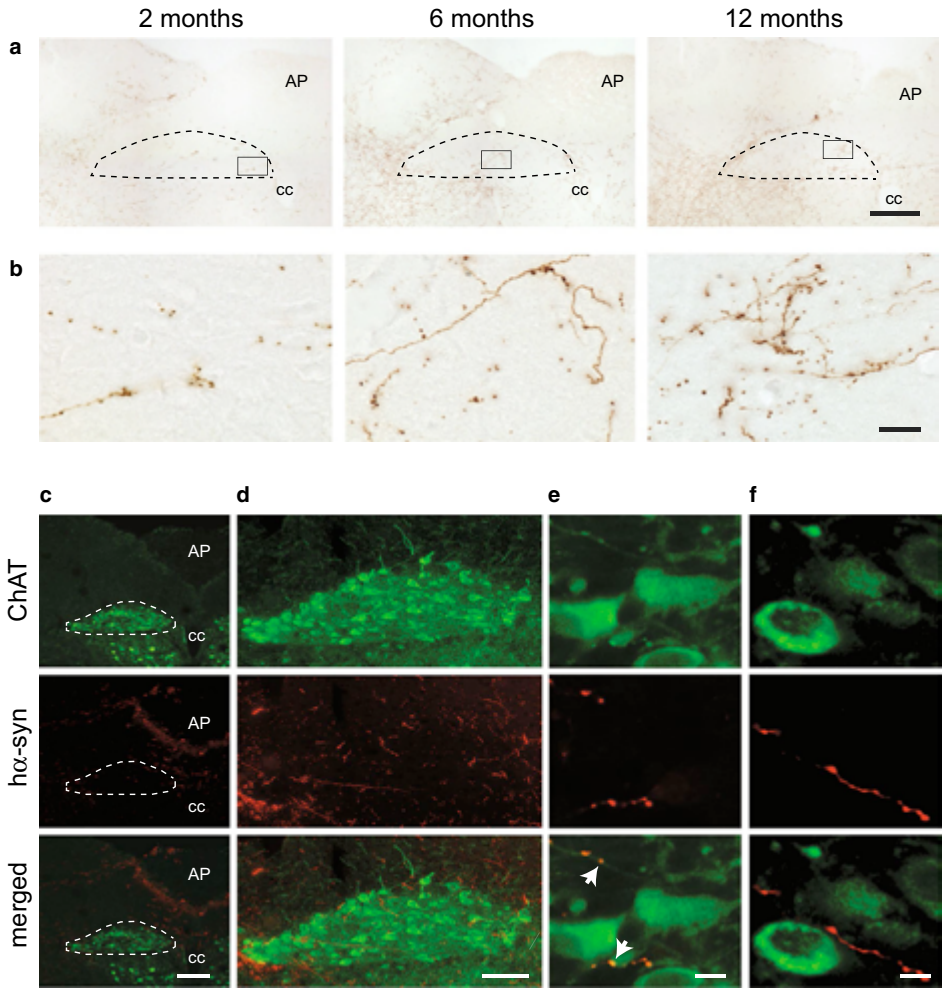

Fig. 6 Human α-synuclein protein in the DMnX of AAV-injected rats. **a**, **b** Medulla oblongata sections from rats injected with hα-synuclein-AAVs ($n \geq 5$/time point) were immunostained with anti-hα-synuclein. Representative images at lower magnification (**a**) show labeled neuronal projections in the right medulla oblongata; the DMnX is delineated by *dashed lines*, and the area postrema (AP) and central canal (cc) are indicated. *Rectangular boxes* encompass portions of the right DMnX that are also shown at higher magnification (**b**). *Scale bars* 200 μm in **a** and 20 μm in **b**. **c**–**f** Rats ($n = 5$) received a single midbrain injection of hα-synuclein-AAVs and were killed 6 months later. Sections of the medulla oblongata were double-stained with anti-ChAT and anti-hα-synuclein (hα-syn). The right DMnX is delineated by *dashed lines* at low magnification (**c**) and shown in its entireness in **d**. Images at high magnification (**e**, **f**) show DMnX axons co-labeled with hα-syn and ChAT (**e** *white arrows* in the merged panel), or immunoreactive for hα-syn but not ChAT (**f**). *Scale bars* 200 μm in **c**, 100 μm in **d** and 10 μm in **e**, **f**

projections even at later time points (Fig. 7c). Syn-O2 immunoreactivity was more robust and readily detectable in all AAV-injected rats. As shown in Fig. 7d, entire profiles of intramedullary vagal fibers could be distinguished by Syn-O2/ChAT co-labeling. For comparative purposes, tissue sections from the high-midbrain were also stained with Syn-F1 or Syn-O2; with either of the two antibodies, intense and diffuse immunoreactivity was observed within and outside the substantia nigra, labeling both neuronal cell bodies and neuronal projections of AAV-injected rats (Supplementary Figure 4).

A final set of experiments was carried out in rats that received unilateral midbrain injections of GFP- rather than hα-synuclein-carrying AAVs. GFP-AAV administration

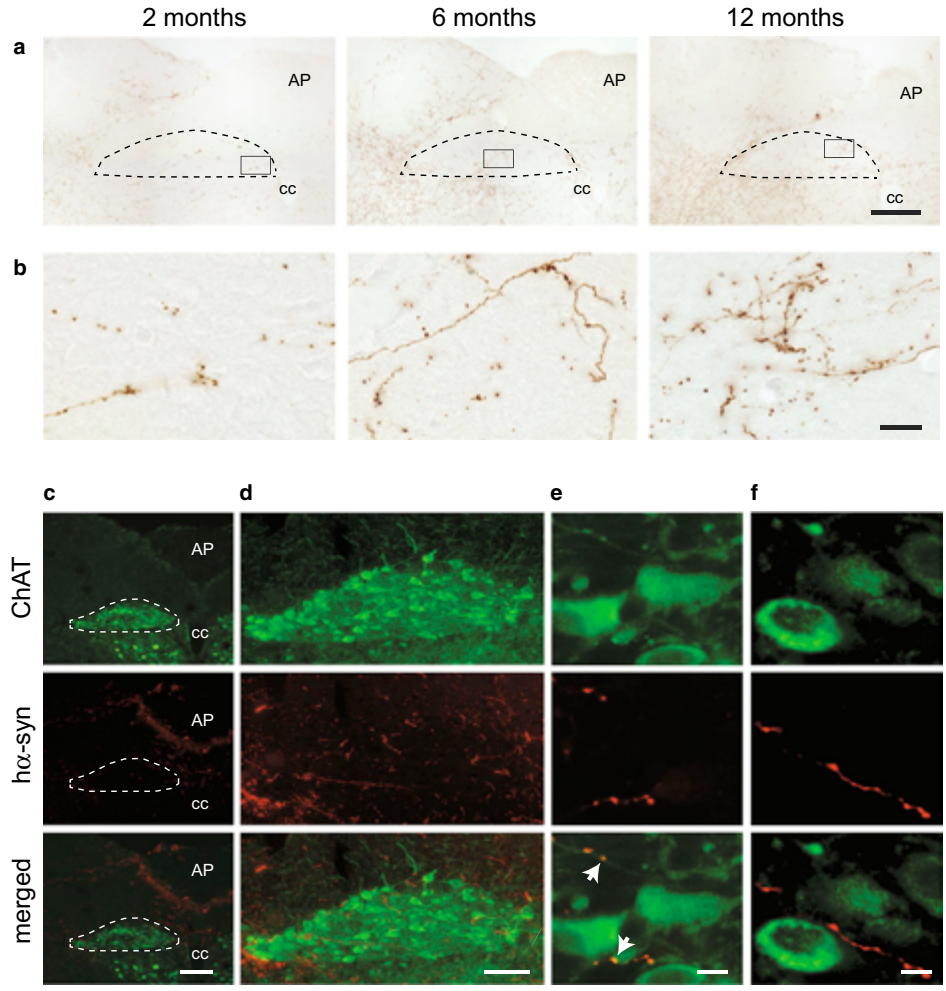

Fig. 6 Human α-synuclein protein in the DMnX of AAV-injected rats. **a**, **b** Medulla oblongata sections from rats injected with hα-synuclein-AAVs ($n \geq 5$/time point) were immunostained with anti-hα-synuclein. Representative images at lower magnification (**a**) show labeled neuronal projections in the right medulla oblongata; the DMnX is delineated by *dashed lines*, and the area postrema (AP) and central canal (cc) are indicated. *Rectangular boxes* encompass portions of the right DMnX that are also shown at higher magnification (**b**). *Scale bars* 200 μm in **a** and 20 μm in **b**. **c**–**f** Rats ($n = 5$) received a single midbrain injection of hα-synuclein-AAVs and were killed 6 months later. Sections of the medulla oblongata were double-stained with anti-ChAT and anti-hα-synuclein (hα-syn). The right DMnX is delineated by *dashed lines* at low magnification (**c**) and shown in its entireness in **d**. Images at high magnification (**e**, **f**) show DMnX axons co-labeled with hα-syn and ChAT (**e** *white arrows* in the merged panel), or immunoreactive for hα-syn but not ChAT (**f**). *Scale bars* 200 μm in **c**, 100 μm in **d** and 10 μm in **e**, **f**

projections even at later time points (Fig. 7c). Syn-O2 immunoreactivity was more robust and readily detectable in all AAV-injected rats. As shown in Fig. 7d, entire profiles of intramedullary vagal fibers could be distinguished by Syn-O2/ChAT co-labeling. For comparative purposes, tissue sections from the high-midbrain were also stained with Syn-F1 or Syn-O2; with either of the two antibodies, intense and diffuse immunoreactivity was observed within and outside the substantia nigra, labeling both neuronal cell bodies and neuronal projections of AAV-injected rats (Supplementary Figure 4).

A final set of experiments was carried out in rats that received unilateral midbrain injections of GFP- rather than hα-synuclein-carrying AAVs. GFP-AAV administration

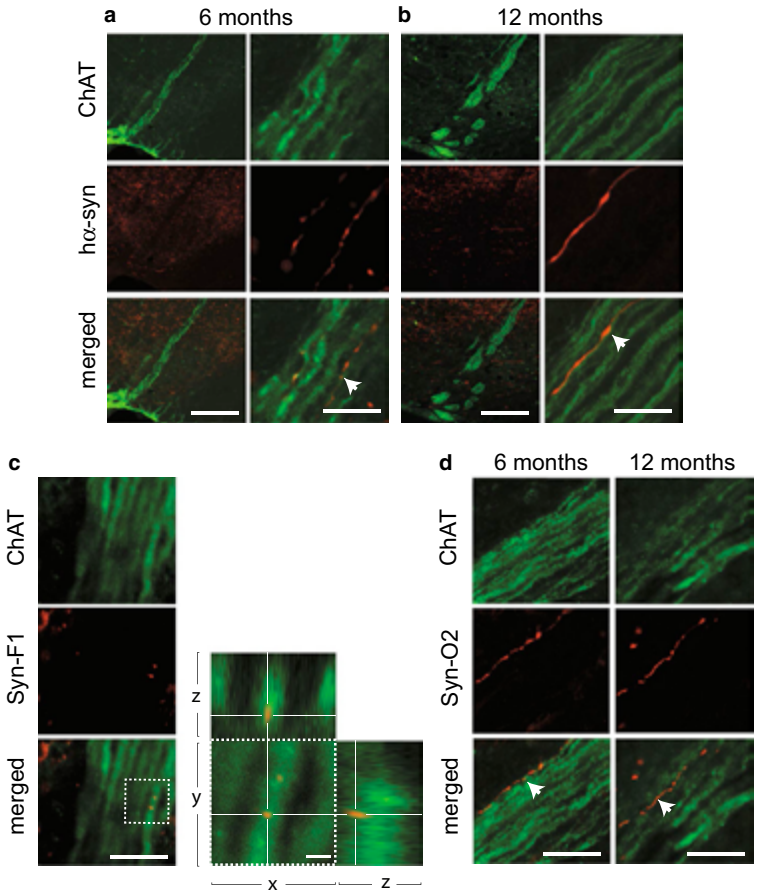

Fig. 7 Human α-synuclein-positive vagal axons in the rat medulla oblongata. **a**, **b** Rats ($n = 5$/time point) received a single midbrain injection of hα-synuclein-AAVs. Sections of the lower medulla oblongata (between Bregma −13.92 and −14.04 mm) were double-stained with anti-ChAT and anti-hα-synuclein. Images at lower magnification (*left panels*) show bundles of fibers that cross the right medulla oblongata converging into the vagus nerve. Higher magnification panels (*right*) show intramedullary vagal fibers co-labeled for ChAT and hα-synuclein (some of these fibers are indicated by *white arrows*). *Scale bars* 200 μm (*lower magnification*) and 10 μm (*higher magnification*). **c** Rats ($n = 5$) were killed at 12 months after a single midbrain injection of hα-synuclein-AAVs. Sections of the lower medulla oblongata were double-stained with anti-ChAT plus an antibody that specifically recognizes mature α-synuclein fibrils (Syn-F1). Images show co-labeled punctae within a vagal axon crossing the reticular formation of the right medulla oblongata. Co-localization was confirmed in the enlarged images showing orthogonal cross-sections in the *x*–*y*, *x*–*z* and *y*–*z* axes. *Scale bars* 10 μm (*lower magnification*) and 2 μm (*higher magnification*). **d** Rats ($n = 5$/time point) were killed at 6 and 12 months after a single midbrain injection of hα-synuclein-AAVs. Sections of the lower medulla oblongata were double-stained with anti-ChAT plus an antibody that recognizes oligomeric and fibrillar forms of α-synuclein (Syn-O2). Images show co-labeled vagal axons (*white arrows* in the merged panels) in the right medulla oblongata. *Scale bar* 10 μm

caused transduction features similar to those observed with hα-synuclein-AAVs; robust transduction was measured in midbrain samples, whereas WPRE mRNA remained undetectable in specimens from the dorsal medulla oblongata (Fig. 5f). In contrast to the results with hα-synuclein-AAVs, however, GFP-AAV injections were not associated with presence of the transduced protein in vagal neurons; no GFP immunoreactivity was indeed observed within DMnX cholinergic axons in the medulla oblongata (Supplementary Figure 5a). Similarly, vagus nerve sections and stomach whole mount preparations were consistently devoid of GFP labeling (Supplementary Figure 5b, c).

Discussion

Results of this study reveal a distinctive role of DMnX-derived vagal efferents in transferring α-synuclein from the brain to peripheral tissues. When hα-synuclein was overexpressed directly in the vagal system (DMnX and vagal ganglia), it efficiently traveled via both efferent and afferent fibers of the vagus nerve and reached visceromotor as well as viscerosensory terminals in the stomach wall (Fig. 8a). Quite in contrast, protein overexpression targeted to the midbrain resulted in detection and accumulation of hα-synuclein only within vagal efferents terminating onto ganglionic neurons of the myenteric plexus (Fig. 8b). This preferential route of protein transmission is particularly remarkable if one considers that preganglionic efferents represent only a small percent of fibers forming the vagus nerve and that, based on their numerical prevalence within this nerve, a greater contribution of sensory afferents to α-synuclein transfer might have been expected. Indeed, according to estimates in various animal species and with different techniques, the ratio of efferent over afferent vagal projections has been reported to range between 1:10 and 1:3 [1, 18]. Our present study focused on α-synuclein transmission from the brain to the gastric wall. However, given the extensive innervation provided to the small intestine by vagal preganglionic efferents [4], it is conceivable that α-synuclein may also travel from the brain to other sections of the gastrointestinal tract, such as the duodenum and jejunum. Further work is warranted to substantiate this possibility and determine whether accumulation of brain-derived α-synuclein throughout the gut may result in overt alterations of gastrointestinal function in this animal model.

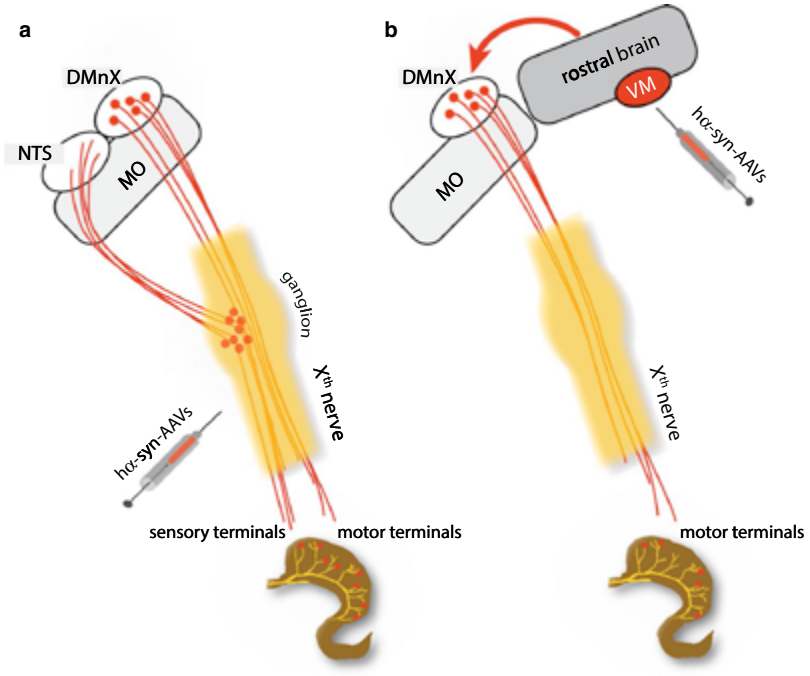

Fig. 8 Schematic representations of patterns of hα-synuclein accumulation after vagal or intraparenchymal injections of hα-synuclein-AAVs. **a** Following AAV injections into the vagus nerve, neuronal cell bodies in the DMnX and nodose ganglion produce hα-synuclein. The exogenous protein is then accumulated within efferent DMnX projections and afferent vagal fibers, reaching both visceromotor and viscerosensory nerve endings in the gastric wall. Afferent fibers also terminate onto neurons of the nucleus of the tractus solitarius (NTS) in the medulla oblongata (MO). **b** Following AAV injections into the ventral mesencephalon (VM), hα-synuclein is overexpressed within neurons that project toward lower brainstem regions. Traveling rostro-caudally through these axons, the exogenous protein reaches the medulla oblongata (MO) and gains access into DMnX neurons. The red arrow underscores the fact that passage into these cells would require a neuron-to-neuron jump. Hα-synuclein then uses efferent projections stemming from the DMnX and contained in the vagus nerve to reach preganglionic vagal nerve endings in the stomach wall

Specific mechanisms underlying the propensity of visceromotor vagal fibers to accrue and deliver α-synuclein remain unclear. Braak and colleagues underscored a potential relationship between axonal length and myelination and vulnerability to α-synuclein pathology; morphological and metabolic differences between long, thin and poorly myelinated axons of the visceromotor vagal system vs. sturdily myelinated fibers relaying viscerosensory inputs may contribute to their distinctive role in pathological processes involving α-synuclein [6]. It is also noteworthy that earlier work investigating endogenous α-synuclein expression in the rat stomach and duodenum found that vagal afferent endings did not contain α-synuclein, whereas virtually all vagal preganglionic projections expressed the protein [16]. It appears therefore that vagal neurons producing, transporting and utilizing α-synuclein under normal conditions may more efficiently serve as conduits for pathological protein transfer and be more vulnerable to α-synuclein accumulation.

Hα-synuclein was detected within cholinergic DMnX axons (by 2 months), within intramedullary fibers of the Xth nerve and within the vagus nerve itself in the rat neck (by 6 months), supporting the conclusion that brain-to-stomach protein advancement progressively occurred through this pathway (Fig. 8b). The DMnX encompasses cholinergic cell bodies that only project outside the brain via axons forming the Xth cranial nerve (Fig. 8b). Data are therefore consistent with the interpretation that hα-synuclein, once generated within transduced midbrain neurons, proceeded toward the medulla oblongata and gained access into DMnX cells as a result of both intra- and inter-neuronal protein transfer. Based on our findings with conformation-specific antibodies, monomeric and oligomeric forms of α-synuclein are likely to be primarily responsible for protein mobility. Crowding of α-synuclein within vagal neurons may subsequently trigger a localized process of further aggregation, leading to the formation of mature α-synuclein fibrils. An alternative explanation for the vagal accumulation of exogenous α-synuclein under our experimental conditions might have been that viral vectors injected into the ventral mesencephalon were able to reach and transduce DMnX cells. Several lines of evidence make this possibility highly unlikely. They include lack of detection of hα-synuclein mRNA and lack of hybridization of multiple oligonucleotides targeting WPRE mRNA (a viral vector marker) in DMnX-containing medullary tissue. Furthermore, midbrain injections of GFP-carrying AAVs did not result in any detection of GFP protein within DMnX neurons, underscoring the inability of these viral vectors to travel to the medulla oblongata and transduce vagal cells. Finally, a relatively non-specific diffusion of hα-synuclein-carrying AAVs would be difficult to reconcile with our observation of a targeted protein accumulation within preganglionic vagal efferents.

Together with earlier observations supporting a gut-to-brain transfer of α-synuclein [13, 15], our current findings indicate that protein transmission can proceed in either direction from distant organs to the brain or from the brain to peripheral tissues. This bidirectional potential is consistent with the ability of α-synuclein to move both anterogradely and retrogradely within neurons [7–9, 23]. An important translational implication of our study concerns the presence of α-synuclein pathology in peripheral tissues of synucleinopathy patients. Pathological forms of the protein have been detected in the gastrointestinal tract of patients with Parkinson's disease as well as multiple system atrophy and dementia with Lewy bodies [3, 17, 20]. In some instances, these peripheral α-synuclein lesions were observed in non-symptomatic individuals, suggesting that they may represent initial or early manifestations of Parkinson's disease [5, 21]. Our current results do not confute this possibility. They clearly indicate, however, that accumulation of α-synuclein in peripheral tissues may not always define site(s) of disease inception or be a marker of prodromal disease stages. The pattern of progression of α-synuclein pathology, caudo-rostral or rostro-caudal, may vary from patient to patient and differ, for example, in typical Parkinson's disease as compared to sub-variants of the disease or other synucleinopathies.

Acknowledgements We thank Sarah A. Jewell for her comments on the manuscript, Omar El-Agnaf for kindly providing conformation-specific antibodies, Raffaella Rusconi for the design of in situ probes, Cherie N. Hudson, Bettina Winzen-Reichert, Franziska Hesse, Laura Jakobi for assistance with the experiments, and Ireen Koenig for assistance with microscopy. This work was supported by the Paul Foundation, the Centres of Excellence in Neurodegeneration Research (CoEN) and NIH Grant DK027627.

References

1. Agostoni E, Chinnock JE, De Daly MB, Murray JG (1957) Functional and histological studies of the vagus nerve and its branches to the heart, lungs and abdominal viscera in the cat. J Physiol 135:182–205
2. Annerino DM, Arshad S, Taylor GM, Adler CH, Beach TG, Greene JG (2012) Parkinson's disease is not associated with gastrointestinal myenteric ganglion neuron loss. Acta Neuropathol 124:665–680. doi:10.1007/s00401-012-1040-2
3. Beach TG, Adler CH, Sue LI, Vedders L, Lue L, White Iii CL, Akiyama H, Caviness JN, Shill HA, Sabbagh MN, Walker DG (2010) Multi-organ distribution of phosphorylated α-synuclein histopathology in subjects with Lewy body disorders. Acta Neuropathol 119:689–702. doi:10.1007/s00401-010-0664-3
4. Berthoud HR, Jedrzejewska A, Powley TL (1990) Simultaneous labeling of vagal innervation of the gut and afferent projections from the visceral forebrain with dil injected into the dorsal vagal complex in the rat. J Comp Neurol 301:65–79

5. Braak H, de Vos RA, Bohl J, Del Tredici K (2006) Gastric α-synuclein immunoreactive inclusions in Meissner's and Auerbach's plexuses in cases staged for Parkinson's disease-related brain pathology. Neurosci Lett 396:67–72. doi:10.1016/j.neulet.2005.11.012
6. Braak H, Rub U, Gai WP, Del Tredici K (2003) Idiopathic Parkinson's disease: possible routes by which vulnerable neuronal types may be subject to neuroinvasion by an unknown pathogen. J Neural Transm 110:517–536. doi:10.1007/s00702-002-0808-2
7. Danzer KM, Kranich LR, Ruf WP, Cagsal-Getkin O, Winslow AR, Zhu L, Vanderburg CR, McLean PJ (2012) Exosomal cell-to-cell transmission of α-synuclein oligomers. Mol Neurodegener 7:42. doi:10.1186/1750-1326-7-42
8. Freundt EC, Maynard N, Clancy EK, Roy S, Bousset L, Sourigues Y, Covert M, Melki R, Kirkegaard K, Brahic M (2012) Neuron-to-neuron transmission of α-synuclein fibrils through axonal transport. Ann Neurol 72:517–524. doi:10.1002/ana.23747
9. George S, Rey NL, Reichenbach N, Steiner JA, Brundin P (2013) α-Synuclein: the long distance runner. Brain Pathol 23:350–357. doi:10.1111/bpa.12046
10. Giasson BI, Jakes R, Goedert M, Duda JE, Leight S, Trojanowski JQ, Lee VM (2000) A panel of epitope-specific antibodies detects protein domains distributed throughout human α-synuclein in Lewy bodies of Parkinson's disease. J Neurosci Res 59:528–533
11. Goedert M, Spillantini MG, Del Tredici K, Braak H (2013) 100 years of Lewy pathology. Nat Rev Neurol 9:13–24. doi:10.1038/nrneurol.2012.242
12. Helwig M, Klinkenberg M, Rusconi R, Musgrove RE, Majbour NK, El-Agnaf OM, Ulusoy A, Di Monte DA (2016) Brain propagation of transduced α-synuclein involves non-fibrillar protein species and is enhanced in α-synuclein null mice. Brain 139:856–870. doi:10.1093/brain/awv376
13. Holmqvist S, Chutna O, Bousset L, Aldrin-Kirk P, Li W, Bjorklund T, Wang ZY, Roybon L, Melki R, Li JY (2014) Direct evidence of Parkinson pathology spread from the gastrointestinal tract to the brain in rats. Acta Neuropathol 128:805–820. doi:10.1007/s00401-014-1343-6
14. Kirik D, Rosenblad C, Burger C, Lundberg C, Johansen TE, Muzyczka N, Mandel RJ, Bjorklund A (2002) Parkinson-like neurodegeneration induced by targeted overexpression of α-synuclein in the nigrostriatal system. J Neurosci 22:2780–2791
15. Pan-Montojo F, Schwarz M, Winkler C, Arnhold M, O'Sullivan GA, Pal A et al (2012) Environmental toxins trigger PD-like progression via increased α-synuclein release from enteric neurons in mice. Sci Rep 2:898. doi:10.1038/srep00898
16. Phillips RJ, Walter GC, Wilder SL, Baronowsky EA, Powley TL (2008) α-Synuclein-immunopositive myenteric neurons and vagal preganglionic terminals: autonomic pathway implicated in Parkinson's disease? Neuroscience 153:733–750. doi:10.1016/j.neuroscience.2008.02.074
17. Pouclet H, Lebouvier T, Coron E, Rouaud T, Flamant M, Toulgoat F, Roy M, Vavasseur F, Bruley des Varannes S, Neunlist M, Derkinderen P (2012) Analysis of colonic α-synuclein pathology in multiple system atrophy. Parkinsonism Relat Disord 18:893–895. doi:10.1016/j.parkreldis.2012.04.020
18. Prechtl JC, Powley TL (1990) The fiber composition of the abdominal vagus of the rat. Anat Embryol 181:101–115
19. Raj A, van den Bogaard P, Rifkin SA, van Oudenaarden A, Tyagi S (2008) Imaging individual mRNA molecules using multiple singly labeled probes. Nat Methods 5:877–879. doi:10.1038/nmeth.1253
20. Sánchez-Ferro Á, Rábano A, Catalán MJ, Rodríguez-Valcárcel FC, Fernández Díez S, Herreros-Rodríguez J, Garcia-Cobos E, Alvarez-Santullano MM, Lopez-Manzanares L, Mosqueira AJ, Vela Desojo L, Lopez-Lozano JJ, Lopez-Valdes E, Sanchez-Sanchez R, Molina-Arjona JA (2015) In vivo gastric detection of α-synuclein inclusions in Parkinson's disease. Mov Disord 30:517–524. doi:10.1002/mds.25988
21. Shannon KM, Keshavarzian A, Dodiya HB, Jakate S, Kordower JH (2012) Is α-synuclein in the colon a biomarker for premotor Parkinson's disease? Evidence from 3 cases. Mov Disord 27:716–719. doi:10.1002/mds.25020
22. Spillantini MG, Schmidt ML, Lee VM, Trojanowski JQ, Jakes R, Goedert M (1997) α-Synuclein in Lewy bodies. Nature 388:839–840. doi:10.1038/42166
23. Uchihara T, Giasson B (2016) Propagation of α-synuclein pathology: hypotheses, discoveries, and yet unresolved questions from experimental and human brain studies. Acta Neuropathol 131:49–73. doi:10.1007/s00401-015-1485-1
24. Ulusoy A, Musgrove RE, Rusconi R, Klinkenberg M, Helwig M, Schneider A, Di Monte DA (2015) Neuron-to-neuron α-synuclein propagation in vivo is independent of neuronal injury. Acta Neuropathol Commun 3:13. doi:10.1186/s40478-015-0198-y
25. Ulusoy A, Rusconi R, Perez-Revuelta BI, Musgrove RE, Helwig M, Winzen-Reichert B, Di Monte DA (2013) Caudo-rostral brain spreading of α-synuclein through vagal connections. EMBO Mol Med 5:1051–1059. doi:10.1002/emmm.201302475
26. Vaikath NN, Majbour NK, Paleologou KE, Ardah MT, van Dam E, van de Berg WD, Forrest SL, Parkkinen L, Gai WP, Hattori N, Takanashi M, Lee SJ, Mann DM, Imai Y, Halliday GM, Li JY, El-Agnaf OM (2015) Generation and characterization of novel conformation-specific monoclonal antibodies for α-synuclein pathology. Neurobiol Dis 79:81–99. doi:10.1016/j.nbd.2015.04.009
27. Walter GC, Phillips RJ, Baronowsky EA, Powley TL (2009) Versatile, high-resolution anterograde labeling of vagal efferent projections with dextran amines. J Neurosci Methods 178:1–9. doi:10.1016/j.jneumeth.2008.11.003
28. Wang FB, Powley TL (2000) Topographic inventories of vagal afferents in gastrointestinal muscle. J Comp Neurol 421:302–324
29. Wang ZY, Lian H, Cai QQ, Song HY, Zhang XL, Zhou L, Zhang YM, Zheng LF, Zhu JX (2014) No direct projection is observed from the substantia nigra to the dorsal vagus complex in the rat. J Parkinsons Dis 4:375–383. doi:10.3233/JPD-130279

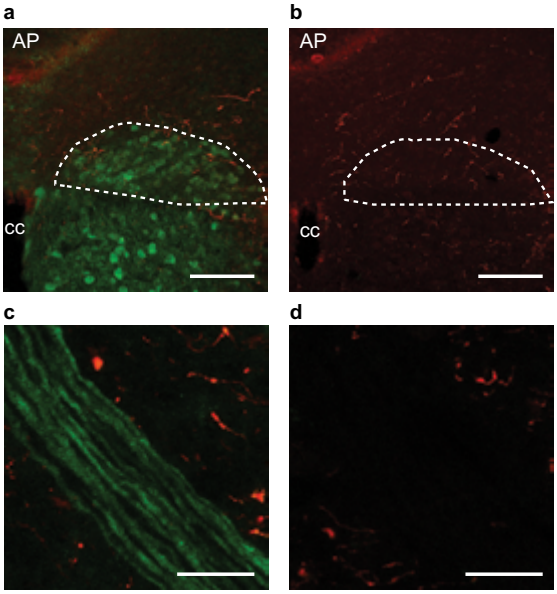

Supplementary Fig. 1 Rats (n = 3) received a single midbrain injection of hα-synuclein-AAVs and were killed at 6 months post-treatment. **a, b** Consecutive sections of the medulla oblongata containing the DMnX were double-stained with anti-hα-synuclein (red) and anti-ChAT (green) (**a**) or incubated with anti-hα-synuclein in the absence of ChAT primary antibody (**b**). The right DMnX is delineated by dashed lines, and the area postrema (AP) and central canal (cc) are indicated. Scale bars = 200 μm. **c**, **d** Consecutive sections of the medulla oblongata at the level where intramedullary fibers of the right vagus nerve are formed were double-stained with anti-hα-synuclein and anti-ChAT (**c**) or incubated with anti-hα-synuclein in the absence of ChAT primary antibody (**d**). Scale bars = 10 μm. Lack of labeling in (**b**) and (**d**) confirms specificity of the ChAT labeling.

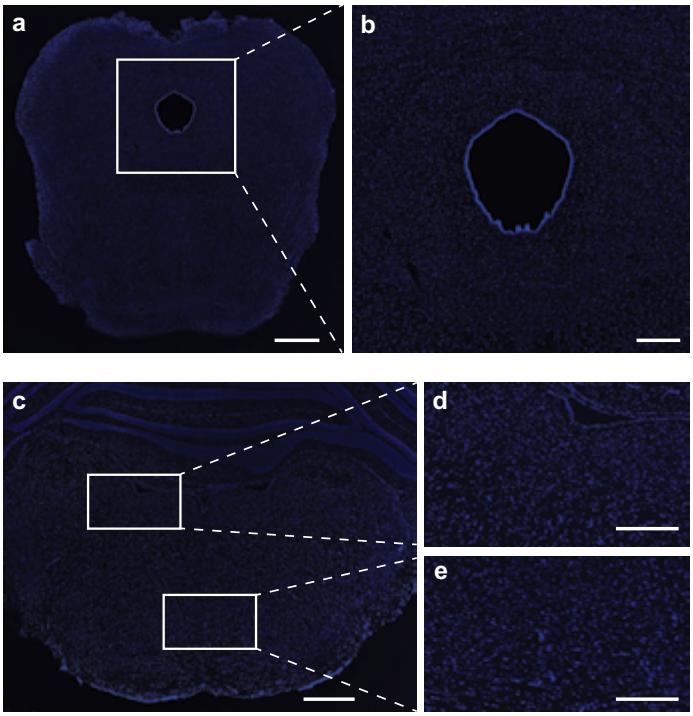

Supplementary Fig. 2 Rats (n = 3) received a single midbrain injection of hα-synuclein-AAVs and were killed at 2 months post-treatment. **a-e** Sections from the lower midbrain (representative images in **a** and **b**) and from the pons (representative images in **c-e**) were processed for fluorescent *in situ* hybridization to detect WPRE mRNA (white). Sections were also counterstained with DAPI (blue). The square box in (**a**) encompasses the periaqueductal gray shown at higher magnification in (**b**). The rectangular boxes in (**c**) encompass the right locus coeruleus / parabrachial nucleus and the pontine reticular nucleus that are shown at higher magnification in (**d**) and (**e**), respectively. No white signal (i.e. no WPRE hybridization) was detected in any of the sections from these brain regions. Scale bars = 1 mm in (**a** and **c**) and 500 μm in (**b**, **d** and **e**).

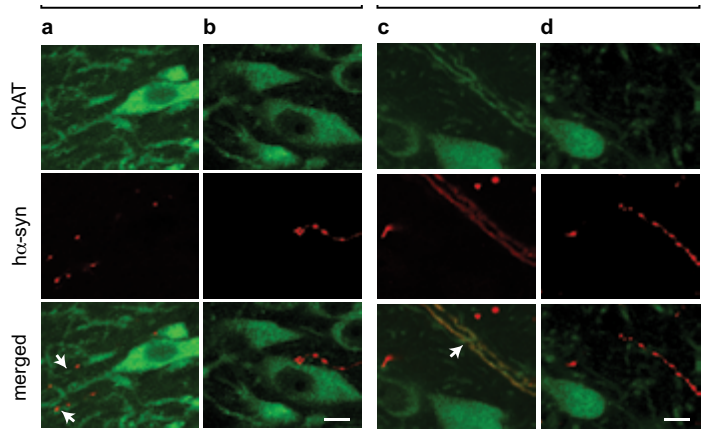

Supplementary Fig. 3 a-d Rats (n ≥ 5/time point) received a single midbrain injection of hα-synuclein-AAVs and were killed at 2 and 12 months post-treatment. Sections of the medulla oblongata were double-stained with anti-ChAT and anti-hα-synuclein (hα-syn). Representative confocal images show DMnX axons co-labeled with hα-syn and ChAT (**a** and **c**; white arrows in the merged panels), or immunoreactive for hα-syn but not ChAT (**b** and **d**). Scale bars = 10 μm.

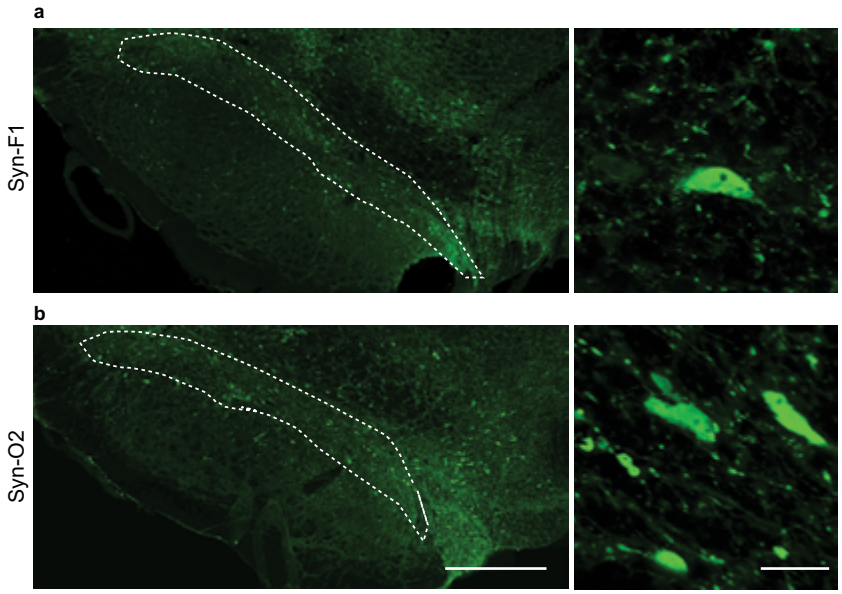

Supplementary Fig. 4 a, b Rats (n = 5) were killed at 6 months after a single midbrain injection of hα-synuclein-AAVs. Sections of the midbrain containing the substantia nigra pars compacta (delineated by dashed lines in the left panels) were stained with an antibody (Syn-F1) that specifically recognizes mature α-synuclein fibrils (**a**) or an antibody (Syn-O2) that recognizes oligomeric and fibrillar forms of α-synuclein (**b**). Higher magnification images (right panels) show nigral cell bodies and neuronal projections containing aggregated α-synuclein. Scale bars = 250 μm (lower magnification) and 20 μm (higher magnification).

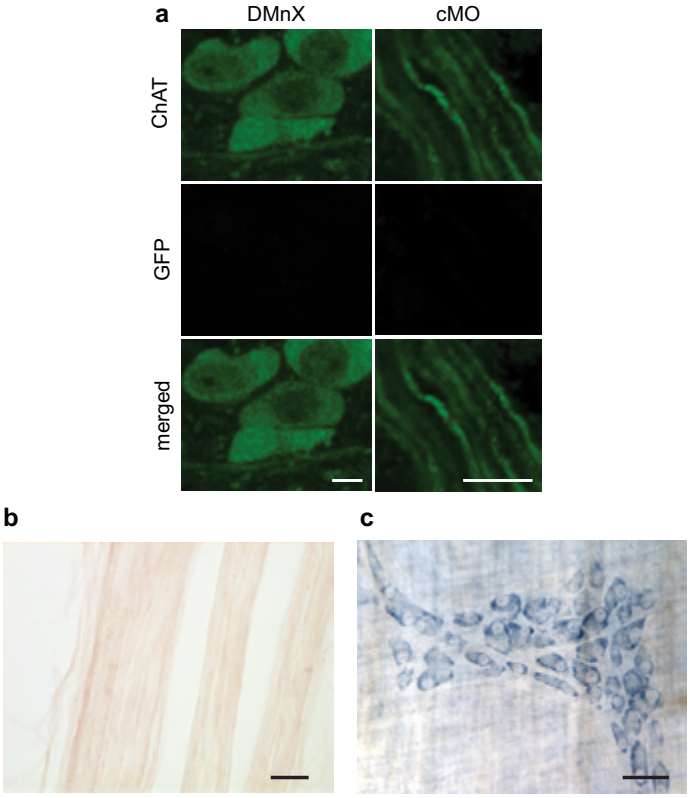

Supplementary Fig. 5 Rats (n = 5) received a single injection of GFP-AAVs in the right midbrain and were killed at 12 months. **a** Sections of the right medulla oblongata were double-stained with anti-ChAT (green) and anti-GFP (false-colored in red). ChAT-positive neurons and neuronal projections are shown in the DMnX (left panels); intramedullary fibers of the vagus nerve were also labeled for ChAT in caudal sections of the medulla oblongata (cMO; right panels). Please note the absence of GFP co-labeling. Scale bars = 10 μm. **b** Longitudinal sections of right vagus nerves were stained with anti-GFP. The representative image shows no specific immunoreactivity. Scale bar = 10 μm. **c** Stomach whole mounts were stained with anti-GFP and counterstained with Cuprolinic Blue. The representative image shows ganglionic cells of the myenteric plexus. No specific GFP immunoreactivity was detected. Scale bar = 50 μm.

Rusconi, R., **Ulusoy, A.,** Aboutalebi, H., and Di Monte, D.A. (2018). Long-lasting pathological consequences of overexpression-induced α-synuclein spreading in the rat brain. Aging Cell 17 :e12727.

Objective: This study aimed to investigate the long-term consequences of overexpression-induced α-syn spreading in the rat brain.

Methods and Results: Following AAV-α-syn injections into the rat vagus nerve, α-syn overexpression in the medulla oblongata and the interneuronal spreading to more rostral brain regions was observed, as described earlier (Helwig et al., 2016; Ulusoy et al., 2015; Ulusoy et al., 2013). The animals were followed for a period of 1 year, and the brain tissue was analyzed for neurodegeneration, α-syn spreading, and inflammatory changes.

Sustained expression of α-syn in the DMX neurons led to neurodegeneration of these recipient neurons. Although we observed a marked spreading of α-syn from the medulla oblongata to more frontal brain regions (i.e., pons, midbrain and basal forebrain), loss of donor neurons in the DMX led to cessation of caudo-rostral protein transmission. In fact, accumulation of α-syn and its spread to distant brain regions were dependent on continuous overexpression. Interestingly, even when spreading ceased, long-lasting pathological changes in the brain occurred/lasted. For example, we observed progressive degeneration of the LC accompanied by microglial activation and astrocytosis. Similarly, the central amygdala also displayed inflammatory changes.

Conclusions: Here we further highlighted the potential for neurodegeneration and sustained glial activation even with temporary overexpression-induced spreading. Thus, even if temporary, overexpression-induced spreading caused long-lasting pathological consequences in brain regions distant from the site of overexpression but anatomically connected to it.

Accepted: 28 December 2017
DOI: 10.1111/acel.12727

ORIGINAL ARTICLE

WILEY Aging Cell

Long-lasting pathological consequences of overexpression-induced α-synuclein spreading in the rat brain

Raffaella Rusconi | Ayse Ulusoy | Helia Aboutalebi | Donato A. Di Monte

German Center for Neurodegenerative Diseases (DZNE), Bonn, Germany

Correspondence
Donato A. Di Monte, German Center for Neurodegenerative Diseases (DZNE), Bonn, Germany.
Email: donato.dimonte@dzne.de

Funding information
This work was supported by the Paul Foundation, the Centres of Excellence in Neurodegeneration Research CoEN and the EU Joint Programme—Neurodegenerative Disease (JPND; 01ED1612).

Summary

Increased expression of α-synuclein can initiate its long-distance brain transfer, representing a potential mechanism for pathology spreading in age-related synucleinopathies, such as Parkinson's disease. In this study, the effects of overexpression-induced α-synuclein transfer were assessed over a 1-year period after injection of viral vectors carrying human α-synuclein DNA into the rat vagus nerve. This treatment causes targeted overexpression within neurons in the dorsal medulla oblongata and subsequent diffusion of the exogenous protein toward more rostral brain regions. Protein advancement and accumulation in pontine, midbrain, and forebrain areas were contingent upon continuous overexpression, because death of transduced medullary neurons resulted in cessation of spreading. Lack of sustained spreading did not prevent the development of long-lasting pathological changes. Particularly remarkable were findings in the locus coeruleus, a pontine nucleus with direct connections to the dorsal medulla oblongata and greatly affected by overexpression-induced transfer in this model. Data revealed progressive degeneration of catecholaminergic neurons that proceeded long beyond the time of spreading cessation. Neuronal pathology in the locus coeruleus was accompanied by pronounced microglial activation and, at later times, astrocytosis. Interestingly, microglial activation was also featured in another region reached by α-synuclein transfer, the central amygdala, even in the absence of frank neurodegeneration. Thus, overexpression-induced spreading, even if temporary, causes long-lasting pathological consequences in brain regions distant from the site of overexpression but anatomically connected to it. Neurodegeneration may be a consequence of severe protein burden, whereas even a milder α-synuclein accumulation in tissues affected by protein transfer could induce sustained microglial activation.

KEYWORDS
axon, locus coeruleus, microglia, neurodegeneration, Parkinson's disease, stereology

1 | INTRODUCTION

The protein α-synuclein plays a key role in the pathogenesis of a number of age-related neurodegenerative diseases, collectively referred to as synucleinopathies, that include Parkinson's disease, dementia with Lewy bodies, and multiple system atrophy. The initial link between α-synuclein and human synucleinopathies was provided by genetic studies showing a causal relationship between a missense

mutation, alanine to threonine, at position 53 (A53T) of the α-synuclein gene (*SNCA*), and the development of autosomal-dominant parkinsonism (Polymeropoulos et al., 1997). Further genetic studies identified additional *SNCA* missense mutations (A30P, E46K, H50Q, G51D, and A53E) linked to hereditary parkinsonism (reviewed in Petrucci, Ginevrino & Valente, 2016). They also revealed an intriguing association between familial parkinsonism and *SNCA* duplication and triplication (Chartier-Harlin et al., 2004; Ibáñez et al., 2004; Singleton et al., 2003). In patients with these multiplication mutations, the severity of clinical presentation is correlated with gene dosage, because triplication carriers display more severe symptoms and earlier disease onset than patients with *SNCA* duplication (Ross et al., 2008). Pathological features triggered by *SNCA* multiplication are similar to those seen in idiopathic Parkinson's disease, including the degeneration of specific neuronal populations and the accumulation of α-synuclein-containing intraneuronal inclusions (Konno, Ross, Puschmann, Dickson & Wszolek, 2016). Taken together, these observations indicate that a sustained increase in protein expression is itself capable of triggering a gain of α-synuclein toxic function, leading to development of Parkinson's disease-like pathology. They also support the possibility that even transient and more localized elevations of brain levels of α-synuclein could have deleterious effects and contribute to the development of synucleinopathies (Ulusoy & Di Monte, 2013).

Studies over the past few years have characterized an α-synuclein property of likely relevance to its pathological role in human diseases: monomeric and aggregated α-synuclein are able to pass across neurons from donor to recipient cells and can thus advance from brain region to brain region following anatomical connections (Desplats et al., 2009; Goedert, Spillantini, Del Tredici & Braak, 2013; Rey, Petit, Bousset, Melki & Brundin, 2013). In Parkinson's disease, this interneuronal protein transfer may account for the stereotypical pattern of progression of α-synuclein pathology that, starting in the lower brainstem, affects higher and higher brain regions and ultimately reaches cortical areas (Braak et al., 2003; Goedert et al., 2013). Recent experimental work has demonstrated that brain spreading of α-synuclein can be initiated by its overexpression. Caudo-rostral protein transmission from the lower brainstem to the forebrain was prompted by targeted α-synuclein overexpression within neurons of the rat or mouse medulla oblongata (Helwig et al., 2016; Ulusoy et al., 2013). Experimental evidence also revealed long-distance α-synuclein diffusion from the brain to peripheral tissues (i.e. the stomach wall) as a result of enhanced protein expression in the rat midbrain (Ulusoy et al., 2017). Thus, a pathogenetic mechanism by which increased protein load could promote the development and progression of a synucleinopathy may be via inter- and intraneuronal transmission of α-synuclein and α-synuclein species (e.g. oligomers) with toxic potential (Helwig et al., 2016; Kim et al., 2013; Rochenstain et al., 2014).

Age-related synucleinopathies are characterized by a chronic disease course and progressive pathology, underscoring the importance of investigations into the long-term consequences of neuron-to-neuron transmission and widespread diffusion of α-synuclein. In this study, α-synuclein spreading triggered by its overexpression in the rat medulla oblongata was assessed over a period of 1 year, significantly extending the observation time of earlier investigations, and was correlated with short- and long-term markers of tissue injury. The new findings elucidate important factors that affect in vivo α-synuclein transfer and its pathological outcomes under conditions of enhanced protein load. Data reveal for the first time that long-term consequences of overexpression-induced spreading include neurodegenerative changes and robust microglial and astrocytic reactions in tissues affected by "secondary" (i.e. post-transfer) α-synuclein burden.

2 | RESULTS

2.1 | Long-term effects of α-synuclein overexpression in the rat medulla oblongata

Unilateral vagal injection of adeno-associated viral vectors (AAVs) carrying human α-synuclein (hα-synuclein) DNA caused overexpression of the exogenous protein in the dorsal medulla oblongata (Figure 1a,b). More precisely, staining of medullary tissue with a monoclonal antibody specific for hα-synuclein (syn211) showed immunoreactivity within cell bodies and axons of neurons in the dorsal motor nucleus of the vagus nerve (DMnX) ipsilateral (left) to the injection side; accumulation of hα-synuclein was also detected within vagal afferent projections terminating into the nucleus of the tractus solitarius on the left and, to a lesser extent, the right medulla oblongata. While this distinct anatomical distribution of transduced neurons was observed at earlier (6 weeks and 3 months) and later (6 months and 1 year) time points after AAV administration, the intensity and extent of hα-synuclein staining were time-dependent. Robust and widespread labeling characterized samples at 6 weeks and 3 months (Figure 1a); in contrast, a weaker and less diffuse immunoreactivity was displayed by medullary sections at 6-month and 1-year postvagal injection (Figure 1b).

Changes in overexpression were also assessed by stereological counting of hα-synuclein-positive neurons in the left (AAV-transduced) DMnX (Figure 1c). Counts revealed a significantly lower number of neurons (−30%) at 3 months as compared to 6 weeks post-treatment. An even more pronounced loss occurred between 3 and 6 months and, by 1 year, only a few neurons immunoreactive for hα-synuclein could be counted in the transduced tissue; indeed, values at 6 months and 1 year were 85% and 95% lower than the initial cell number at 6 weeks (Figure 1c). Reduced counts of hα-synuclein-positive cells were not due to a loss of transduction effect but rather to degeneration of neurons accumulating the exogenous protein. Data supporting this conclusion were obtained by counting the total number of Nissl-stained neurons in the left DMnX. When compared to control values in naïve animals and in the right (contralateral to the injection side) DMnX, total neuronal counts were unchanged at 6 weeks but reduced by approximately 10, 25, and 30% at 3 months, 6 months, and 1 year, respectively (Figure 1d). Of note, at each time point, the decrease in Nissl-stained neurons (e.g.

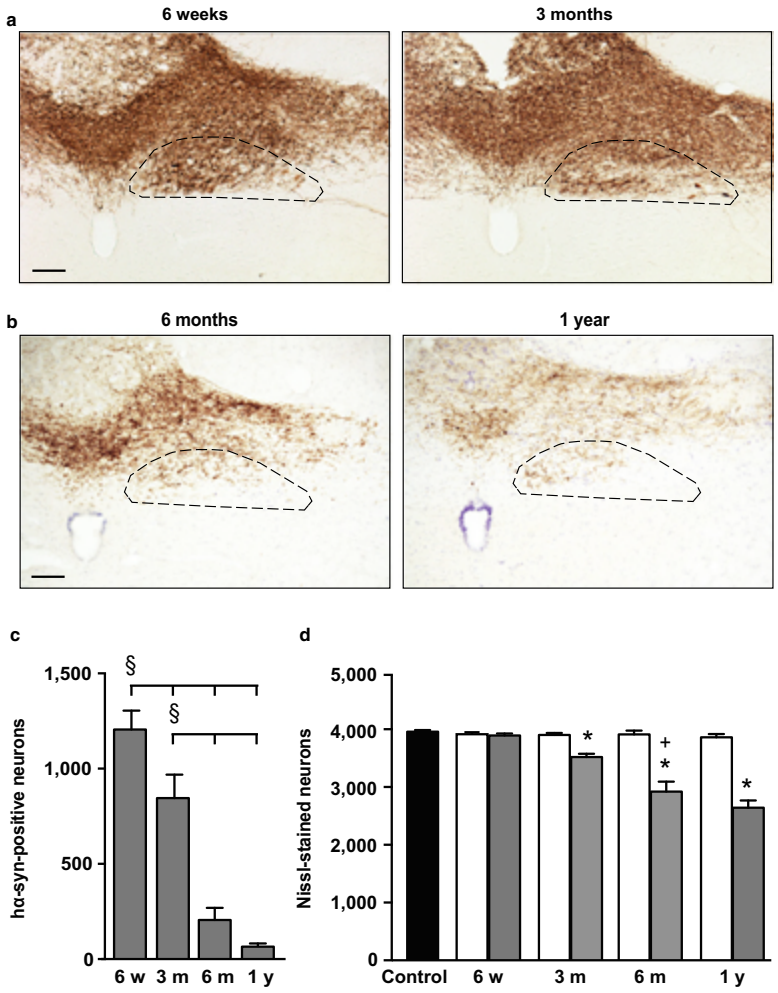

FIGURE 1 Time-dependent degeneration of hα-synuclein-overexpressing neurons in the rat medulla oblongata. Rats received a single injection of hα-synuclein-carrying adeno-associated viral vectors (AAVs) into the left vagus nerve and were killed at different time points after treatment. (a and b) Representative sections of the dorsal medulla oblongata from animals killed at early (a) or later (b) time points were labeled with an anti-hα-synuclein antibody. In each section, the left dorsal motor nucleus (DMnX) is delineated by dashed lines. Scale bar = 100 μm. (c) The number of hα-synuclein-positive neurons was counted in the left (AAV-transduced) DMnX at different time points post-treatment ($n \geq 5$ animals/time point). Error bars indicate *SEM*. $^{\S}p < .05$ (one-way ANOVA). (d) Stereological counts of Nissl-stained neurons were carried out in the DMnX of untreated naïve rats (black bar; $n = 4$) as well as in the right (contralateral to the injection side, white bars; $n \geq 5$) and left (ipsilateral to vagal injections, gray bars; $n \geq 6$) DMnX of AAV-treated animals. Error bars indicate *SEM*. $^{*}p < .05$ vs. the contralateral side value at the corresponding time point (Student's *t* test). $^{+}p < .05$ vs. the value at the earlier time point in the left DMnX (one-way ANOVA)

−1,036 ± 172 cells at 6 months) matched the loss of hα-synuclein-immunoreactive cells (−999 ± 53 neurons at 6 months), underscoring a causal relationship between hα-synuclein overexpression and neurodegeneration.

2.2 | Overexpression-induced spreading of α-synuclein

Overexpression of hα-synuclein triggers its neuron-to-neuron transmission from medullary donor neurons into recipient axons reaching the dorsal medulla oblongata from higher brain regions; through these axons, hα-synuclein then spreads toward the pons, midbrain, and forebrain (Helwig et al., 2016; Ulusoy et al., 2013). The next set of analyses was designed to assess how death of donor neurons at later times post-transduction affected hα-synuclein brain propagation. Spreading was estimated by counting the number of axons immunoreactive for hα-synuclein in brain sections at predetermined Bregma coordinates. A distinct pattern emerged, with progressive caudo-rostral protein spreading occurring only during the first 3-month post-AAV injection (Figure 2a). At 3 months, hα-synuclein

had spread from the medulla oblongata first to the pons and caudal midbrain (by 6 weeks) and then to the rostral midbrain and forebrain. No further advancement occurred thereafter and, in fact, a pronounced decrease in counts of hα-synuclein-positive fibers was found in all brain regions at 6 months and 1 year; at these later time points, positive axons became sparse in the pons, rare in the caudal midbrain and virtually undetectable in the rostral midbrain and forebrain (Figure 2a). Axonal counts obtained in syn211-stained sections were validated in a separate set of samples labeled with a polyclonal antibody recognizing both human and rodent α-synuclein (AB5038P). The pattern and extent of protein spreading were similar between syn211- and AB5038P-stained samples, and, in particular, data confirmed a dramatic loss of immunoreactive fibers between 3 and 6 months after AAV administration (Figure 2b).

2.3 | Neuronal and glial pathology associated with α-synuclein spreading

Spreading of hα-synuclein and its consequent accumulation within recipient neurons were accompanied by morphological evidence of axonal pathology; syn211- or AB5038P-labeled fibers appeared as tortuous threads with irregularly spaced and intensely labeled swellings (Figure 2c and Figure S1). The volume of these swellings is an indicator of hα-synuclein burden (Ulusoy et al., 2013). Mean volumes of axonal varicosities were compared in pontine sections of AAV-injected rats at different time points post-treatment. Interestingly, they varied significantly, reaching their peak at 3 months and then declining by 25% at 6 months and 50% at 1 year (Figure 2c,d). Further characterization of axonal pathology was carried out using antibodies that recognize modified or aggregated forms of α-synuclein. Phosphorylation at serine 129 is often used as a marker of α-synuclein pathology (Neumann et al., 2002). However, when pontine, midbrain, and forebrain sections from AAV-injected rats were stained for phospho-Ser129 α-synuclein, no immunoreactivity was detected at any time point post-treatment (data not shown). To assess protein aggregation, tissues were labeled with two conformation-specific antibodies: Syn-O2 recognizes both early (oligomers) and late (fibrils) α-synuclein aggregates, whereas Syn-F1 specifically reacts against fibrillar α-synuclein (Helwig et al., 2016; Vaikath et al., 2015). Immunoreactivity could be seen in sections labeled with Syn-O2 but not Syn-F1, indicating the presence of oligomeric but not fibrillar protein within abnormal axons (Figure 2e).

Recipient axons accumulating hα-synuclein under our experimental conditions would stem from brain nuclei that send direct projections into the dorsal medulla oblongata. The next set of analyses focused on a detailed assessment of pathological changes in two of these nuclei, namely the locus coeruleus in the pons and the amygdala in the medial temporal lobe (van der Kooy, Koda, McGinty, Gerfen & Bloom, 1984; Ter Horst, Toes & Van Willigen, 1991). The vast majority of neurons in the locus coeruleus is noradrenergic and displays immunoreactivity for tyrosine hydroxylase. Tyrosine hydroxylase labeling was less robust in the locus coeruleus of AAV-injected rats killed at 1 year as compared to age-matched naïve animals (Figure 3a). Following delineation of the locus coeruleus on pontine sections (Figure S2), the total number of neurons stained with cresyl violet was counted stereologically and compared in the left (ipsilateral to the injection side) locus coeruleus of rats killed at different times post-AAV injection *vs.* the locus coeruleus of naïve age-matched controls. While counts in animals killed at 6 weeks post-treatment were similar to control values, a progressive neuronal loss occurred at later time points, with counts being reduced by 4% at 3 months, 11% at 6 months, and 15% at 1 year (Figure 3d).

Next, the number and morphology of microglial cells were monitored in the left locus coeruleus of control (naïve) and treated rats. In control animals, counts of cells immunoreactive for ionized calcium-binding adapter molecule 1 (IBA1, a marker of microglia) revealed age-dependent changes because, as compared to values at 6 weeks and 3 months, the number of microglia was 25% and 50% greater at 6 months and 1 year, respectively (Figure 3e). In AAV-injected rats, the number of IBA1-positive cells was markedly elevated at 3 months and remained higher at 6 months and 1 year (Figure 3b,e). When compared to age-matched control values, counts in these treated animals showed no change at 6 weeks, but significant increases at 3 months (+50%), 6 months (+40%), and 1 year (+15%). Subpopulations of IBA1-labeled cells were also separately analyzed based on four distinct microglial phenotypes: (i) "resting", surveying cells with small, round cell bodies and elongated, thin processes; (ii) "hyper-ramified" cells with bigger, less circular cell bodies and dense ramifications of variable thickness; (iii) "hypertrophic" cells with big, irregular cell bodies and only a few, shorter, and poorly ramified processes; and (iv) "amoeboid" cells with an ovoid-shaped body devoid of extensions or with one or two thick, unramified processes (Jimenez-Ferrer, Jewett, Tontanahal, Romero-Ramos & Swanberg, 2017; Torres-Platas et al., 2014) (Figure 4a). The age-dependent increase in microglial counts seen in the locus coeruleus of naïve rats was primarily due to an enhanced number of resting and hypertrophic cells (Figure 4b). Resting, hypertrophic but also amoeboid cells accounted for the higher microglial number in AAV-injected animals (Figure 4b).

Astrogliosis is another typical reaction to brain tissue injury and was therefore evaluated as a potential pathological consequence of hα-synuclein spreading and hα-synuclein-induced neurodegeneration. The number of astrocytes immunoreactive for glial fibrillary acidic protein (GFAP) was first estimated in the locus coeruleus of naïve rats. Similar to the effect of aging on microglia, astrocyte counts were found to be elevated by 40% and 75% at 6 months and 1 year, respectively, as compared to earlier time points (Figure 3f). AAV injections caused a small but statistically significant increase (+15%) in GFAP-positive cells in the left locus coeruleus of rats killed at 3 months. This astrogliosis became much more pronounced, however, at 6 months and 1 year post-treatment (Figure 3c); counts in animals killed at these later time points were approximately 100% higher than the corresponding values in age-matched controls (Figure 3f). Of note, immunohistochemical analyses of either microglial or astrocytic cells in the locus coeruleus of AAV-injected animals showed no evidence of accumulation of the exogenous hα-synuclein protein within these cells (data not shown).

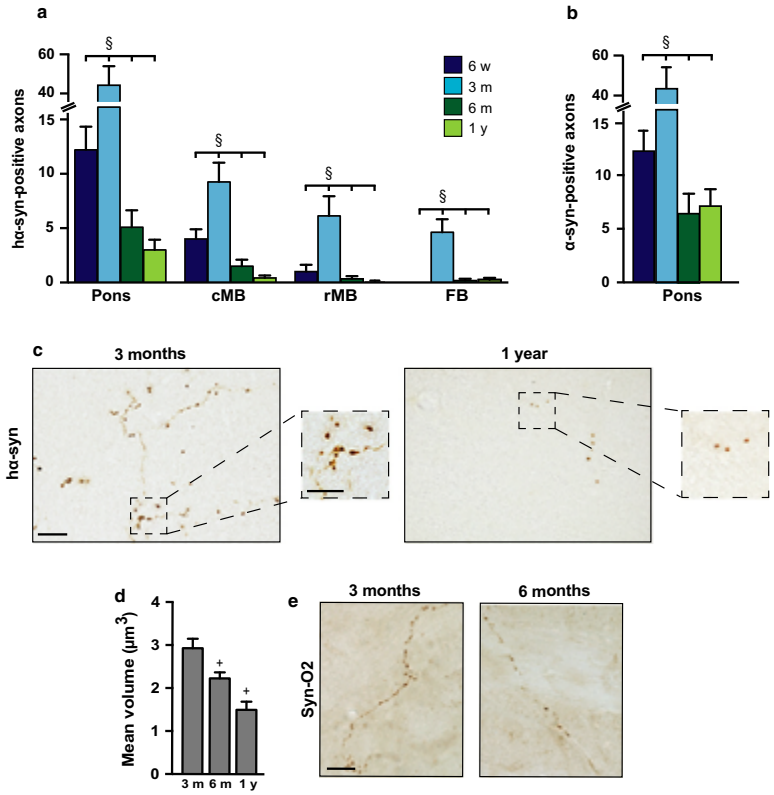

FIGURE 2 Long-term reduction in hα-synuclein-loaded axons in brain regions affected by protein spreading. (a) The number of axons immunostained for hα-synuclein with syn211 was counted in the brain of rats killed at different time points ($n \geq 4$ animals/time point) after vagal AAV injections. Sections of the left (ipsilateral to the injection side) pons (Bregma: −9.6 mm), caudal midbrain (cMB; Bregma: −7.8), rostral midbrain (rMB; Bregma: −6.0), and forebrain (FB; Bregma: −2.4) were used for this analysis. Error bars indicate *SEM*. $^{\S}p < .05$ (one-way ANOVA). (b) The number of axons immunostained for total (human plus rat) α-synuclein with AB5038P was counted in sections of the left pons at different time points ($n = 4$ animals/time point) after vagal AAV injections. Error bars indicate *SEM*. $^{\S}p < .05$ (one-way ANOVA). (c) Representative images show hα-synuclein-immunoreactive axons in the left (ipsilateral to the treatment side) pons of rats sacrificed at 3 months or 1 year after vagal AAV injections. The number of positive axons was markedly reduced at the later time point. The square boxes delineate two pontine areas shown at higher magnification in the smaller panels; at this higher magnification, the volume of axonal varicosities appears to be decreased at 1 year as compared to 3 months. Scale bar = 20 μm (large panels) and 10 μm (smaller panels). (d) The volume of axonal varicosities was measured in left pontine sections of rats killed at 3 months, 6 months, or 1 year after AAV injections ($n \geq 4$ animals/time point). Data are expressed as geometric means ± 95% confidence interval. $^{+}p < .05$ vs. the value at the earlier time point (Kruskal–Wallis test). (e) Representative images show pontine axons stained with the Syn-O2 antibody, recognizing both oligomeric and fibrillar α-synuclein. Sections of the left pons were collected from rats killed at 3 or 6 months after vagal AAV injections. Scale bar = 20 μm

In a final set of analyses, potential pathological changes associated with hα-synuclein spreading were evaluated in the central amygdala. Following delineation criteria illustrated in Figure S3, the number of Nissl-stained neurons as well as IBA1- and GFAP-positive cells was counted in the left central amygdala and compared in naïve vs. AAV-injected rats at different ages and different time points post-treatment. No significant changes were found when neuronal and astrocyte counts were carried out in tissue specimens from naïve animals of different ages (Figure 5a,c). Similarly, the number of Nissl-stained and GFAP-immunoreactive cells remained unaffected in the central amygdala of AAV-injected rats as compared to age-matched control animals (Figure 5a,c). Quite in contrast, both aging and AAV treatment had an effect on microglia. Total microglial counts were increased by 10% in naïve rats at 1 year as compared to younger animals (Figure 5b). They were also significantly enhanced at 6 months (+15%) and 1 year (+25%) post-AAV injection (Figure 5b,d); IBA1-positive hyper-ramified and hypertrophic cells contributed to this elevation at both time points (Figure 5e,f).

3 | DISCUSSION

Evidence supporting a relationship between enhanced expression, neuron-to-neuron transfer, and long-distance spreading of α-

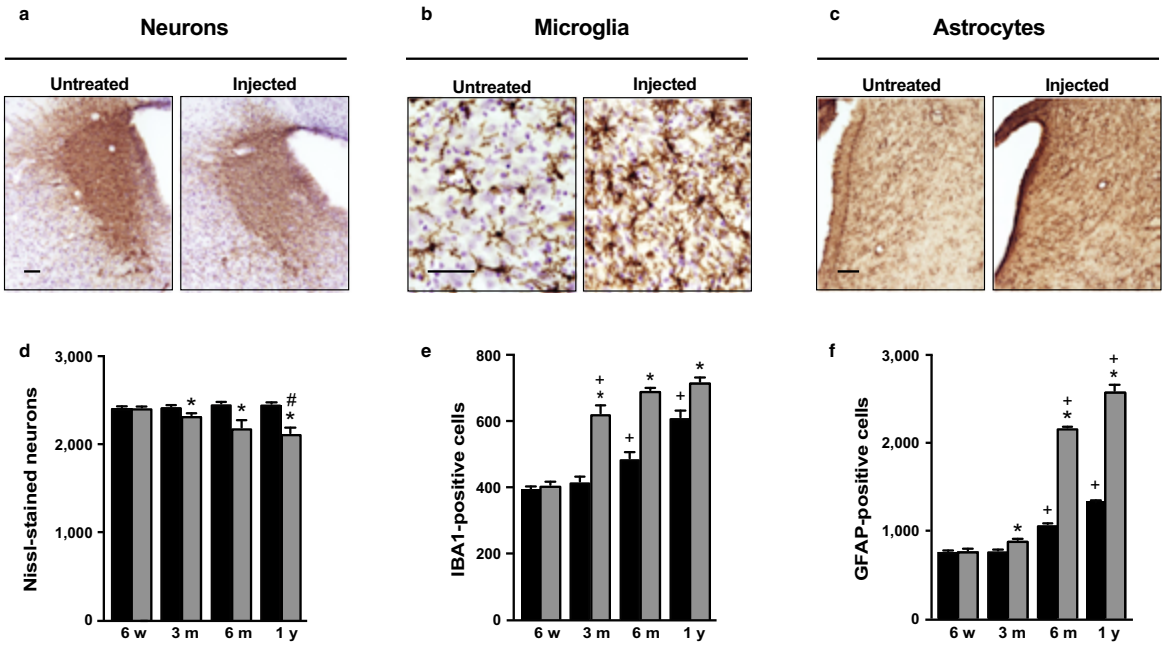

FIGURE 3 Neurodegeneration and gliosis as consequences of hα-synuclein spreading in the locus coeruleus. (a-c) Pontine sections were obtained from age-matched naïve (untreated) rats and animals that were injected with AAVs in the left vagus nerve and killed at 6 months (microglia and astrocytes) or 1 year (neurons) post-treatment. Sections were stained with antityrosine hydroxylase plus Nissl (a), anti-IBA1 plus Nissl (b), or anti-GFAP (c). Representative images show neuronal (a), microglial (b), and astrocytic (c) cells in the left locus coeruleus. Scale bars = 50 μm. (d-f) Stereological counts of Nissl-stained neurons (d), IBA1-positive microglia (e) and GFAP-immunoreactive astrocytes (f) were carried out in the locus coeruleus of untreated naïve rats (black bars; $n \geq 3$/time point) and the left locus coeruleus of AAV-injected animals (gray bars; $n \geq 3$/time point). Error bars indicate *SEM*. $^{*}p < .05$ vs. the value in age-matched controls at the corresponding time point (Student's *t* test). $^{+}p < .05$ vs. the value at the earlier time point in the respective treatment group (age-matched controls or AAV-injected rats) (one-way ANOVA). $^{\#}p < .05$ vs. the value at the 3-month time point (one-way ANOVA)

synuclein bears important pathogenetic implications for human synucleinopathies. Several conditions (including aging, environmental insults, genetic variations of the *SNCA* promoter region, and mutations of the glucocerebrosidase gene) are associated with α-synuclein elevation, underscoring the possibility that protein spreading may also occur under these conditions and contribute to an increased synucleinopathy risk (Mazzulli et al., 2011; Ulusoy & Di Monte, 2013). The present study elucidates important features of overexpression-induced α-synuclein transmission and, in particular, reveals long-lasting effects that could be relevant to disease development and progression in the aging brain. First, data indicate that progressive spreading of α-synuclein is strictly dependent upon its sustained overexpression within donor neurons. Under the experimental conditions used for this work, increased content of hα-synuclein within neurons in the medulla oblongata caused its initial brain spreading; on the other hand, a subsequent demise of these donor neurons represented a limiting factor, leading to cessation of caudo-rostral protein transmission. A second important finding of this study is that, upon death of the donor cells, the number of recipient axons accumulating hα-synuclein not only did not further increase but actually receded. At least two mechanisms, not mutually exclusive, could account for this long-term effect. The number of hα-synuclein-loaded fibers may decrease as a result of clearance of the exogenous protein, and/or persistent protein load could induce severe axonal injury and, ultimately, death of the recipient neurons. Either of these possibilities is supported by the observation that the mean volume of axonal varicosities, a marker of α-synuclein burden, declined over time in the pons of AAV-injected rats. Progressive protein clearance would result in smaller-sized swellings; alternatively or at the same time, a reduction in mean volume of axonal varicosities could arise from a preferential loss of neurons with greater α-synuclein burden and larger swellings.

To determine whether protein spreading and consequent axonal hα-synuclein burden ultimately led to frank neurodegeneration, detailed pathological analyses were carried out and compared in two brain regions, the locus coeruleus and central amygdala. Several reasons justify the choice of these regions. They are both significantly affected by α-synuclein pathology in the brain of Parkinson's disease patients. According to the Braak staging of disease progression, pathological α-synuclein lesions appear relatively early in the locus coeruleus (stage 2) and then reach the amygdala at later stages (stages 3 and 4); among the amygdalar nuclei, the central subnucleus

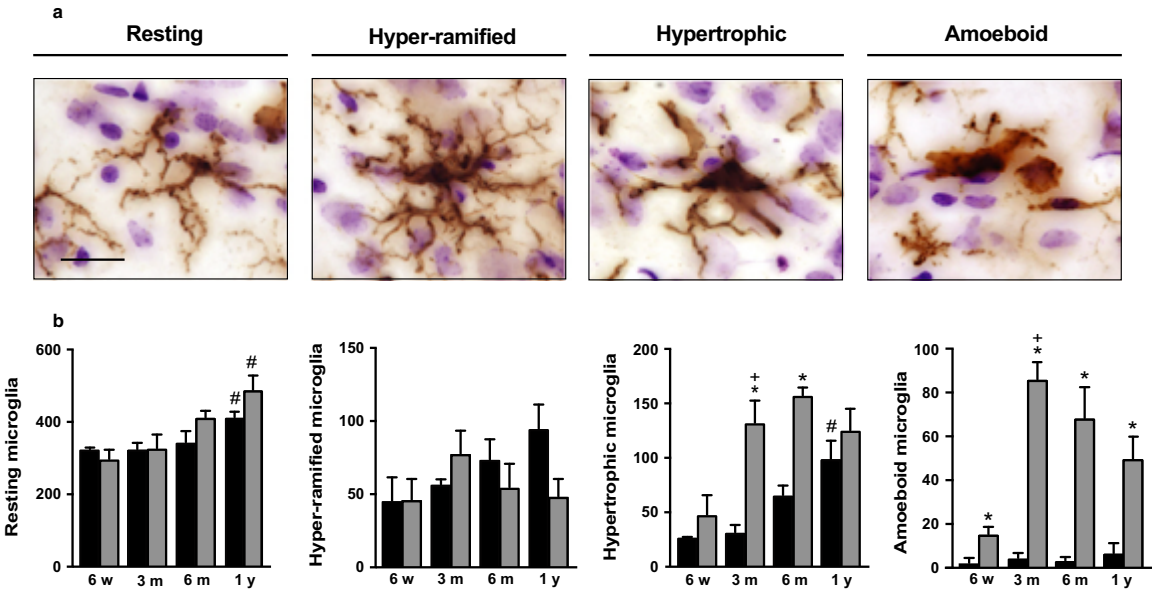

FIGURE 4 Changes in microglial phenotypes as a consequence of hα-synuclein spreading in the locus coeruleus. (a) Pontine sections from AAV-injected animals were immunolabeled with an anti-IBA1 antibody. Representative images show typical morphological features of resting, hyper-ramified, hypertrophic, and amoeboid microglia in the left locus coeruleus. Scale bar = 20 μm. (b) IBA1-positive cells with morphological features of resting, hyper-ramified, hypertrophic, or amoeboid microglia were stereologically counted in the locus coeruleus of untreated naïve rats (black bars; $n \geq 3$/time point) and the left (ipsilateral to the AAV injection side) locus coeruleus of AAV-injected animals (gray bars; $n \geq 3$/time point). Error bars indicate *SEM*. $^{*}p < .05$ vs the value in age-matched controls at the corresponding time point (Student's *t* test). $^{+}p < .05$ vs. the value at the earlier time point (one-way ANOVA). $^{\#}p < .05$ vs. the value at the 3-month time point in the respective treatment group (age-matched controls or AAV-injected rats) (one-way ANOVA)

represents a primary site of pathological α-synuclein accumulation (Braak, Rüb, Gai & Del Tredici, 2003 and Braak et al., 2003). Pathological features of both the locus coeruleus and central amygdala in Parkinson's disease brain also include neuronal cell loss, underscoring the relevance of these two regions for studies on the relationship between α-synuclein pathology and neurodegeneration (German et al., 1992; Harding, Stimson, Henderson & Halliday, 2002). The locus coeruleus and central amygdala densely project to the DMnX and, for this reason, may represent preferential sites of caudo-rostral α-synuclein spreading in Parkinson's disease as well as in our present model of overexpression-induced protein transmission (Braak, et al., 2003). In this model, hα-synuclein burden in brain regions affected by protein spreading is inversely correlated with their distance from the medulla oblongata and, indeed, the number of hα-synuclein-loaded axons and the extent of axonal protein accumulation are much greater in the locus coeruleus (pons) than in the amygdala (forebrain) (Ulusoy et al., 2013). This difference allowed us to assess whether potential long-term tissue injury was dependent upon severity of the initial α-synuclein burden.

Findings of this study provide first experimental evidence linking overexpression-induced α-synuclein spreading to neurodegeneration. A buildup of hα-synuclein into axonal projections stemming from the locus coeruleus caused a "dying back" neurodegenerative process and resulted in a progressive loss of catecholaminergic cells in this pontine nucleus. Neurodegeneration did not involve formation of fibrillar or hyperphosphorylated α-synuclein, consistent with a pathological/toxic role of accumulation of monomeric and oligomeric forms of the protein (Roberts, Wade-Martins & Alegre-Abarrategui, 2015; Rochenstain et al., 2014). The sequence of pathological events leading from protein spreading to neurodegeneration is also noteworthy. Neuronal death proceeded after cessation of spreading (at 6 months and 1 year), supporting the concept that even temporary increases in α-synuclein expression could have sustained consequences in brain regions distant from the site of overexpression but anatomically connected to it.

A marked gliosis characterized the locus coeruleus of AAV-injected rats. Counts of IBA1-positive and GFAP-immunoreactive cells were both significantly enhanced after overexpression-induced spreading. The time courses of these microglial and astrocytic changes revealed clear differences, however. In particular, a pronounced increase in total microglial number as well as in counts of hypertrophic and amoeboid microglia was already evident at 3 months and was maintained at later time points; marked astrocyte elevations were instead seen only at 6 months and 1 year post-treatment. Microglial activation at 3 months paralleled and could be a consequence of the initial degeneration of catecholaminergic neurons. It is also possible, however, that these glial changes may be initiated or accentuated by interactions between α-synuclein and

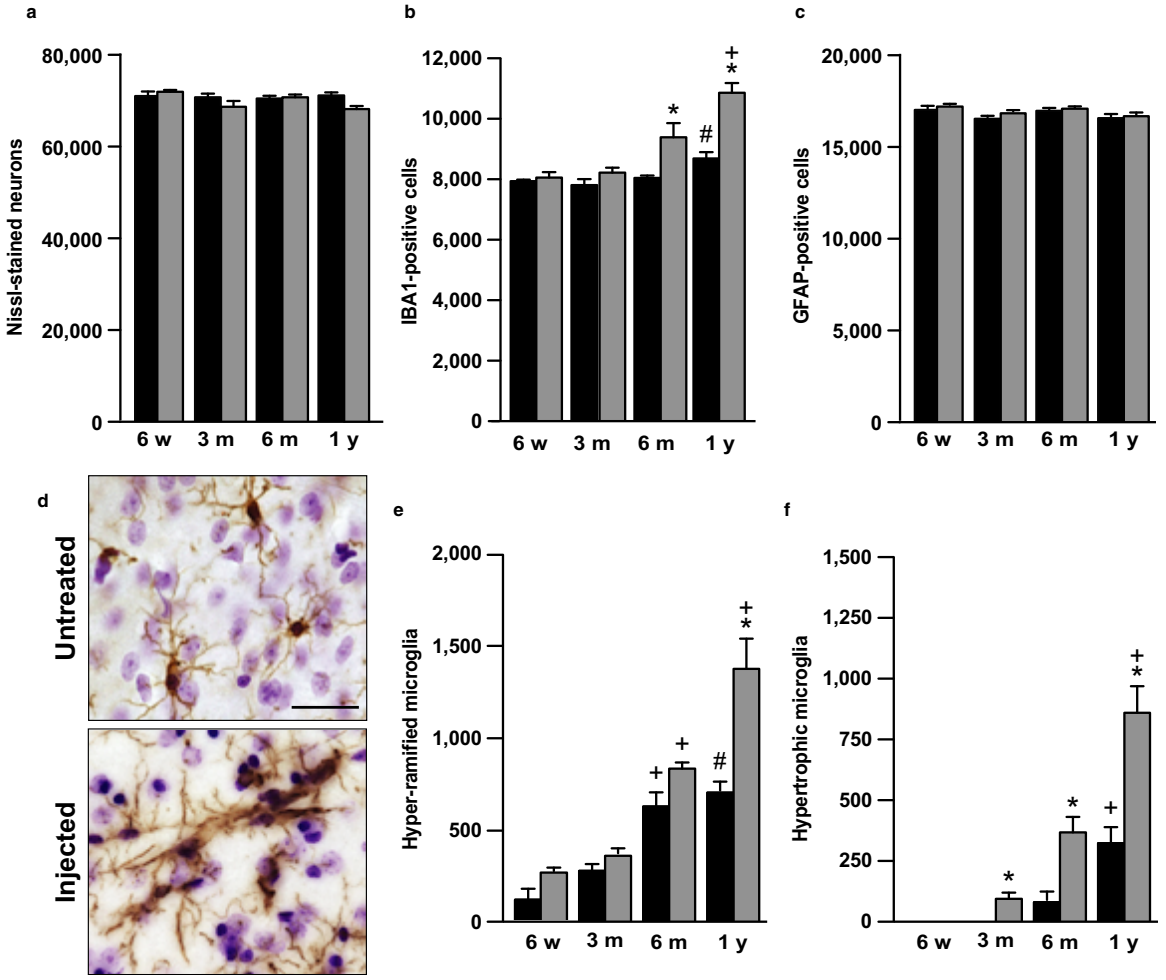

FIGURE 5 Microgliosis as a long-term consequence of hα-synuclein spreading in the central amygdala. (a-c) Stereological analyses were performed on tissue sections encompassing the entire left central amygdala of rats that received a unilateral (left) vagal injection of hα-synuclein-carrying AAVs (gray bars). Animals were sacrificed at different time points post-treatment ($n \geq 3$ animals/time point). Comparisons were made with control values obtained from age-matched naïve animals (black bars; $n \geq 3$ rats/time point). The number of Nissl-stained neurons (a), IBA1-positive microglia (b), and GFAP-immunoreactive astrocytes (c) was estimated. (d) Representative sections of the left central amygdala of an age-matched naïve (untreated) rat and an AAV-injected animal killed at 1 year post-treatment were immunostained with an anti-IBA1 antibody. Scale bar = 25 μm. (e and f) The number of IBA1-immunoreactive cells with morphological features of hyper-ramified (e) or hypertrophic (f) microglia was counted stereologically in the left central amygdala of age-matched naïve controls (black bars) and AAV-injected (gray bars) rats. Error bars indicate *SEM*. $^{*}p < .05$ vs. the value in age-matched controls at the corresponding time point (Student's *t* test). $^{+}p < .05$ vs. the value at the earlier time point in the respective treatment group (age-matched controls or AAV-injected rats) (one-way ANOVA). $^{\#}p < .05$ vs. the value at the 3-month time point in the respective treatment group (one-way ANOVA)

microglia. Earlier work has shown that, once released from neurons, oligomeric α-synuclein is capable of inducing microglial activation by acting as a ligand of the Toll-like receptor 2 (TLR2) (Kim et al., 2013). Our results show an elevated number of hα-synuclein-loaded axons at 3 months and also reveal that oligomeric α-synuclein is formed and accumulated within these recipient neurons. Thus, mechanisms leading to an early inflammatory response in the locus coeruleus may include a release of oligomeric α-synuclein from damaged axons and ensuing TLR2-mediated microglial activation. The increase in counts of GFAP-labeled astrocytes displayed a delayed pattern as compared to microglial activation and peaked later than the acute onset of neurodegeneration. It appears to reflect therefore postinjury processes and/or to be part of a more chronic reaction to ongoing degenerative lesions at 6 months and 1 year post-treatment. Micro- and astrogliosis triggered by protein transmission in this model was not accompanied by overt evidence of hα-synuclein accumulation within these glial cells. This negative observation should be interpreted with a degree of caution, however. Further studies are

warranted to rule out the possibility, for example, that a more discrete protein transfer might have been overlooked due to limitations of the detection methods used in our present investigation.

Findings in the locus coeruleus were compared to results of parallel analyses in the central amygdala where, as discussed above, the extent of hα-synuclein spreading was significantly less pronounced. No evidence of neurodegeneration was found in the central amygdala, thus suggesting that a less severe hα-synuclein burden is compatible with clearance of the overloaded protein and neuronal survival. Less severe forebrain injury is also likely to explain the lack of astrocytic reaction in the central amygdala of AAV-injected rats even at late time points post-treatment. Quite in contrast, an intriguing long-term effect of hα-synuclein spreading in the central amygdala was an increase in counts of IBA1-positive cells at 6 months and 1 year. Taken together, data indicate that astrogliosis is more strictly associated with neurodegenerative changes while activation of microglia can still occur in the absence of severe tissue injury; data are also consistent with the possibility that milder axonal pathology may facilitate the release of hα-synuclein into the extracellular space and its consequent binding to microglial TLR2. As compared to findings in the locus coeruleus where neuronal cell loss was associated with higher counts of hypertrophic and amoeboid microglia, changes in the central amygdala were accounted for by increases in hyper-ramified and hypertrophic cells. In line with earlier results (Sanchez-Guajardo, Febbraro, Kirik & Romero-Ramos, 2010), these observations suggest that microglial morphology is in part dependent upon the severity of α-synuclein-induced pathology; in particular, a marked elevation of IBA1-positive cells with amoeboid phenotype appears to be a reflection of pronounced tissue injury leading to neurodegeneration.

In summary, results of this study have elucidated a number of important factors and mechanisms affecting overexpression-induced α-synuclein spreading and pathology. They include the survival/demise of donor neurons, the extent of protein burden within recipient cells, and the response of brain tissue to α-synuclein accumulation/release. A potential addition to this list is suggested by our findings in untreated naïve animals. Neuronal counts were similar among naïve rats of different ages in either the locus coeruleus or central amygdala. Age-related and region-specific differences were seen, however, in glial counts. In the locus coeruleus, the number of microglia and astrocytes was progressively higher at 6 months and 1 year, whereas, in the central amygdala, a slight but statistically significant elevation of microglia was detected only at 1 year. The pathophysiological relevance of glial changes in the aging brain and their involvement in the pathogenesis of human synucleinopathies are far from being fully understood (Askew et al., 2017; Cotrina & Nedergaard, 2002; Hefendehl et al., 2014). It is reasonable to speculate, however, that age- and region-dependent increases in astrocyte and microglial counts could play a role in modulating long-term α-synuclein pathology and may contribute to selective vulnerability to α-synuclein spreading.

4 | EXPERIMENTAL PROCEDURES

A detailed description of the experimental procedures can be found in the online supporting information (Appendix S1).

4.1 | Animals and surgical procedures

Experimental protocols/procedures were approved by the ethical committee of the State Agency for Nature, Environment and Consumer Protection in North Rhine Westphalia. Some of the animals received intravagal injections of recombinant AAVs (serotype 2 genome and serotype 6 capsids) for transgene expression of hα-synuclein. The surgical procedure for vagal AAV injection has been previously described (Ulusoy et al., 2013).

4.2 | Tissue preparation and histology

Animals were killed under pentobarbital anesthesia and perfused through the ascending aorta with paraformaldehyde. Brains were removed, immersion-fixed in paraformaldehyde, and cryopreserved. Coronal sections (40 μm) throughout the brain were cut and stored. Immunohistochemistry was performed on free-floating sections. The following primary antibodies were used: monoclonal mouse anti-hα-synuclein clone syn211 (Merck Millipore, Darmstadt, Germany; 1:10,000), polyclonal rabbit anti-α-synuclein (AB5038P, Merck Millipore; 1:750), monoclonal mouse antibody recognizing both α-synuclein fibrils and oligomers (Syn-O2, courtesy of Dr. Omar El-Agnaf; 1:12,000), monoclonal mouse antibody recognizing mature α-synuclein fibrils (Syn-F1, courtesy of Dr. Omar El-Agnaf; 1:10,000), monoclonal rabbit anti-phospho-Ser129 α-synuclein (clone EP15361Y, Abcam, Cambridge, UK; 1:10,000), polyclonal rabbit anti-GFAP (DAKO, Waldbronn, Germany; 1:500), polyclonal rabbit anti-IBA1 (WAKO, Neuss, Germany; 1:500), polyclonal guinea pig anti-IBA1 (Synaptic Systems, Goettingen, Germany; 1:500), and polyclonal rabbit antityrosine hydroxylase (Merck Millipore; 1:10,000). All histological quantifications were performed by investigators blinded to the experimental groups. Unbiased stereology using the optical fractionator probe was carried out to estimate cell numbers (neurons, microglia, and/or astrocytes). The number of axons immunoreactive for hα-synuclein and the volume of hα-synuclein-positive axonal varicosities were quantified as previously described (Ulusoy et al., 2013).

4.3 | Statistical analysis

Statistical analyses were performed with PRISM software (version 7.0a; GraphPad Software, La Jolla, CA, USA). For normally distributed data, means between two groups were compared with two-tailed Student's *t* test, and comparisons between multiple groups were carried out with one-way ANOVA followed by Tukey post hoc test. For non-normally distributed data, Kruskal–Wallis test was applied. Statistical significance was set at $p < .05$. The number of animals used for each experiment/analysis is indicated in Table S1.

ACKNOWLEDGMENTS

We thank Sarah A. Jewell for her comments on the manuscript; Omar El-Agnaf for kindly providing conformation-specific antibodies; Bettina Winzen-Reichert, Franziska Hesse, Laura Jakobi for assistance with the experiments; and Ireen Koenig (DZNE Light Microscopy Facility) for assistance with microscopy.

CONFLICT OF INTEREST

The authors declare that they have no competing interests.

AUTHOR CONTRIBUTIONS

RR designed experiments and carried out histological analyses, neuronal counts in the DMnX, and volumetric measurements of axonal varicosities; AU performed surgeries and carried out stereological cell counting (neurons and glia) in the central amygdala and axonal counts; HA performed stereological cell counting in the locus coeruleus; DADM designed experiments, analyzed data, and wrote the manuscript with input from the other authors.

REFERENCES

Askew, K., Li, K., Olmos-Alonso, A., Garcia-Moreno, F., Liang, Y., Richardson, P., … Gomez-Nicola, D. (2017). Coupled proliferation and apoptosis maintain the rapid turnover of microglia in the adult brain. *Cell Reports*, *18*, 391–405. https://doi.org/10.1016/j.celrep.2016.12.041

Braak, H., Del Tredici, K., Rub, U., de Vos, R. A., Jansen Steur, E. N., & Braak, E. (2003). Staging of brain pathology related to sporadic Parkinson's disease. *Neurobiology of Aging*, *24*(2), 197–211. https://doi.org/10.1016/S0197-4580(02)00065-9

Braak, H., Rüb, U., Gai, W. P., & Del Tredici, K. (2003). Idiopathic Parkinson's disease: Possible routes by which vulnerable neuronal types may be subject to neuroinvasion by an unknown pathogen. *Journal of Neural Transmission*, *110*(5), 517–536. https://doi.org/10.1007/s00702-002-0808-2

Chartier-Harlin, M. C., Kachergus, J., Roumier, C., Mouroux, V., Douay, X., Lincoln, S., … Destée, A. (2004). α-Synuclein locus duplication as a cause of familial Parkinson's disease. *Lancet*, *364*(9440), 1167–1169. https://doi.org/10.1016/S0140-6736(04)17103-1

Cotrina, M. L., & Nedergaard, M. (2002). Astrocytes in the aging brain. *Journal of Neuroscience Research*, *67*(1), 1–10. https://doi.org/10.1002/(ISSN)1097-4547

Desplats, P., Lee, H. J., Bae, E. J., Patrick, C., Rockenstein, E., Crews, L., … Lee, S. J. (2009). Inclusion formation and neuronal cell death through neuron-to-neuron transmission of α-synuclein. *Proceedings of the National Academy of Sciences of the United States of America*, *106*(31), 13010–13015. https://doi.org/10.1073/pnas.0903691106

German, D. C., Manaye, K. F., White, C. L., Woodward, D. J., McIntire, D. D., Smith, W. K., … Mann, D. M. (1992). Disease-specific patterns of locus coeruleus cell loss. *Annals of Neurology*, *32*(5), 667–676. https://doi.org/10.1002/ana.410320510

Goedert, M., Spillantini, M. G., Del Tredici, K., & Braak, H. (2013). 100 years of Lewy pathology. *Nature Reviews Neurology*, *9*(1), 13–24. https://doi.org/10.1038/nrneurol.2012.242

Harding, A. J., Stimson, E., Henderson, J. M., & Halliday, G. M. (2002). Clinical correlates of selective pathology in the amygdala of patients with Parkinson's disease. *Brain*, *125*(11), 2431–2445. https://doi.org/10.1093/brain/awf251

Hefendehl, J. K., Neher, J. J., Sühs, R. B., Kohsaka, S., Skodras, A., & Jucker, M. (2014). Homeostatic and injury-induced behavior in the aging brain. *Aging Cell*, *13*(1), 60–69. https://doi.org/10.1111/acel.12149

Helwig, M., Klinkenberg, M., Rusconi, R., Musgrove, R. E., Majbour, N. K., El-Agnaf, O. M., … Di Monte, D. A. (2016). Brain propagation of transduced α-synuclein involves non-fibrillar protein species and is enhanced in α-synuclein null mice. *Brain*, *139*(3), 856–870. https://doi.org/10.1007/s00401-016-1661-y

Ibáñez, P., Bonnet, A. M., Débarges, B., Lohmann, E., Tison, F., Pollak, P., … Brice, A. (2004). Causal relation between α-synuclein gene duplication and familial Parkinson's disease. *Lancet*, *364*(9440), 1169–1171. https://doi.org/10.1016/S0140-6736(04)17104-3

Jimenez-Ferrer, I., Jewett, M., Tontanahal, A., Romero-Ramos, M., & Swanberg, M. (2017). Allelic difference in Mhc2ta confers altered microglial activation and susceptibility to α-synuclein-induced dopaminergic neurodegeneration. *Neurobiology of Disease*, *106*, 279–290. https://doi.org/10.1016/j.nbd.2017.07.016

Kim, C., Ho, D. H., Suk, J. E., You, S., Michael, S., Kang, J., … Lee, S. J. (2013). Neuron-released oligomeric α-synuclein is an endogenous agonist of TLR2 for paracrine activation of microglia. *Nature Communications*, *4*, 1562. https://doi.org/10.1038/ncomms2534

Konno, T., Ross, O. A., Puschmann, A., Dickson, D. W., & Wszolek, Z. K. (2016). Autosomal dominant Parkinson's disease caused by SNCA duplications. *Parkinsonism & Related Disorders*, *1*(Supple 1), S1–S6. https://doi.org/10.1016/j.parkreldis.2015.09.007

van der Kooy, D., Koda, L. Y., McGinty, J. F., Gerfen, C. R., & Bloom, F. E. (1984). The organization of projections from the cortex, amygdala, and hypothalamus to the nucleus of the solitary tract in rat. *The Journal of Comparative Neurology*, *224*(1), 1–24.

Mazzulli, J. R., Xu, Y. H., Sun, Y., Knight, A. L., McLean, P. J., Caldwell, G. A., & Krainc, D. (2011). Gaucher disease glucocerebrosidase and α-synuclein form a bidirectional pathogenic loop in synucleinopathies. *Cell*, *146*(1), 37–52. https://doi.org/10.1016/j.cell.2011.06.001

Neumann, M., Kahle, P. J., Giasson, B. I., Ozmen, L., Borroni, E., Spooren, W., … Haass, C. (2002). Misfolded proteinase K-resistant hyperphosphorylated α-synuclein in aged transgenic mice with locomotor deterioration and in human alpha-synucleopathies. *The Journal of Clinical Investigation*, *110*(10), 1429–1439. https://doi.org/10.1172/JCI200215777

Petrucci, S., Ginevrino, M., & Valente, E. M. (2016). Phenotypic spectrum of α-synuclein mutations: New insights from patients and cellular models. *Parkinsonism & Related Disorders*, *22*(Suppl 1), S16–S20. https://doi.org/10.1016/j.parkreldis.2015.08.015

Polymeropoulos, M. H., Lavedan, C., Leroy, E., Ide, S. E., Dehejia, A., Dutra, A., … Nussbaum, R. L. (1997). Mutation in the α-synuclein gene identified in families with Parkinson's disease. *Science*, *276*(5321), 2045–2047.

Rey, N. L., Petit, G. H., Bousset, L., Melki, R., & Brundin, P. (2013). Transfer of human α-synuclein from the olfactory bulb to interconnected brain regions in mice. *Acta Neuropathologica*, *126*(4), 555–573. https://doi.org/10.1007/s00401-013-1160-3

Roberts, R. F., Wade-Martins, R., & Alegre-Abarrategui, J. (2015). Direct visualization of α-synuclein oligomers reveals previously undetected pathology in Parkinson's disease brain. *Brain*, *138*(6), 1642–1657. https://doi.org/10.1093/brain/awv040

Rochenstain, E., Nuber, S., Overk, C. R., Ubhi, K., Mante, M., Patrick, C., … Masliah, E. (2014). Accumulation of oligomer-prone α-synuclein exacerbates synaptic and neuronal degeneration in vivo. *Brain*, *137*(5), 1496–1513. https://doi.org/10.1093/brain/awu057

Ross, O. A., Braithwaite, A. T., Skipper, L. M., Kachergus, J., Hulihan, M. M., Middleton, F. A., … Farrer, M. J. (2008). Genomic investigation of α-synuclein multiplication and parkinsonism. *Annals of Neurology*, *63*(6), 743–750. https://doi.org/10.1002/ana.21380

Sanchez-Guajardo, V., Febbraro, F., Kirik, D., & Romero-Ramos, M. (2010). Microglia acquire distinct activation profiles depending on the degree of α-synuclein neuropathology in a rAAV based model of Parkinson's disease. *PLoS One*, *5*(1), e8784. https://doi.org/10.1371/journal.pone.0008784

Singleton, A. B., Farrer, M., Johnson, J., Singleton, A., Hague, S., Kachergus, J., … Gwinn-Hardy, K. (2003). α-Synuclein locus triplication causes Parkinson's disease. *Science*, *302*(5646), 841. https://doi.org/10.1126/science.1090278

Ter Horst, G. J., Toes, G. J., & Van Willigen, J. D. (1991). Locus coeruleus projections to the dorsal motor vagus nucleus in the rat. *Neuroscience*, *45*(1), 153–160. https://doi.org/10.1016/0306-4522(91)90111-Z

Torres-Platas, S. G., Comeau, S., Rachalski, A., Bo, G. D., Cruceanu, C., Turecki, G., & Mechawar, N. (2014). Morphometric characterization of microglia phenotypes in human cerebral cortex. *Journal of Neuroinflammation*, *11*, 12. https://doi.org/10.1186/1742-2094-11-12

Ulusoy, A., & Di Monte, D. A. (2013). α-Synuclein elevation in human neurodegenerative diseases: Experimental, pathogenic and therapeutic implications. *Molecular Neurobiology*, *47*(2), 484–494. https://doi.org/10.1007/s12035-012-8329-y

Ulusoy, A., Philips, R. J., Helwig, M., Klinkenberg, M., Powley, T. L., & Di Monte, D. A. (2017). Brain-to-stomach transfer of α-synuclein via vagal preganglionic projections. *Acta Neuropathologica*, *133*(3), 381–393. https://doi.org/10.1007/s00401-016-1661-y

Ulusoy, A., Rusconi, R., Pérez-Revuelta, B. I., Musgrove, R. E., Helwig, M., Winzen-Reichert, B., & Di Monte, D. A. (2013). Caudo-rostral brain spreading of α-synuclein through vagal connections. *EMBO Molecular Medicine*, *5*(7), 1119–1127. https://doi.org/10.1002/emmm.201302475

Vaikath, N. N., Majbour, N. K., Paleologou, K. E., Ardah, M. T., van Dam, E., van de Berg, W. D., … El-Agnaf, O. M. (2015). Generation and characterization of novel conformation-specific monoclonal antibodies for α-synuclein pathology. *Neurobiology of Disease*, *79*, 81–99. https://doi.org/10.1038/mt.2015.232

SUPPORTING INFORMATION

Additional Supporting Information may be found online in the supporting information tab for this article.

How to cite this article: Rusconi R, Ulusoy A, Aboutalebi H, Di Monte DA. Long-lasting pathological consequences of overexpression-induced α-synuclein spreading in the rat brain. *Aging Cell*. 2018;e12727. https://doi.org/10.1111/acel.12727

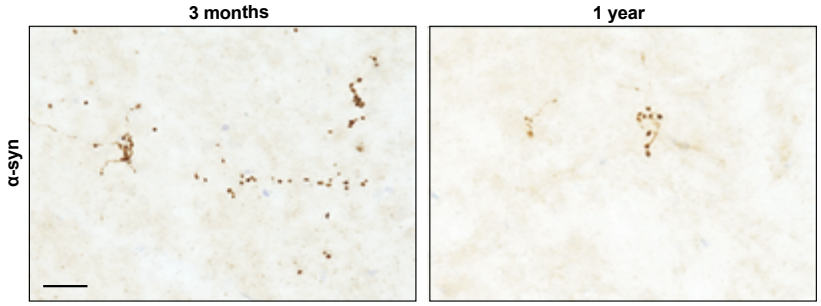

Fig. S1 Axonal pathology caused by hα-synuclein spreading. Pontine sections were stained with AB5038P, an antibody recognizing both human and rat α-synuclein. Representative images show α-synuclein-immunoreactive axons in the left (ipsilateral to the treatment side) pons of rats sacrificed at 3 months or 1 year after vagal AAV injections. Scale bar = 20 μm.

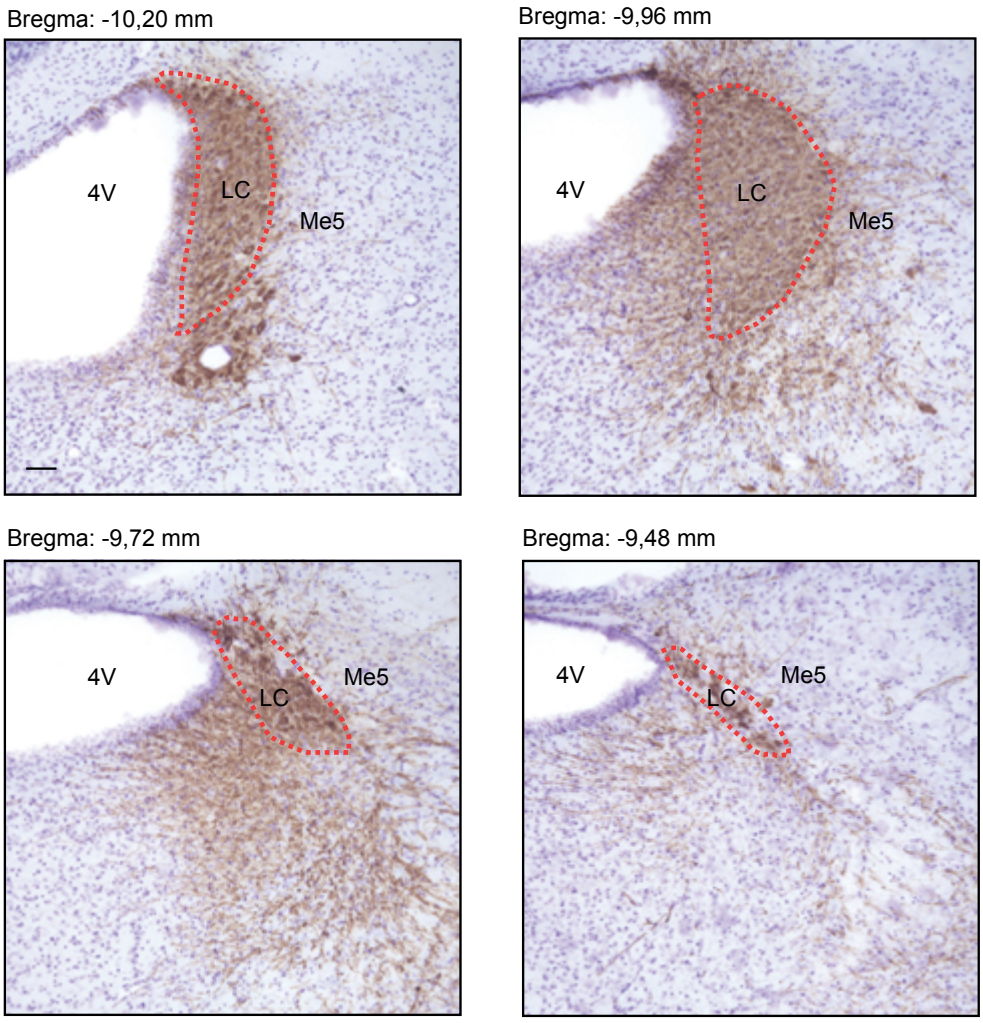

Fig. S2 Delineation of the counting area for stereological analysis in the locus coeruleus. The entire locus coeruleus was encompassed within four coronal sections (40-µm-thick) of the rat pons. Images show each of these sections at the corresponding caudo-rostral Bregma coordinate (-10.20 to -9.48 mm). The locus coeruleus (LC) is delineated by dashed red lines. The mesencephalic trigeminal nucleus (Me5) and 4th ventricle (4V) are also marked. Scale bar = 50 µm.

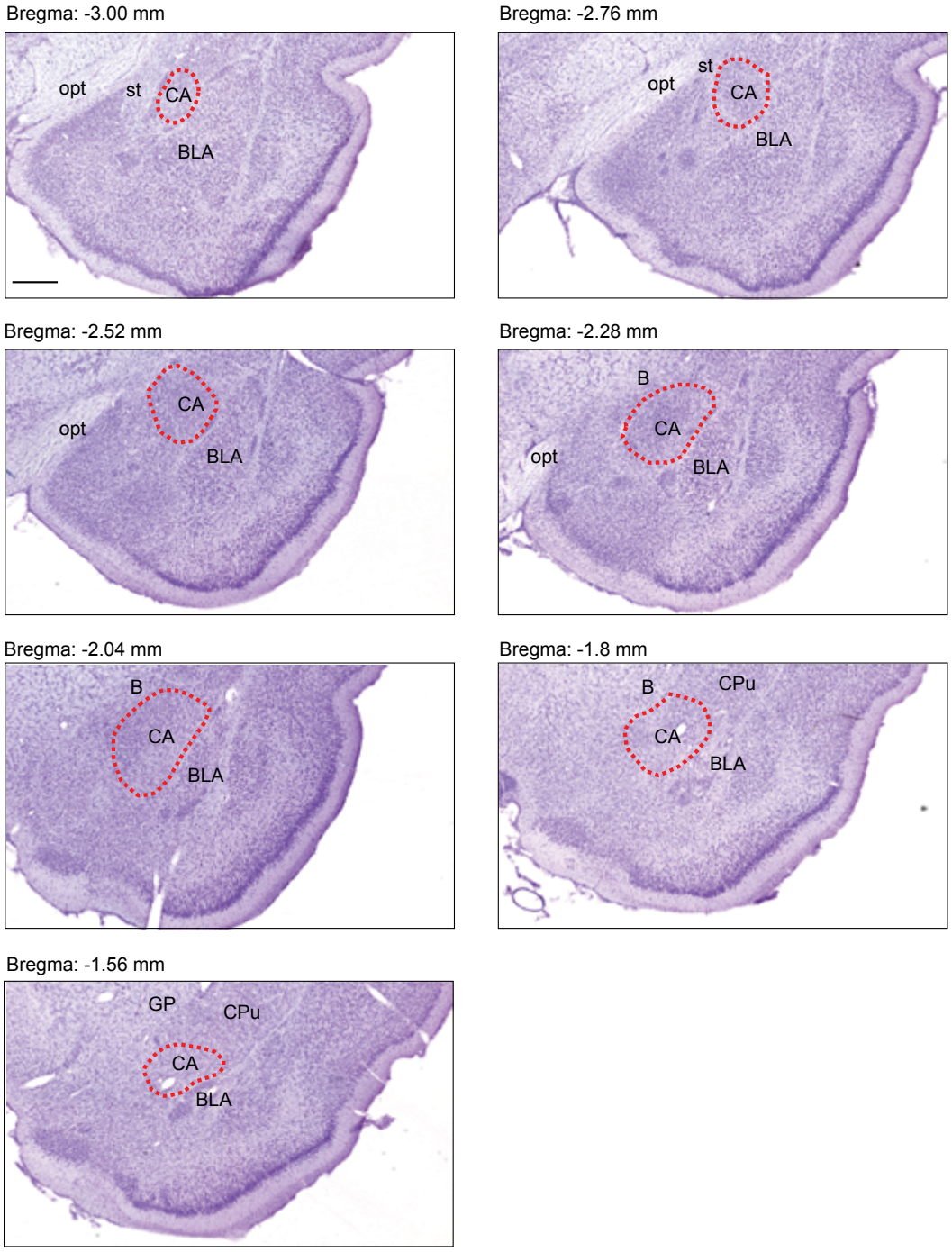

Fig. S3 Delineation of the counting area for stereological analysis in the central amygdala. The entire central amygdala was encompassed within seven coronal sections (40-µm-thick) of the medial temporal lobe. Images show each of these sections at the corresponding caudo-rostral Bregma coordinate (-3.00 to -1.56 mm). The central amygdala (CA) is delineated by dashed red lines, and the following structures/areas are marked: nucleus basalis of Meynert (B); basolateral amygdaloid nucleus (BLA); caudate putamen (CPu); globus pallidus (GP); optic tract (opt); stria terminalis (st). Scale bar = 500 µm.

FIGURE 1

	Fig 1C	Fig 1D	
	ipsi[1]	contra[2]	ipsi
6 weeks	5	6	6
3 months	5	7	8
6 months	6	8	8
1 year	5	5	6

FIGURE 2

	Fig 2A	Fig 2B	Fig 2D
	ipsi	ipsi	ipsi
6 weeks	4	4	
3 months	8	4	4
6 months	12	4	5
1 year	12	4	4

FIGURE 3

	Fig 3D		Fig 3E		Fig 3F	
	naïve[3]	AAV[1]	naïve	AAV	naïve	AAV
6 weeks	4	4	3	4	4	3
3 months	6	5	6	5	6	4
6 months	10	5	6	3	6	4
1 year	8	6	6	5	6	5

FIGURE 4

	Fig 4B	
	naïve	AAV
6 weeks	3	4
3 months	6	5
6 months	6	3
1 year	6	5

FIGURE 5

	Fig 5A		Fig 5B/E/F		Fig 5C	
	naïve	AAV	naïve	AAV	naïve	AAV
6 weeks	3	3	4	3	4	3
3 months	3	4	3	4	3	4
6 months	3	3	4	3	5	4
1 year	4	4	5	4	5	6

Table S1 Number of rats used for the experiments illustrated in Figs. 1-5.

[1]ipsi/AAV = rats received AAV injections, and analyses were made on the left side of the brain, ipsilateral to the injections.

[2]contra = rats received AAV injections, and analyses were made on the right side of the brain, contralateral to the injections.

[3]naïve = analyses were made in control, non-injected rats

Musgrove, R.E., Helwig, M., Bae, E.J., Aboutalebi, H., Lee, S.J., **Ulusoy, A.,** and Di Monte, D.A. (2019). **Oxidative stress in vagal neurons promotes parkinsonian pathology and intercellular α-synuclein transfer.** J Clin Invest 129, 3738-3753.

Objective: We next investigated possible molecular mechanisms that may trigger interneuronal α-syn spreading. We hypothesized that oxidative stress, a well-known cause of neurodegeneration, may also be implicated in pathology spreading.

Methods and results: To study the relationship between oxidative stress, neurodegeneration, and α-syn pathology, we overexpressed α-syn in the mouse DMX using the vagus nerve injection paradigm and induced oxidative stress by treating mice with a reactive oxygen species (ROS) generating agent paraquat (**Figure 4**). Overexpression of α-syn in these neurons triggered oxidative stress, which was exacerbated by paraquat exposure. A novel and translationally significant observation of this study was the finding that DMX neurons are particularly susceptible to oxidative challenges and the accumulation of ROS.

Severe oxidative stress led to increased production of oxidatively modified forms of α-syn (i.e., nitrated α-syn), enhanced α-syn aggregation, and degeneration of DMX neurons. Spreading of α-syn from the DMX to other brain regions under conditions of enhanced oxidative stress was also augmented, supporting the role of oxidative stress in promoting α-syn spreading. In vitro experiments confirmed the transfer of α-syn between cells under pro-oxidant conditions, with nitrated forms of α-syn being highly transferable. These findings demonstrate the relevance of oxidative stress in PD pathogenesis, establish a link between oxidative stress and vulnerability to α-syn pathology, and identify enhanced cell-to-cell α-syn transmission as a mechanism by which oxidative stress could promote PD development and progression.

Conclusions: This study highlights the susceptibility of DMX cholinergic neurons to oxidative stress and suggests that this vulnerability is a predisposing factor common to PD-vulnerable neuronal populations. The metabolic properties of these neurons, including calcium-dependent pacemaking (Surmeier et al., 2017), contribute to their high susceptibility to oxidative stress. The findings support the importance of oxidative injury and define a potential mechanism by which oxidative stress contributes to the development and progression of PD.

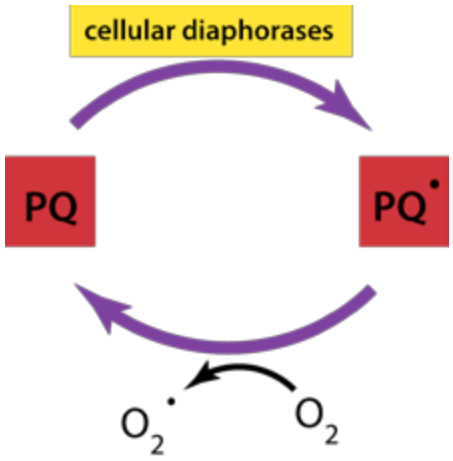

Figure 4. Paraquat's mechanism of action. Paraquat (PQ) is a herbicide that is known to induce the production of reactive oxygen species (ROS). When paraquat enters cells, it undergoes redox cycling. During this process, paraquat accepts an electron from a cellular molecule and is converted to a reduced form. The reduced form of PQ can then react with molecular oxygen to generate superoxide anions ($O_2^{\bullet-}$). Superoxide anions can further react with other molecules, leading to the production of additional ROS such as hydrogen peroxide (H_2O_2) and hydroxyl radicals (•OH). These ROS are highly reactive and can cause oxidative damage to cellular components, including proteins, lipids, and DNA.

JCI The Journal of Clinical Investigation

Oxidative stress in vagal neurons promotes parkinsonian pathology and intercellular α-synuclein transfer

Ruth E. Musgrove, … , Ayse Ulusoy, Donato A. Di Monte

J Clin Invest. 2019;129(9):3738-3753. https://doi.org/10.1172/JCI127330.

Research Article **Neuroscience**

Specific neuronal populations display high vulnerability to pathological processes in Parkinson's disease (PD). The dorsal motor nucleus of the vagus nerve (DMnX) is a primary site of pathological α-synuclein deposition and may play a key role in the spreading of α-synuclein lesions within and outside the CNS. Using in vivo models, we show that cholinergic neurons forming this nucleus are particularly susceptible to oxidative challenges and accumulation of ROS. Targeted α-synuclein overexpression within these neurons triggered an oxidative stress that became more pronounced after exposure to the ROS-generating agent paraquat. A more severe oxidative stress resulted in enhanced production of oxidatively modified forms of α-synuclein, increased α-synuclein aggregation into oligomeric species, and marked degeneration of DMnX neurons. Enhanced oxidative stress also affected neuron-to-neuron protein transfer, causing an increased spreading of α-synuclein from the DMnX toward more rostral brain regions. In vitro experiments confirmed a greater propensity of α-synuclein to pass from cell to cell under prooxidant conditions and identified nitrated α-synuclein forms as highly transferable protein species. These findings substantiate the relevance of oxidative injury in PD pathogenetic processes, establish a relationship between oxidative stress and vulnerability to α-synuclein pathology, and define a mechanism, enhanced cell-to-cell α-synuclein transmission, by which oxidative stress could promote PD development and progression.

RESEARCH ARTICLE The Journal of Clinical Investigation

Oxidative stress in vagal neurons promotes parkinsonian pathology and intercellular α-synuclein transfer

Ruth E. Musgrove,[1] Michael Helwig,[1] Eun-Jin Bae,[1,2] Helia Aboutalebi,[1] Seung-Jae Lee,[2] Ayse Ulusoy,[1] and Donato A. Di Monte[1]

[1]German Center for Neurodegenerative Diseases (DZNE), Bonn, Germany. [2]Departments of Biomedical Sciences and Medicine, Neuroscience Research Institute, Seoul National University College of Medicine, Seoul, South Korea.

Specific neuronal populations display high vulnerability to pathological processes in Parkinson's disease (PD). The dorsal motor nucleus of the vagus nerve (DMnX) is a primary site of pathological α-synuclein deposition and may play a key role in the spreading of α-synuclein lesions within and outside the CNS. Using in vivo models, we show that cholinergic neurons forming this nucleus are particularly susceptible to oxidative challenges and accumulation of ROS. Targeted α-synuclein overexpression within these neurons triggered an oxidative stress that became more pronounced after exposure to the ROS-generating agent paraquat. A more severe oxidative stress resulted in enhanced production of oxidatively modified forms of α-synuclein, increased α-synuclein aggregation into oligomeric species, and marked degeneration of DMnX neurons. Enhanced oxidative stress also affected neuron-to-neuron protein transfer, causing an increased spreading of α-synuclein from the DMnX toward more rostral brain regions. In vitro experiments confirmed a greater propensity of α-synuclein to pass from cell to cell under prooxidant conditions and identified nitrated α-synuclein forms as highly transferable protein species. These findings substantiate the relevance of oxidative injury in PD pathogenetic processes, establish a relationship between oxidative stress and vulnerability to α-synuclein pathology, and define a mechanism, enhanced cell-to-cell α-synuclein transmission, by which oxidative stress could promote PD development and progression.

Introduction

Oxidative stress has long been implicated in the pathogenesis of Parkinson's disease (PD), the second most common human neurodegenerative disorder. Pathological hallmarks of PD are the degeneration of discrete neuronal populations and progressive accumulation of α-synuclein–containing intraneuronal inclusions called Lewy bodies and Lewy neurites. Initial evidence linking oxidative stress to selective neurodegeneration focused on dopaminergic neurons in the substantia nigra pars compacta and led to the notion that their high vulnerability to PD pathology was due, at least in part, to a prooxidant environment generated by reactions involving dopamine itself (1, 2). More recent experimental work has elucidated a cascade of toxic events that could further explain the severe loss of dopaminergic cells and pronounced buildup of nigral Lewy inclusions seen in PD. A cell-autonomous pacemaking activity was found to cause large oscillations in intracellular calcium concentration within vulnerable nigral neurons, leading to mitochondrial oxidant stress, dopamine oxidation, lysosomal dysfunction, and α-synuclein accumulation (3–5). Once α-synuclein burden is enhanced within dopaminergic cells, a vicious cycle may be set in motion, since increased α-synuclein could promote the formation of protein aggregates and these aggregates may in turn exacerbate oxidative stress (6, 7).

Besides nigral dopaminergic cells, other neuronal populations are targeted by PD pathology. However, the role of oxidative stress as a mechanism contributing to this extranigral susceptibility and its involvement in pathogenetic processes that affect neurons devoid of dopamine content remain relatively unclear. In this study, the relationship among oxidative stress, neurodegeneration, and α-synuclein pathology was investigated in vivo in the mouse dorsal motor nucleus of the vagus (Xth) nerve (DMnX). Several lines of consideration underscore the rationale for choosing this specific brain region. The DMnX contains cholinergic neurons that are vulnerable to degeneration in PD (8–10). Similarly to nigral dopaminergic cells, DMnX neurons are spontaneously active; they exhibit autonomous pacemaking activity that is associated with a sustained calcium entry and high metabolic demands (11). The relevance of investigations focusing on DMnX neurons is further indicated by our current knowledge of α-synuclein pathophysiology. In postmortem PD brain, DMnX neurons are primary sites of accumulation of Lewy inclusions and are affected by α-synuclein aggregate pathology at the earliest stages of disease development (12). Pathological α-synuclein can be transferred from neuron to neuron, and through this mechanism, α-synuclein lesions may spread throughout the brain and reach vulnerable brain regions (13–16). As one of the initial sites of α-synuclein pathology, the DMnX could therefore play a critical role in the early process of protein accumulation and interneuronal protein transmission. Finally, evidence of α-synuclein lesions in the peripheral nervous system has prompted the suggestion that

▶ Related Commentary: p. 3530

Conflict of interest: SJL is a founder and CEO of Neuramedy Ltd.

Submitted: January 16, 2019; **Accepted:** June 6, 2019; **Published:** August 5, 2019.
Reference information: *J Clin Invest*. 2019;129(9):3738–3753.
https://doi.org/10.1172/JCI127330.

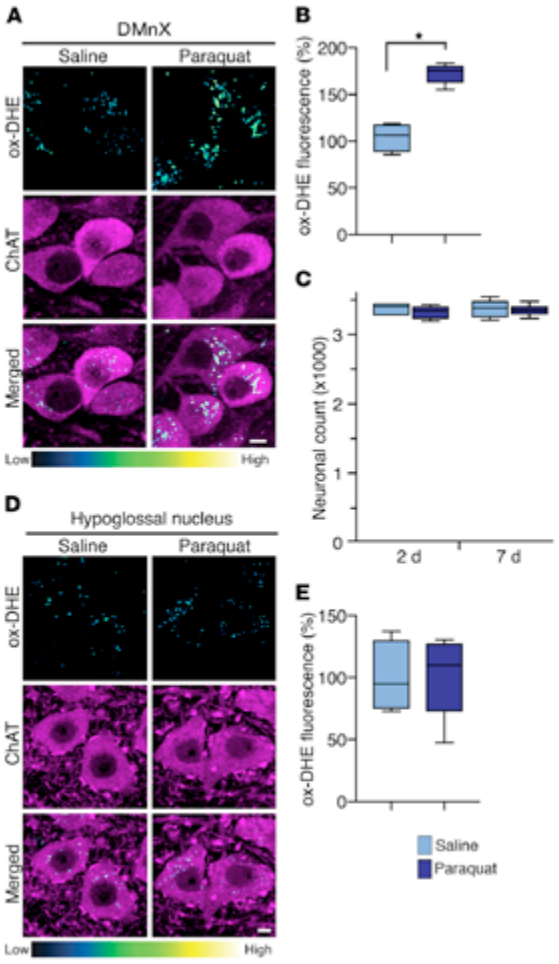

Figure 1. Paraquat-induced oxidative stress causes ROS accumulation in the DMnX, but not the hypoglossal nucleus. (**A**) Mice received 2 i.p. injections of either saline or paraquat separated by a 1-week interval and were sacrificed at 2 days after treatment. They were also injected with DHE 1 hour before the time of sacrifice. Representative confocal images show fluorescent puncta of ox-DHE (a marker of ROS formation, blue-green-yellow color graded) within ChAT-immunoreactive neurons (magenta) in the DMnX. Scale bar: 5 μm. (**B**) Comparison of the integrated density of fluorescent ox-DHE puncta within ChAT-positive DMnX neurons from mice treated with saline (n = 4, light blue bar) or paraquat (n = 5, dark blue bar). Approximately 100 neurons/animal were analyzed and averaged. Values were calculated as percentage of the mean value in saline-injected animals. (**C**) Mice injected with saline (n = 4/time point) or paraquat (n = 4/time point) were sacrificed at 2 and 7 days after treatment, and the number of Nissl-stained neurons was counted unilaterally in the DMnX. (**D**) Representative confocal images show ChAT-positive hypoglossal neurons (magenta) containing fluorescent ox-DHE from mice injected with saline or paraquat and sacrificed 2 days after treatment. Scale bar: 5 μm. (**E**) Integrated density of ox-DHE puncta within ChAT-positive neurons in the hypoglossal nucleus. Analyses were carried out on tissue sections from mice treated with saline (n = 4) or paraquat (n = 5). Approximately 30 neurons/animal were analyzed and averaged. Values were calculated as percentage of the mean value in saline-injected animals. Box and whisker plots show median (middle line), upper and lower quartiles, and maximum and minimum as whiskers. *$P \leq 0.05$, Mann-Whitney U test.

pathological forms of the protein may travel long distance from peripheral tissues to the brain and vice versa, from the brain to peripheral tissues (16). Both clinical and experimental observations support the likelihood that DMnX neurons, with their long visceromotor projections, represent key carriers of α-synuclein pathology on this central-to-peripheral route (17–19).

In the present study, targeted accumulation of α-synuclein within cholinergic DMnX neurons was achieved by a single injection of adeno-associated viral vectors (AAVs) carrying human α-synuclein (hα-synuclein) DNA into the mouse vagus nerve. Features of this model include aggregation and neuron-to-neuron transmission of hα-synuclein as well as selective degeneration of the overexpressing DMnX cells (20, 21). To induce oxidative stress both in vivo and in vitro, mice and cells in culture were treated with paraquat, a bipirydyl agent capable of generating substantial amounts of ROS via redox cycling with molecular oxygen (22). In vivo results revealed pronounced vulnerability of DMnX cholinergic neurons to oxidative challenges. Severe oxidative stress, as induced by paraquat exposure together with α-synuclein overexpression, caused an accumulation of oxidatively modified forms of α-synuclein, enhanced protein aggregation, and marked neurodegeneration, indicating a contribution of oxidative stress to PD-relevant pathological processes in the DMnX. Quite remarkably, both in vivo and in vitro evidence also revealed the ability of oxidative stress to promote cell-to-cell α-synuclein transfer and supported the conclusion that oxidized/nitrated forms of the protein are characterized by pronounced cell-to-cell mobility.

Results

Vulnerability of DMnX neurons to oxidative stress. Oxidative stress was compared in the DMnX of mice that received 2 i.p. injections (separated by a 1-week interval) of either vehicle (saline) or paraquat (15 mg/kg) and were sacrificed at 2 days after the second administration. To visualize and quantify ROS formation, the superoxide indicator dihydroethidium (DHE) was injected s.c. shortly before the time of sacrifice. Reaction of DHE with superoxide generates the fluorescent ethidium cation (ox-DHE); this cation can then be accumulated into mitochondria via the mitochondrial transmembrane potential, generating a punctate pattern of intracellular fluorescent signal (23, 24). Punctate fluorescence was observed within choline acetyltransferase–immunoreactive (ChAT-immunoreactive) DMnX neurons in sections of the mouse medulla oblongata from both control and paraquat-exposed mice; histology also revealed, however, that the number and intensity of labeled puncta were markedly augmented in specimens from the latter group of animals (Figure 1A). Intraneuronal quantification of the ethidium-generated fluorescent signal showed a significantly higher integrated density after paraquat administration, consistent with an increase in ROS formation (Figure 1B). Oxidative stress was further investigated by measurements of malondialdehyde, a marker of lipid peroxidation, in tissue specimens of the dorsal medulla oblongata. A prooxidant effect was indicated by a significant increase in malondialdehyde levels in samples

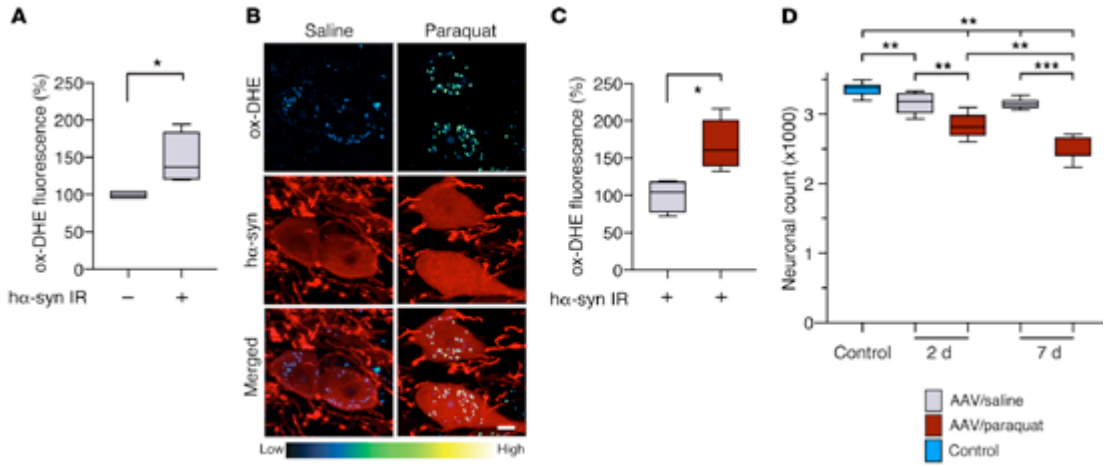

Figure 2. hα-Synuclein overexpression causes an oxidative stress that is augmented by paraquat administration. (**A**) Mice (n = 4) received a unilateral (left) intravagal injection of hα-synuclein–carrying AAVs. They were then treated with 2 i.p. injections of saline and were sacrificed at 2 days after the second saline administration. They also received an injection of DHE 1 hour before the time of sacrifice. Ox-DHE fluorescent signal was compared in the left DMnX between transduced neurons immunoreactive for hα-synuclein (hα-syn IR) and neurons devoid of hα-synuclein immunoreactivity. Approximately 50 neurons/animal were analyzed and averaged. Values were calculated as percentage of the mean value in hα-synuclein–devoid cells. (**B** and **C**) hα-Synuclein AAV–injected mice were treated with saline (n = 4) or paraquat (n = 5) and sacrificed at 2 days. They also received a DHE injection. (**B**) Representative confocal images show hα-synuclein–positive neurons (red) containing fluorescent ox-DHE (blue-green-yellow) in the left DMnX. Scale bar: 5 μm. (**C**) Integrated density of ox-DHE fluorescence within hα-synuclein–immunoreactive neurons in the left DMnX of mice treated with saline (gray bar) or paraquat (red bar). Approximately 50 neurons/animal were analyzed and averaged. Values were calculated as percentage of the mean value in hα-synuclein AAV/saline–injected animals. (**D**) hα-Synuclein AAV-injected mice were treated with either saline or paraquat and sacrificed at 2 (n ≥ 5/treatment) or 7 (n = 7/treatment) days after treatment. A group of control animals (n = 8, light blue bar) were only injected with saline. The number of Nissl-stained neurons was counted stereologically in the left DMnX. Box and whisker plots show median, upper and lower quartiles, and maximum and minimum as whiskers. $^*P \le 0.05$; $^{**}P \le 0.01$; $^{***}P \le 0.001$, Mann-Whitney U test (**A** and **C**) or Kruskal-Wallis followed by Conover-Iman post hoc test (**D**).

from paraquat-injected as compared with saline-injected mice (Supplemental Figure 1). To assess the neurotoxic consequences of paraquat-induced oxidative stress, the number of Nissl-stained neurons was counted stereologically in the DMnX. Results showed no difference in cell counts between saline- and paraquat-treated mice at 2 days after the second saline or paraquat injection. Also, no significant difference in neuronal number between the 2 groups of animals was seen at a later time point, namely 7 days after administration (Figure 1C).

Susceptibility to oxidative stress was then evaluated within other populations of cholinergic cells. First, analyses focused on ChAT-positive neurons that lie immediately below the DMnX and constitute the hypoglossal nucleus. In findings similar to those in the DMnX, oxidation-induced DHE fluorescence was detected within hypoglossal neurons in saline- and paraquat-injected mice (Figure 1D). In contrast with data in the DMnX, however, histological observations and measurements of integrated fluorescence density showed no significant changes as a result of paraquat exposure (Figure 1, D and E). Next, analyses were carried out to assess ox-DHE fluorescence within striatal cholinergic interneurons and ChAT-positive cells in the medial septal nucleus. In both regions, data showed ROS levels that were similar in saline- and paraquat-treated animals (Supplemental Figure 2).

Oxidative stress and α-synuclein burden in the DMnX. To investigate the relationship between α-synuclein accumulation and oxidative stress, mice were first injected with hα-synuclein AAVs into the left vagus nerve. Then, 2 weeks later, at a time when transduction and overexpression of the exogenous protein are fully attained in the DMnX (20, 25), they received 2 injections (at a 1-week interval) of either saline or paraquat. Sections of the medulla oblongata were immunostained with a specific antibody recognizing human but not rodent α-synuclein (MJFR1). Counts of neurons positive and negative for hα-synuclein showed that AAV-induced transduction caused overexpression in approximately 40% of neurons in the left DMnX (ipsilateral to the AAV injection); no hα-synuclein–containing cells were detected in the contralateral DMnX. Transduction efficiency was similar in control and paraquat-treated mice (data not shown). Oxidative stress was evaluated in animals sacrificed at 2 days after the second saline or paraquat administration; these mice also received a DHE injection prior to the time of sacrifice. To determine whether hα-synuclein overexpression was itself capable of inducing oxidative stress, ethidium-generated fluorescence was quantified in AAV-injected animals treated with saline and compared between neurons devoid of detectable hα-synuclein versus hα-synuclein–containing neurons in the left DMnX. Results revealed that a higher fluorescent signal characterized the transduced cells (Figure 2A). To test the possibility that paraquat administration may induce a further increase in ROS production over the one caused by hα-synuclein, fluorescence was compared between hα-synuclein–immunoreactive neurons in saline-treated mice and hα-synuclein–positive neurons in paraquat-injected animals. Paraquat exposure indeed triggered a

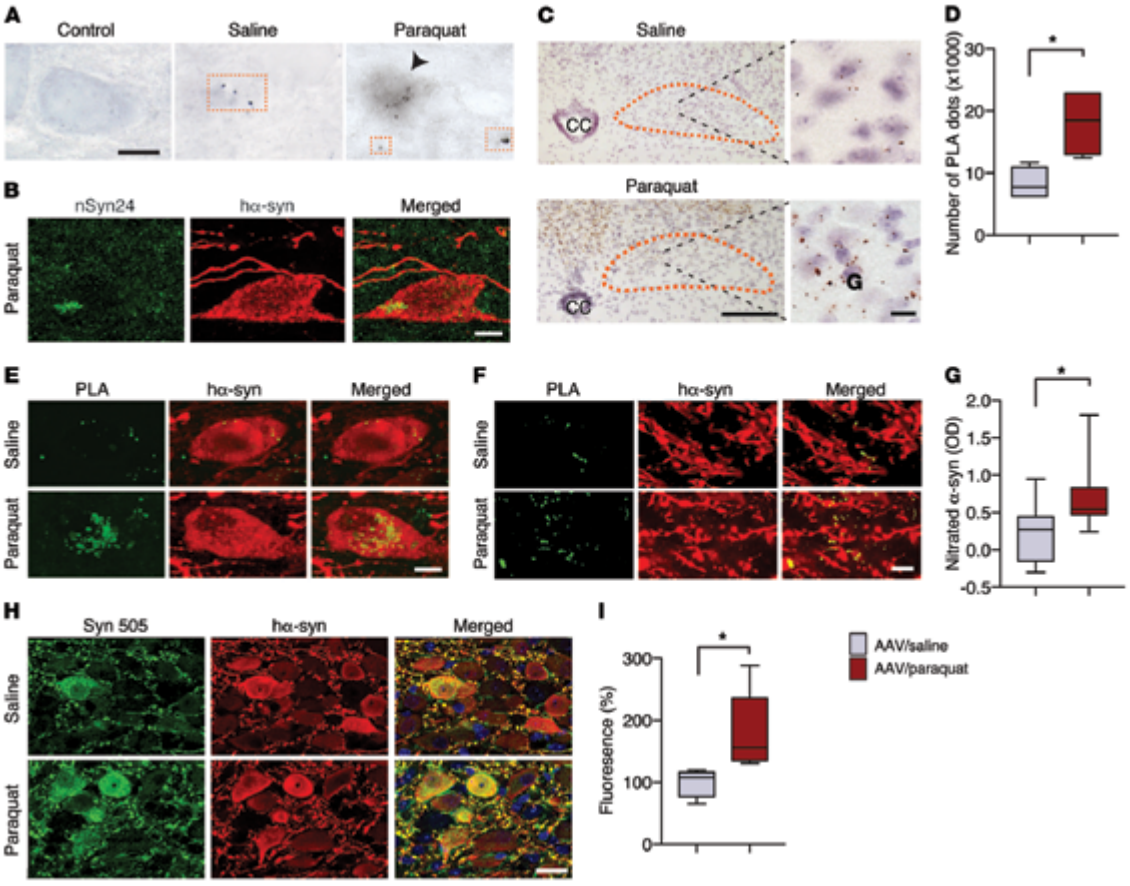

Figure 3. Severity of oxidative stress affects the degree of hα-synuclein oxidative modifications. Mice received an infusion of hα-synuclein–carrying AAVs into the left vagus nerve and were injected i.p. with either saline or paraquat and sacrificed at 2 days after treatment. (**A**) Representative images show left DMnX tissue stained with anti-nitrated α-synuclein (nSyn24). Squares highlight neuritic immunoreactivity, while the arrowhead indicates a DMnX immunoreactive cell body. Scale bar: 10 μm. (**B**) Confocal images show a neuron immunoreactive for both nSyn24 and hα-synuclein in the left DMnX of a mouse treated with hα-synuclein AAVs/paraquat. Scale bar: 5 μm. (**C**) Representative low- and high-magnification images of the left DMnX (delineated in orange) show specific signal for nitrated hα-synuclein detected by indirect hα-synuclein/3-NT PLA. CC, central canal. Scale bars: 200 μm (left); 10 μm (right). (**D**) The number of PLA dots was counted in the left DMnX of mice treated with hα-synuclein AAVs/saline (n = 4, gray bar) or hα-synuclein AAVs/paraquat (n = 4, red bar). (**E** and **F**) Sections of the medulla oblongata were double labeled with PLA and anti–hα-synuclein. Representative images show cell bodies (**E**) and neurites (**F**) in the left DMnX. Scale bars: 5 μm. (**G**) Nitrated α-synuclein was measured in the dorsal left medulla oblongata by ELISA. OD was compared in samples from mice treated with hα-synuclein AAVs/saline (n = 9) versus hα-synuclein AAVs/paraquat (n = 9). (**H** and **I**) Medullary sections were double stained with Syn 505 and anti–hα-synuclein. (**H**) Representative confocal images show left DMnX tissue. Scale bar: 10 μm. (**I**) Fluorescence densities for Syn 505 and hα-synuclein were measured on images of the left DMnX of mice treated with hα-synuclein AAVs/saline (n = 4) or hα-synuclein AAVs/paraquat (n = 5). At least 6 images/animal were analyzed. Values were calculated as the ratio of Syn 505/hα-synuclein fluorescence and are expressed as percentage of the mean value in hα-synuclein AAV/saline–injected animals. Box and whisker plots are shown. *$P \leq 0.05$, Mann-Whitney U test.

more robust DHE oxidation within cell bodies and neurites in the left DMnX, as assessed histologically as well as by quantification of the perikaryal fluorescent signal (Figure 2, B and C). The more severe oxidative stress caused by combined hα-synuclein overexpression and paraquat challenge was associated with enhanced neurotoxicity. Overexpression of hα-synuclein followed by 2 saline injections induced a 5% decrease in the number of DMnX neurons at both 2 and 7 days after treatment (Figure 2D). In contrast, cotreatment with hα-synuclein AAVs and paraquat caused a 15% reduction of DMnX Nissl–stained neurons already at 2 days after the second paraquat injection; this reduction progressed to a 25% loss at the 7-day time point (Figure 2D).

Oxidative modifications of α-synuclein in the DMnX. Oxidative α-synuclein modifications are typically observed in human synucleinopathies. Antibodies that specifically detect nitrated α-synuclein or react against 3-nitrotyrosine–modified (3-NT–modified) protein residues robustly label α-synuclein–containing inclusions in the brain of patients with PD and other synucle-

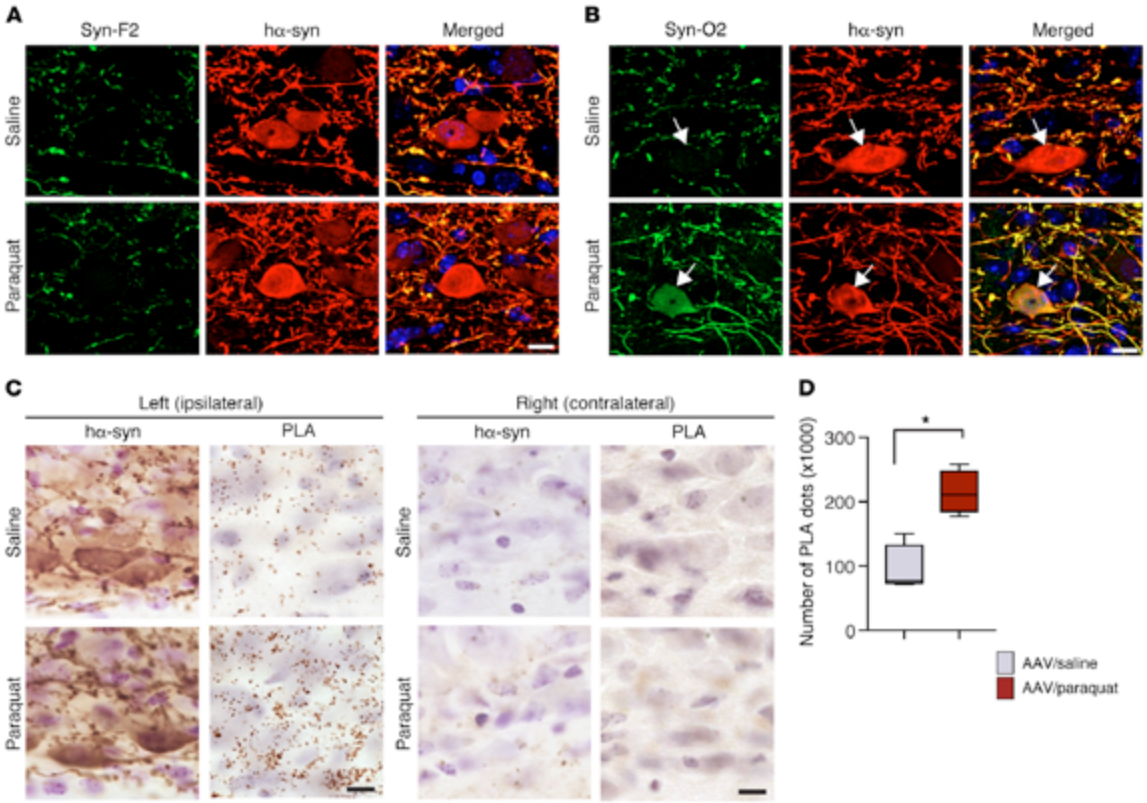

Figure 4. Severity of oxidative stress affects the extent of α-synuclein aggregation. Mice received an injection of hα-synuclein–carrying AAVs into the left vagus nerve and were injected systemically with either saline or paraquat and sacrificed at 2 days after treatment. (**A**) Representative confocal images show left DMnX tissue double labeled with an antibody that recognizes only mature α-synuclein fibrils (Syn-F2) and with anti–hα-synuclein. Scale bar: 5 μm. (**B**) Representative confocal images of left DMnX tissue. One of the antibodies used for double staining detects oligomeric and fibrillar forms of α-synuclein (Syn-O2). The other antibody was anti–hα-synuclein. Arrows indicate 2 hα-synuclein–positive neurons, one from a mouse injected with saline and the other from an animal treated with paraquat; the latter is also Syn-O2 immunoreactive. Scale bar: 5 μm. (**C**) Sections of the medulla oblongata were labeled with anti–hα-synuclein or with syn/syn PLA, which detects aggregated (preferentially oligomeric) hα-synuclein. Protein overexpression and aggregation were visualized in the left (ipsilateral to AAV infusion) and right (contralateral) DMnX and compared in mice treated with hα-synuclein AAVs/saline versus hα-synuclein AAVs/paraquat. Scale bars: 10 μm. (**D**) The number of syn/syn PLA dots was counted stereologically in the left DMnX from mice treated with hα-synuclein AAVs/saline (n = 4, gray bar) or with hα-synuclein AAVs/paraquat (n = 4, red bar). Box and whisker plots show median, upper and lower quartiles, and maximum and minimum as whiskers. *$P \leq 0.05$, Mann-Whitney U test.

inopathies (26, 27). Furthermore, monoclonal antibodies (i.e., Syn 505, Syn 506, Syn 514, and Syn 303) that are raised against oxidized/nitrated recombinant hα-synuclein recognize conformational α-synuclein variants that are preferentially associated with PD pathological lesions (28, 29). Here, the relationship between ROS formation and α-synuclein nitration was investigated in the DMnX of AAV-injected animals and compared under conditions of milder (AAV/saline treatment) versus severe (AAV/paraquat treatment) oxidative stress. Mice were sacrificed at 2 days after the second saline or paraquat treatment, and tissue sections of the medulla oblongata were immunostained with mouse anti-nitrated α-synuclein clone 24.8 (nSyn24), an antibody that detects α-synuclein nitrated at positions Y125 and Y133 (26). NSyn24 labeling was sparse in the left (AAV-injected side) DMnX from saline-treated animals and revealed a neuritic, dot-like accumulation of the modified protein (Figure 3A). More robust staining characterized the DMnX of paraquat-injected mice in which nSyn24 immunoreactivity not only labeled neuritic projections, but could also be detected within neuronal cell bodies overexpressing hα-synuclein (Figure 3, A and B). To further evaluate and quantify α-synuclein nitration, fixed medullary tissue sections and homogenates from snap-frozen medulla oblongata specimens were processed for proximity ligation assay (PLA) and ELISA, respectively. PLA has previously been shown to enable visualization of proteins with specific posttranslational modifications, such as phosphorylation, SUMOylation, and acetylation (30–32). In the present study, a pair of antibodies, namely anti–3-NT and MJFR1, was used to detect nitrated hα-synuclein by direct or indirect PLA; the former involved direct conjugation of the primary antibodies to oligonucleotide probes, whereas for the latter, reactive oligo-

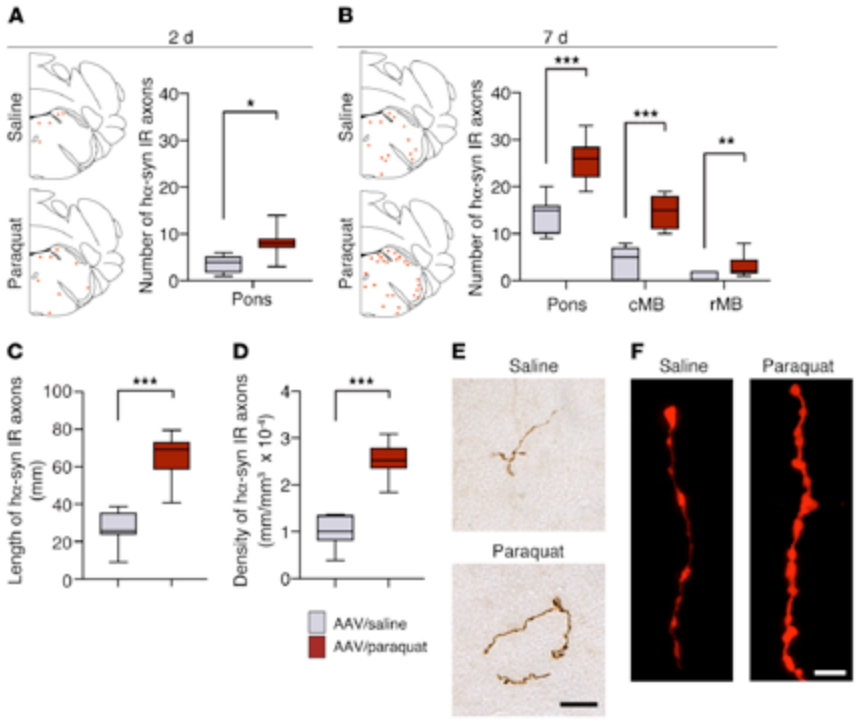

Figure 5. Oxidative stress promotes caudo-rostral spreading of hα-synuclein in the mouse brain. Mice received an infusion of hα-synuclein–carrying AAVs into the left vagus nerve and were injected i.p. with either saline or paraquat and sacrificed at 2 or 7 days after treatment. Tissue sections were immunostained with anti–hα-synuclein. (**A** and **B**) The schematic plots show the distribution of hα-synuclein–labeled axons (each red dot represents one of these axons) in the left (AAV-injected side) pons. In the graphs, data show the counts of hα-synuclein–immunoreactive axons in the left pons at 2 and 7 days and in the caudal (cMB) and rostral midbrain (rMB) at 7 days. Tissue was obtained from mice treated with hα-synuclein AAVs/saline (n = 6 at 2 days and n = 7 at 7 days, gray bars) or with hα-synuclein AAVs/paraquat (n = 7 at 2 days and n = 9 at 7 days, red bars). (**C** and **D**) Length and density of hα-synuclein–positive axons were estimated at 7 days after treatment in a pontine area encompassing the locus coeruleus and the nucleus parabrachialis using the Spaceballs stereological tool. Analyses were made in the left pons in samples collected from mice treated with hα-synuclein AAVs/saline (n = 7) or with hα-synuclein AAVs/paraquat (n = 9). (**E** and **F**) Representative images of pontine axons immunolabeled with anti–hα-synuclein and visualized using brightfield (brown) or fluorescent (red) microscopy. Scale bars: 20 μm (**E**); 5 μm (**F**). Box and whisker plots show median, upper and lower quartiles, and maximum and minimum as whiskers. $*P \le 0.05$; $**P \le 0.01$; $***P \le 0.001$, Mann-Whitney U test.

nucleotides were conjugated to the secondary antibodies. Both hα-synuclein/3-NT PLA procedures yielded similar findings. Specific chromogenic dots were detected in the left but not the right DMnX of all AAV-injected mice, and a marked enhancement of signal characterized sections from paraquat- as compared with saline-treated animals (Figure 3C and Supplemental Figure 3). This effect was confirmed and quantified by PLA dot counts (Figure 3D). Furthermore, using an in situ fluorescent PLA protocol, neuronal cell bodies and neuritic projections accumulating nitrated hα-synuclein were frequently observed in the DMnX of mice injected with paraquat and were instead very scarce in saline-treated animals (Figure 3, E and F). Levels of nitrated α-synuclein were finally measured by ELISA in tissue specimens of the dorsal left medulla oblongata encompassing the transduced DMnX. Using an antibody against total (human and mouse) α-synuclein as capture reagent and anti–3-NT as a detection antibody, we found protein nitration to be significantly increased as a consequence of paraquat administration (Figure 3G).

Medullary tissue sections were then double-immunostained with Syn 505, one of the antibodies raised against oxidized/nitrated hα-synuclein (28), and anti–hα-synuclein. Results showed immunoreactivity within transduced cell bodies and neurites in the left DMnX of saline-injected mice. The extent of protein modifications detected by Syn 505 was more pronounced, however, in animals treated with paraquat (Figure 3H). Similarly, when the ratio of fluorescent Syn 505/hα-synuclein signals was measured in DMnX sections, a significant increase was found after paraquat administration (Figure 3I).

Oxidative stress–induced α-synuclein aggregation in the DMnX. Oxidative stress may exacerbate α-synuclein's tendency to aggregate (33–36). Furthermore, nitrative modifications of α-synuclein induced by oxidative stress could affect the kinetics of protein aggregation and modulate pathways of protein assembly, leading to the formation of oligomeric and/or fibrillar species (37–40). Conformation-specific antibodies were used to determine whether oxidative stress enhanced α-synuclein aggregation in

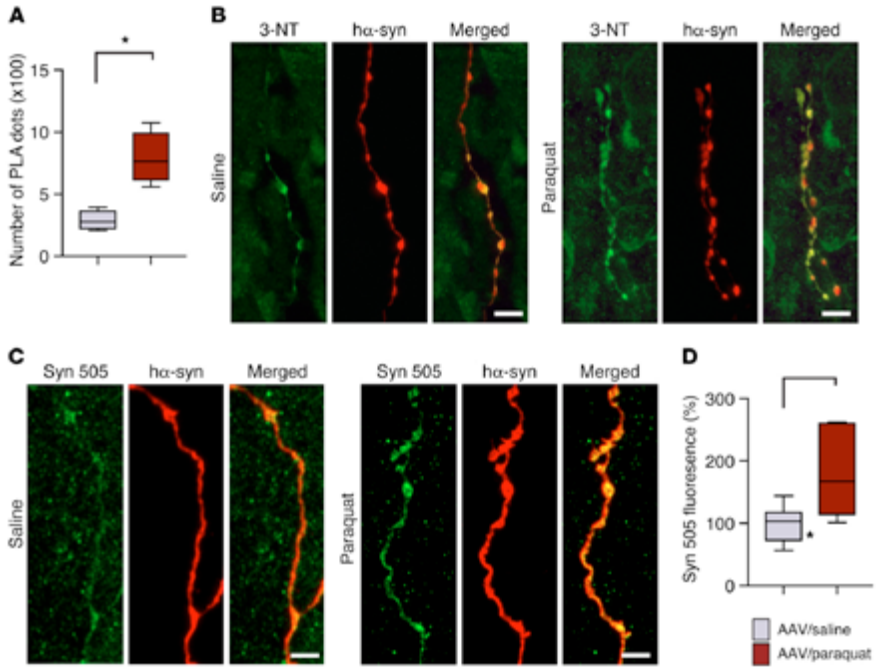

Figure 6. Oxidatively modified hα-synuclein is accumulated within pontine axons during caudo-rostral spreading of the protein. Mice received an infusion of hα-synuclein–carrying AAVs into the left vagus nerve and were injected systemically with either saline or paraquat and sacrificed at 7 days after treatment. (**A**) Nitrated hα-synuclein was detected by indirect hα-synuclein/3-NT PLA. The number of PLA dots in the left pons from mice treated with hα-synuclein AAVs/saline (n = 4, gray bar) or with hα-synuclein AAVs/paraquat (n = 5, red bar) was counted. (**B**) Pontine tissue sections were costained with anti–3-NT and anti–hα-synuclein. Representative confocal images show labeled axons in the left pons. Scale bars: 5 μm. (**C**) Representative confocal images show axons in the left pons stained with anti-Syn 505 and anti–hα-synuclein. Scale bar: 5 μm. (**D**) Measurements of Syn 505 fluorescence were carried out in the left pons of mice treated with hα-synuclein AAVs/saline (n = 7) or with hα-synuclein AAVs/paraquat (n = 6). At least 3 axons/animal were analyzed and averaged. Values are expressed as percentage of the mean value in hα-synuclein AAV/saline-injected animals. Box and whisker plots show median, upper and lower quartiles, and maximum and minimum as whiskers. *$P \leq 0.05$, Mann-Whitney U test.

the DMnX and whether it promoted the accumulation of specific aggregate forms (i.e., fibrillar or oligomeric). First, medullary tissue sections from hα-synuclein–overexpressing mice were stained with an antibody, Syn-F2, that recognizes only mature amyloid α-synuclein fibrils (20, 41). Immunoreactivity for Syn-F2 labeled hα-synuclein–containing neuronal processes in the left DMnX, with no apparent difference in the distribution and robustness of labeling between overexpressing mice injected with saline and overexpressing animals treated with paraquat (Figure 4A). Tissue sections were then probed with a second antibody, Syn-O2, capable of detecting both α-synuclein oligomers and α-synuclein fibrils (20, 41). Syn-O2 staining was overtly more pronounced in specimens from paraquat- as compared with saline-injected mice, as indicated by a denser network of labeled neurites and by the presence of DMnX cell bodies immunoreactive for both Syn-O2 and hα-synuclein (Figure 4B). Taken together, these findings indicate that, as a result of paraquat-induced oxidative stress, α-synuclein aggregation is enhanced and leads to the formation of predominantly oligomeric protein species. Similar conclusions could be drawn from experiments in which protein aggregation was assessed using a PLA protocol (syn/syn PLA) that preferentially detects pathological hα-synuclein oligomers in PD brain and in the brain of hα-synuclein–overexpressing mice (20, 42). Syn/syn PLA labeling was observed in medullary sections from all AAV-injected mice, and its distribution closely matched the pattern of hα-synuclein overexpression. In particular, distinct chromogenic spots characterized the left DMnX (ipsilateral to the AAV injection side), whereas no specific signal was detected on the contralateral side of the brain (Figure 4C). PLA reactivity was then compared between overexpressing mice treated with saline versus paraquat; results in this latter group of animals showed enhanced tissue labeling, a significant increase in PLA dot counts, and a more pronounced accumulation of PLA-labeled α-synuclein oligomers within DMnX-overexpressing cell bodies and neurites (Figure 4, C and D, and Supplemental Figure 4).

Oxidative stress and neuron-to-neuron α-synuclein transfer. Overexpression of hα-synuclein in the rodent DMnX, as induced by vagal AAV injections, has been shown to trigger a discrete, progressive accumulation of the exogenous protein within dystrophic axons in the pons, midbrain, and forebrain. Since DMnX cholinergic neurons do not have central axons projecting toward higher brain regions, this observation of extramedullary pathol-

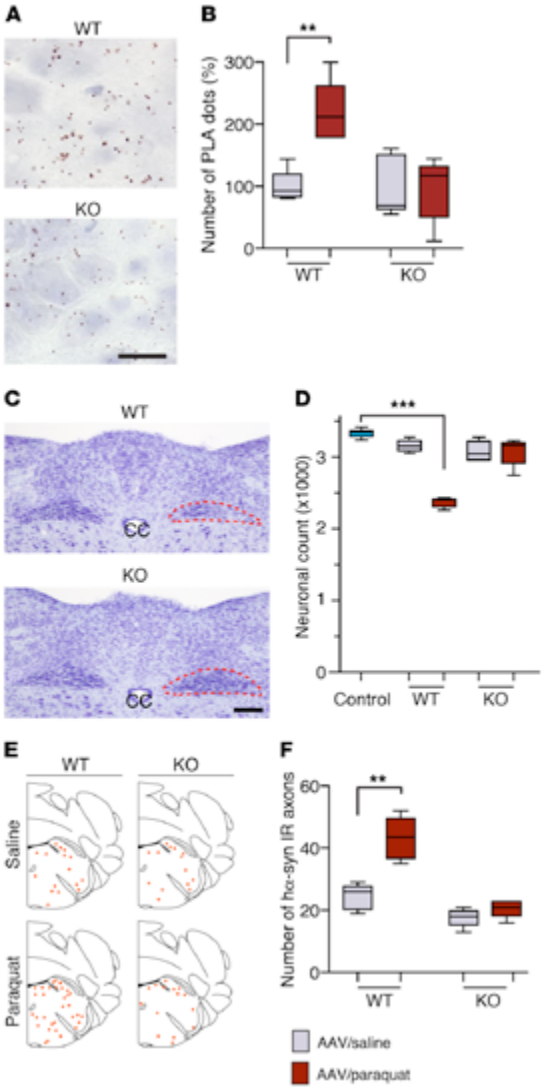

Figure 7. Gp91phox-deficient mice are resistant to paraquat-induced DMnX pathology. WT and gp91phox-deficient (KO) mice received an injection of hα-synuclein AAVs into the left vagus nerve and were injected systemically with either saline ($n \geq 4$/genotype, gray bars) or paraquat ($n \geq 4$/genotype, red bars) and sacrificed at 7 days. (**A**) Medullary tissue sections were processed for indirect hα-synuclein/3-NT PLA. Representative images show the left DMnX of a WT and a KO mouse injected with hα-synuclein AAVs/paraquat. Specific PLA signal was apparently reduced in the KO mouse. Scale bar: 10 μm. (**B**) The number of hα-synuclein/3-NT PLA dots was counted in the left DMnX of WT and KO mice injected with hα-synuclein AAVs/saline or hα-synuclein AAVs/paraquat. Values are expressed as percentage of the mean value in the corresponding hα-synuclein AAV/saline–injected animals. (**C**) Representative images of Nissl-stained neurons in the dorsal medulla oblongata. Tissues were obtained from a WT and a KO mouse injected with hα-synuclein AAVs/paraquat. The left DMnX is delineated in red. Neuronal loss is evident only in the left (ipsilateral to AAV infusion) DMnX from the WT animal. Scale bar: 100 μm. (**D**) The number of Nissl-stained neurons was counted stereologically in the left DMnX of WT and KO mice treated with hα-synuclein AAVs/saline or hα-synuclein AAVs/paraquat. Control counts ($n = 5$, light blue bar) were obtained from the right DMnX of WT animals injected with hα-synuclein AAVs/saline. (**E** and **F**) Pontine tissue sections were immunostained with anti–hα-synuclein. The schematic plots show the distribution of hα-synuclein–labeled axons in the left pons. In the graph, data show the counts of hα-synuclein–positive axons in the left pons. Box and whisker plots show median, upper and lower quartiles, and maximum and minimum as whiskers. $^{**}P \leq 0.01$; $^{***}P \leq 0.001$, Mann-Whitney *U* test (saline- versus paraquat-injected mice) or Kruskal-Wallis followed by Dunn's post hoc (**D**).

ogy reflects an interneuronal transfer and subsequent retrograde spreading of hα-synuclein (20, 25, 43). The next set of experiments was designed to investigate whether vulnerability of the DMnX to oxidative stress may affect neuron-to-neuron α-synuclein transmission in this model of caudorostral protein spreading. Tissue sections of the left pons and midbrain were collected from mice that first received hα-synuclein AAVs and were then treated with 2 injections of saline or paraquat. Samples were stained with a hα-synuclein–specific antibody (Syn211) and analyzed for the presence of the exogenous protein. A few axonal projections immunoreactive for hα-synuclein were already present in pontine sections at 2 days after the second saline/paraquat administration, and interestingly, counts of these labeled axons revealed a higher number in paraquat- as compared with saline-treated animals (Figure 5A). Additional measurements were carried out at a later time point, namely 7 days after saline/paraquat treatment. The number of hα-synuclein–positive axons was increased in pontine sections at 7 days, and at this later time point, immunoreactive fibers were also detected in the caudal and rostral midbrain. In findings similar to those at 2 days, counts of axons containing hα-synuclein were consistently higher in pontine and midbrain sections from mice injected with paraquat (Figure 5B). Length and density of labeled fibers were then measured at the 7-day time point in a defined pontine region encompassing the locus coeruleus and parabrachial nucleus (20, 44). Both measurements showed values that were more than doubled as a result of paraquat administration (Figure 5, C and D). Axons accumulating hα-synuclein generally appeared enlarged, tortuous, and with irregularly spaced varicosities. When fiber morphology was compared in sections from saline- versus paraquat-treated mice, these features were noticeably more prominent in the latter group of animals. In particular, axons from the paraquat-exposed group were more swollen, had larger varicosities, and displayed stronger diaminobenzidine and fluorescent labeling, all consistent with an enhanced hα-synuclein load (Figure 5, E and F).

Further characterization of the spreading protein involved detection and quantification of nitrated and Syn 505–immunoreactive hα-synuclein in pontine tissue. Specific hα-synuclein/3-NT PLA labeling (indirect PLA) was very scant in samples from saline-treated mice, but became more evident and abundant after paraquat administration (Figure 6A). Similarly, double staining of pontine sections with anti–3-NT and anti–hα-synuclein revealed fibers with more pronounced colocalization in paraquat-injected mice (Figure 6B). Severe oxidative stress and

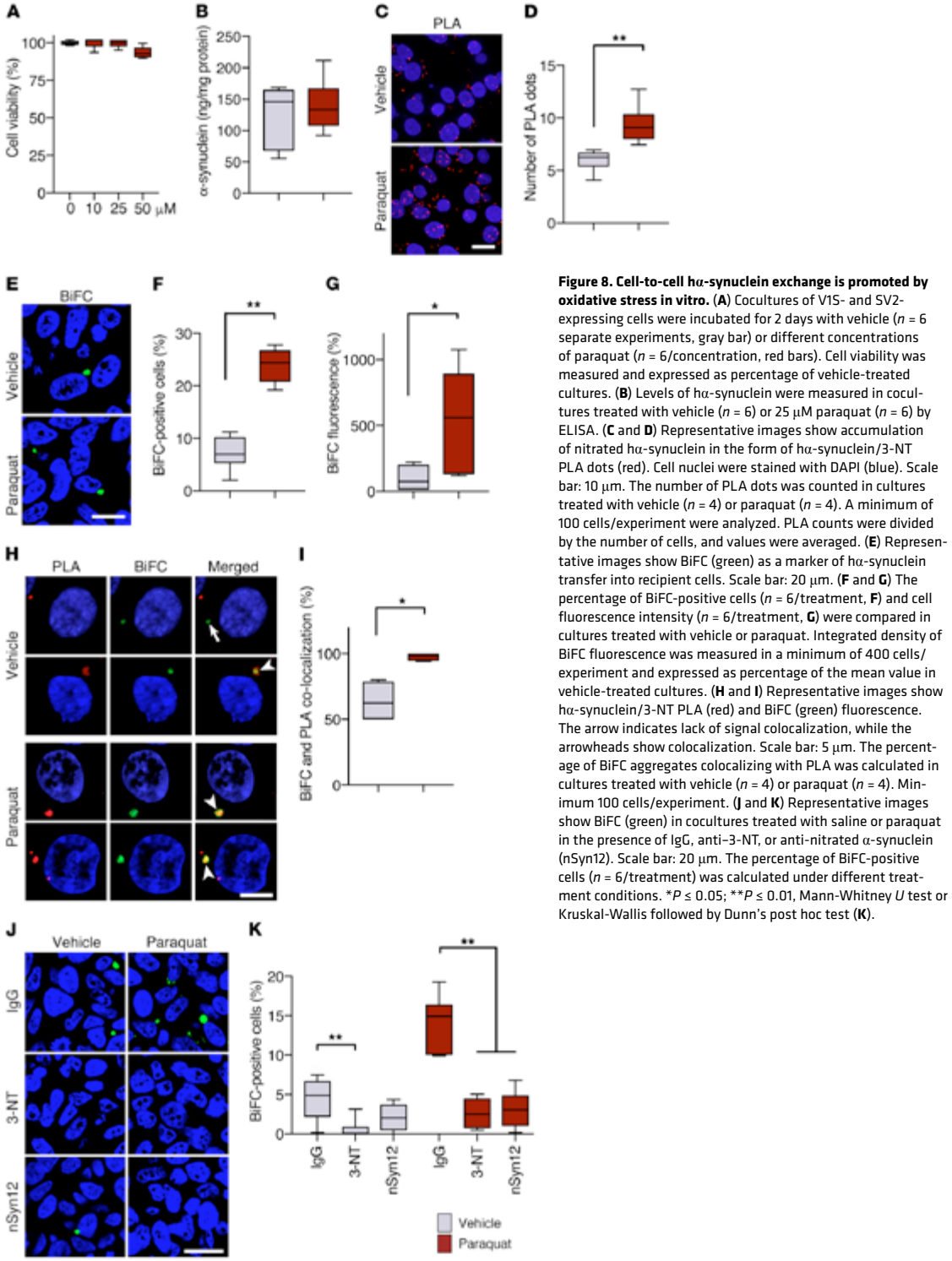

Figure 8. Cell-to-cell hα-synuclein exchange is promoted by oxidative stress in vitro. (**A**) Cocultures of V1S- and SV2-expressing cells were incubated for 2 days with vehicle (n = 6 separate experiments, gray bar) or different concentrations of paraquat (n = 6/concentration, red bars). Cell viability was measured and expressed as percentage of vehicle-treated cultures. (**B**) Levels of hα-synuclein were measured in cocultures treated with vehicle (n = 6) or 25 μM paraquat (n = 6) by ELISA. (**C** and **D**) Representative images show accumulation of nitrated hα-synuclein in the form of hα-synuclein/3-NT PLA dots (red). Cell nuclei were stained with DAPI (blue). Scale bar: 10 μm. The number of PLA dots was counted in cultures treated with vehicle (n = 4) or paraquat (n = 4). A minimum of 100 cells/experiment were analyzed. PLA counts were divided by the number of cells, and values were averaged. (**E**) Representative images show BiFC (green) as a marker of hα-synuclein transfer into recipient cells. Scale bar: 20 μm. (**F** and **G**) The percentage of BiFC-positive cells (n = 6/treatment, **F**) and cell fluorescence intensity (n = 6/treatment, **G**) were compared in cultures treated with vehicle or paraquat. Integrated density of BiFC fluorescence was measured in a minimum of 400 cells/experiment and expressed as percentage of the mean value in vehicle-treated cultures. (**H** and **I**) Representative images show hα-synuclein/3-NT PLA (red) and BiFC (green) fluorescence. The arrow indicates lack of signal colocalization, while the arrowheads show colocalization. Scale bar: 5 μm. The percentage of BiFC aggregates colocalizing with PLA was calculated in cultures treated with vehicle (n = 4) or paraquat (n = 4). Minimum 100 cells/experiment. (**J** and **K**) Representative images show BiFC (green) in cocultures treated with saline or paraquat in the presence of IgG, anti–3-NT, or anti-nitrated α-synuclein (nSyn12). Scale bar: 20 μm. The percentage of BiFC-positive cells (n = 6/treatment) was calculated under different treatment conditions. *$P \le 0.05$; **$P \le 0.01$, Mann-Whitney U test or Kruskal-Wallis followed by Dunn's post hoc test (**K**).

increased spreading induced by the AAV/paraquat treatment was also associated with enhanced accumulation of Syn 505–reactive hα-synuclein species within pontine fibers; after labeling with anti–Syn 505, the fluorescent signal within these fibers was almost doubled in sections from AAV/paraquat- compared with AAV/saline-treated animals (Figure 6, C and D).

Prevention of paraquat-induced DMnX pathology. A likely mechanism contributing to ROS production after paraquat exposure involves paraquat-microglia interactions. More specifically, microglial membrane-bound NADPH oxidase could catalyze the 1-electron reduction of paraquat, thus promoting its redox cycling with molecular oxygen and enhancing the formation of superoxide and other ROS (45, 46). To assess this mechanism and further evaluate the contribution of ROS production to DMnX pathology, experiments were carried out in mutant mice lacking the gp91phox subunit of NADPH oxidase. Absence of this subunit prevents assembly of the enzyme at the plasma membrane and thus abolishes its catalytic activity (45, 47). Gp91phox-deficient mice on the C57BL/6J background strain and C57BL/6J WT animals were administered hα-synuclein AAVs intravagally and then injected twice with saline or paraquat. They were sacrificed at 7 days after the second saline/paraquat treatment. To evaluate oxidative/nitrative stress, sections of the medulla oblongata were processed for indirect hα-synuclein/3-NT PLA, and the number of PLA dots was compared in the DMnX of WT and mutant mice after saline or paraquat administration (Figure 7, A and B). Stereological counts of DMnX neurons were carried out to compare the neurodegenerative effects of paraquat administration in WT verus mutant mice (Figure 7, C and D). Finally, the number of neuronal fibers immunoreactive for hα-synuclein was counted in the pons as a measure of neuron-to-neuron protein transfer and retrograde axonal spreading (Figure 7, E and F). Results showed that, as seen in the earlier experiments, paraquat administration caused an enhancement of hα-synuclein nitration, DMnX neuronal loss, and hα-synuclein spreading in WT animals. Quite remarkably, these effects were abolished in gp91phox-deficient mice. In these animals, the counts of DMnX PLA dots, DMnX neurons, and pontine hα-synuclein–containing axons were comparable regardless of treatment with AAV/saline or AAV/paraquat (Figure 7, B, D, and F).

Oxidative stress and cell-to-cell α-synuclein transfer in vitro. Results in vivo indicating enhanced hα-synuclein spreading in paraquat-treated mice are consistent with the interpretation that paraquat-induced oxidative stress promotes α-synuclein transfer from donor to recipient neurons. Cell-to-cell α-synuclein transmission in the absence or presence of oxidative stress was further investigated next using an in vitro system in which 2 separate SH-SY5Y–derived cell lines are cocultured; the 2 cell lines stably express hα-synuclein fused with either the N (V1S) or C terminal (SV2) fragment of the fluorescent protein Venus. In this system, bimolecular fluorescence complementation (BiFC) indicates dimerization or oligomerization of hα-synuclein as a consequence of its transmission and exchange between V1S- and SV2-containing cells (48). In a set of initial experiments, V1S- and SV2-expressing cells were cocultured in the presence of vehicle or different concentrations of paraquat. Measurements of cell viability determined that no toxicity occurred after a 48-hour incubation with 10 or 25 μM paraquat; with 50 μM paraquat, a 10% loss of viability occurred, although this effect did not reach statistical significance (Figure 8A). Based on these findings, all subsequent experiments were carried out on cells treated with vehicle or 25 μM paraquat for 48 hours. Under these conditions, treatment with paraquat did not significantly change cellular levels of hα-synuclein as assessed by ELISA (Figure 8B). To assess the oxidative effect of paraquat, nitration of intracellular hα-synuclein was visualized and quantified with hα-synuclein/3-NT PLA (indirect PLA). Nitrated hα-synuclein was detected within control cells incubated in the presence of vehicle; however, a significantly higher count of PLA dots characterized cells in paraquat-exposed cultures (Figure 8, C and D). Cell-to-cell hα-synuclein transfer was assessed by counting the number of cells with BiFC-positive structures (48). Furthermore, total cell fluorescence caused by bimolecular complementation was measured and compared in randomly selected cells from vehicle- versus paraquat-treated cultures. Both measurements revealed a significant increase in BiFC caused by paraquat, supporting an association between paraquat-induced oxidative stress and enhanced hα-synuclein transmission (Figure 8, E–G). Further evidence of this association derived from experiments in which cocultures of V1S- and SV2-expressing cells were challenged with oxidative stress–inducing agents other than paraquat. In particular, the percentage of BiFC-positive cells was found to be more than doubled in cultures treated with hydrogen peroxide versus vehicle; it was also increased by approximately 5 times over control levels when hydrogen peroxide was added together with iron sulfate to the incubation medium (Supplemental Figure 5).

Coaggregates of V1S and SV2 proteins formed as a consequence of bimolecular complementation contained nitrated hα-synuclein, as indicated by colocalization of fluorescent dots generated by hα-synuclein/3-NT PLA within BiFC-positive structures (Figure 8H). hα-Synuclein/3-NT PLA colabeled approximately 60% of BiFC-positive aggregates in vehicle-treated cultures, whereas almost 100% colocalization of PLA and BiFC was found in cells exposed to paraquat (Figure 8I). These findings raise the possibility that nitrated forms of hα-synuclein may play an important role in protein transmission, particularly under conditions of oxidative stress. Cell-to-cell transfer of nitrated hα-synuclein would likely involve its initial release into the extracellular space. A final set of experiments was therefore designed to test the hypothesis that addition of antibodies capable of binding extracellular nitrated hα-synuclein may counteract protein transfer and formation of BiFC-positive oligomers in this in vitro system. Two specific antibodies were used for these experiments, namely anti–3-NT or anti-nitrated α-synuclein clone nSyn12. A control antibody, mouse IgG, was also used to account for nonspecific protein binding. IgG, anti–3-NT, or nSyn12 was added to cultures treated with either vehicle or paraquat. In vehicle-treated cultures, a comparison of the percentage of cells containing BiFC-positive aggregates after addition of IgG versus anti–3-NT or nSyn12 revealed decreased fluorescence in the presence of specific nitrated protein–binding antibodies; this decrease reached statistical significance with anti–3-NT, but not nSyn12, however (Figure 8, J and K). In paraquat-treated cultures, the effects of the 2 specific antibodies were both statistically significant ($P \leq 0.01$).

Addition of either anti–3-NT or nSyn12 largely prevented the increase in hα-synuclein transfer caused by paraquat and reduced cellular formation of BiFC-positive aggregates by approximately 80% (Figure 8, J and K).

Discussion

Oxidative challenges are likely to be common events in the CNS, underscoring the relevance of oxidative stress for pathogenetic processes in human neurodegenerative diseases. They can result from cellular dysfunction, such as mitochondrial impairment, and tissue reactions, such as activation of innate immunity (49–51). In PD, oxidative stress could also be promoted by disease risk factors, including aging, environmental exposures, and genetic variants (22, 49). Here, we demonstrate a high susceptibility of DMnX neurons to oxidative stress; our data also indicate that these neurons are relatively more vulnerable to oxidative stress than other populations of cholinergic cells. Following exposure to paraquat, DMnX neurons accumulated substantial amounts of ROS, whereas under the same toxic conditions, no apparent ROS buildup was detected within cholinergic cells in the nearby hypoglossal nucleus nor in the striatum and medial septal nucleus.

This differential vulnerability, in spite of the same neurotransmitter phenotype, is not unique to cholinergic neurons, but is instead reminiscent of differences seen between midbrain dopaminergic cells. Dopaminergic neurons in the substantia nigra pars compacta are markedly more susceptible to oxidative challenges and ROS accumulation than dopaminergic cells in the adjacent ventral tegmental area (3, 52, 53). The substantia nigra pars compacta is also known to be more vulnerable than the ventral tegmental area to the neurodegenerative process of PD (54, 55). Similarly, earlier and more prominent PD pathology, in the form of both α-synuclein lesions and neurodegeneration, characterizes the DMnX and distinguishes DMnX neurons from other cholinergic cells in the hypoglossal nucleus, striatum, and medial septum (10, 56–58). Thus, taken together, previous and current observations support the likelihood that sensitivity to oxidative stress represents a predisposing factor common to PD-vulnerable neuronal populations. The finding that both nigral and DMnX neurons display a high vulnerability to oxidative challenges is also noteworthy. A nigro-vagal pathway that controls gastric tone and motility has recently been shown to connect these 2 brain regions, raising the possibility that the pathological consequences of an oxidative injury may be relayed and possibly amplified through this anatomical and functional connection (59).

Nigral dopaminergic neurons and DMnX cholinergic cells share metabolic properties that could ultimately contribute to their high vulnerability to oxidative stress. In particular, a prooxidant environment characterizing both nigral and DMnX neurons has been proposed to arise from their reliance on calcium currents for pacemaking firing activity. The high metabolic demands associated with cytosolic calcium oscillations could stimulate mitochondrial oxidative phosphorylation, increase mitochondrial ROS production, and predispose these neurons to ROS accumulation after oxidative challenges (4, 11, 50, 60). Our present findings are therefore compatible with the interpretation that, acting on the background of this prooxidant metabolism, challenges with α-synuclein and paraquat, alone or in combination, caused an oxidative burden within susceptible DMnX neurons.

Both intra- and extraneuronal mechanisms could contribute to an enhanced ROS production after hα-synuclein overexpression and/or paraquat exposure. Within neurons, protein overexpression may induce ROS accumulation as a consequence of mitochondria–α-synuclein interactions. This possibility is supported by a recent investigation revealing that modified forms of α-synuclein, such as α-synuclein oligomers, inhibited mitochondrial protein import by binding with high affinity to the translocase of the outer membrane 20 (TOM20) receptor; when levels of α-synuclein were elevated, deleterious consequences of this inhibition included an impairment of mitochondrial respiration and increased ROS production (61). An important role of extraneuronal mechanisms in DMnX oxidative stress and ensuing pathology is indicated by our present results in transgenic mice lacking microglial NADPH oxidase activity. In these animals, inhibition of the NADPH oxidase–dependent redox cycling of paraquat and reduced generation of microglia-derived ROS dramatically protected DMnX neurons from severe oxidative injury after combined hα-synuclein overexpression and paraquat exposure. Of note, the involvement of microglial NADPH oxidase in neuronal oxidative injury represents another feature shared by the DMnX and substantia nigra. Earlier investigations have indeed shown that, in models of nigrostriatal degeneration, lack of functional NADPH oxidase is associated with neuroprotection (45, 62).

During oxidative stress, both superoxide anion and nitric oxide are likely to be generated. In particular, within neurons with calcium-dependent pacemaking, mitochondrial calcium influx has been shown to stimulate nitric oxide synthase activity, thus promoting nitric oxide production (63). Reaction of nitric oxide with superoxide generates the peroxynitrite anion, which can readily dissociate into hydroxyl and nitrogen dioxide radicals; nitrogen dioxide directly reacts with tyrosine residues of proteins, resulting in their nitration to 3-NT (64). α-Synuclein, with its 4 tyrosine residues, can be a target for nitration, and here, a direct relationship between oxidative stress and α-synuclein nitration was documented in the DMnX using immunohistochemistry, ELISA, and a new PLA. hα-Synuclein/3-NT PLA proved to be a highly sensitive assay to detect nitrated hα-synuclein under conditions of milder (single treatment with hα-synuclein AAVs) or severe (combined hα-synuclein AAVs plus paraquat treatment) ROS production. It also allowed a quantitative assessment of the extent of α-synuclein nitration on histological tissue sections, indicating a 2- to 3-fold increase after combined as compared with single treatment. Based on both immunohistochemical and PLA observations, mild oxidative stress was associated with a buildup of nitrated α-synuclein mostly within dystrophic DMnX neurites; on the other hand, accumulation of nitrated α-synuclein became overt within neuronal cell bodies only after more pronounced ROS generation. Data suggest, therefore, that neuronal projections may represent preferential and/or early sites for the pathological accumulation of nitrated α-synuclein during oxidative challenges.

Syn 505, an antibody raised against peroxynitrite-treated α-synuclein, recognizes both nitrated and nonnitrated α-synuclein (28, 29). In line with this biochemical characterization, staining of DMnX tissue with Syn 505 produced a more robust signal than

that generated by staining with anti-nitrated α-synuclein nSyn24 or with hα-synuclein/3-NT PLA. It is noteworthy, however, that, despite its relative lack of specificity toward nitrated α-synuclein, immunoreactivity for Syn 505 was still a sensitive indicator of oxidative stress, since labeling was more robust after a more severe ROS challenge. In the brain of patients affected by synucleinopathies, staining with Syn 505 has been shown to preferentially recognize pathological as compared with normal α-synuclein. It detected extensive dot-like lesions in brain regions known to be targeted by Lewy inclusions as well as in regions with previously underestimated α-synuclein pathology (28, 29). Based on our current findings, this distinct Syn 505 labeling of smaller pathological aggregates further supports and may actually signify an important contribution of oxidative stress to the development of α-synuclein pathology in humans.

α-Synuclein aggregation was also evaluated as part of this study. Protein assembly occurred within DMnX neurons of hα-synuclein–overexpressing mice, but was overtly more pronounced when overexpression was followed by paraquat administration, suggesting a relationship between enhanced ROS formation and increased α-synuclein aggregation in vivo. It is conceivable that oxidative α-synuclein modifications, which were detected in ROS-challenged DMnX tissue, could play a significant role in this relationship. In particular, structural and conformational variants of oxidized α-synuclein that are recognized by Syn 505 may underlie a greater propensity to protein assembly (29). Similarly, the ability of nitrated α-synuclein to modulate pathways of protein aggregation has long been recognized and documented by in vitro studies. Results of these earlier investigations suggest that either oligomerization or fibrillation of α-synuclein can be promoted by its nitration (38–40, 65). Here, we found that severe oxidative stress, as induced by combined α-synuclein overexpression and paraquat administration, triggered early intraneuronal accumulation of predominantly oligomeric α-synuclein species. Nitration-dependent changes in protein conformation may be stabilized by assembly into oligomers, thus contributing to this effect (38, 65). Furthermore, intraneuronal generation of mixed nitrated α-synuclein species (nitrated monomers, dimers, and oligomers) as well as α-synuclein nitration at all of its 4 tyrosine residues may favor the accumulation of oligomers as seen under our present experimental conditions (39, 40).

Another consideration arising from our analyses in the DMnX of AAV- and paraquat-injected animals concerns the contribution of α-synuclein aggregation to neuronal degeneration. If it is assumed that accumulation of aggregate pathology plays a role in neuronal demise, then toxic oligomeric species would likely mediate this effect and contribute to the marked loss of DMnX neurons seen after severe oxidative stress. This conclusion is in line with increasing in vitro and in vivo experimental evidence as well as neuropathological observations supporting a deleterious potential of α-synuclein oligomers (42, 66–68). Small protein aggregates may be accumulated and play a more relevant role at early stages of pathogenetic processes, including early damage after oxidative challenges (20, 42). Formation and accumulation of fibrillar α-synuclein species may, on the other hand, underlie the development of more advanced pathological processes, such as prion-like α-synuclein propagation and deposition of intraneuronal Lewy inclusions (20, 69, 70).

In PD, neuron-to-neuron transfer and consequent spreading of pathogenic α-synuclein from the lower brain stem toward higher brain regions may contribute to pathological disease progression (12, 16). Using our models of hα-synuclein overexpression and oxidative stress in the DMnX, we found that enhanced ROS production caused by paraquat was associated with an increased advancement of hα-synuclein from the DMnX to the pons and then to the mouse midbrain. To the best of our knowledge, this is the first report of a distinct role of oxidative stress in hα-synuclein brain spreading. Evidence strengthening this conclusion includes the findings of rescue experiments in which enhanced spreading by paraquat was virtually abolished in mice with reduced NADPH oxidase–dependent ROS generation. These results in gp91phox-deficient mice also underscore a mechanism by which microglial cells could contribute to pathogenetic processes involving hα-synuclein; microglial activation is likely to result in enhanced ROS production and, through this mechanism, could not only play a role in inducing oxidative stress, but also promote neuron-to-neuron transfer of pathogenic hα-synuclein.

Caudo-rostral advancement of hα-synuclein triggered by its overexpression in the DMnX is dependent upon protein transfer from medullary donor neurons into recipient axons that project into the dorsal medulla oblongata from higher brain regions (20, 21, 25, 43). A likely explanation for the present findings is therefore that oxidative stress affects neuron-to-neuron protein transmission, with increased ROS production promoting interneuronal hα-synuclein mobility. This interpretation of the in vivo data is strongly supported by results of our in vitro experiments carried out in cocultures of cells expressing hα-synuclein fused with V1S or SV2 Venus fragments (48). Indeed, enhanced BiFC after incubations in the presence of paraquat, hydrogen peroxide, or hydrogen peroxide plus iron sulfate indicated a higher propensity of hα-synuclein to pass from cell to cell during an oxidative challenge. It is noteworthy that increased in vitro cell crossing as well as enhanced in vivo spreading were unlikely to be a mere consequence of hα-synuclein release from damaged/dead cells. In the in vitro setting, paraquat-induced increase in BiFC occurred in the absence of any overt evidence of cytotoxicity. In mice, severe oxidative stress after cotreatment with hα-synuclein AAVs and paraquat did cause a more pronounced neuronal death. This enhanced neurodegeneration, however, would not be expected to cause an increase in protein spreading, since earlier investigations found that overexpression-induced hα-synuclein transfer is more efficient between relatively healthy cells and is in fact lessened after degeneration of DMnX neurons (21, 44).

Our in vivo and in vitro data support the likelihood that, following an oxidative challenge, oxidatively modified forms of hα-synuclein that are readily transferable from cell to cell are generated. An initial clue of mobility of oxidized/nitrated hα-synuclein was provided by the in vivo observation that, following a more severe oxidative stress, increased levels of Syn 505–immunoreactive and nitrated protein were present within donor DMnX neurons as well as within recipient pontine axons. In vitro evidence then revealed that fluorescent hα-synuclein oligomers formed as a result of bimolecular complementation within recipient cells contained nitrated hα-synuclein. Incubations in the presence of paraquat not only promoted BiFC, but also enhanced the extent of nitration of

the fluorescent oligomers. Finally, addition of antibodies capable of blocking nitrated α-synuclein in the incubation medium prevented this protein exchange and markedly suppressed BiFC. Taken together, these findings suggest that, following increased production of oxidized/nitrated α-synuclein during oxidative stress, greater amounts of modified protein were exchanged between donor and recipient cells. Oxidative modifications likely denote pathogenetic forms of α-synuclein with pronounced conformational and structural abnormalities (29, 39, 40). Therefore, high mobility of oxidized/nitrated α-synuclein could result in the exchange of deleterious protein species and contribute to their propagation throughout the brain. Brain regions with higher vulnerability to oxidative stress may be at higher risk for the spreading of these pathogenetic hα-synuclein forms. Further work is warranted to determine whether a distinct pattern of connectome-dependent spreading may arise, at least in part, from tissue/cellular vulnerability to oxidative pathology. Future investigations will also establish feasibility and efficacy of therapeutic strategies that, targeting oxidized/nitrated α-synuclein, may help counteract the progression of disease pathology in PD and other human synucleinopathies.

Methods

Viral vectors. Transgenic expression of hα-synuclein was induced using recombinant AAVs (AAV2/6; Sirion Biotech). Gene expression was regulated by the human synapsin 1 promoter and enhanced using a woodchuck hepatitis virus posttranscriptional regulatory element and a polyadenylation signal sequence.

Animals and treatment. The majority of the experiments were conducted on male C57BL/6NRj mice (Janvier) between 12 and 16 weeks of age. For experiments aimed at determining the effects of NADPH oxidase deficiency on paraquat-induced pathology, male gp91phox-deficient mice on a C57BL/6J background strain and C57BL/6J WT animals (B6.129S-*Cybb*^{tm1Din}/J, Jackson Laboratory) were used. Animals were housed in a specific pathogen–free facility under a 12-hour light/12-hour dark cycle with ad libitum access to food and water. Paraquat dichloride hydrate (Sigma-Aldrich) was dissolved in 0.9% saline and administered i.p. at 2 doses of 15 mg/kg separated by a 1-week interval. Animals injected with 0.9% saline served as controls. hα-Synuclein AAVs (7×10^{11} genome copies/ml) were injected into the left vagus nerve as previously described (20). DHE was dissolved in DMSO (40% in saline) and injected s.c. at a dose of 5 mg/kg 1 hour prior to sacrifice. Mice were sacrificed with an i.p. injection of 140 mg/kg sodium pentobarbital. They were then perfused through the ascending aorta with 4% (w/v) paraformaldehyde (PFA). Brains were removed and immersed in 4% PFA for 24 hours before being cryopreserved in 30% (w/v) sucrose. For analyses requiring nonfixed tissue (e.g., ELISA), mice were perfused with 0.9% saline, and brains were snap-frozen and stored at –80 °C until use.

Immunohistochemistry and image acquisition. A summary of primary antibodies and their source and working dilutions is shown in Supplemental Table 1. Coronal brain sections (35 μm) were cut using a freezing microtome. Single and double labeling were carried out for fluorescence and brightfield microscopy using established protocols with a few modifications (20, 25). Free-floating medulla oblongata sections for double-fluorescence staining were treated with an antigen-retrieval solution (10 mM sodium citrate in 0.05% Tween 20, pH = 6.0) at 98°C for 5 minutes. For nSyn24.8/hα-synuclein immunolabeling, sections were incubated for an additional hour in 0.01% SDS in Tris-HCl. Endogenous mouse IgG reactivity was blocked using Mouse on Mouse (MOM) Blocking Reagent (Vector Laboratories). Following blocking in 5% normal serum, sections were incubated with primary antibodies. hα-Synuclein antibodies were directly labeled with DyLight-594–conjugated secondary antibody (1:300). Other mouse monoclonal antibodies were labeled by a 2-step protocol using first a horse anti-mouse biotinylated secondary antibody (1:200) and then DyLight-488 streptavidin (1:300). All secondary antibodies were purchased from Vector Laboratories. In some instances, sections were counterstained with 300 nM DAPI (Thermo Fisher Scientific), a nuclear marker, prior to mounting. Sections stained with nSyn24.8 and processed for brightfield microscopy were also treated with antigen-retrieval solution (see above) and developed with Vector SG Peroxidase Substrate Kit (Vector Laboratories). Fluorescence images were collected on Zeiss microscopes (LSM700 or LSM800) with a ×63 Plan-Apochromat objective. They were processed and analyzed with Fiji software (ImageJ, NIH, version 2.0.0) unless otherwise specified. A mouse brain atlas was used as reference for brain coordinates (71).

Ox-DHE and MDA quantification. Ox-DHE fluorescent signal was acquired from ChAT-immunoreactive neurons in the DMnX (bregma –7.48 to –7.32 mm), hypoglossal nucleus (–7.48 to –7.32 mm), striatum (+0.26 to +1.10 mm), and medial septal nucleus (+0.26 to +1.10 mm) or from hα-synuclein–immunoreactive DMnX neurons. Using confocal images, neurons were delineated based on ChAT or hα-synuclein immunoreactivity. Ox-DHE puncta within the delineated cells were selected by applying a constant intensity threshold and outlined using the "analyze particles" function. The total integrated density of the outlined puncta was quantified for each image, divided by the number of neurons, and averaged for each animal. For quantification of MDA, brains were removed and snap-frozen on dry ice. Specimens of the dorso-medial medulla oblongata (10 mg wet tissue/animal) were assayed using a Colorimetric MDA Assay Kit (Abcam) according to the manufacturer's protocol.

Quantification of transduction. Investigators performing histological analyses were blinded to sample treatment. AAV-induced transduction was estimated from confocal images of medulla oblongata sections immunostained for hα-synuclein (MJFR1). Every fifth section of the entire left DMnX between bregma –7.32 and –7.20 mm was acquired with a ×20 objective. The total number of hα-synuclein–positive and DAPI-stained neurons was counted using the cell counter plugin.

Counting of DMnX neurons. The number of Nissl-stained neurons was quantified throughout the entire DMnX using every fifth section. Stereological counts were performed on an IX2 UCB Olympus microscope using an optical fractionator (Stereo Investigator, version 9, MBF Bioscience). Coefficients of error were less than 0.10.

Quantification of Syn 505 fluorescence. Fluorescence intensity was measured in DMnX-containing tissue sections immunostained with Syn 505 antibody and anti-hα-synuclein (15G7). Every fifth medulla oblongata section between bregma –7.48 and –7.20 mm was used to acquire single-plane images of the left DMnX. For each image, a Gaussian blur and background subtraction were applied. An intensity threshold was also selected to detect and outline 15G7-positive structures. The median fluorescence of either 15G7 or Syn 505 labeling was measured. Data were calculated as the median ratio of Syn 505 over 15G7 fluorescence. Fluorescence intensity was also quantified within pontine axons immunolabeled with Syn 505 and 15G7. Confocal

images taken within the locus coeruleus or parabrachial nucleus between bregma –5.68 and –5.34 mm were used for these analyses. Each axon was outlined based on a constant fluorescence threshold for 15G7 immunoreactivity. The mean fluorescence intensity of Syn 505 labeling was measured within the delineated area and corrected for background fluorescence.

Axonal counts and quantification of spreading. The total number of hα-synuclein–immunoreactive (Syn211) axons was counted in sections of the left pons (bregma –5.40 mm) and the left caudal (bregma –4.60 mm) and rostral (bregma –3.40 mm) midbrain. Measurements of axonal length and density were carried out in pontine sections (bregma –5.68, –5.51, and –5.34 mm) after delineation of an area encompassing the locus coeruleus and parabrachial nucleus, using the Spaceballs stereological probe (Stereo Investigator software, version 9, MBF Biosciences) (20). High-magnification images of Syn211-immunoreactive axons were acquired on an Observer.Z1 microscope (Zeiss), using a ×63 Plan-Apochromat objective.

PLA. PLA was performed using Duolink (Sigma-Aldrich) according to the manufacturer's protocols. Aggregated hα-synuclein was detected using PLA probes conjugated to a hα-synuclein–specific antibody (Syn211), as previously described (20, 42). Nitrated hα-synuclein was detected by either direct or indirect PLA. For direct PLA, PLUS and MINUS oligonucleotide probes were conjugated with a hα-synuclein antibody (MJFR1) and anti–3-NT, respectively (Duolink Probemaker, Sigma-Aldrich). For indirect PLA, sections were first incubated overnight in primary antibodies (3-NT and MJFR1) and then incubated with secondary antibodies conjugated with oligonucleotide probes, i.e., anti-rabbit PLUS and anti-mouse MINUS (Sigma-Aldrich). Following ligation and amplification, specific PLA signals were visualized using brightfield or fluorescence detection kits (Duolink, Sigma-Aldrich). In some instances, sections were counterstained with hematoxylin or DAPI. For PLA/immunohistochemistry double labeling, the PLA signal was detected using the Duolink Green Detection Kit (Sigma-Aldrich). Tissue sections were then immunolabeled for hα-synuclein (4B12) using DyLight-594 as a secondary antibody. In SH-SY5Y cells, the PLA signal was visualized using the Duolink Red Fluorescence Detection Kit (Sigma-Aldrich). Specificity of hα-synuclein/3-NT PLA was confirmed by experiments in which medulla oblongata sections were first incubated with a cocktail of concentrated monoclonal antibodies raised against nitrated α-synuclein (nSyn12, nSyn14, and nSyn24.8) for 48 hours at 4°C. These sections were then processed for direct hα-synuclein/3-NT PLA, as described above. Preincubation with nitrated α-synuclein antibodies completely abolished the PLA signal (Supplemental Figure 1). For quantification of the syn/syn and hα-synuclein/3-NT PLA signals in the DMnX, medullary sections encompassing the entire DMnX were used. The DMnX was delineated at low magnification (×10 objective) on every tenth section (between bregma –6.96 and –8.00 mm), and the number of PLA dots was counted stereologically. Coefficients of error were less than 0.10. Analysis of hα-synuclein/3-NT PLA dots in the pons was performed on a single section corresponding to bregma –5.34 mm. Counts were performed in the entire left hemisphere using the meander scan function of Stereo Investigator (MBF Bioscience).

ELISA. For measurements of nitrated α-synuclein in vivo, the left dorso-medial medulla oblongata was dissected under a stereomicroscope and sonicated in RIPA buffer (×10 w/v) with protease inhibitors (Sigma-Aldrich). Tissue homogenates were centrifuged at 16,000 *g* for 15 minutes at 4°C. Protein concentration was determined from the supernatants by BCA assay (Pierce Biotechnology). 96-Well ELISA plates (MaxiSorp, Nunc) coated with 1 μg/ml of the capture antibody, i.e., anti–α-synuclein (Syn-1) in 50 mM carbonate buffer (pH 9.6), were washed with PBS containing 0.05% Tween 20 and blocked with SuperBlock T20 (Thermo Fisher Scientific) for 1 hour at room temperature. Samples (0.1 mg protein) were added to the wells and incubated at room temperature for 2.5 hours with shaking. After washing, further incubations were carried out first with the biotinylated detection antibody, i.e., 3-NT (1 μg/ml), for 1.5 hours and then with avidin-conjugated peroxidase (ExtrAvidin; Sigma-Aldrich). Final steps of the protocol involved subsequent additions of 3,3′5,5′-tetramethylbenzidine solution (Sigma-Aldrich) and 2 N sulfuric acid. Absorbance was measured at 450 nm using an Anthos 2010 plate reader (Biochrome Ltd.). For measurements of hα-synuclein in vitro, cells were lysed in RIPA buffer. Syn-1 was used as capture antibody. Coating of 96-well plates and washing procedures were similar to those described above. Samples (20 μg protein with 1% SDS) and recombinant hα-synuclein monomers (for generation of a standard curve) were added to the wells. MJFR1 antibody (1 μg/ml) was then used for detection together with horseradish peroxidase–conjugated anti-rabbit IgG (1:1000; Promega).

In vitro experiments/analyses. SH-SY5Y human neuroblastoma cell lines stably expressing the N-terminal half of Venus YFP-tagged hα-synuclein (V1S) or the C-terminal half of Venus YFP-tagged hα-synuclein (SV2) were cocultured in equivalent numbers and maintained as previously described (48). Paraquat, hydrogen peroxide, and iron sulfate were dissolved in sterile PBS or distilled water. To determine cell viability, cells were trypsinized and stained with acridine orange/propidium iodide (Logos Biosystems) prior to automated cell counting (LUNA-FLTM Dual Fluorescence Cell Counter). All other analyses were made on cells grown on poly-L-lysine–coated coverslips and fixed in 4% PFA. Nuclei were stained with DAPI. Assessment of BiFC fluorescence and quantification of in vitro hα-synuclein/3-NT PLA were carried out on confocal stack images acquired on a Zeiss LSM710 microscope (BiFC) or a Zeiss LSM800 microscope with airy scan (PLA) under a ×63 Apochrome objective. The number of both total and BiFC-positive cells was counted using the cell counter plugin (48). For assessment of BiFC-integrated density, the intracellular fluorescent signal was measured after delineation the BiFC-positive cells. The number of PLA dots per cell was counted on representative images randomly acquired from multiple areas on the coverslip. Counts were made using the spots function of the Imaris software (version 8) and averaged over the number of DAPI-stained nuclei. The number of BiFC aggregates with or without PLA dots was counted on the entire coverslip to calculate the percentage of colocalization. In experiments in which antibodies were added to the incubation medium, IgG, anti–3-NT, or nSyn12 was used at a concentration of 50 μg/ml.

Statistics. Analyses were performed with GraphPad Prism (8.0) or R software (3.5.2) using nonparametric Mann-Whitney *U* test for comparisons between 2 groups. Comparisons among more than 2 groups were carried out using Kruskal-Wallis 1-way ANOVA followed by Dunn's or Conover-Iman post hoc tests. *P* values of less than 0.05 were considered statistically significant.

Study approval. Animal experiments were approved by the State Agency for Nature, Environment, and Consumer Protection in North Rhine Westphalia, Germany.

Author contributions

REM designed and performed in vivo experiments and analyzed data. MH performed surgical procedures and contributed to histological quantifications. EJB designed and performed in vitro experiments and analyzed their results. HA contributed to analysis and quantification of the in vitro work. AU carried out PLA and other histological evaluations. SJL, AU, and DADM supervised different aspects of the project. DADM designed experiments, analyzed data, and wrote the manuscript with input from the other authors.

Acknowledgments

The authors thank Sarah A. Jewell for her comments on the manuscript, Omar El-Agnaf (Qatar Biomedical Research Institute) for kindly providing conformation-specific antibodies, Celine Galvagnion for the production of α-synuclein standards, Bettina Winzen-Reichert and Laura Jakobi for assistance with the experiments, and personnel at the DZNE Light Microscope Facility, Image and Data Analysis Facility, and Preclinical Center. This work was supported by the Paul Foundation, the EU Joint Programme-Neurodegenerative Disease (JPND 01ED1612) and National Research Foundation (NRF) grants by the Korean Government (Ministry of Science, ICT, and Future Planning [MSIP]; NRF-2018R1A2A1A05078261 and NRF-2018R1A5A2025964).

Address correspondence to: Donato A. Di Monte, German Center for Neurodegenerative Diseases, Venusberg-Campus 1, Building 99, 53127 Bonn, Germany. Phone: 49.228.43302650; Email: donato.dimonte@dzne.de.

1. Graham DG. Oxidative pathways for catecholamines in the genesis of neuromelanin and cytotoxic quinones. *Mol Pharmacol*. 1978;14(4):633–643.
2. Sulzer D. Multiple hit hypotheses for dopamine neuron loss in Parkinson's disease. *Trends Neurosci*. 2007;30(5):244–250.
3. Chan CS, et al. 'Rejuvenation' protects neurons in mouse models of Parkinson's disease. *Nature*. 2007;447(7148):1081–1086.
4. Guzman JN, et al. Oxidant stress evoked by pacemaking in dopaminergic neurons is attenuated by DJ-1. *Nature*. 2010;468(7324):696–700.
5. Burbulla LF, et al. Dopamine oxidation mediates mitochondrial and lysosomal dysfunction in Parkinson's disease. *Science*. 2017;357(6357):1255–1261.
6. Dryanovski DI, et al. Calcium entry and α-synuclein inclusions elevate dendritic mitochondrial oxidant stress in dopaminergic neurons. *J Neurosci*. 2013;33(24):10154–10164.
7. Tapias V, Hu X, Luk KC, Sanders LH, Lee VM, Greenamyre JT. Synthetic alpha-synuclein fibrils cause mitochondrial impairment and selective dopamine neurodegeneration in part via iNOS-mediated nitric oxide production. *Cell Mol Life Sci*. 2017;74(15):2851–2874.
8. Eadie MJ. The pathology of certain medullary nuclei in parkinsonism. *Brain*. 1963;86:781–792.
9. Halliday GM, Blumbergs PC, Cotton RG, Blessing WW, Geffen LB. Loss of brainstem serotonin- and substance P-containing neurons in Parkinson's disease. *Brain Res*. 1990;510(1):104–107.
10. Gai WP, Blumbergs PC, Geffen LB, Blessing WW. Age-related loss of dorsal vagal neurons in Parkinson's disease. *Neurology*. 1992;42(11):2106–2111.
11. Goldberg JA, et al. Calcium entry induces mitochondrial oxidant stress in vagal neurons at risk in Parkinson's disease. *Nat Neurosci*. 2012;15(10):1414–1421.
12. Braak H, Del Tredici K, Rüb U, de Vos RA, Jansen Steur EN, Braak E. Staging of brain pathology related to sporadic Parkinson's disease. *Neurobiol Aging*. 2003;24(2):197–211.
13. Kordower JH, Chu Y, Hauser RA, Freeman TB, Olanow CW. Lewy body-like pathology in long-term embryonic nigral transplants in Parkinson's disease. *Nat Med*. 2008;14(5):504–506.
14. Desplats P, et al. Inclusion formation and neuronal cell death through neuron-to-neuron transmission of alpha-synuclein. *Proc Natl Acad Sci U S A*. 2009;106(31):13010–13015.
15. Freundt EC, et al. Neuron-to-neuron transmission of α-synuclein fibrils through axonal transport. *Ann Neurol*. 2012;72(4):517–524.
16. Goedert M, Spillantini MG, Del Tredici K, Braak H. 100 years of Lewy pathology. *Nat Rev Neurol*. 2013;9(1):13–24.
17. Holmqvist S, et al. Direct evidence of Parkinson pathology spread from the gastrointestinal tract to the brain in rats. *Acta Neuropathol*. 2014;128(6):805–820.
18. Svensson E, et al. Vagotomy and subsequent risk of Parkinson's disease. *Ann Neurol*. 2015;78(4):522–529.
19. Ulusoy A, Phillips RJ, Helwig M, Klinkenberg M, Powley TL, Di Monte DA. Brain-to-stomach transfer of α-synuclein via vagal preganglionic projections. *Acta Neuropathol*. 2017;133(3):381–393.
20. Helwig M, et al. Brain propagation of transduced α-synuclein involves non-fibrillar protein species and is enhanced in α-synuclein null mice. *Brain*. 2016;139(Pt 3):856–870.
21. Rusconi R, Ulusoy A, Aboutalebi H, Di Monte DA. Long-lasting pathological consequences of overexpression-induced α-synuclein spreading in the rat brain. *Aging Cell*. 2018;17(2):e12727.
22. Di Monte DA. The environment and Parkinson's disease: is the nigrostriatal system preferentially targeted by neurotoxins? *Lancet Neurol*. 2003;2(9):531–538.
23. Budd SL, Castilho RF, Nicholls DG. Mitochondrial membrane potential and hydroethidine-monitored superoxide generation in cultured cerebellar granule cells. *FEBS Lett*. 1997;415(1):21–24.
24. Andrews ZB, et al. Uncoupling protein-2 is critical for nigral dopamine cell survival in a mouse model of Parkinson's disease. *J Neurosci*. 2005;25(1):184–191.
25. Ulusoy A, et al. Caudo-rostral brain spreading of α-synuclein through vagal connections. *EMBO Mol Med*. 2013;5(7):1119–1127.
26. Giasson BI, et al. Oxidative damage linked to neurodegeneration by selective alpha-synuclein nitration in synucleinopathy lesions. *Science*. 2000;290(5493):985–989.
27. Duda JE, et al. Widespread nitration of pathological inclusions in neurodegenerative synucleinopathies. *Am J Pathol*. 2000;157(5):1439–1445.
28. Duda JE, Giasson BI, Mabon ME, Lee VM, Trojanowski JQ. Novel antibodies to synuclein show abundant striatal pathology in Lewy body diseases. *Ann Neurol*. 2002;52(2):205–210.
29. Waxman EA, Duda JE, Giasson BI. Characterization of antibodies that selectively detect alpha-synuclein in pathological inclusions. *Acta Neuropathol*. 2008;116(1):37–46.
30. Elfineh L, Classon C, Asplund A, Pettersson U, Kamali-Moghaddam M, Lind SB. Tyrosine phosphorylation profiling via in situ proximity ligation assay. *BMC Cancer*. 2014;14:435.
31. Sahin U, Jollivet F, Berthier C, de Thé H, Lallemand-Breitenbach V. Detection of protein SUMOylation in situ by proximity ligation assays. *Methods Mol Biol*. 2016;1475:139–150.
32. Avin A, Levy M, Porat Z, Abramson J. Quantitative analysis of protein-protein interactions and post-translational modifications in rare immune populations. *Nat Commun*. 2017;8(1):1524.
33. Hashimoto M, et al. Oxidative stress induces amyloid-like aggregate formation of NACP/alpha-synuclein in vitro. *Neuroreport*. 1999;10(4):717–721.
34. Ischiropoulos H, Beckman JS. Oxidative stress and nitration in neurodegeneration: cause, effect, or association? *J Clin Invest*. 2003;111(2):163–169.
35. Brahmachari S, et al. Activation of tyrosine kinase c-Abl contributes to α-synuclein–induced neurodegeneration. *J Clin Invest*. 2016;126(8):2970–2988.
36. Scudamore O, Ciossek T. Increased oxidative stress exacerbates α-synuclein aggregation in vivo. *J Neuropathol Exp Neurol*. 2018;77(6):443–453.
37. Paxinou E, et al. Induction of alpha-synuclein aggregation by intracellular nitrative insult. *J Neurosci*. 2001;21(20):8053–8061.
38. Uversky VN, et al. Effects of nitration on the structure and aggregation of alpha-synuclein. *Brain Res Mol Brain Res*. 2005;134(1):84–102.
39. Hodara R, et al. Functional consequences of alpha-synuclein tyrosine nitration: diminished binding to lipid vesicles and increased fibril formation. *J Biol Chem*. 2004;279(46):47746–47753.
40. Burai R, Ait-Bouziad N, Chiki A, Lashuel HA. Elucidating the role of site-specific nitration of α-synuclein in the pathogenesis of Parkinson's disease via protein semisynthesis and mutagenesis. *J Am Chem Soc*. 2015;137(15):5041–5052.

41. Vaikath NN, et al. Generation and characterization of novel conformation-specific monoclonal antibodies for α-synuclein pathology. *Neurobiol Dis*. 2015;79:81–99.
42. Roberts RF, Wade-Martins R, Alegre-Abarrategui J. Direct visualization of alpha-synuclein oligomers reveals previously undetected pathology in Parkinson's disease brain. *Brain*. 2015;138 (Pt 6):1642–1657.
43. Bae EJ, et al. LRRK2 kinase regulates α-synuclein propagation via RAB35 phosphorylation. *Nat Commun*. 2018;9(1):3465.
44. Ulusoy A, et al. Neuron-to-neuron α-synuclein propagation in vivo is independent of neuronal injury. *Acta Neuropathol Commun*. 2015;3:13.
45. Purisai MG, McCormack AL, Cumine S, Li J, Isla MZ, Di Monte DA. Microglial activation as a priming event leading to paraquat-induced dopaminergic cell degeneration. *Neurobiol Dis*. 2007;25(2):392–400.
46. Bonneh-Barkay D, Reaney SH, Langston WJ, Di Monte DA. Redox cycling of the herbicide paraquat in microglial cultures. *Brain Res Mol Brain Res*. 2005;134(1):52–56.
47. Pollock JD, et al. Mouse model of X-linked chronic granulomatous disease, an inherited defect in phagocyte superoxide production. *Nat Genet*. 1995;9(2):202–209.
48. Bae EJ, et al. Glucocerebrosidase depletion enhances cell-to-cell transmission of α-synuclein. *Nat Commun*. 2014;5:4755.
49. Schapira AH. Mitochondria in the aetiology and pathogenesis of Parkinson's disease. *Lancet Neurol*. 2008;7(1):97–109.
50. Surmeier DJ, Obeso JA, Halliday GM. Selective neuronal vulnerability in Parkinson disease. *Nat Rev Neurosci*. 2017;18(2):101–113.
51. Heneka MT, McManus RM, Latz E. Inflammasome signalling in brain function and neurodegenerative disease. *Nat Rev Neurosci*. 2018;19(10):610–621.
52. McCormack AL, Atienza JG, Langston JW, Di Monte DA. Decreased susceptibility to oxidative stress underlies the resistance of specific dopaminergic cell populations to paraquat-induced degeneration. *Neuroscience*. 2006;141(2):929–937.
53. Mosharov EV, et al. Interplay between cytosolic dopamine, calcium, and alpha-synuclein causes selective death of substantia nigra neurons. *Neuron*. 2009;62(2):218–229.
54. Hirsch E, Graybiel AM, Agid YA. Melanized dopaminergic neurons are differentially susceptible to degeneration in Parkinson's disease. *Nature*. 1988;334(6180):345–348.
55. German DC, Manaye KF, Sonsalla PK, Brooks BA. Midbrain dopaminergic cell loss in Parkinson's disease and MPTP-induced parkinsonism: sparing of calbindin-D28k-containing cells. *Ann N Y Acad Sci*. 1992;648:42–62.
56. Seidel K, et al. The brainstem pathologies of Parkinson's disease and dementia with Lewy bodies. *Brain Pathol*. 2015;25(2):121–135.
57. Mori F, Tanji K, Zhang H, Kakita A, Takahashi H, Wakabayashi K. alpha-Synuclein pathology in the neostriatum in Parkinson's disease. *Acta Neuropathol*. 2008;115(4):453–459.
58. Hall H, et al. Hippocampal Lewy pathology and cholinergic dysfunction are associated with dementia in Parkinson's disease. *Brain*. 2014;137(Pt 9):2493–2508.
59. Anselmi L, Toti L, Bove C, Hampton J, Travagli RA. A nigro-vagal pathway controls gastric motility and is affected in a rat model of Parkinsonism. *Gastroenterology*. 2017;153(6):1581–1593.
60. Guzman JN, et al. Systemic isradipine treatment diminishes calcium-dependent mitochondrial oxidant stress. *J Clin Invest*. 2018;128(6):2266–2280.
61. Di Maio R, et al. α-Synuclein binds to TOM20 and inhibits mitochondrial protein import in Parkinson's disease. *Sci Transl Med*. 2016;8(342):342ra78.
62. Wu DC, et al. NADPH oxidase mediates oxidative stress in the 1-methyl-4-phenyl-1,2,3,6-tetrahydropyridine model of Parkinson's disease. *Proc Natl Acad Sci USA*. 2003;100(10):6145–6150.
63. Sanchez-Padilla J, et al. Mitochondrial oxidant stress in locus coeruleus is regulated by activity and nitric oxide synthase. *Nat Neurosci*. 2014;17(6):832–840.
64. Schildknecht S, et al. Oxidative and nitrative alpha-synuclein modifications and proteostatic stress: implications for disease mechanisms and interventions in synucleinopathies. *J Neurochem*. 2013;125(4):491–511.
65. Yamin G, Uversky VN, Fink AL. Nitration inhibits fibrillation of human alpha-synuclein in vitro by formation of soluble oligomers. *FEBS Lett*. 2003;542(1-3):147–152.
66. Rockenstein E, et al. Accumulation of oligomer-prone α-synuclein exacerbates synaptic and neuronal degeneration in vivo. *Brain*. 2014;137 (Pt 5):1496–1513.
67. Deas E, et al. Alpha-synuclein oligomers interact with metal ions to induce oxidative stress and neuronal death in Parkinson's disease. *Antioxid Redox Signal*. 2016;24(7):376–391.
68. Mor DE, et al. Dopamine induces soluble α-synuclein oligomers and nigrostriatal degeneration. *Nat Neurosci*. 2017;20(11):1560–1568.
69. Luk KC, et al. Pathological α-synuclein transmission initiates Parkinson-like neurodegeneration in nontransgenic mice. *Science*. 2012;338(6109):949–953.
70. Mao X, et al. Pathological α-synuclein transmission initiated by binding lymphocyte-activation gene 3. *Science*. 2016;353(6307):aah3374.
71. Franklin KBJ, Paxinos G. *Paxinos and Franklin's the mouse brain in stereotaxic coordinates*. 4th ed. Amsterdam, the Netherlands: Academic Press; 2013.

Supplemental Figure 1

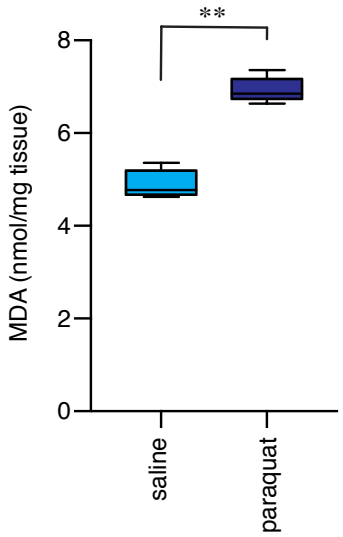

Supplemental Figure 1. Paraquat exposure causes an increase in lipid peroxidation in the DMnX. Mice received 2 intraperitoneal injections of either saline (n=5) or paraquat (n=5) separated by a 1-week interval and were sacrificed at 2 days post treatment. DMnX-containing specimens of the dorsal medulla oblongata were used for measurements of malondialdehyde (MDA) using a colorimetric assay. Box and whisker plots show median (middle line), upper and lower quartiles, and the maximum and minimum as whiskers. $^{**}P \leq 0.01$, Mann-Whitney test.

Supplemental Figure 2

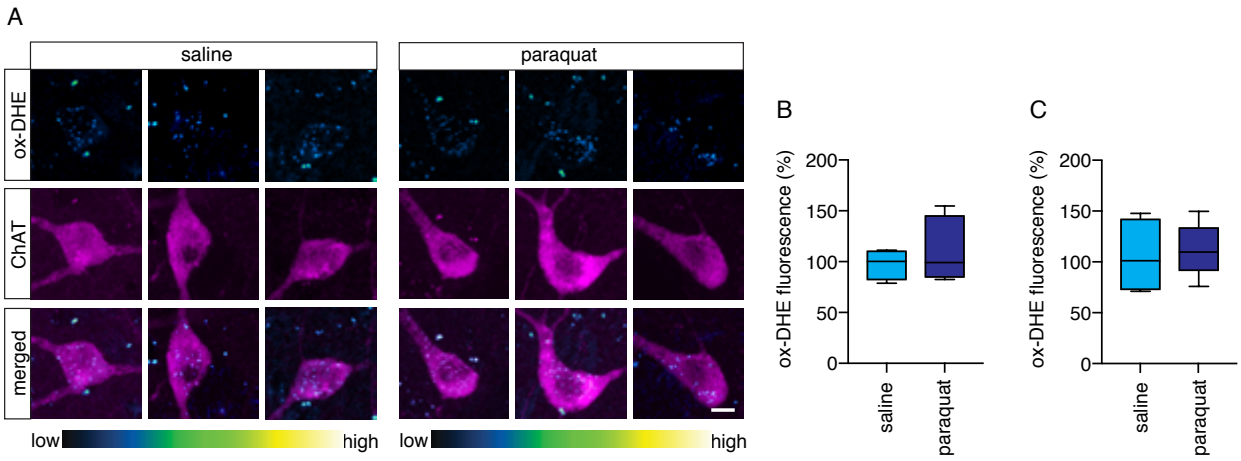

Supplemental Figure 2. Paraquat administration does not cause overt oxidative stress within cholinergic neurons in the striatum and medial septal nucleus. Mice received 2 intraperitoneal injections of either saline or paraquat separated by a 1-week interval and were sacrificed at 2 days post treatment. They were also injected with DHE 1 hour before the time of sacrifice. (**A**) Representative confocal images show ox-DHE fluorescence (blue-green-yellow color graded) within neurons immunoreactive for choline acetyltransferase (ChAT, magenta) in the striatum. Three neurons from 3 different animals injected with saline or paraquat are shown. Scale bar: 5 µm. (**B** and **C**) Comparison of the integrated density of fluorescent ox-DHE puncta within cholinergic (ChAT-positive) neurons in the striatum (B) and medial septal nucleus (C) from mice treated with saline (n=4, azure bar) or paraquat (n=5, dark blue bar). Approximately 14 and 12 neurons/animal were analyzed and averaged in the striatum and medial septal nucleus, respectively. Values were calculated as percent of the mean value in saline-injected animals. Box and whisker plots show median, upper and lower quartiles, and the maximum and minimum as whiskers.

Supplemental Figure 3

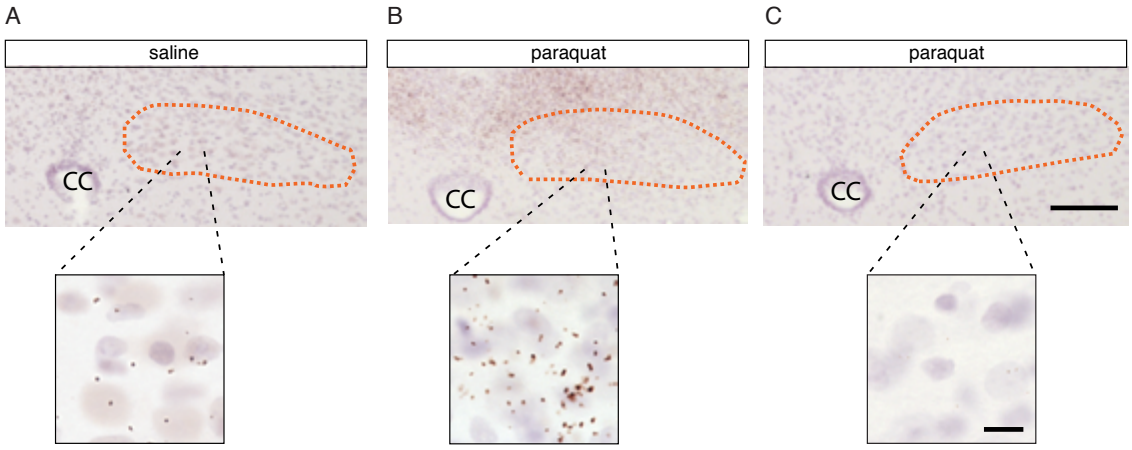

Supplemental Figure 3. Oxidative stress causes nitration of hα-synuclein that can be detected by specific PLA-generated signal. Mice received an injection of hα-synuclein-carrying AAVs into the left vagus nerve, were treated with either saline or paraquat and sacrificed at 2 days post treatment. (**A** and **B**) Representative low-(top panels) and high-(bottom panels) magnification images of the left DMnX (delineated in orange at low magnification) show specific signal for nitrated hα-synuclein detected by direct hα-synuclein/3-NT PLA. (**C**) Tissue sections of the medulla oblongata from a paraquat-injected mouse were pre-incubated with a cocktail of antibodies against nitrated α-synuclein and then processed for direct hα-synuclein/3-NT PLA. Representative images show that, in these tissue specimens, the PLA signal was abolished. CC=central canal. Scale bars: 100 μm (low) and 10 μm (high magnification).

Supplemental Figure 4

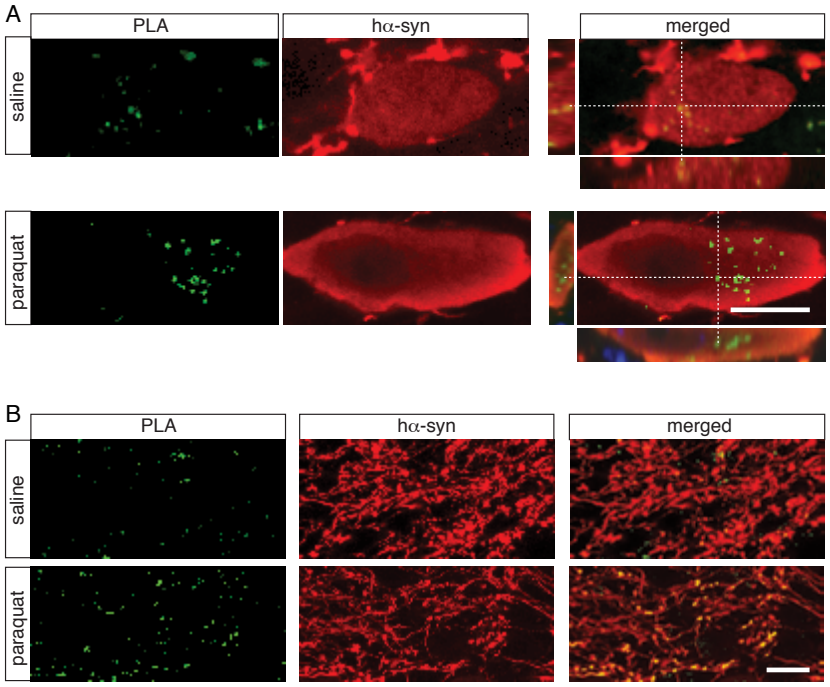

Supplemental Figure 4. Oxidative stress causes intraneuronal accumulation of oligomeric hα-synuclein. Mice received an injection of hα-synuclein-carrying AAVs into the left vagus nerve, were treated with either saline or paraquat and sacrificed at 2 days post treatment. Sections of the medulla oblongata were double-labeled with syn/syn PLA and anti-hα-synuclein. (**A**) Representative images show neuronal cell bodies in the left DMnX. Co-localization was confirmed in merged images showing orthogonal cross-sections in the x–z and y–z axes. Scale bar: 5 µm. (**B**) Representative images show neuritic labeling in the left DMnX. Syn/syn PLA and hα-synuclein co-localization (merged panels) was enhanced in the paraquat-treated animal. Scale bar: 10 µm.

Supplemental Figure 5

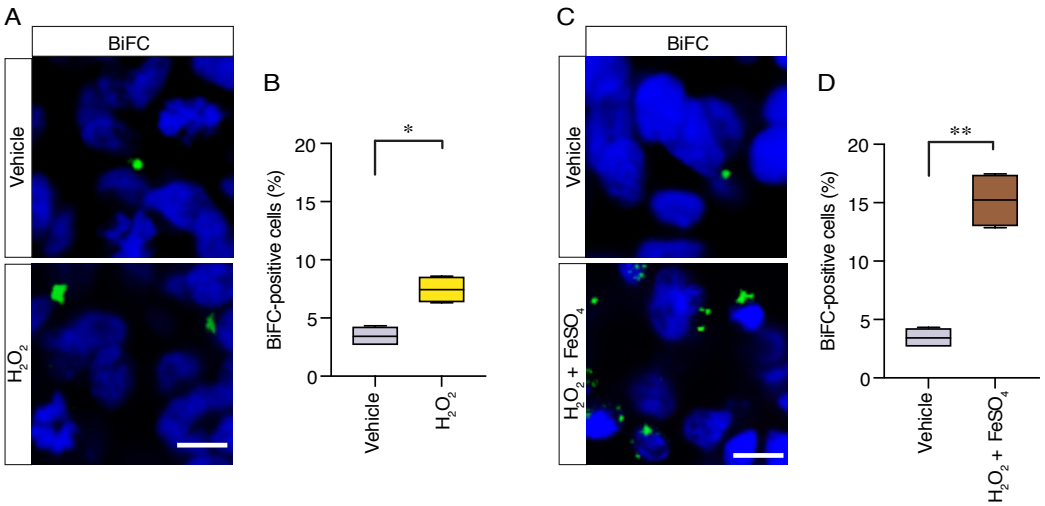

Supplemental Figure 5. ROS-induced oxidative stress promotes cell-to-cell hα-synuclein transfer in vitro. Co-cultures of V1S- and SV2-expressing cells were incubated for 2 days with vehicle, 100 µM hydrogen peroxide or 100 µM hydrogen peroxide plus 10 mM iron sulfate. At the end of these incubations, no significant differences in cell viability were found among the 3 treatment groups (data not shown). (**A** and **C**) Representative images show BiFC (green) as a marker of hα-synuclein transfer into recipient cells. Scale bar: 10 µm. (**B** and **D**) The percent of BiFC-positive cells (n=4 separate experiments/treatment) was compared in cultures treated with vehicle vs. hydrogen peroxide (B) or with vehicle vs. hydrogen peroxide plus iron sulfate (D). For each experiment, at least 1000 cells were analyzed and values were averaged. Box and whisker plots show median (middle line), upper and lower quartiles, and the maximum and minimum as whiskers. *$P \leq 0.05$, **$P \leq 0.01$, Mann-Whitney test.

Supplemental Table 1

Primary antibodies used in the study

Protein target	Antibody	Host	Supplier/ Catalog	Application	Concentration
α-Synuclein (human-specific)	Monoclonal clone MJFR1	Rabbit	Abcam ab138501	IF BM PLA (direct) PLA (indirect)	1:20,000 1:20,000 1 mg/ml 1:5,000
α-Synuclein (human-specific)	Monoclonal clone Syn 211	Mouse	Abcam 36-008	BM PLA (direct)	1:30,000 1 mg/ml
α-Synuclein (human-specific)	Monoclonal clone 4B12	Mouse	BioLegend 103-108	IF	1:500
α-Synuclein (human-specific)	Monoclonal clone 15G7	Rat	Enzo ALX-804-258	IF	1:1,000
α-Synuclein (total)	Monoclonal clone Syn-1 42/α-synuclein	Mouse	BD Biosciences 610787	ELISA	1 µg/ml
Choline acetyltransferase	Polyclonal	Goat	Millipore AB144P	IF	1:200
Nitrated α-synuclein	Monoclonal clone nSyn24.8	Mouse	Thermo Fisher MA5-16142	IF BM PLA blocking	1:100 1:500 1:50
Nitrated α-synuclein	Monoclonal clone nSyn12	Mouse	Upstate 36-011	PLA blocking *In vitro* blocking	1:20 50 µg/ml
Nitrated α-synuclein	Monoclonal clone nSyn14	Mouse	Upstate 36-012	PLA blocking	1:20
3-Nitrotyrosine (3-NT)	Monoclonal clone 39B6	Mouse	Abcam ab61392	IF *In vitro* blocking PLA (direct) PLA (indirect) ELISA	1:400 50 µg/ml 1 mg/ml 1:400 1 µg/ml
Oxidized α-synuclein	Monoclonal clone Syn 505	Mouse	Thermo Fisher 35-8300	IF	1:1,000
Aggregated α-synuclein	Monoclonal clone Syn-O2	Mouse	Custom	IF	1:5,000
Fibrillar α-synuclein	Monoclonal clone Syn-F1	Mouse	Custom	IF	1:5,000

IF = immunofluorescence; BM = brightfield microscopy; PLA = proximity ligase assay;
ELISA = Enzyme-linked immunosorbent assay
Custom antibodies were a kind gift from Dr. Omar El-Agnaf

Helwig, M*., Ulusoy, A*., Rollar, A., O'Sullivan, S.A., Lee, S.S.L., Aboutalebi, H., Pinto-Costa, R., Jevans, B., Klinkenberg, M., and Di Monte, D.A. (2022). Neuronal hyperactivity-induced oxidant stress promotes in vivo α-synuclein brain spreading. Sci Adv 8, eabn0356.

* Equal contribution

Objective: Here we sought to further scrutinize the causes and mechanisms of interneuronal α-syn and its relationship with oxidative stress. Based on previous work indicating that oxidative stress triggers neuron-to-neuron α-syn transfer, we hypothesized that increased neuronal activity in DMX neurons, known for their calcium-dependent pacemaking properties (Surmeier et al., 2017), could lead to elevated oxidative stress and promote interneuronal α-syn spreading.

Methods and results: To test this hypothesis, we induced α-syn transduction in the vagal complex. Instead of directly overexpressing α-syn through AAV-α-syn injections as described above, here, we utilized a conditional mouse line expressing Cre-recombinase dependent human α-syn. We induced α-syn expression by injecting AAV vectors encoding for Cre-recombinase (AAV-Cre) into the vagus nerve. This experimental approach allowed us to perform multiple Cre-dependent expressions simultaneously (e.g., α-syn and DREADD expression - see below). Injection of AAV-Cre into the vagus nerve resulted in transgene expression specifically in the vagal complex, reproducing the same anatomical distribution observed in wild-type mice after intravagal administration of AAV-α-syn.

To modulate neuronal activity, we employed intravagal injections of AAV vectors encoding DREADDs (designer receptors exclusively activated by designer drugs): Gq-coupled hM3D (human M_3 muscarinic DREADD) to increase activity and Gi-coupled hM4D (human M_3 muscarinic DREADD) to reduce activity. These receptors were activated explicitly by systemic administration of the synthetic ligand clozapine-N-oxide (CNO) (Roth, 2016). We injected a mixture of AAV-Cre and AAV-hM3D- or AAV-hM4D into the vagus nerve of mutant mice to investigate the impact of activity changes on the spreading process. Subsequently, the mice were treated with either CNO or a control vehicle. Cre-mediated α-syn expression induced interneuronal transfer and caudo-rostral spreading in vehicle-treated animals. This effect was significantly enhanced in mice expressing hM3D (increased neuronal activity) upon CNO administration, whereas it was significantly reduced in mice expressing hM4D (decreased neuronal activity). These results indicated a direct association between interneuronal α-syn spreading and neuronal activity.

Next, we examined the consequences of increased neuronal activity and demonstrated that besides promoting protein transfer, neuronal hyperactivity significantly exacerbated intraneuronal aggregate pathology, ROS formation, and increased accumulation of nitrated α-syn within DMX neurons. Notably, oxidative stress was particularly associated with mitochondrial dysfunction. In a final set of experiments, we tested whether overexpression of the mitochondrial superoxide scavenging enzyme SOD2 could counteract ROS formation and prevent interneuronal α-syn spreading under these experimental conditions. The data showed that SOD2 overexpression indeed reversed protein nitration and the enhanced α-syn spreading caused by neuronal hyperactivity.

Conclusions: The findings of this study provide valuable insights into the role of neuronal activity and oxidative stress in the spreading and pathology of interneuronal α-syn. Understanding these mechanisms

could have implications for the development of therapeutic strategies targeting α-synucleinopathies. Future studies could focus on investigating the specific molecular pathways underlying the link between neuronal activity, oxidative stress, and α-syn spreading, as well as exploring additional therapeutic approaches that modulate these pathways to mitigate disease progression.

SCIENCE ADVANCES | RESEARCH ARTICLE

NEUROSCIENCE

Neuronal hyperactivity–induced oxidant stress promotes in vivo α-synuclein brain spreading

Michael Helwig[1]†, Ayse Ulusoy[1,2]†, Angela Rollar[1], Sinead A. O'Sullivan[1], Shirley S. L. Lee[1], Helia Aboutalebi[1], Rita Pinto-Costa[1], Benjamin Jevans[1], Michael Klinkenberg[1], Donato A. Di Monte[1,2]*

Interneuronal transfer and brain spreading of pathogenic proteins are features of neurodegenerative diseases. Pathophysiological conditions and mechanisms affecting this spreading remain poorly understood. This study investigated the relationship between neuronal activity and interneuronal transfer of α-synuclein, a Parkinson-associated protein, and elucidated mechanisms underlying this relationship. In a mouse model of α-synuclein brain spreading, hyperactivity augmented and hypoactivity attenuated protein transfer. Important features of neuronal hyperactivity reported here were an exacerbation of oxidative and nitrative reactions, pronounced accumulation of nitrated α-synuclein, and increased protein aggregation. Data also pointed to mitochondria as key targets and likely sources of reactive oxygen and nitrogen species within hyperactive neurons. Rescue experiments designed to counteract the increased burden of reactive oxygen species reversed hyperactivity-induced α-synuclein nitration, aggregation, and interneuronal transfer, providing first evidence of a causal link between these pathological effects of neuronal stimulation and indicating a mechanistic role of oxidant stress in hyperactivity-induced α-synuclein spreading.

INTRODUCTION

A prominent pathological feature of human neurodegenerative diseases is the intra- and/or extracellular deposition of proteinaceous aggregates (*1*). In Parkinson's disease (PD), aggregates containing the protein α-synuclein (αS) are accumulated within neuronal cell bodies and neurites, forming typical inclusions known as Lewy bodies and Lewy neurites (*2*, *3*). Thorough assessment of Lewy pathology at early presymptomatic stages as well as during disease progression has yielded a number of intriguing observations. αS deposition not only affects neurons in the brain but also occurs within neurons of the peripheral nervous system (*4*–*7*). In the brain, specific anatomically interconnected regions are preferentially targeted by Lewy pathology, and the buildup of αS lesions often follows a stereotypical caudo-rostral pattern, advancing from the lower brainstem toward higher brain regions (*3*, *8*). Together, these pathological features prompted the hypothesis that cell-to-cell transfer of pathogenic αS species plays an important role in the progressive spread of αS lesions throughout the brain and between the brain and peripheral tissues (*9*–*12*). As a corollary to this hypothesis, much attention has been focused on neurons of the dorsal motor nucleus of the vagus (X^{th}) nerve (DMnX) in the medulla oblongata (MO). These cholinergic cells are among the earliest sites of αS deposition during PD development and could therefore represent a source of initial pathological spreading (*3*, *8*). Furthermore, long efferent projections of DMnX neurons reach peripheral tissues through the vagus nerve, supporting a role of the DMnX as a relay center for peripheral-to-central (or central-to-peripheral) αS transmission (*13*–*15*).

Evidence of a relationship between interneuronal protein transfer and progressive spreading of pathological lesions underscores the relevance of investigations into pathophysiological conditions that may prompt or affect these processes. Growing experimental data are consistent with the ability of neuronal activity to modulate both the pathogenicity and interneuronal mobility of disease-associated proteins, namely, β-amyloid, tau, and αS. Chronic optogenetic neuronal stimulation and chemogenetic reduction of neuronal activity have been found to exacerbate and attenuate, respectively, β-amyloid peptide deposition (*16*–*18*). Similarly, in transgenic mouse models of human tau overexpression, tau pathology was enhanced and more widely spread under conditions of increased neuronal activity (*19*, *20*). In regard to αS, pharmacological induction of neuronal activity has been reported to promote αS aggregation and trafficking after "seeding" of organotypic brain slice cultures with αS preformed fibrils (PFFs) (*21*). Moreover, when PFFs were injected into the mouse dorsal striatum, motor deficits and αS pathology became more or less pronounced after chemogenetic induction of striatal hyper- or hypoactivity (*21*). The possibility that hyper- or hypoactivity may affect protein-induced pathology by modulating interneuronal protein transfer is further supported by data showing that secretion of β-amyloid, tau, or αS into the extracellular space and protein exchange from donor into recipient cells are clearly influenced by neuronal activity (*16*, *19*, *20*, *22*, *23*).

Despite increasing recognition of this pathophysiological role of neuronal activity, key questions concerning the relationship between hyper-/hypoactivity and protein spreading remain unanswered. First, very little is known about mechanisms by which changes in neuronal activity could modulate interneuronal protein transfer. Second, hyper- and hypoactivity not only affect protein spreading but also appear to influence the severity of aggregate pathology, raising the question of whether these activity-dependent changes are mediated through similar or different mechanisms (*16*, *19*, *21*). Last, it is conceivable that mechanisms underlying the relationship between neuronal activity and protein spreading may have a more or less pronounced

[1]German Center for Neurodegenerative Diseases (DZNE), Bonn 53127, Germany. [2]Aligning Science Across Parkinson's (ASAP) Collaborative Research Network, Chevy Chase, MD 20815, USA.
*Corresponding author. Email: donato.dimonte@dzne.de
†These authors contributed equally to this work.

impact on different neuronal populations, thus contributing to their discrete vulnerability to protein spreading and ensuing pathology. The aim of the current study was to further our understanding of these important mechanistic issues. In particular, experiments were designed to test the hypothesis that oxidant stress is a mechanism by which changes in neuronal activity can modulate interneuronal transfer and brain spreading of αS.

Several considerations prompted this hypothesis. A major cellular source of reactive oxygen species (ROS) is the mitochondrial electron transfer chain (ETC). During oxidative phosphorylation (OXPHOS), the flux of electrons through the ETC not only generates the energy gradient needed for adenosine triphosphate (ATP) production but also is accompanied by leakage of superoxide primarily from complex I and complex III (*24*–*26*). It is quite plausible therefore that, as a consequence of hyper- or hypoactivity, changes in neuronal energy demands could affect mitochondrial OXPHOS and electron transfer rates, resulting in increased or lowered ROS production. If hyper- or hypoactivity is associated with enhanced or reduced oxidant stress, the likelihood that this effect may ultimately impinge upon interneuronal protein spreading is supported by the results of an earlier investigation. These findings revealed that, under prooxidant conditions characterized by neuronal accumulation of both ROS and reactive nitrogen species (RNS), neuron-to-neuron transmission and consequent brain spreading of αS were significantly exacerbated (*27*). A potential relationship between neuronal activity, oxidant stress, and interneuronal αS transfer may be of particular relevance for DMnX neurons. These cells feature a distinct physiological trait that also characterizes other neuronal populations highly susceptible to αS pathology, including dopaminergic cells in the substantia nigra pars compacta and noradrenergic cells in the locus coeruleus (*28*–*31*). They autonomously generate a broad rhythmic action potential that is accompanied by slow oscillations of cytosolic calcium. This pacemaking activity creates a high basal metabolic demand, promotes calcium entry into mitochondria, and stimulates mitochondrial OXPHOS (*32*, *33*). It may also render these neurons particularly susceptible to activity-dependent oxidant stress and consequent protein spreading.

Experiments here were carried out using a unique paradigm of transgene expression targeting neurons in the DMnX-containing dorsal MO (DMnX-MO). This paradigm involved the use of transgenic Cre-inducible human αS (h-αS) knock-in mice and administration of adeno-associated viral vectors (AAVs) into the mouse vagus nerve. Intravagal treatment with AAVs carrying Cre recombinase DNA (Cre-AAVs) induced targeted h-αS expression that was followed by interneuronal transfer of the exogenous protein and its spreading from the dorsal MO toward higher brain regions. The intravagal route was also used for administration of AAVs delivering DREADD (Designer Receptor Exclusively Activated by Designer Drugs) DNAs. Targeted expression and pharmacologic stimulation of hyperactivity- or hypoactivity-inducing DREADDs allowed us to achieve tissue-specific changes in neuronal activity that markedly affected caudo-rostral h-αS spreading. Other findings revealed that increased protein spreading after neuronal hyperactivity was associated with pronounced ROS burden, nitrative modifications of both cytosolic and mitochondrial proteins, and enhanced h-αS assembly. Rescue experiments aimed at preventing neuronal ROS accumulation established a clear relationship between these pathological effects of neuronal stimulation and demonstrated a key mechanistic role of oxidant stress in hyperactivity-induced h-αS transfer.

RESULTS

Cre-induced expression of h-αS in the DMnX-MO of conditional transgenic mice triggered its caudo-rostral spreading

Targeted transgene insertion at the *Rosa26* locus on chromosome 6 is an effective strategy to generate transgenic mice and induce stable gene expression in these animals (*34*–*36*). Conditional expression can also be achieved by cloning the transgene into a Rosa26-targeting vector downstream to a *loxP*-flanked neo/STOP cassette (Fig. 1A, I to III). Under these conditions, gene expression would only occur upon Cre-mediated excision of the transcriptional termination sequence (Fig. 1A, IV and V). Transgenic Cre-inducible h-αS knock-in mice (iR26-αS) were generated using this approach, bred to homozygosity, and used for this study. To induce h-αS expression in the DMnX-MO, iR26-αS mice received a single unilateral injection of Cre-AAVs driving Cre recombinase expression under control of the human synapsin promoter into the left vagus nerve (Fig. 1B). At 4 weeks after this treatment, animals were sacrificed, their brains were dissected, and medullary tissue sections were stained with an antibody that specifically recognizes h-αS. Immunoreactivity showed a reproducible pattern of expression consistent with AAV-induced transduction of neuronal cell bodies in the DMnX and inferior vagal ganglion (*37*–*40*). H-αS–loaded perikarya and neurites were observed in the ipsilateral DMnX, while h-αS–positive axons originating from ganglionic cells projected into the nucleus of the tractus solitarius (NTS) both ipsi- and contralaterally (Fig. 1C). A dose-dependent effect of Cre-induced transgene expression was indicated by an increasing number of h-αS–positive DMnX neurons and increasing densities of immunoreactive NTS axons after injections with low, middle, and high AAV titers (Fig. 1C).

To determine whether Cre-induced DMnX-MO expression of h-αS resulted in its interneuronal spreading toward more rostral brain regions, titer- and time-dependent experiments were carried out. First, iR26-αS mice received an intravagal injection of different titers of Cre-AAVs, i.e., 1×10^{12}, 2×10^{12}, or 4×10^{12} genome copies (gc)/ml, and were sacrificed at 4 weeks after administration. Coronal tissue sections were collected throughout the brain and stained with anti–h-αS. Spreading was assessed by counting the number of h-αS–immunoreactive axons in the pons, midbrain, and forebrain. Moreover, the length and density of h-αS–positive fibers were estimated in a defined pontine area encompassing the locus coeruleus and the nucleus parabrachialis using the Space Balls stereological probe. At 4 weeks after treatment, enlarged h-αS–positive axons with densely labeled and irregularly spaced varicosities could be detected in brain regions rostral to the MO (Fig. 2A). The number of these axons was highest in the pons and progressively lower in the caudal and rostral midbrain and forebrain, indicating that regions closer to the MO were more severely affected by the spreading pathology (Fig. 2, B and C). Axonal counts as well as Space Balls measurements were dependent upon the titer of Cre-AAV injections. Higher titers were associated with higher count, length, and density values, underscoring a relationship between the extent of AAV-induced h-αS expression and degree of protein transfer (Fig. 2, C and D).

For the time-course experiments, mice were injected with Cre-AAVs (2×10^{12} gc/ml) and sacrificed 4, 5, or 6 weeks after treatment. Results of these experiments provided further evidence of ascending protein spreading that became more and more pronounced at increasing time intervals. Axonal counts in the pons, midbrain, and forebrain and measurements of fiber length and density in pontine

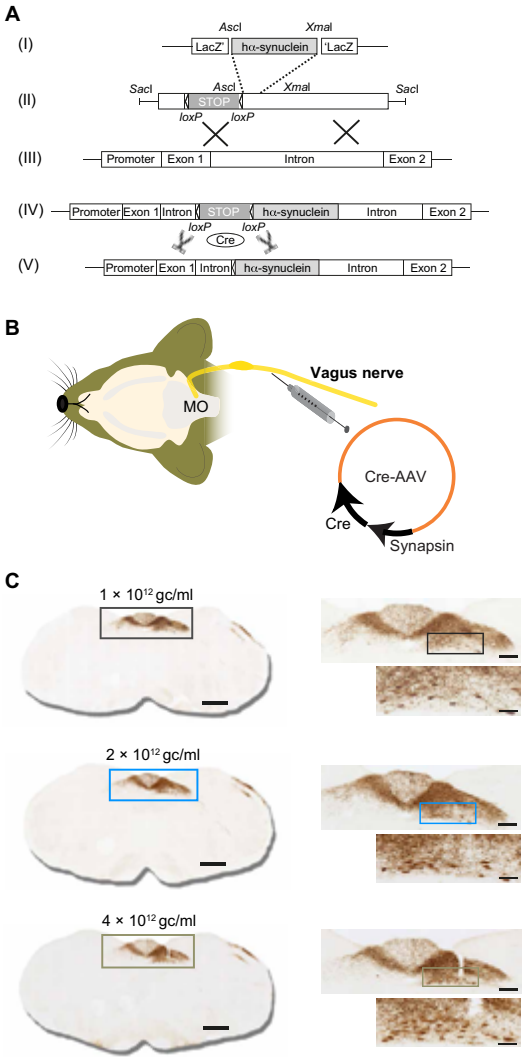

Fig. 1. Cre-inducible expression of h-αS in the dorsal medulla oblongata of iR26-αS mice. (**A**) Gene targeting strategy for the generation of transgenic iR26-αS mice involved insertion of wild-type h-αS cDNA (I) into a Rosa26 targeting vector downstream to a *loxP*-flanked transcriptional termination (neo/STOP) cassette (II). Following homologous recombination at the murine *Rosa26* genomic locus (III), correctly targeted clones contained the neo/STOP cassette and the h-αS DNA sequence adjacent to the endogenous Rosa26 promoter (IV). In mice carrying this transgene, Cre recombinase–dependent excision of the neo/STOP cassette (V) drove the inducible expression of h-αS. (**B**) Transgenic expression of h-αS in the MO was induced by a unilateral injection of Cre-AAVs into the left vagus nerve. Gene expression was regulated by the human synapsin 1 promoter. (**C**) Mice were sacrificed at 4 weeks after a vagal injection of 1×10^{12} gc/ml (black boxes), 2×10^{12} gc/ml (light blue boxes), or 4×10^{12} gc/ml (green-brown boxes) of Cre-AAVs. Coronal sections of the MO were immunostained with anti–h-αS. Representative images show titer-dependent h-αS expression (brown staining) at low, medium, and high magnification. Boxes in the low-magnification images encompass an area of the dorsal MO that is shown at medium magnification. Boxes in the medium-magnification images encompass an area of the DMnX that is also shown at high magnification. Scale bars, 500, 200, and 50 μm in low-, medium-, and high-magnification images, respectively.

sections indicated a progressive buildup of h-αS–positive neurites between 4 and 6 weeks after AAV administration (Fig. 2, E to H). Primary sites of pathological h-αS accumulation included the coeruleus-subcoeruleus complex in the pons, the dorsal raphae and periacqueductal gray in the midbrain, the hypothalamus in the diencephalon, and the amygdala in the medial temporal lobe. Together, these results indicated that conditional expression of h-αS could be reproducibly achieved in the DMnX-MO of iR26-αS mice after a vagal Cre-AAV injection and that enhanced protein expression effectively triggered h-αS caudo-rostral brain advancement. On the basis of these initial findings, mice used in subsequent experiments were all injected with a Cre-AAV titer of 2×10^{12} gc/ml; h-αS spreading was then consistently assessed at 5 weeks after treatment.

Increased activity of DMnX neurons exacerbated h-αS spreading

Expression of synthetically designed receptors and binding of these receptors with specific ligands can be used for transient activation or inactivation of targeted brain regions (*21*, *41*, *42*, *43*). This DREADD approach has been successfully applied to induce hyper- or hypoactivity of DMnX neurons that was validated using electrophysiological recordings and functional outcomes (*31*, *44*). Experiments were carried out here to assess the effects of chemogenetically induced DMnX hyperactivity on h-αS brain transfer. iR26-αS mice received an injection of a cocktail of two viral vectors into the left vagus nerve. The injected solution contained Cre-AAVs and AAVs designed to express Gq-coupled hM3D DREADD fused with mCherry under control of the human synapsin promoter; conditional expression was achieved using a double-floxed inverse ORF (DIO) (hM3D^{fl}-AAVs; Fig. 3A). hM3D is a DREADD variant commonly used for neuronal excitation (*41*, *42*). Animals were kept for 5 weeks after AAV vagal administration and, starting at the beginning of week 4, also received a daily intraperitoneal injection of clozapine *N*-oxide (CNO), a synthetic ligand and DREADD activator. To define the distribution of AAV transduction and demonstrate confinement of AAVs within the MO, Cre recombinase mRNA was assessed by RT-PCR (reverse transcription polymerase chain reaction) as a marker of Cre-AAV–dependent transduction. Assays were carried out on tissue specimens of the dorsal MO, pons, and midbrain. RT-PCR products, when run on agarose gel, revealed clear bands for Cre recombinase mRNA in all samples from the DMnX-MO; quite in contrast, specimens from the pons and midbrain were consistently devoid of AAV-derived mRNA (Fig. 3B). No differences in Cre transduction were observed between saline- or CNO-treated mice (Fig. 3B). Expression of Cre recombinase was also assessed at the protein level by immunostaining medullary and pontine tissue sections from both saline and CNO-treated mice with a specific antibody against this protein. In all animals, reactivity with anti-Cre clearly labeled nuclei within neurons of the left (ipsilateral to the AAV injection side) DMnX; this observation sharply contrasted with findings in pontine sections, showing the absence of specific immunoreactivity (fig. S1).

Further analyses were performed using immunohistochemistry to verify that coadministration of Cre- and hM3D^{fl}-AAVs resulted in Cre-induced expression of both h-αS and mCherry-fused hM3D proteins. For these analyses, coronal sections of the MO were stained with either anti–h-αS or an mCherry-recognizing antibody raised against red fluorescent protein (RFP). In all animals treated with Cre-/hM3D^{fl}-AAVs plus saline or Cre-/hM3D^{fl}-AAVs plus CNO, staining with either of the two antibodies showed robust DMnX-MO

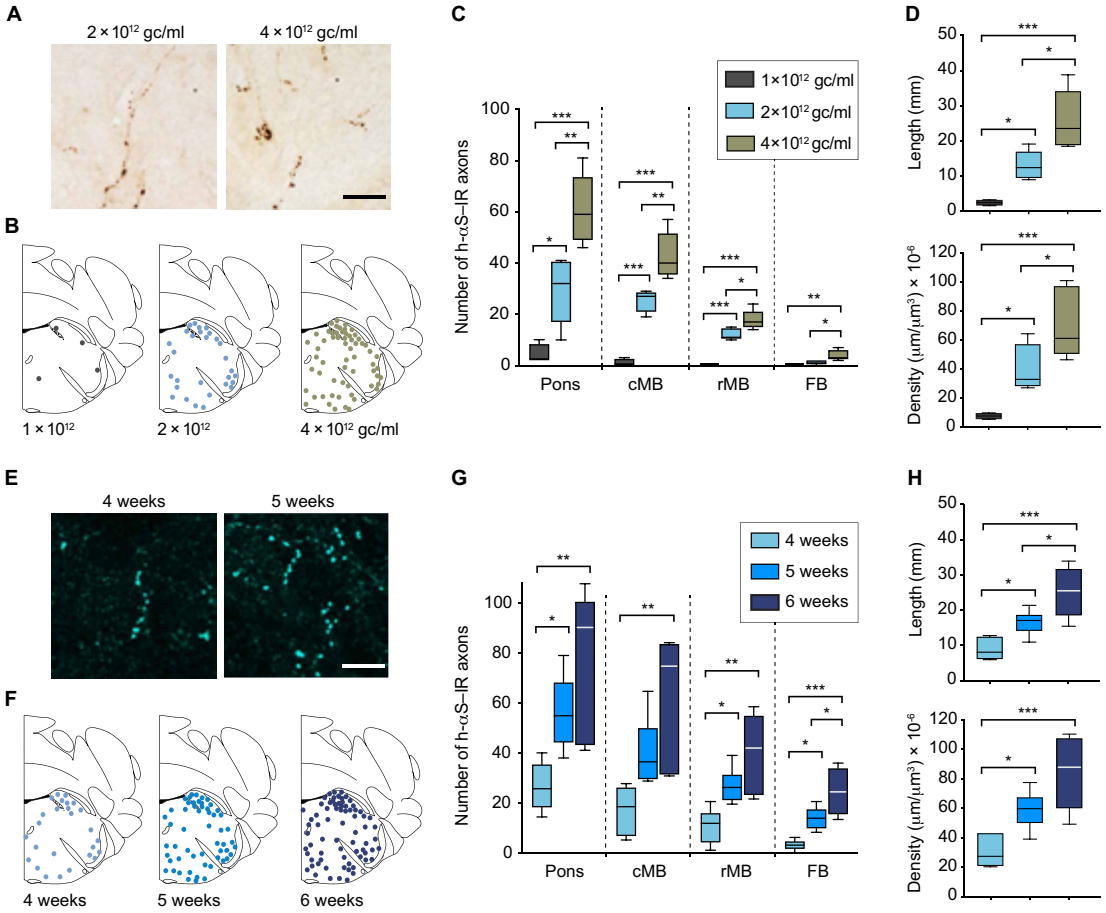

Fig. 2. Caudo-rostral h-αS spreading is triggered by Cre-induced h-αS expression in the DMnX-MO. (**A** to **D**) iR26-αS mice received a single injection of 1×10^{12} gc/ml ($n = 4$, black), 2×10^{12} gc/ml ($n = 5$, light blue), or 4×10^{12} gc/ml ($n = 5$, green-brown) of Cre-AAVs into the left vagus nerve and were sacrificed 4 weeks later. Tissue sections were immunostained with anti–h-αS. Representative bright-field images show h-αS–positive axons in the left pons. Scale bar, 20 μm (A). Schematic plots of the distribution of h-αS–immunoreactive (h-αS–IR) axons in left pontine sections (bregma −5.40 mm) from three representative mice; each dot represents a separate single axon (B). The number of h-αS–immunoreactive axons was counted in tissue sections of the left pons, caudal midbrain (cMB), rostral midbrain (rMB), and forebrain (FB) (C). Length and density of h-αS–positive axons were estimated in a defined pontine area using the Space Balls stereological tool (D). (**E** to **H**) Mice received a single injection of Cre-AAVs (2×10^{12} gc/ml) into the left vagus nerve and were sacrificed 4 weeks ($n = 6$, light blue), 5 weeks ($n = 6$, blue), and 6 weeks ($n = 5$, dark blue) later. Representative confocal images show h-αS–positive axons (cyan) in tissue sections of the left pons. Scale bar, 20 μm (E). Schematic plots of the distribution of h-αS–immunoreactive axons in left pontine sections (F). The number of h-αS–immunoreactive axons was counted in tissue sections of the left pons, caudal midbrain, rostral midbrain, and forebrain (G). The length and density of h-αS–immunoreactive axons were estimated in a defined pontine area using the Space Balls stereological tool (H). Box and whisker plots show median, upper and lower quartiles, and maximum and minimum as whiskers. *$P < 0.05$, **$P < 0.01$, and ***$P < 0.001$.

immunoreactivity, indicating successful expression of both h-αS and hM3D proteins (Fig. 3C shows images from a saline-injected mouse). Separate medullary sections were double-stained with anti–h-αS and anti-RFP and processed for immunofluorescence. In these sections, images of the DMnX showed signal colocalization within neuronal cell bodies that were immunoreactive for both h-αS and RFP (Fig. 3D). In contrast to findings in the MO, sections of the pons stained with anti-RFP were found to be consistently (e.g., in saline- or CNO-treated mice) devoid of immunoreactivity (fig. S2A). Furthermore, when pontine sections were double-labeled with anti–h-αS and anti-RFP, h-αS–loaded axons were observed, reflecting the MO-to-pons transfer of this protein; the same axons, however, showed no immunoreactivity for the RFP/mCherry protein (fig. S2B). Together, these observations further support the conclusion that AAV transduction and consequent protein expression targeted and remained strictly confined within medullary vagus–associated neurons.

Expression of the immediate early gene c-fos is an indirect marker of neuronal activity and was therefore used to assess DREADD activation upon treatment with its ligand and consequent neuronal hyperactivity. Samples analyzed for c-fos expression were obtained from mice injected with Cre-/hM3D^{fl}-AAVs and then, after 3 weeks, treated with either saline or CNO for 1 or 2 weeks. Staining of medullary

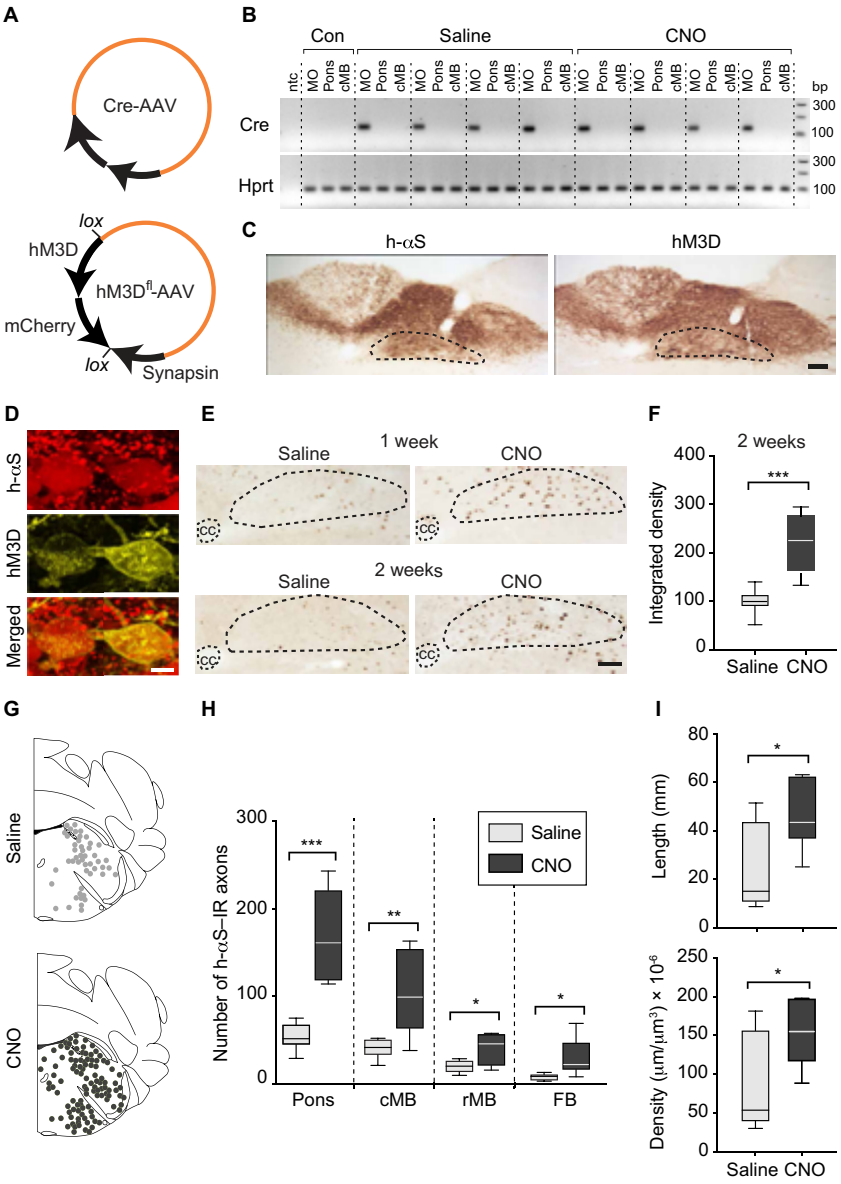

Fig. 3. Neuronal hyperactivity exacerbates caudo-rostral h-αS spreading. (**A** and **B**) Mice were coinjected with Cre-AAVs together with AAVs designed for conditional hM3D DREADD expression (hM3D^{fl}-AAVs) (A). They also received saline or CNO for 2 weeks (weeks 4 and 5) before sacrifice. Tissue specimens from the left dorsal MO, pons, and caudal midbrain were processed for RT-PCR; specific bands at 116 (Cre) and 90 (Hprt) bp; control samples (Con) from untreated mice; nontemplate control (ntc) (B). (**C** and **D**) Mice were coinjected with Cre- and hM3D^{fl}-AAVs and treated with saline as above. Medullary sections were immunostained with anti–h-αS or anti-RFP; the DMnX is delineated. Scale bar, 100 μm (C). Confocal images of DMnX neurons double-labeled with anti–h-αS and anti-RFP. Scale bar, 10 μm (D). (**E** and **F**) Mice received an injection of Cre- and hM3D^{fl}-AAVs and were treated with saline or CNO for 1 or 2 weeks. Medullary sections were labeled with anti–c-fos; the central canal (cc) and DMnX are delineated. Scale bar, 100 μm (E). Density measurements of c-fos immunoreactivity in the DMnX of mice injected with Cre- and hM3D^{fl}-AAVs and treated with saline or CNO ($n = 8$ per group); data were calculated as percentage of the mean value in the saline group (F). (**G** to **I**) Mice received an injection of Cre- and hM3D^{fl}-AAVs and were treated with saline ($n = 6$, gray) or CNO ($n = 7$, black). Brain sections were immunostained with anti–h-αS. Schematic plots of the distribution of h-αS–immunoreactive axons in left pontine sections (G). The number of h-αS–immunoreactive axons was counted in the left pons, caudal and rostral midbrain, and forebrain (H). The length and density of h-αS–immunoreactive axons were measured in pontine sections (I). Plots show median, upper and lower quartiles, and maximum and minimum as whiskers. *$P < 0.05$, **$P < 0.01$, and ***$P < 0.001$.

tissue sections with anti–c-fos revealed a significantly greater number of labeled DMnX neurons and significantly enhanced c-fos immunoreactivity as consequences of 1- or 2-week CNO administration, consistent with neuronal hyperactivity throughout the period of hM3D activation (Fig. 3, E and F). Next, treatment of iR26-αS mice with Cre-/hM3D^{fl}-AAVs and subsequent injections with saline or CNO (during weeks 4 and 5 after AAV administration) were used to compare h-αS spreading in the absence or presence of hM3D activation. Tissue sections of the pons, caudal and rostral midbrain, and forebrain were stained with anti–h-αS and used for quantitative assessment of h-αS–immunoreactive axons. Axonal counts were consistently (i.e., in all brain regions) found to be much greater in CNO-treated as compared to saline-treated animals and, similarly, Space Balls measurements of pontine fiber length and density yielded values that were two to three times higher after hM3D activation (Fig. 3, G to I). Thus, hyperactivity had a pronounced effect on neuron-to-neuron protein transfer and significantly exacerbated h-αS advancement from the lower brainstem toward higher brain regions.

Neuronal hyperactivity caused oxidant stress and accumulation of nitrated h-αS

Experiments and analyses were carried out to determine whether increased neuronal activity was associated with oxidant stress, suggesting a relationship between hyperactivity, augmented ROS/RNS formation, and enhanced h-αS transfer. iR26-αS mice were injected with Cre-/hM3D^{fl}-AAVs, treated for 2 weeks (weeks 4 and 5) with saline or CNO, and sacrificed at 5 weeks after AAV administration. One hour before the time of sacrifice, they also received an intraperitoneal injection of the superoxide indicator dihydroethidium (DHE). Microscopic examination of medullary sections from these mice revealed a punctate pattern of fluorescent signal within h-αS–loaded DMnX neurons (Fig. 4A). This signal is an indicator of the reaction between DHE and superoxide, leading to the formation of fluorescent ethidium cations (ox-DHEs) and their accumulation into mitochondria (*27*, *45*). Neurons displayed a wide range of number and intensity of fluorescent puncta, likely reflecting cell-to-cell variability of oxidant burden. Nevertheless, this punctate fluorescence was increased in sections from CNO-treated mice, and quantification of the intraneuronal ox-DHE signal revealed significantly higher intensity values after hM3D stimulation (Fig. 4, A and B).

During oxidant stress, enhanced ROS and RNS production may lead to nitration of αS at one or more of its four tyrosine residues (*46*). Accumulation of nitrated h-αS was therefore assessed in tissue sections of the MO of h-αS and hM3D coexpressing mice using a proximity ligation assay (PLA). For this assay, samples were incubated first with a pair of primary antibodies and then with secondary antibodies conjugated with PLA oligonucleotide probes; the two primary antibodies were anti–h-αS and anti–3-nitrotyrosine (3-NT), an antibody that recognizes 3-NT–modified protein residues (*27*). Following signal amplification, bright-field detection showed specific chromogenic dots in the left (ipsilateral to the vagal AAV injection) DMnX and revealed a marked signal enhancement in samples from CNO-treated as compared to saline-treated animals (Fig. 4C). When the number of PLA dots was estimated using unbiased stereological counting, this number was found to be increased by three to four times following stimulation of neuronal activity (Fig. 4D). 3-NT/h-αS PLA was then used to determine whether nitrated h-αS was also present in pontine tissue sections, i.e., within axons that accumulated h-αS as a result of MO-to-pons protein transfer. Specific labeling was scant in sections from saline-treated mice but more abundant after CNO administration, and stereological counts of pontine PLA dots were significantly higher in samples from the latter as compared to the former treatment group (Fig. 4E).

Neuronal hyperactivity was associated with mitochondrial nitrative damage

To assess the involvement of mitochondria in hyperactivity-induced oxidative reactions, new PLA-based assays were developed and used for detection and quantification of nitrative modifications of key mitochondrial proteins. In particular, these analyses evaluated levels of nitrated mitochondrial complex I subunit NDUFB8 [NADH (reduced form of nicotinamide adenine dinucleotide) dehydrogenase (ubiquinone) I beta subcomplex subunit 8] and nitrated superoxide dismutase 2 (SOD2) within unstimulated versus hyperactive DMnX neurons. Medullary tissue sections from iR26-αS mice injected with Cre-/hM3D^{fl}-AAVs and treated with saline or CNO were incubated with anti–3-NT and anti-NDUFB8 for assessment of nitrated NDUFB8 or with anti–3-NT and anti-SOD2 for the detection of nitrated SOD2. Samples were then incubated with oligonucleotide-labeled secondary antibodies and hybridizing connector oligonucleotides before amplification and visualization of the PLA signal with fluorescence detection. These sections were also stained with anti–h-αS. Confocal microscopy showed weak PLA signal in sections from saline-treated animals (Fig. 5, A and C), whereas robust labeling indicated accumulation of either nitrated NDUFB8 (Fig. 5A) or nitrated SOD2 (Fig. 5C) within h-αS–immunoreactive DMnX neurons after CNO administration. This marked effect of neuronal hyperactivity was confirmed by image analysis and quantification of intraneuronal PLA signal intensity as well as by counts of the PLA dots (Fig. 5, B and D). These findings not only provided additional evidence of oxidant stress within hyperactive neurons but also pointed to mitochondria as key targets of ROS/RNS-induced modifications during neuronal stimulation.

Evidence of oxidant stress after stimulation of h-αS–loaded DMnX neurons raised the question of whether ROS/RNS burden is a direct consequence of neuronal hyperactivity or represents a specific feature of neuronal stimulation in the presence of enhanced h-αS expression. To address this question, a separate set of experiments was designed using iR26-αS mice that received an intravagal injection of AAVs carrying nonfloxed hM3D DNA (Fig. 6A). This treatment aimed at expressing the excitatory DREADD in the absence of concurrent h-αS expression. At 3 weeks after AAV treatment, the animals were divided into two groups that received daily saline or CNO injections for 2 weeks before being sacrificed. Medullary tissue sections were processed for fluorescent microscopy and double-labeled with 3-NT/NDUFB8 PLA and anti-RFP. Microscopic examination revealed an overt increase in PLA signal in samples from CNO-treated mice (Fig. 6B). Similarly, when PLA signal intensity was measured within RFP-positive DMnX neurons and compared between saline- and CNO-injected animals, significantly higher fluorescence characterized the latter set of samples (Fig. 6C). Thus, neuronal hyperactivity was itself capable of inducing nitrative modifications of mitochondrial NDUFB8.

Accumulation of nitrated h-αS and protein spreading were reduced after suppression of neuronal activity

Expression and CNO-induced activation of the DREADD hM4D result in membrane hyperpolarization and suppression of neuronal activity (*31*, *41*, *42*). Experiments were therefore carried out using

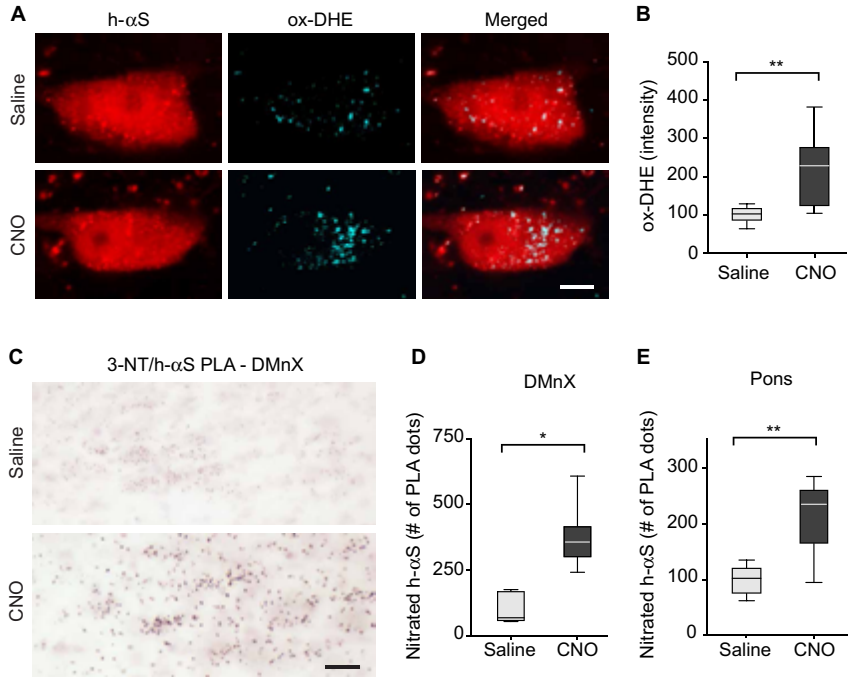

Fig. 4. Neuronal hyperactivity induces oxidant and nitrative stress. (**A** and **B**) iR26-αS mice were coinjected with Cre- and hM3D^{fl}-AAVs and treated with daily injections of either saline ($n = 8$) or CNO ($n = 7$) during weeks 4 and 5 after AAV injection. At the end of week 5, they received an injection of DHE 1 hour before sacrifice. Sections of the MO were immunostained with anti–h-αS. Representative confocal images show fluorescent puncta of ox-DHE within h-αS–positive DMnX neurons. Scale bar, 10 μm (A). Ox-DHE fluorescent intensity was measured within h-αS–positive DMnX neurons (approximately 30 neurons per animal). For each animal, neuronal intensity values were averaged; the averaged value was then calculated as percentage of the mean value in the saline group (B). (**C** to **E**) Mice injected with Cre- and hM3D^{fl}-AAVs also received either saline ($n = 6$) or CNO ($n = 7$). To detect nitrated h-αS, sections of the MO and pons were processed for 3-NT/h-αS PLA. Representative images show specific chromogenic PLA dots in the left (injected side) DMnX. Scale bars, 50 μm (C). For each animal, the number of PLA dots was estimated in the left DMnX using unbiased stereology; data were calculated as percentage of the mean value in the saline group (D). The number of PLA dots was counted in left pontine sections; for each mouse, counts were done on a single section corresponding to bregma −5.34 mm, and data were calculated as percentage of the mean value in the saline group (E). Box and whisker plots show median, upper and lower quartiles, and maximum and minimum as whiskers. *$P < 0.05$ and **$P < 0.01$.

hM4D expression as a tool for assessing the effects of neuronal hypoactivity on h-αS nitration and h-αS spreading. Mice received an intravagal coinjection of Cre-AAVs and AAVs designed to express Gi-coupled hM4D DREADD fused with mCherry under control of the human synapsin promoter; conditional expression was achieved using a DIO system (hM4D^{fl}-AAVs, Fig. 7A). They were also treated for 2 weeks (weeks 4 and 5 after AAV injection) with saline or CNO before being sacrificed at 5 weeks after AAV administration. Postmortem analyses of medullary tissue sections that were double-labeled for h-αS and RFP showed colocalization of immunoreactivities within DMnX neurons, thus confirming cotransduction and coexpression (Fig. 7B). To evaluate potential changes in h-αS nitration, tissue sections of the MO were processed for 3-NT/h-αS PLA. Microscopic examination revealed that the number of PLA-specific chromogenic dots was reduced in the DMnX of CNO-treated as compared to saline-treated mice (Fig. 7C). Similarly, when the number of these PLA dots was estimated by unbiased stereological counting, a significant decrease in h-αS nitration was seen after CNO administration (Fig. 7D). Coronal tissue sections of the pons, caudal and rostral midbrain, and forebrain were then immunostained with anti–h-αS, and the presence of h-αS–positive axons was evaluated in these samples as evidence of caudo-rostral protein spreading. As shown in Fig. 7E, axonal counts yielded numbers that were consistently lower in all regions of the brain of CNO-injected animals, indicating that caudo-rostral protein spreading was attenuated as a result of neuronal hypoactivity targeted to the DMnX-MO. Thus, hypoactivity was associated with effects that were the opposite of those seen after induction of hyperactivity, further supporting a relationship between neuronal activity, ROS/RNS production, and h-αS spreading.

Enhanced SOD2 expression reversed hyperactivity-induced h-αS spreading

The next set of experiments was aimed at directly testing the role of oxidant stress as a mechanism underlying hyperactivity-induced h-αS spreading. More specifically, these experiments were designed to determine whether enhanced expression of the superoxide scavenging enzyme SOD2 would be effective in counteracting ROS/RNS accumulation and thus preventing h-αS transfer from hyperactive neurons. To achieve the expression of h-αS, activity-inducing DREADD and SOD2, a group of iR26-αS mice (SOD2 group) received a single injection of a solution containing three different viral vectors into the left vagus nerve; Cre- and hM3D^{fl}-AAVs were injected together

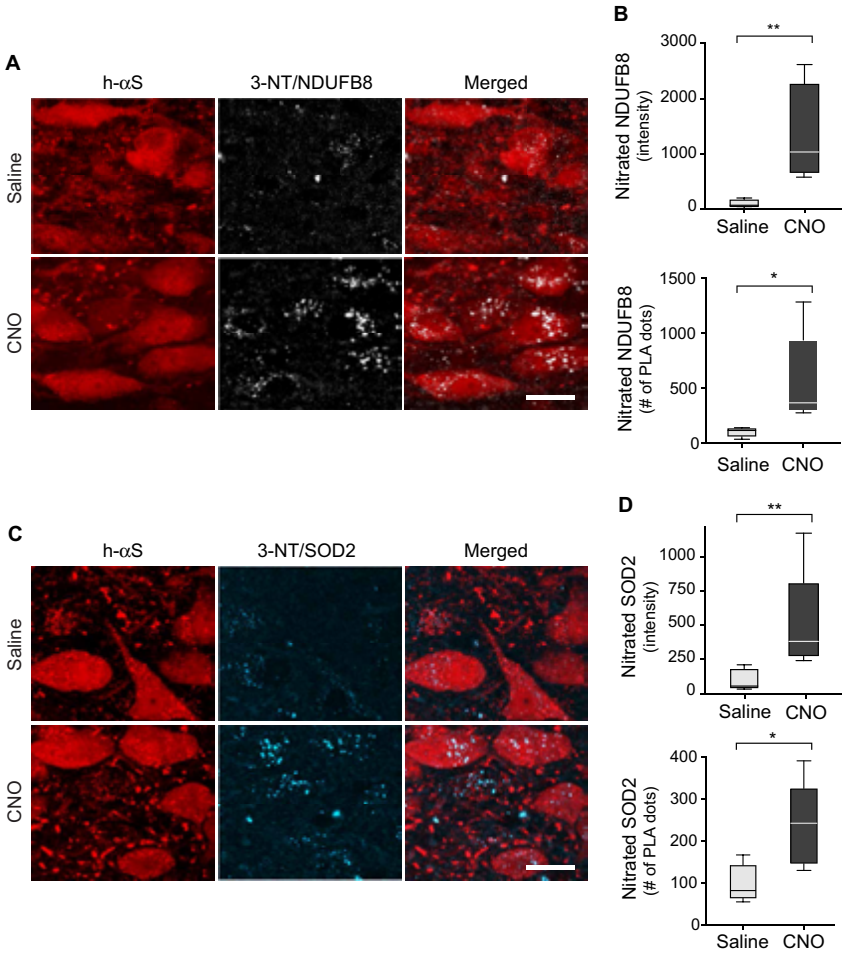

Fig. 5. Mitochondrial nitrative damage within hyperactive h-αS–loaded neurons. (**A** to **D**) iR26-αS mice were injected intravagally with a solution containing Cre- and hM3D^{fl}-AAVs, treated with either saline ($n = 5$) or CNO ($n = 5$) during weeks 4 and 5, and sacrificed at 5 weeks after AAV injection. To detect nitrated NDUFB8 (A and B) or nitrated SOD2 (C and D), sections of the MO were processed for either 3-NT/NDUFB8 or 3-NT/SOD2 PLA. They were also labeled with anti–h-αS. Representative confocal images show fluorescent PLA dots within h-αS–immunoreactive DMnX neurons. Scale bars, 20 μm (A and C). Fluorescent intensity and number of PLA dots were measured within h-αS–positive DMnX neurons. Approximately 15 neurons per animal were analyzed, and for each animal, intensity values and PLA counts were averaged. Data were then calculated as percentage of the mean value in the saline group (B and D). Box and whisker plots show median, upper and lower quartiles, and maximum and minimum as whiskers. *$P < 0.05$ and **$P < 0.01$.

with AAVs carrying human SOD2 DNA under the control of the CAG promoter (Fig. 8A). A separate group of animals (control group) also received an intravagal injection of a cocktail of three viral vectors consisting of Cre- and hM3D^{fl}-AAVs together with empty AAVs lacking protein coding sequence (Fig. 8A). Mice in the control and SOD2 groups were further divided into two experimental groups and treated with either saline or CNO. Daily saline/CNO administrations were carried out during weeks 4 and 5 after vagal AAV injection; animals were then sacrificed at the end of week 5.

Initial analyses were carried out to assess transgene expression and to verify CNO-induced hyperactivity. Levels of exogenous h-αS, endogenous mouse αS, and total αS (human plus mouse) mRNAs were analyzed by quantitative real-time PCR (qPCR) and compared in the dorsal MO of control versus SOD2 mice. Data showed comparable αS (exogenous, endogenous, or total) expression between the two experimental groups (Fig. 8B). Immunohistochemistry was carried out to assess expression of h-αS and hM3D proteins in medullary sections that were stained with either anti–h-αS or anti-RFP. Microscopic examination and densitometric analysis of the stained sections showed comparable h-αS or RFP immunoreactivity in samples from control and SOD2 mice; either of the two proteins was specifically expressed in the DMnX-MO, consistent with targeted Cre and hM3D transduction after AAV vagal administration (Fig. 8, C and D). Coexpression was further evaluated in medullary tissue sections triple-stained with anti–h-αS, anti-RFP, and anti-SOD2. Coimmunoreactivity for h-αS and hM3D, but not SOD2, was observed in samples from

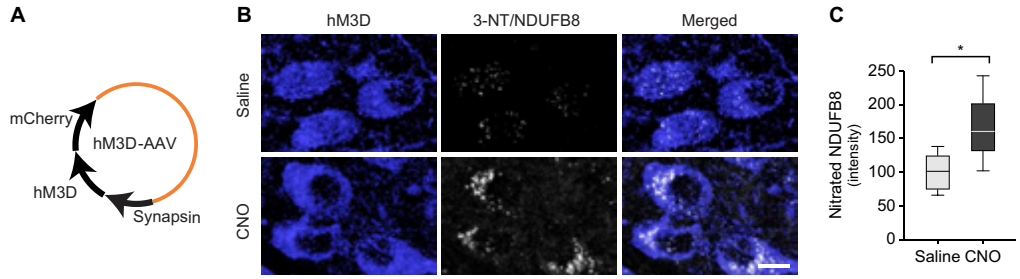

Fig. 6. Nitration of mitochondrial NDUFB8 during neuronal hyperactivity in the absence of h-αS overexpression. (**A**) iR26-αS mice were injected with AAVs delivering (nonfloxed) hM3D fused with mCherry under control of the human synapsin promoter. (**B** and **C**) Mice received an intravagal injection of hM3D-AAVs and were then treated with daily injections of either saline ($n = 5$, gray bar) or CNO ($n = 5$, black bar) during weeks 4 and 5 after AAV injection. They were then sacrificed at the end of week 5. Medullary tissue sections were processed for fluorescent microscopy and double-labeled with 3-NT/NDUFB8 PLA and anti-RFP (for the detection of mCherry-tagged hM3D). Representative confocal images show fluorescent PLA dots within hM3D/RFP-positive DMnX neurons. Scale bar, 10 μm (B). Fluorescent intensity was measured within hM3D/RFP-positive DMnX neurons. Approximately 40 neurons per animal were analyzed, and for each animal, intensity values were averaged and calculated as percentage of the mean value in the saline group. Box and whisker plots show median, upper and lower quartiles, and maximum and minimum as whiskers. *$P < 0.05$ (C).

control mice, whereas coexpression of h-αS, hM3D, and SOD2 was evident within DMnX neurons from SOD2 animals (Fig. 8E). The effectiveness of hM3D stimulation and consequent induction of hyperactivity was assayed in medullary tissue sections stained with anti–c-fos. Comparative analyses were done in samples from control and SOD2 mice treated with saline or CNO. Data showed a marked increase in DMnX c-fos expression in all samples from CNO-treated animals, indicating robust and comparable hM3D stimulation and neuronal hyperactivity regardless of whether vagal injections with Cre- and hM3D^{fl}-AAVs were associated with coadministration of empty or SOD2-carrying viral vectors (Fig. 8F).

Formation and accumulation of nitrated proteins were compared during hyperactivity in the absence or presence of human SOD2 expression. Medullary tissue sections were processed for 3-NT/NDUFB8 or 3-NT/h-αS PLA and analyzed using fluorescent or bright-field detection. In the DMnX of control mice, PLA signals for nitrated NDUFB8 and nitrated h-αS were noticeably affected by hM3D stimulation; microscopic observation (Fig. 9, A and D), measurement of fluorescent intensity (Fig. 9B), and count of PLA dots (Fig. 9, C and E) all revealed CNO-induced increases in neuronal labeling. These findings sharply contrasted to the results in SOD2 animals in which levels of NDUFB8 and h-αS nitration remained unchanged after CNO administration (Fig. 9, A to E). In a parallel set of analyses, h-αS nitration was also compared in tissue sections of the pons from control and SOD2 mice with or without CNO treatment. Samples were processed for 3-NT/h-αS PLA with bright-field detection, and the number of chromogenic PLA dots was counted using unbiased stereology. PLA counts were found to be significantly increased in pontine sections from control animals injected with CNO. They were instead quite similar in samples from the SOD2 treatment group after administration of either saline or CNO (Fig. 9F).

Caudo-rostral h-αS spreading was finally evaluated in the pons, midbrain, and forebrain of saline- and CNO-injected control and SOD2 mice. Coronal brain sections were stained with anti–h-αS, and the number, length, and density of h-αS–immunoreactive axons were compared under these different experimental conditions. Axonal counts were significantly higher in all brain sections from control animals injected with CNO, whereas CNO administration had no effect on the number of h-αS–positive axons in samples from SOD2 mice (Fig. 9G). Moreover, measurements of length and density of h-αS–loaded axons in pontine sections yielded values that were significantly increased after hM3D stimulation in control but not SOD2 animals (Fig. 9, H and I). Together, these data provided direct evidence of a protective effect of ROS scavenging against h-αS spreading and thus indicated a key role of ROS and RNS accumulation in promoting the transfer of h-αS from hyperactive neurons.

Hyperactivity promoted h-αS aggregation, and this effect was reversed by SOD2 expression

Enhanced neuronal activity has been reported to promote αS aggregation (*21*). Earlier studies also indicate that the tendency of αS to aggregate may be exacerbated by oxidant stress (*27*, *47*–*49*). Whether a relationship exists between neuronal activity, oxidant stress, and protein aggregation remains elusive, however. Here, a series of experiments were designed to address this question and to assess h-αS aggregation in the absence and presence of neuronal stimulation as well as in the absence and presence of SOD2 expression. First, iR26-αS mice were injected with Cre-/hM3D^{fl}-AAVs, treated with saline or CNO for 2 weeks (weeks 4 and 5 after AAV treatment), and sacrificed at the end of week 5. Protein aggregation was assayed using a conformation-specific antibody, Syn-O2, capable of detecting aggregated but not monomeric αS (*27*, *40*, *50*). Further analyses were carried out using a PLA protocol (h-αS/h-αS PLA) well characterized in human and mouse brain specimens; this protocol allows the detection of aggregated and, in particular, oligomeric forms of the protein with a high degree of sensitivity and specificity (*27*, *40*, *51*). Results were similar in medullary tissue sections stained with Syn-O2 or processed for h-αS/h-αS PLA since, with both assays, enhanced protein aggregation was detected in samples from CNO-treated as compared to saline-treated mice (Fig. 10, A and B). When sections from saline-injected animals were double-stained for h-αS and Syn-O2 fluorescence, Syn-O2 immunoreactivity predominantly labeled neuritic projections and terminals (Fig. 10A). Quite in contrast, Syn-O2 staining was obviously present not only within neurites but also within DMnX cell bodies in sections from CNO-treated mice; quantification of signal intensity within h-αS–expressing neurons yielded significantly higher values after hM3D stimulation (Fig. 10, A and C). Signal quantification was also carried out in the DMnX of PLA-processed

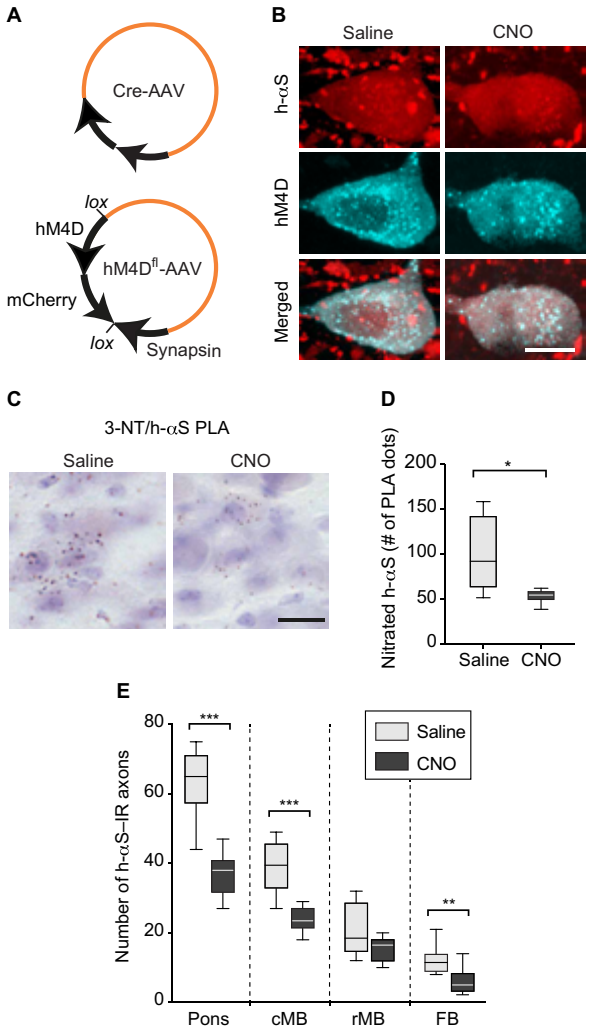

Fig. 7. Caudo-rostral h-αS spreading is reduced after suppression of neuronal activity. (**A**) iR26-αS mice were injected with Cre-AAVs together with AAVs designed to express Gi-coupled hM4D DREADD fused with mCherry under control of the human synapsin promoter; conditional expression was achieved using a DIO system (hM4D^{fl}-AAVs). (**B**) Mice received an injection of Cre- and hM4D^{fl}-AAVs and were then treated with daily injections of either saline or CNO during weeks 4 and 5 after AAV treatment. They were then sacrificed at the end of week 5. Medullary sections were double-labeled with anti–h-αS and anti-RFP and processed for confocal microscopy. Scale bar, 10 μm. (**C** and **D**) Mice were injected with Cre- and hM3D^{fl}-AAVs and received either saline ($n = 6$) or CNO ($n = 6$). Tissue sections of the MO were processed for 3-NT/h-αS PLA and counterstained with Nissl; representative images show specific chromogenic PLA dots in the left DMnX. Scale bar, 20 μm (C). For each mouse, the number of PLA dots was stereologically counted in the left DMnX; data were calculated as percentage of the mean value in the saline group (D). (**E**) Mice received an injection of Cre- and hM4D^{fl}-AAVs and were then treated with either saline ($n = 8$) or CNO ($n = 10$). Tissue sections throughout the brain were immunostained with anti–h-αS, and the number of h-αS–immunoreactive axons was counted in predefined tissue sections of the left pons, caudal midbrain, rostral midbrain, and forebrain. Box and whisker plots show median, upper and lower quartiles, and maximum and minimum as whiskers. *$P < 0.05$, **$P < 0.01$, and ***$P < 0.001$.

samples; increased counts of h-αS/h-αS PLA dots in sections from CNO-injected mice provided additional evidence of enhanced aggregation after neuronal stimulation (Fig. 10D).

To investigate the involvement of oxidant stress in hyperactivity-induced h-αS assembly, iR26-αS mice received an intravagal cocktail injection of either Cre-, hM3D^{fl}-, and empty-AAVs (control mice) or Cre-, hM3D^{fl}-, and SOD2-AAVs (SOD2 mice). Both control and SOD2 mice were also treated with saline or CNO as described above. Medullary tissue sections from all these animals were processed for h-αS/h-αS PLA, and the number of chromogenic PLA dots was stereologically counted in the DMnX. Data revealed that dot counts were markedly increased after CNO administration in control mice; they remain unchanged, however, after hM3D stimulation in sections from SOD2 animals (Fig. 10E). Thus, oxidant stress during neuronal hyperactivity, as documented in this study, played an important role in promoting h-αS aggregation that could be counteracted by boosting intraneuronal ROS scavenging.

DISCUSSION

The vagus nerve can be used as a conduit for delivering viral vectors to the brain (*27*, *31*, *39*, *40*, *52*). In this study, Cre/*loxP* conditional h-αS knock-in mice received an intravagal injection of Cre-AAVs to achieve stable expression of h-αS driven by the endogenous Rosa26 promoter. AAV-induced transduction targeted vagus-associated neurons and remained strictly confined to areas of the MO that are occupied by efferent (the DMnX) and afferent (the NTS) vagal neurons. This anatomical restriction was confirmed by detection of Cre recombinase mRNA in the DMnX-MO but not in other higher brain regions and is in line with the results of earlier investigations in rats and mice injected with viral vectors into the vagus nerve (*39*, *40*). Expression of h-αS protein was also initially restricted to the dorsal MO. Starting a few weeks later, however, neuron-to-neuron protein transfer was indicated by the detection of h-αS in brain regions outside the MO. Overexpressing cells in the DMnX and/or overexpressing afferent projections in the NTS could conceivably act as donor neurons and sources of the spreading protein. However, it is noteworthy that, while a contribution of NTS nerve terminals, albeit possible, warrants further investigation, several lines of evidence are consistent with an important role played by DMnX neurons in h-αS transfer. Earlier studies demonstrated, for example, that caudo-rostral protein spreading triggered by overexpression of h-αS in the dorsal MO was strictly contingent upon the integrity and viability of DMnX neurons; partial or complete loss of these cells resulted in reduction or cessation, respectively, of h-αS advancement (*52*, *53*).

The initial step of the spreading process involved the passage of h-αS between overexpressing donor neurons and recipient axons innervating the dorsal MO and connecting it to higher brain regions. Following this transfer, retrograde protein spreading through axonal projections resulted in a progressive accumulation of h-αS first in pontine, then in midbrain, and finally in forebrain sites. Brain regions with strong, direct connections to the dorsal MO, such as the locus coeruleus, dorsal raphae, hypothalamus, and amygdala, were primarily affected by this secondary (i.e., posttransfer) h-αS burden, supporting a transfer mechanism that involves anatomically interconnected neurons (*54*, *55*). A feature of h-αS pathology in areas affected by the spreading process was the presence of an increasing number of dystrophic axons loaded with the exogenous protein. This observation of axonal burden, which contrasted with the apparent

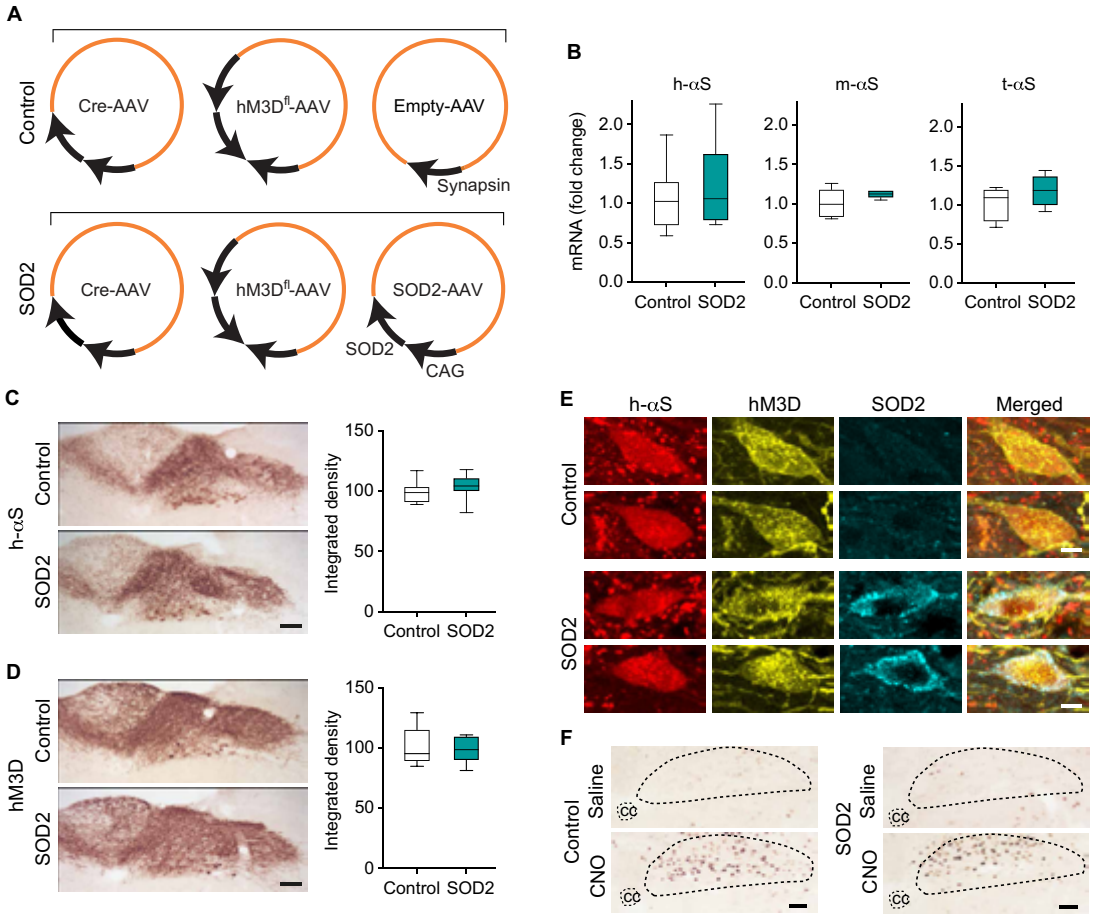

Fig. 8. H-αS, hM3D, and SOD2 are coexpressed after AAV-induced transduction. (**A**) iR26-αS mice were coinjected with Cre- and hM3D^{fl}-AAVs together with either empty AAVs or AAVs delivering human SOD2 under control of the CAG promoter. (**B**) Mice treated with Cre-, hM3D^{fl}-, and empty-AAVs (control mice, $n = 8$) and animals treated with Cre-, hM3D^{fl}-, and SOD2-AAVs (SOD2 mice, $n = 6$) were sacrificed at 5 weeks after AAV injection. Levels of h-αS, mouse αS (m-αS), total (human + mouse) αS (t-αS), and, as housekeeping control, Hprt mRNAs were measured in the left DMnX-MO by qPCR. (**C** and **D**) Coronal sections of the MO from control ($n = 10$) and SOD2 ($n = 10$) mice were immunostained with either anti–h-αS or anti-RFP (for detection of mCherry-tagged hM3D). Representative images show robust immunoreactivity of either protein in the DMnX-MO. Scale bars, 100 μm. Integrated density measurements were performed in the left (injected side) DMnX; data were calculated as percentage of the mean value in the control group. (**E**) Coronal sections of the MO were triple-labeled with anti–h-αS, anti-RFP, and anti-SOD2. Colocalization of h-αS and hM3D was seen in DMnX neurons from control mice, whereas all three proteins were coexpressed within DMnX neurons of SOD2 animals; representative images of two cells from a control mouse (top two rows) and two neurons from an SOD2 animal (bottom rows). Scale bars, 10 μm. (**F**) Control and SOD2 animals were treated with daily injections of saline or CNO during weeks 4 and 5 after AAV injection. They were then sacrificed at the end of week 5. Medullary tissue sections were labeled with anti–c-fos; representative images show an area of the dorsal MO where the central canal and DMnX are delineated with dashed lines. Scale bars, 100 μm. Box and whisker plots show median, upper and lower quartiles, and maximum and minimum as whiskers.

lack of h-αS buildup within neuronal cell bodies, supports the notion that neuronal projections represent earlier and more vulnerable targets of αS accumulation and pathology (*56*–*58*). Crowding and aggregation of h-αS within nerve fibers may promote axonal pathology but, at the same time, limit protein flow and reduce access of h-αS into neuronal perikarya. Furthermore, as discussed below, a dying-back process triggered by axonal injury during h-αS spreading may lead to cell degeneration before and in the absence of overt h-αS accumulation within neuronal cell bodies (*52*).

To induce h-αS expression and, at the same time, stimulate or inhibit neuronal activity, Cre-AAVs were co-administered with either hM3D^{fl}- or hM4D^{fl}-AAVs into the vagus nerve of iR26-αS mice. DREADD-induced hyper- or hypoactivity had a significant effect on h-αS spreading; upward protein advancement was markedly enhanced after expression and stimulation of hM3D, an excitatory DREADD, whereas expression and stimulation of the inhibitory receptor hM4D were associated with reduced accumulation of h-αS in brain regions rostral to the MO. Together, these findings provide

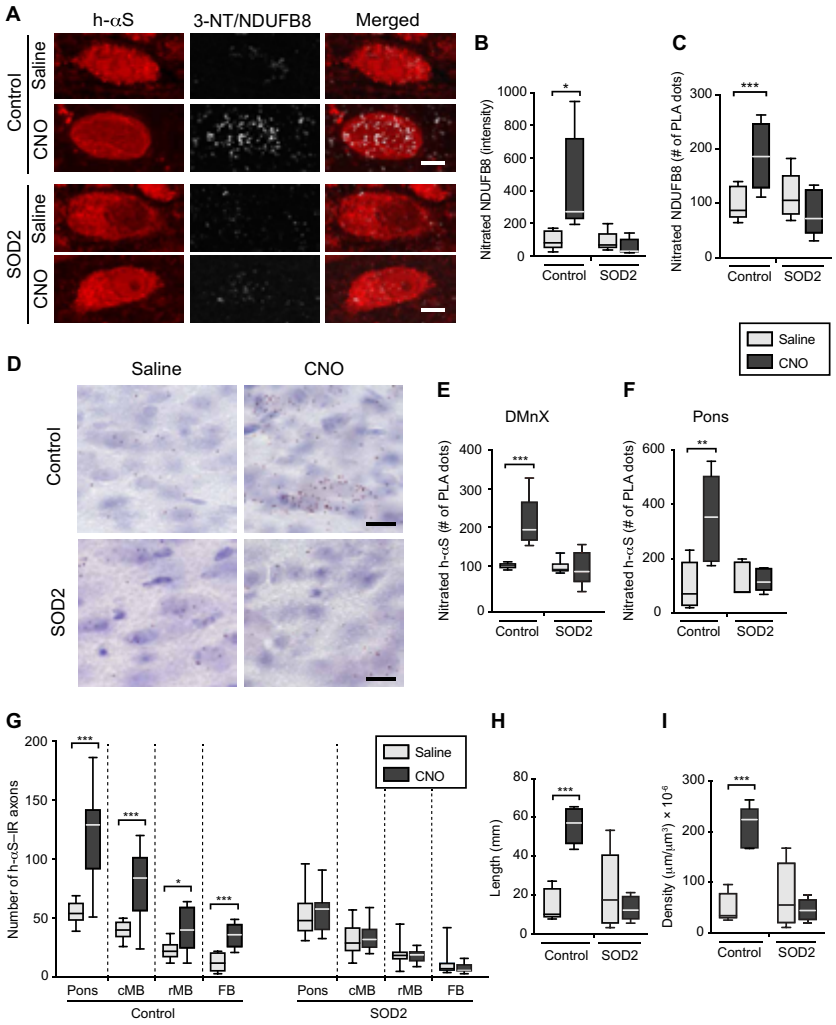

Fig. 9. SOD2 overexpression prevents protein nitration and h-αS spreading during neuronal hyperactivity. Mice were coinjected with Cre-, hM3D^{fl}-, and empty-AAVs (control mice) or Cre-, hM3D^{fl}-, and SOD2-AAVs (SOD2 animals). Animals were also treated with saline (gray) or CNO (black). (**A** to **C**) Mice were divided into four groups: control/saline ($n = 5$), control/CNO ($n = 5$), SOD2/saline ($n = 5$), and SOD2/CNO ($n = 5$). Sections of the MO were processed for 3-NT/NDUFB8 PLA and also labeled with anti–h-αS. Images show DMnX neurons. Scale bars, 10 μm (A). Fluorescent intensity and number of PLA dots were measured within h-αS–positive DMnX neurons; 10 to 15 neurons per animal were analyzed, and for each animal, intensity values and PLA counts were averaged. Data are expressed as percentage of the mean value in the corresponding saline-injected group (B and C). (**D** to **F**) Four groups ($n \geq 5$ per group) of mice were treated as above. To detect nitrated h-αS, sections of the MO and pons were processed for 3-NT/h-αS PLA and counterstained with Nissl. PLA dots are shown in the left DMnX. Scale bars, 50 μm (D). For each animal, the number of PLA dots was counted in the left DMnX (E) and in left pontine sections (F); data were calculated as percentage of the mean value in the corresponding saline-injected group. (**G**) Four groups ($n \geq 7$ per group) of mice were treated as above. The number of h-αS–immunoreactive axons was counted in sections of the left pons, caudal midbrain, rostral midbrain, and forebrain immunostained with anti–h-αS. (**H** and **I**) The length (H) and density (I) of h-αS–immunoreactive axons were measured in the pons ($n = 5$ per group). Plots show median, upper and lower quartiles, and maximum and minimum as whiskers. *$P < 0.05$, **$P < 0.01$, and ***$P < 0.001$.

compelling evidence that neuronal activity affects neuron-to-neuron transfer of h-αS and, by doing so, is able to promote or attenuate protein spreading throughout the brain. It is noteworthy that these findings were obtained under pathophysiological conditions (enhanced αS expression) and mimicked pathological features (progressive caudo-rostral diffusion of αS lesions and αS-induced axonal injury) of likely relevance to PD (*2*, *3*, *56*, *59*–*61*). Under these conditions, neuronal activity could play an important pathogenetic role; it could, for example, modulate the extent and severity of αS burden, affect the exchange of toxic αS species, and/or render specific neuronal populations more or less susceptible to protein exchange and accumulation. Protein spreading, once triggered by enhanced h-αS expression within medullary neurons, has been shown to cause neurodegeneration and a pronounced tissue inflammatory

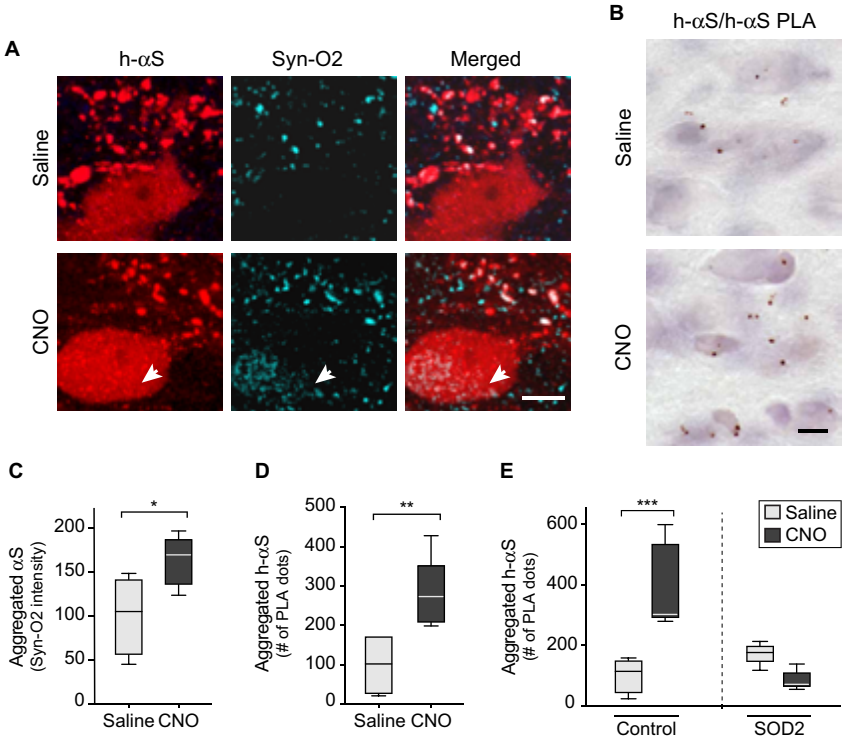

Fig. 10. SOD2 overexpression prevents hyperactivity-induced h-αS aggregation. (**A** and **B**) Mice received an injection of a solution containing Cre- and hM3D^{fl}-AAVs into the left vagus nerve. They were then divided into two groups and treated with saline or CNO. Medullary sections from mice treated with saline ($n = 4$) or CNO ($n = 5$) were double-stained with anti–h-αS and Syn-O2, an antibody recognizing aggregated αS forms. Images show neurites and cell bodies in the left DMnX; the arrow indicates a cell body colabeled for h-αS and Syn-O2. Scale bar, 10 μm (A). Sections of the MO from mice treated with saline ($n = 5$) or CNO ($n = 5$) were processed for h-αS/h-αS PLA. Images show PLA dots in the left DMnX. Scale bar, 20 μm (B). (**C**) Analysis of sections stained with anti–h-αS and Syn-O2. Syn-O2 fluorescent intensity was measured within h-αS–positive DMnX neurons; an average of 30 neurons per animal was analyzed. Cell intensity values were averaged for each animal, and data were calculated as percentage of the mean value in the saline-injected group. (**D**) Analysis of sections processed for h-αS/h-αS PLA. For each mouse, the number of PLA dots was counted in the left DMnX; data were calculated as percentage of the mean value in the corresponding saline group (D). (**E**) Mice were coinjected with Cre-, hM3D^{fl}-, and empty-AAVs (control mice) or Cre-, hM3D^{fl}-, and SOD2-AAVs (SOD2 animals). Animals were also treated with saline or CNO. Sections of the MO from control/saline ($n = 5$), control/CNO ($n = 5$), SOD2/saline ($n = 5$), and SOD2/CNO ($n = 5$) mice were processed for h-αS/h-αS PLA. The number of PLA dots was counted in the left DMnX; data were calculated as percentage of the mean value in the corresponding saline-injected group. Plots show median, upper and lower quartiles, and maximum and minimum as whiskers. *$P < 0.05$, **$P < 0.01$, and ***$P < 0.001$.

response in higher brain regions affected by spreading-induced h-αS accumulation; these effects were observed at 3, 6, and 12 months after the initial protein transfer event (*52*). Thus, neuronal h-αS burden associated with caudo-rostral protein spreading bears significant and long-lasting pathophysiological consequences that could be exacerbated or lessened by hyper- or hypoactivity, respectively.

A key finding of this study was the demonstration of a relationship between neuronal activity and oxidant stress, which led us to interrogate the role of oxidant stress in hyperactivity-induced h-αS spreading. A higher rate of superoxide formation was detected in the form of ox-DHE accumulation within hyperactive DMnX neurons. Further evidence of hyperactivity-induced oxidative reactions was then obtained from analyses of intraneuronal proteins carrying nitrative modifications. In particular, we evaluated and quantified activity-dependent changes in nitrated h-αS, NDUFB8, and SOD2. During oxidant stress, reaction of superoxide with nitric oxide can generate highly unstable peroxynitrite anions that can in turn react with tyrosine residues of proteins (*46*). Oxidative/nitrative reactions have long been known to modify αS in the human brain. In PD and other human synucleinopathies, Lewy inclusions are robustly labeled with antibodies that react against nitrated αS or recognize 3-NT–modified protein residues, underscoring the relevance that any condition capable of affecting αS nitration may have from the pathophysiological standpoint (*62*, *63*). We report here that enhanced production of 3-NT–modified h-αS occurred after neuronal expression and stimulation of hM3D in vivo. On the other hand, hypoactivity that was induced by expression of hM4D and treatment with CNO lowered the intraneuronal burden of nitrated h-αS. Together, these findings indicate a direct relationship between neuronal activity, oxidant stress, and protein nitration and point to neuronal activity as a potential modulator of pathogenetic processes involving nitrated h-αS accumulation.

Mitochondria could conceivably play an important role as sources of increased ROS production during neuronal hyperactivity due to higher energy demand, stimulation of OXPHOS, enhanced leakage

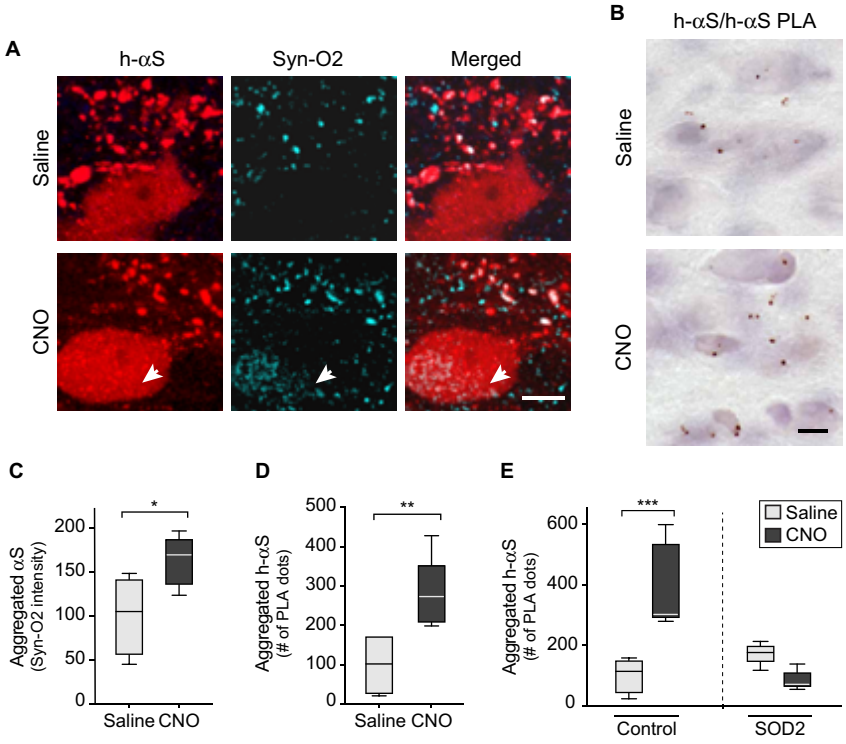

Fig. 10. SOD2 overexpression prevents hyperactivity-induced h-αS aggregation. (**A** and **B**) Mice received an injection of a solution containing Cre- and hM3D^{fl}-AAVs into the left vagus nerve. They were then divided into two groups and treated with saline or CNO. Medullary sections from mice treated with saline ($n = 4$) or CNO ($n = 5$) were double-stained with anti–h-αS and Syn-O2, an antibody recognizing aggregated αS forms. Images show neurites and cell bodies in the left DMnX; the arrow indicates a cell body colabeled for h-αS and Syn-O2. Scale bar, 10 μm (A). Sections of the MO from mice treated with saline ($n = 5$) or CNO ($n = 5$) were processed for h-αS/h-αS PLA. Images show PLA dots in the left DMnX. Scale bar, 20 μm (B). (**C**) Analysis of sections stained with anti–h-αS and Syn-O2. Syn-O2 fluorescent intensity was measured within h-αS–positive DMnX neurons; an average of 30 neurons per animal was analyzed. Cell intensity values were averaged for each animal, and data were calculated as percentage of the mean value in the saline-injected group. (**D**) Analysis of sections processed for h-αS/h-αS PLA. For each mouse, the number of PLA dots was counted in the left DMnX; data were calculated as percentage of the mean value in the corresponding saline group (D). (**E**) Mice were coinjected with Cre-, hM3D^{fl}-, and empty-AAVs (control mice) or Cre-, hM3D^{fl}-, and SOD2-AAVs (SOD2 animals). Animals were also treated with saline or CNO. Sections of the MO from control/saline ($n = 5$), control/CNO ($n = 5$), SOD2/saline ($n = 5$), and SOD2/CNO ($n = 5$) mice were processed for h-αS/h-αS PLA. The number of PLA dots was counted in the left DMnX; data were calculated as percentage of the mean value in the corresponding saline-injected group. Plots show median, upper and lower quartiles, and maximum and minimum as whiskers. *$P < 0.05$, **$P < 0.01$, and ***$P < 0.001$.

response in higher brain regions affected by spreading-induced h-αS accumulation; these effects were observed at 3, 6, and 12 months after the initial protein transfer event (*52*). Thus, neuronal h-αS burden associated with caudo-rostral protein spreading bears significant and long-lasting pathophysiological consequences that could be exacerbated or lessened by hyper- or hypoactivity, respectively.

A key finding of this study was the demonstration of a relationship between neuronal activity and oxidant stress, which led us to interrogate the role of oxidant stress in hyperactivity-induced h-αS spreading. A higher rate of superoxide formation was detected in the form of ox-DHE accumulation within hyperactive DMnX neurons. Further evidence of hyperactivity-induced oxidative reactions was then obtained from analyses of intraneuronal proteins carrying nitrative modifications. In particular, we evaluated and quantified activity-dependent changes in nitrated h-αS, NDUFB8, and SOD2. During oxidant stress, reaction of superoxide with nitric oxide can generate highly unstable peroxynitrite anions that can in turn react with tyrosine residues of proteins (*46*). Oxidative/nitrative reactions have long been known to modify αS in the human brain. In PD and other human synucleinopathies, Lewy inclusions are robustly labeled with antibodies that react against nitrated αS or recognize 3-NT–modified protein residues, underscoring the relevance that any condition capable of affecting αS nitration may have from the pathophysiological standpoint (*62*, *63*). We report here that enhanced production of 3-NT–modified h-αS occurred after neuronal expression and stimulation of hM3D in vivo. On the other hand, hypoactivity that was induced by expression of hM4D and treatment with CNO lowered the intraneuronal burden of nitrated h-αS. Together, these findings indicate a direct relationship between neuronal activity, oxidant stress, and protein nitration and point to neuronal activity as a potential modulator of pathogenetic processes involving nitrated h-αS accumulation.

Mitochondria could conceivably play an important role as sources of increased ROS production during neuronal hyperactivity due to higher energy demand, stimulation of OXPHOS, enhanced leakage

of electrons from the ETC, and consequent reduction of molecular oxygen to superoxide (*24*, *25*). Our data support this possibility and provide intriguing evidence of ROS- and RNS-induced mitochondrial damage during neuronal hyperactivity. Being close to sites of superoxide generation, mitochondrial proteins are highly susceptible to oxidative modifications (*64*). It is also noteworthy that a mitochondrial form of nitric oxide synthase (mitoNOS) could significantly contribute to mitochondrial protein nitration. This mitoNOS is stimulated by calcium influx into mitochondria, and its activity has been proposed to generate larger amounts of NO in neurons with calcium-dependent autonomous pacemaking, including DMnX neurons (*30*, *65*). In our study, increased production of ROS and RNS and pronounced nitration of mitochondrial proteins were indicated by an accumulation of nitrated NDUFB8 and SOD2 and represented an important feature of neuronal hyperactivity. The NDUFB8 subunit is central to complex I assembly, stability, and function that could be severely affected by nitrative reactions (*66*, *67*). Similarly, peroxynitrite-dependent nitration of SOD2 leads to enzyme inactivation (*68*, *69*). Thus, accumulation of these nitrated proteins during neuronal hyperactivity could ultimately set off a self-amplifying toxic loop: superoxide and nitric oxide react together to generate the nitrated proteins, and this nitration may in turn exacerbate superoxide leakage from the ETC (via complex I inhibition) while impairing mitochondrial ROS scavenging (via SOD2 inactivation). Hyperactivity-induced mitochondrial protein nitration (in particular, NDUFB8 nitration) was observed not only in brain tissue from iR26-αS mice coinjected with Cre- and hM3D^{fl}-AAVs but also in samples from animals treated with non–Cre-dependent hM3D-AAVs. These findings indicate that hyperactivity itself is capable of promoting mitochondrial nitrative reactions and that overexpression of h-αS is not a necessary requirement for the protein-modifying effect of neuronal stimulation to become overt. It is noteworthy, however, that, although hyperactivity-induced mitochondrial protein nitration may occur in the absence or presence of h-αS accumulation, the toxic consequences of these nitrative modifications are likely to be more severe within h-αS–loaded neurons. This worsening effect may arise, for example, from direct interactions between αS and mitochondria that could exacerbate mitochondrial dysfunction within hyperactive neurons and, together with oxidative/nitrative reactions, ultimately contribute to neuronal injury (*70*, *71*).

Increased superoxide production and enhanced protein nitration indicated the occurrence of oxidant stress within hyperactive neurons and raised interesting pathophysiological scenarios. These findings did not specifically demonstrate, however, that oxidant stress was a primary mechanism responsible for hyperactivity-induced h-αS spreading. Rescue experiments were therefore designed to determine whether this interneuronal protein transfer could be counteracted by preventing ROS/RNS accumulation. We also aimed at further evaluating the relationship between hyperactivity, ROS production, and mitochondrial damage, and for this reason, the strategy for these experiments was to enhance neuronal expression of the mitochondrial superoxide scavenging enzyme SOD2. SOD2 transduction was achieved together with h-αS and hM3D expression via vagal coadministration of Cre-, hM3D^{fl}-, and SOD2-AAVs. Transgene tissue expression and cellular protein colocalization were carefully verified to confirm efficacy and reliability of this triple-treatment paradigm. Proper assessment of the effects of human SOD2 expression was also ensured by comparing data in the group of animals injected with Cre-, hM3D^{fl}-, and SOD2-AAVs (SOD2 mice) versus another group of mice that received Cre- and hM3D^{fl}-AAVs together with empty vectors (control mice). Stimulation of hM3D receptors by CNO treatment caused neuronal hyperactivity in both control and SOD2 mice. The consequences of this hyperactivity were markedly different, however, between these two groups of animals. In control mice, hM3D stimulation was associated with oxidant stress and enhanced h-αS spreading. Quite in contrast, levels of nitrated h-αS and nitrated NDUFB8 remained unchanged despite CNO-induced hyperactivity in SOD2 animals; similarly, hyperactivity had no significant effect on h-αS transfer in the presence of human SOD2 expression. Thus, ROS scavenging by SOD2 protected against the pro-oxidant and nitrative effects of neuronal stimulation and, at the same time, was sufficient to completely prevent hyperactivity-induced h-αS spreading. An important additional finding obtained from these experiments concerns the relationship between neuronal hyperactivity, oxidant stress, and protein aggregation. While stimulation of hM3D receptors in control mice resulted in enhanced h-αS assembly, the same treatment had no effect on protein aggregation in neurons with increased SOD2 expression. Data therefore indicate that oxidant stress not only exacerbates activity-dependent protein spreading but also mediates, at least in part, the development of aggregate pathology within hyperactive neurons.

Different h-αS species, including posttranslationally modified forms of the protein, are likely to have distinct interneuronal mobility and therefore play a more or less pronounced role in spreading processes. On the basis of these premises, accumulation of 3-NT–modified h-αS, as seen in this study, warrants careful evaluation and bears significant implications. Here, we found that nitrated h-αS, detected by 3-NT/h-αS PLA, was present within donor neurons in the DMnX-MO as well as recipient axons in the pons. During neuronal hyperactivity, enhanced protein spreading was associated with increased levels of 3-NT–modified h-αS in the DMnX-MO and pons. Quite in contrast, both h-αS transfer and levels of nitrated h-αS were significantly lowered as a result of neuronal hypoactivity. Last, when SOD2 expression counteracted hyperactivity-induced oxidant stress, decreased h-αS transfer was paralleled by a reduction of nitrated protein within both medullary and pontine neurons. Together, these findings underscore a strict relationship between neuronal activity, oxidant stress, nitrated h-αS burden, and protein spreading. They also suggest that detection of 3-NT–modified αS not only is a marker of oxidant stress but also may characterize neurons that, under pro-oxidant conditions such as those triggered by hyperactivity, become more active sites of h-αS transfer. Another, not mutually exclusive interpretation of our present results is suggested by data of an earlier investigation, showing that nitrative modifications may generate h-αS species with greater propensity to pass from cell to cell (*27*). Nitrated h-αS, with its high motility, could therefore directly participate in interneuronal protein exchanges, and its enhanced formation during neuronal hyperactivity could itself contribute to protein spreading exacerbation.

In summary, experimental evidence presented here reveals a mechanistic link between neuronal activity, oxidant stress, and αS pathology in the form of protein spreading and aggregation. Our in vivo data also identify mitochondria as key targets of oxidant stress and likely sources of ROS/RNS production within hyperactive neurons. The feasibility of protective intervention against hyperactivity-induced αS pathology is demonstrated by the results of rescue experiments; these results show that protein spreading and aggregation can be effectively counteracted by enhancing neuronal ROS

scavenging capabilities. Last, evidence from this study underscores the significance of nitrated αS accumulation as a marker of neurons with greater susceptibility to αS transfer and supports a direct involvement of nitrated αS in the spreading process. Further work is warranted to develop and evaluate protective strategies aimed at counteracting nitrated αS burden; this targeted intervention may mitigate αS pathology during neuronal hyperactivity and under other pathophysiological conditions associated with oxidative/nitrative neuronal injury.

MATERIALS AND METHODS

Generation of iR26-αS mice

Wild-type human h-αS cDNA (pCR2.1-Topo-αS) was cloned into a Rosa26 targeting vector (PolyGene) downstream to a loxP-flanked neo/STOP cassette. The SacI-linearized vector was electroporated into C57Bl/6N-derived embryonic stem cells, and G418-resistant clones were isolated and screened for correct homologous recombination. Selected clones were injected into gray C57Bl/6 blastocysts, and blastocysts were transferred into CD-1 foster mice for the generation of chimeric animals. Chimeric mice were then bred to C57Bl/6N mice to pass the mutation through the germ line and to obtain homozygous transgenics on a C57Bl/6N background. The following mixture of three primers was used for genotyping purposes: 5′-GCTGTGCTCCACGTTGTCAC-3′, 5′-GGAAAGCTGGGCTTGCATCTC-3′, and 5′-GGAGCGGCGATACCGTAAAG-3′.

The reaction resulted in two bands: one band of 512 base pairs (bp), which indicated integration of the neomycin cassette, and a second band (control fragment) of 380 bp. Homozygous transgenics were viable and fertile. Maintenance and expansion of the colony were achieved through breeding of homozygous mating pairs. Homozygous animals were used for all experiments.

Viral vectors

All AAVs used in this study were generated using a backbone plasmid of AAV2-derived genome encapsulated into an AAV6 capsid. Most AAVs contained a woodchuck hepatitis virus posttranscriptional regulatory element (WPRE) and a polyadenylation signal sequence downstream to the promoter and transgene sequences. Cre-AAVs lacked the WPRE sequence, and empty-AAV had no transgene protein coding sequence. Production and titration of the AAVs were carried out by Vector Biolabs (hM3D-, $hM3D^{fl}$-, $hM4D^{fl}$-, SOD2-, and empty-AAVs) or Sirion Biotech (Cre-AAVs). High-titer stock AAV preparations were diluted with phosphate-buffered saline. Final titers were (i) 1×10^{12} gc/ml, 2×10^{12} gc/ml, or 4×10^{12} gc/ml for Cre-AAVs; (ii) 3×10^{12} gc/ml for hM3D-, $hM3D^{fl}$-, and $hM4D^{fl}$-AAVs; and (iii) 2×10^{12} gc/ml for SOD2- and empty-AAVs.

Animal procedures and tissue processing

Animal experiments were approved by the State Agency for Nature, Environment and Consumer Protection in North Rhine Westphalia, Germany. Experiments were conducted in female and male iR26-αS mice between 15 and 22 weeks of age. Animals were housed in individually ventilated cages, in a specific pathogen–free facility, and kept on a 12-hour light/dark cycle with ad libitum access to food and water. To induce expression of transgene(s) in the DMnX, a solution containing a single AAV preparation or multiple AAVs was injected into the left vagus nerve. Mice were anaesthetized with isoflurane, a small incision was made at the midline of the neck, and the left vagus nerve was isolated (*40*). The AAV-containing solution (800 nl) was injected at a flow rate of 350 nl/min using a 35-gauge blunt steel needle fitted onto a 10-μl NanoFil syringe. After injection, the needle was kept in place for one additional minute to avoid backflow. To stimulate DREADDs, CNO (Tocris) was administered intraperitoneally at a dose of 1 mg/kg dissolved in 0.9% saline. DHE (Abcam) was dissolved in saline/dimethyl sulfoxide (DMSO) (1:1 ratio) and injected intraperitoneally at a dose of 15 mg/kg. Animals were monitored daily throughout the duration of the experiments. No overt changes in body weight, basic motility, and general welfare were noticed as consequences of the surgical procedures or any of the experimental treatments. At the end of the experiments, mice were sacrificed with an injection of sodium pentobarbital (600 mg/kg) (intraperitoneally) and perfused through the ascending aorta with 4% (w/v) paraformaldehyde. Brains were removed and immersed in 4% paraformaldehyde for 24 hours before cryopreservation in 30% (w/v) sucrose. Subsequent analyses were carried out on coronal sections (35 μm) of the brain that were obtained using a freezing microtome.

Immunohistochemistry with bright-field detection and density analysis

For bright-field microscopy, free-floating sections were quenched by incubation in a mixture of 3% H_2O_2 and 10% methanol in tris-buffered saline (pH 7.6). Nonspecific binding sites were blocked by incubation in 5% normal serum. Samples were kept overnight at room temperature in a solution containing the primary antibody: rabbit anti–h-αS (1:50,000; ab138501, Abcam), rabbit anti-RFP (1:20,000; 600-401-379, Rockland), mouse anti–Cre recombinase (1:4000; MAB3120, Millipore), rabbit anti–c-fos (1:2000; 2250, Cell Signaling Technology), and rabbit anti-SOD2 (1:5000; ADI-SOD-110, Enzo Life Sciences). Sections were rinsed and incubated in biotinylated secondary antibody solution (1:200; Vector Laboratories). Following treatment with avidin-biotin–horseradish peroxidase complex (ABC Elite kit, Vector Laboratories), color reaction was developed using a 3,3′-diaminobenzidine kit with or without nickel (Vector Laboratories). Sections were mounted on coated slides, coverslipped with Depex (Sigma-Aldrich), and imaged using a Zeiss Observer.Z1 Microscope (Carl Zeiss) equipped with a motorized stage and AxioCam MRm camera (Carl Zeiss). For bright-field density measurements, slides containing MO sections were scanned (AxioScan.Z1, Carl Zeiss). The DMnX was delineated on three equally spaced sections, and integrated density values were obtained using Fiji (ImageJ version 2.1.0/1.53c).

Immunofluorescence

For single fluorescent labeling, samples were blocked with 5% normal serum and incubated overnight at 4°C with rabbit anti–h-αS (1:3000). For double fluorescence, sections were first incubated overnight with either rabbit anti-RFP (1:3000) or mouse anti–Syn-O2 (1:2000; TAB-0748CLV, Creative Biolabs) and then incubated with anti–h-αS. Labeling of these primary antibodies was achieved using a secondary antibody conjugated with DyLight 488 or DyLight 594 (1:300; Vector Laboratories). Sections were rinsed, mounted on coated slides, and coverslipped with Vectamount mounting medium (Vector Laboratories). For triple fluorescence, tissue sections were processed using the following sequential labeling procedures. First, for detection of mCherry-conjugated hM3D, mCherry was labeled by incubations with rabbit anti-RFP (1:3000), donkey anti-rabbit Fab fragment (1:200; Jackson ImmunoResearch), and goat anti-donkey

Alexa Fluor 594 (1:300; Abcam). Second, SOD2 was labeled by incubations with rabbit anti-SOD2 (1:1000) and goat anti-rabbit Alexa Fluor 647 (1:300, Abcam). Last, h-αS was labeled by overnight incubation with rabbit anti–h-αS conjugated with Alexa Fluor 488 (1:400; ab216124, Abcam). Fluorescence images were collected on Zeiss microscopes (LSM700, LSM800, LSM880, or LSM900) using the ZEN software (Carl Zeiss).

Axonal counts and quantification of spreading

The total number of h-αS–immunoreactive axons was counted using sections of the left pons, caudal midbrain, rostral midbrain, and forebrain at predefined bregma levels: −5.40 mm (pons), −4.60 mm (caudal midbrain), −3.40 mm (rostral midbrain), and −2.18 mm (forebrain). For measurements of axonal length and density, three equally spaced pontine sections (bregma −5.68, −5.51, and −5.34 mm) were used. After delineation of an area encompassing the locus coeruleus and parabrachial nucleus, measurements were performed using the Space Balls stereological probe (Stereo Investigator software, version 9, MBF Biosciences) (*40*). High-magnification images of h-αS–immunoreactive axons were analyzed on an Observer.Z1 microscope (Carl Zeiss), using a 63× Plan-Apochromat objective.

Ox-DHE and Syn-O2 quantification

Fluorescence intensity analyses were performed on DMnX-containing medullary sections using an LSM800 or LSM880 confocal microscope. Confocal z-stack images were collected and analyzed with Imaris 9.5 software. Ox-DHE fluorescent signal was acquired on three sections per animal, as previously described (*27*). Briefly, a three-dimensional (3D) surface rendering model of h-αS–immunoreactive DMnX neurons was created. A second 3D surface was created for ox-DHE puncta by applying a constant intensity threshold and was then filtered through h-αS–positive neuronal surfaces. This allowed for specific detection of ox-DHE puncta within immunoreactive neurons and for quantification of these puncta on a per-cell basis. Syn-O2 fluorescence intensity was quantified on 2D images that were generated from 5-μm-thick z-stack images using maximum intensity projection function of the Zen software (Carl Zeiss). Neuronal cell bodies immunoreactive for h-αS were selected by applying a size exclusion filter (120 μm^2), and Syn-O2 intensity was quantified within these cells.

In situ proximity ligase assay

Free-floating medullary sections containing the DMnX were processed using Duolink In-Situ PLA (Sigma-Aldrich) according to the manufacturer's protocols. Aggregated h-αS was detected using a previously described "direct" PLA method (*27*, *51*). This method involved an overnight incubation of sections in solutions containing PLA probes (1:120) directly conjugated to a h-αS–specific antibody (mouse anti-Syn211, Millipore). Detection of nitrated h-αS, nitrated NDUFB8, and nitrated SOD2 was performed using "indirect" PLA. For this assay, sections were first incubated overnight in a solution containing two primary antibodies and then incubated with secondary antibodies conjugated with oligonucleotide probes. For detection of nitrated h-αS, the two antibodies were mouse anti–3-NT (1:250; ab61392, Abcam) and rabbit anti–h-αS (1:4000) (*27*). For detection of nitrated NDUFB8, the two antibodies were mouse anti–3-NT (1:250) and rabbit anti-NDUFB8 (1:300; 14794, Proteintech), and for detection of nitrated SOD2, they were mouse anti–3-NT (1:250) and rabbit anti-SOD2 (1:1000; ADI-SOD-110, Enzo Life Sciences). Samples were then incubated with secondary antibodies conjugated with oligonucleotide probes, namely, anti-rabbit PLUS and anti-mouse MINUS (Duolink, Sigma-Aldrich). Following ligation and amplification, specific PLA signals were visualized using a bright-field or fluorescence detection kit (Duolink, Sigma-Aldrich). As negative controls, sections were processed using the same procedures with the exception that anti–h-αS, anti-NDUFB8, or anti-SOD2 was omitted. In these control specimens, no PLA signal was present.

Bright-field detection was used for assessment of nitrated (3-NT/h-αS PLA) or aggregated (h-αS/h-αS PLA) h-αS in the left DMnX. In these sections, which were counterstained with hematoxylin, quantification of PLA dots was obtained by stereological counts using the optical dissector (Stereo Investigator, MBF Bioscience). The DMnX was delineated at low magnification (10× objective) on every 10th section between bregma −6.96 and −8.00 mm. Coefficients of error of the PLA counts were less than 0.10. Bright-field detection was also used for visualization and quantification of nitrated h-αS in the left pons. For each animal, the number of PLA dots was counted on a single pontine section at the level of bregma −5.34 mm using the meander scan function of Stereo Investigator (MBF Biosciences). For double fluorescent labeling detecting PLA (nitrated NDUFB8 or nitrated SOD2) and h-αS or RFP, the PLA signal was first detected using the Duolink Green Detection Kit (Sigma-Aldrich). Then, sections were incubated with anti–h-αS or anti-RFP, and labeling was detected using DyLight 594 (1:300). Quantification of the fluorescent PLA signal within h-αS–positive DMnX neurons was performed on a single section at the level of the obex. Quantification of the PLA signal within RFP-immunoreactive neurons was carried out on six equally spaced DMnX-containing MO sections. Confocal z-stack images (4 μm thick) were acquired with a 63× Plan-Apochromat objective using an LSM 700 or LSM 900 scanning confocal microscope (Carl Zeiss). Maximum intensity projection images were generated with the ZEN software and, on these images, DMnX neurons immunoreactive for h-αS were delineated using Fiji (ImageJ version 2.1.0/1.53c). A fixed intensity threshold was set for the delineation of PLA dots that was automatically done using the "analyze particles" function of ImageJ. Intensity of the PLA signal and number of PLA dots were quantified on a per-cell basis.

RT-PCR and qPCR analyses

Tissue dissection, RNA extraction, and cDNA preparation were carried out as previously described (*40*). For RT-PCR assessment of Cre recombinase expression, mRNA was extracted from tissue specimens of the left (ipsilateral to the AAV injection) dorsal MO, pons, and caudal midbrain. For each sample, cDNA amplification was done using Power SYBR Green Master Mix (Applied Biosystems) and forward and reverse primers specific for Cre (i) and Hprt [housekeeping control, (ii)]: (i) 5′-CGCGGTCTGGCAGTAAAAAC and 5′-CGCCGCATAACCAGTGAAAC and (ii) 5′-TCCTCCTCAGACCGCTTTT and 5′-CCTGGTTCATCATCGCTAATC.

PCR products were mixed with 6× sample buffer (New England Biolabs) with 5% DMSO and loaded on a 2.0% SeaKem agarose gel (Lonza Bioscience) pre-stained with RedSafe dye (1:20,000, Intron Biotechnology). Images were acquired with an InGenius3 imaging system and GeneSys software (Syngene). qPCR measurements of human, mouse, and total αS RNA expression were carried out on tissue extracts from the left dorsal MO. Samples were analyzed with a StepOnePlus Real-Time PCR instrument (Applied Biosystems). Triplicate measurements of cDNA (2.5 ng) were done using Power

SYBR Green Master Mix (Applied Biosystems) and forward and reverse primers specific for h-αS (i), mouse αS (ii), total αS (iii), and Hprt (see above): (i) 5′-AATGAAGAAGGAGCCCCACAG and 5′-AAGGCATTTCATAAGCCTCATTGTC, (ii) 5′-AGTGGAGGGAGCTGGGAATATAG and 5′-CCAGGATTCCTTCCTGTGGGTAC, and (iii) 5′-GCTCAGAAGACAGTGGAGGG and 5′-TCTTCCAGAATTCCTTCCTGTGGG. Fold change expression levels were calculated using the $2^{-\Delta\Delta CT}$ method.

Statistical analysis

Unless specified differently in the figure legends, at least five animals per treatment group were used for all histological, biochemical, and molecular biology analyses. Statistical analyses were performed with GraphPad Prism (8.0) using unpaired *t* test for axonal counts/measurements and PLA stereological counts, and nonparametric Mann-Whitney *U* test for intensity image analyses and qPCR measurements. Analysis of variance (ANOVA) followed by Tukey post hoc test was used when comparisons were made among four treatment groups. *P* values of less than 0.05 were considered statistically significant.

SUPPLEMENTARY MATERIALS

Supplementary material for this article is available at https://science.org/doi/10.1126/sciadv.abn0356

View/request a protocol for this paper from *Bio-protocol*.

REFERENCES AND NOTES

1. B. N. Dugger, D. W. Dickson, Pathology of neurodegenerative diseases. *Cold Spring Harb. Perspect. Biol.* **9**, a028035 (2017).
2. M. G. Spillantini, M. L. Schmidt, V. M. Lee, J. Q. Trojanowski, R. Jakes, M. Goedert, α-Synuclein in Lewy bodies. *Nature* **388**, 839–840 (1997).
3. M. Goedert, M. G. Spillantini, K. Del Tredici, H. Braak, 100 years of Lewy pathology. *Nat. Rev. Neurol.* **9**, 13–24 (2013).
4. H. Braak, R. A. de Vos, J. Bohl, K. Del Tredici, Gastric α-synuclein immunoreactive inclusions in Meissner's and Auerbach's plexuses in cases staged for Parkinson's disease-related brain pathology. *Neurosci. Lett.* **396**, 67–72 (2006).
5. K. Del Tredici, C. H. Hawkes, E. Ghebremedhin, H. Braak, Lewy pathology in the submandibular gland of individuals with incidental Lewy body disease and sporadic Parkinson's disease. *Acta Neuropathol.* **119**, 703–713 (2010).
6. T. G. Beach, C. H. Adler, L. I. Sue, L. Vedders, L. Lue, C. L. White III, H. Akiyama, J. N. Caviness, H. A. Shill, M. N. Sabbagh, D. G. Walker; Arizona Parkinson's Disease Consortium, Multi-organ distribution of phosphorylated α-synuclein histopathology in subjects with Lewy body disorders. *Acta Neuropathol.* **119**, 689–702 (2010).
7. K. A. Jellinger, Neuropathobiology of non-motor symptoms in Parkinson disease. *J. Neural Transm.* **122**, 1429–1440 (2015).
8. H. Braak, K. Del Tredici, U. Rub, R. A. de Vos, E. N. Jansen Steur, E. Braak, Staging of brain pathology related to sporadic Parkinson's disease. *Neurobiol. Aging* **24**, 197–211 (2003).
9. H. McCann, H. Cartwright, G. M. Halliday, Neuropathology of α-synuclein propagation and Braak hypothesis. *Mov. Disord.* **31**, 152–160 (2016).
10. D. M. Walsh, D. J. Selkoe, A critical appraisal of the pathogenic protein spread hypothesis of neurodegeneration. *Nat. Rev. Neurosci.* **17**, 251–260 (2016).
11. C. Peng, J. Q. Trojanowski, V. M. Lee, Protein transmission in neurodegenerative disease. *Nat. Rev. Neurol.* **16**, 199–212 (2020).
12. I. C. Brás, T. F. Outeiro, α-Synuclein: Mechanisms of release and pathology progression in synucleinopathies. *Cells* **10**, 375 (2021).
13. H. Braak, U. Rub, W. P. Gai, K. Del Tredici, Idiopathic Parkinson's disease: Possible routes by which vulnerable neuronal types may be subject to neuroinvasion by an unknown pathogen. *J. Neural Transm.* **110**, 517–536 (2003).
14. D. P. Breen, G. M. Halliday, A. E. Lang, Gut-brain axis and the spread of α-synuclein pathology: Vagal highway or dead end? *Mov. Disord.* **34**, 307–316 (2019).
15. A. Ulusoy, R. J. Phillips, M. Helwig, M. Klinkenberg, T. L. Powley, D. A. Di Monte, Brain-to-stomach transfer of α-synuclein via vagal preganglionic projections. *Acta Neuropathol.* **133**, 381–393 (2017).
16. A. W. Bero, P. Yan, J. H. Roh, J. R. Cirrito, F. R. Stewart, M. E. Raichle, J. M. Lee, D. M. Holtzman, Neuronal activity regulates the regional vulnerability to amyloid-β deposition. *Nat. Neurosci.* **14**, 750–756 (2011).
17. K. Yamamoto, Z. I. Tanei, T. Hashimoto, T. Wakabayashi, H. Okuno, Y. Naka, O. Yizhar, L. E. Fenno, M. Fukayama, H. Bito, J. R. Cirrito, D. M. Holtzman, K. Deisseroth, T. Iwatsubo, Chronic optogenetic activation augments Aβ pathology in a mouse model of Alzheimer disease. *Cell Rep.* **11**, 859–865 (2015).
18. P. Yuan, J. Grutzendler, Attenuation of ß-amyloid deposition and neurotoxicity by chemogenetic modulation of neural activity. *J. Neurosci.* **36**, 632–641 (2016).
19. J. W. Wu, S. A. Hussaini, I. M. Bastille, G. A. Rodriguez, A. Mrejeru, K. Rilett, D. W. Sanders, C. Cook, H. Fu, R. A. Boonen, M. Herman, E. Nahmani, S. Emrani, Y. H. Figueroa, M. I. Diamond, C. L. Clelland, S. Wray, K. E. Duff, Neuronal activity enhances tau propagation and tau pathology in vivo. *Nat. Neurosci.* **19**, 1085–1092 (2016).
20. M. K. Schultz Jr., R. Gentzel, M. Usenovic, C. Gretzula, C. Ware, S. Parmentier-Batteur, J. B. Schachter, H. A. Zariwala, Pharmacogenetic neuronal stimulation increases human tau pathology and trans-synaptic spread of tau to distal brain regions in mice. *Neurobiol. Dis.* **118**, 161–176 (2018).
21. Q. Wu, M. A. Shaikh, E. S. Meymand, B. Zhang, K. C. Luk, J. Q. Trojanowski, V. M.-Y. Lee, Neuronal activity modulates alpha-synucle in aggregation and spreading in organotypic brain slice cultures and in vivo. *Acta Neuropathol.* **140**, 831–849 (2020).
22. K. Yamada, J. K. Holth, F. Liao, F. R. Stewart, T. E. Mahan, H. Jiang, J. R. Cirrito, T. K. Patel, K. Hochgrafe, E. M. Mandelkow, D. M. Holtzman, Neuronal activity regulates extracellular tau in vivo. *J. Exp. Med.* **211**, 387–393 (2014).
23. K. Yamada, T. Iwatsubo, Extracellular α-synuclein levels are regulated by neuronal activity. *Mol. Neurodegener.* **13**, 9 (2018).
24. P. S. Brookes, Y. Yoon, J. L. Robotham, M. W. Anders, S. S. Sheu, Calcium, ATP, and ROS: A mitochondrial love-hate triangle. *Am. J. Physiol. Cell Physiol.* **287**, C817–C833 (2004).
25. M. P. Murphy, How mitochondria produce reactive oxygen species. *Biochem. J.* **417**, 1–13 (2009).
26. E. Zampese, D. J. Surmeier, Calcium, bioenergetics, and Parkinson's disease. *Cells* **9**, 2045 (2020).
27. R. E. Musgrove, M. Helwig, E. J. Bae, H. Aboutalebi, S. J. Lee, A. Ulusoy, D. A. Di Monte, Oxidative stress in vagal neurons promotes parkinsonian pathology and intercellular α-synuclein transfer. *J. Clin. Invest.* **129**, 3738–3753 (2019).
28. J. A. Goldberg, J. N. Guzman, C. M. Estep, E. Ilijic, J. Kondapalli, J. Sanchez-Padilla, D. J. Surmeier, Calcium entry induces mitochondrial oxidant stress in vagal neurons at risk in Parkinson's disease. *Nat. Neurosci.* **15**, 1414–1421 (2012).
29. J. N. Guzman, J. Sanchez-Padilla, D. Wokosin, J. Kondapalli, E. Ilijic, P. T. Schumacker, D. J. Surmeier, Oxidant stress evoked by pacemaking in dopaminergic neurons is attenuated by DJ-1. *Nature* **468**, 696–700 (2010).
30. J. Sanchez-Padilla, J. N. Guzman, E. Ilijic, J. Kondapalli, D. J. Galtieri, B. Yang, S. Schieber, W. Oertel, D. Wokosin, P. T. Schumacker, D. J. Surmeier, Mitochondrial oxidant stress in locus coeruleus is regulated by activity and nitric oxide synthase. *Nat. Neurosci.* **17**, 832–840 (2014).
31. W. H. Chiu, L. Kovacheva, R. E. Musgrove, H. Arien-Zakay, J. B. Koprich, J. M. Brotchie, R. Yaka, D. Ben-Zvi, M. Hanani, J. Roeper, J. A. Goldberg, α-Synuclein-induced Kv4 channelopathy in mouse vagal motoneurons drives nonmotor parkinsonian symptoms. *Sci. Adv.* **7**, eabd3994 (2021).
32. D. Sulzer, D. J. Surmeier, Neuronal vulnerability, pathogenesis, and Parkinson's disease. *Mov. Disord.* **28**, 715–724 (2013).
33. P. Gonzalez-Rodriguez, E. Zampese, D. J. Surmeier, Selective neuronal vulnerability in Parkinson's disease. *Prog. Brain Res.* **252**, 61–89 (2020).
34. P. Soriano, Generalized lacZ expression with the ROSA26 Cre reporter strain. *Nat. Genet.* **21**, 70–71 (1999).
35. S. Srinivas, T. Watanabe, C. S. Lin, C. M. William, Y. Tanabe, T. M. Jessell, F. Costantini, Cre reporter strains produced by targeted insertion of EYFP and ECFP into the ROSA26 locus. *BMC Dev. Biol.* **1**, 4 (2001).
36. J. P. Daher, M. Ying, R. Banerjee, R. S. McDonald, M. D. Hahn, L. Yang, M. Flint Beal, B. Thomas, V. L. Dawson, T. M. Dawson, D. J. Moore, Conditional transgenic mice expressing C-terminally truncated human α-synuclein (αSyn119) exhibit reduced striatal dopamine without loss of nigrostriatal pathway dopaminergic neurons. *Mol. Neurodegener.* **4**, 34 (2009).
37. M. Kalia, J. M. Sullivan, Brainstem projections of sensory and motor components of the vagus nerve in the rat. *J. Comp. Neurol.* **211**, 248–265 (1982).
38. R. A. Leslie, D. G. Gwyn, D. A. Hopkins, The central distribution of the cervical vagus nerve and gastric afferent and efferent projections in the rat. *Brain Res. Bull.* **8**, 37–43 (1982).
39. A. Ulusoy, R. Rusconi, B. I. Perez-Revuelta, R. E. Musgrove, M. Helwig, B. Winzen-Reichert, D. A. Di Monte, Caudo-rostral brain spreading of α-synuclein through vagal connections. *EMBO Mol. Med.* **5**, 1119–1127 (2013).
40. M. Helwig, M. Klinkenberg, R. Rusconi, R. E. Musgrove, N. K. Majbour, O. M. El-Agnaf, A. Ulusoy, D. A. Di Monte, Brain propagation of transduced α-synuclein involves non-fibrillar protein species and is enhanced in α-synuclein null mice. *Brain* **139**, 856–870 (2016).
41. B. L. Roth, DREADDs for neuroscientists. *Neuron* **89**, 683–694 (2016).

42. K. S. Smith, D. J. Bucci, B. W. Luikart, S. V. Mahler, DREADDS: Use and application in behavioral neuroscience. *Behav. Neurosci.* **130**, 137–155 (2016).
43. T. Torre-Muruzabal, J. Devoght, C. Van den Haute, B. Brone, A. Van der Perren, V. Baekelandt, Chronic nigral neuromodulation aggravates behavioral deficits and synaptic changes in an α-synuclein based rat model for Parkinson's disease. *Acta Neuropathol. Commun.* **7**, 160 (2019).
44. C. NamKoong, W. J. Song, C. Y. Kim, D. H. Chun, S. Shin, J. W. Sohn, H. J. Choi, Chemogenetic manipulation of parasympathetic neurons (DMV) regulates feeding behavior and energy metabolism. *Neurosci. Lett.* **712**, 134356 (2019).
45. S. L. Budd, R. F. Castilho, D. G. Nicholls, Mitochondrial membrane potential and hydroethidine-monitored superoxide generation in cultured cerebellar granule cells. *FEBS Lett.* **415**, 21–24 (1997).
46. S. Schildknecht, H. R. Gerding, C. Karreman, M. Drescher, H. A. Lashuel, T. F. Outeiro, D. A. Di Monte, M. Leist, Oxidative and nitrative alpha-synuclein modifications and proteostatic stress: Implications for disease mechanisms and interventions in synucleinopathies. *J. Neurochem.* **125**, 491–511 (2013).
47. M. Hashimoto, L. J. Hsu, Y. Xia, A. Takeda, A. Sisk, M. Sundsmo, E. Masliah, Oxidative stress induces amyloid-like aggregate formation of NACP/α-synuclein in vitro. *Neuroreport* **10**, 717–721 (1999).
48. H. Ischiropoulos, J. S. Beckman, Oxidative stress and nitration in neurodegeneration: Cause, effect, or association? *J. Clin. Invest.* **111**, 163–169 (2003).
49. O. Scudamore, T. Ciossek, Increased oxidative stress exacerbates α-synuclein aggregation in vivo. *J. Neuropathol. Exp. Neurol.* **77**, 443–453 (2018).
50. N. N. Vaikath, N. K. Majbour, K. E. Paleologou, M. T. Ardah, E. van Dam, W. D. van de Berg, S. L. Forrest, L. Parkkinen, W. P. Gai, N. Hattori, M. Takanashi, S. J. Lee, D. M. Mann, Y. Imai, G. M. Halliday, J. Y. Li, O. M. El-Agnaf, Generation and characterization of novel conformation-specific monoclonal antibodies for α-synuclein pathology. *Neurobiol. Dis.* **79**, 81–99 (2015).
51. R. F. Roberts, R. Wade-Martins, J. Alegre-Abarrategui, Direct visualization of alpha-synuclein oligomers reveals previously undetected pathology in Parkinson's disease brain. *Brain* **138**, 1642–1657 (2015).
52. R. Rusconi, A. Ulusoy, H. Aboutalebi, D. A. Di Monte, Long-lasting pathological consequences of overexpression-induced α-synuclein spreading in the rat brain. *Aging Cell* **17**, e12727 (2018).
53. A. Ulusoy, R. E. Musgrove, R. Rusconi, M. Klinkenberg, M. Helwig, A. Schneider, D. A. Di Monte, Neuron-to-neuron α-synuclein propagation in vivo is independent of neuronal injury. *Acta Neuropathol. Commun.* **3**, 13 (2015).
54. D. van der Kooy, L. Y. Koda, J. F. McGinty, C. R. Gerfen, F. E. Bloom, The organization of projections from the cortex, amygdala, and hypothalamus to the nucleus of the solitary tract in rat. *J. Comp. Neurol.* **224**, 1–24 (1984).
55. G. J. Ter Horst, G. J. Toes, J. D. Van Willigen, Locus coeruleus projections to the dorsal motor vagus nucleus in the rat. *Neuroscience* **45**, 153–160 (1991).
56. H. C. Cheng, C. M. Ulane, R. E. Burke, Clinical progression in Parkinson disease and the neurobiology of axons. *Ann. Neurol.* **67**, 715–725 (2010).
57. M. Decressac, B. Mattsson, M. Lundblad, P. Weikop, A. Bjorklund, Progressive neurodegenerative and behavioural changes induced by AAV-mediated overexpression of α-synuclein in midbrain dopamine neurons. *Neurobiol. Dis.* **45**, 939–953 (2012).
58. D. Games, P. Seubert, E. Rockenstein, C. Patrick, M. Trejo, K. Ubhi, B. Ettle, M. Ghassemiam, R. Barbour, D. Schenk, S. Nuber, E. Masliah, Axonopathy in an α-synuclein transgenic model of Lewy body disease is associated with extensive accumulation of C-terminal-truncated α-synuclein. *Am. J. Pathol.* **182**, 940–953 (2013).
59. M. J. Devine, K. Gwinn, A. Singleton, J. Hardy, Parkinson's disease and α-synuclein expression. *Mov. Disord.* **26**, 2160–2168 (2011).
60. J. Grundemann, F. Schlaudraff, O. Haeckel, B. Liss, Elevated α-synuclein mRNA levels in individual UV-laser-microdissected dopaminergic substantia nigra neurons in idiopathic Parkinson's disease. *Nucleic Acids Res.* **36**, e38 (2008).
61. L. Mu, S. Sobotka, J. Chen, H. Su, I. Sanders, C. H. Adler, H. A. Shill, J. N. Caviness, J. E. Samanta, T. G. Beach; Arizona Parkinson's Disease Consortium, Alpha-synuclein pathology and axonal degeneration of the peripheral motor nerves innervating pharyngeal muscles in Parkinson disease. *J. Neuropathol. Exp. Neurol.* **72**, 119–129 (2013).
62. B. I. Giasson, J. E. Duda, I. V. Murray, Q. Chen, J. M. Souza, H. I. Hurtig, H. Ischiropoulos, J. Q. Trojanowski, V. M. Lee, Oxidative damage linked to neurodegeneration by selective α-synuclein nitration in synucleinopathy lesions. *Science* **290**, 985–989 (2000).
63. J. E. Duda, B. I. Giasson, Q. Chen, T. L. Gur, H. I. Hurtig, M. B. Stern, S. M. Gollomp, H. Ischiropoulos, V. M. Lee, J. Q. Trojanowski, Widespread nitration of pathological inclusions in neurodegenerative synucleinopathies. *Am. J. Pathol.* **157**, 1439–1445 (2000).
64. N. Ugarte, I. Petropoulos, B. Friguet, Oxidized mitochondrial protein degradation and repair in aging and oxidative stress. *Antioxid. Redox Signal.* **13**, 539–549 (2010).
65. N. Traaseth, S. Elfering, J. Solien, V. Haynes, C. Giulivi, Role of calcium signaling in the activation of mitochondrial nitric oxide synthase and citric acid cycle. *Biochim. Biophys. Acta* **1658**, 64–71 (2004).
66. J. Murray, S. W. Taylor, B. Zhang, S. S. Ghosh, R. A. Capaldi, Oxidative damage to mitochondrial complex I due to peroxynitrite: Identification of reactive tyrosines by mass spectrometry. *J. Biol. Chem.* **278**, 37223–37230 (2003).
67. C. W. Davis, B. J. Hawkins, S. Ramasamy, K. M. Irrinki, B. A. Cameron, K. Islam, V. P. Daswani, P. J. Doonan, Y. Manevich, M. Madesh, Nitration of the mitochondrial complex I subunit NDUFB8 elicits RIP1- and RIP3-mediated necrosis. *Free Radic. Biol. Med.* **48**, 306–317 (2010).
68. F. Yamakura, H. Taka, T. Fujimura, K. Murayama, Inactivation of human manganese-superoxide dismutase by peroxynitrite is caused by exclusive nitration of tyrosine 34 to 3-nitrotyrosine. *J. Biol. Chem.* **273**, 14085–14089 (1998).
69. R. Radi, Protein tyrosine nitration: Biochemical mechanisms and structural basis of functional effects. *Acc. Chem. Res.* **46**, 550–559 (2013).
70. L. J. Hsu, Y. Sagara, A. Arroyo, E. Rockenstein, A. Sisk, M. Mallory, J. Wong, T. Takenouchi, M. Hashimoto, E. Masliah, α-Synuclein promotes mitochondrial deficit and oxidative stress. *Am. J. Pathol.* **157**, 401–410 (2000).
71. R. Di Maio, P. J. Barrett, E. K. Hoffman, C. W. Barrett, A. Zharikov, A. Borah, X. Hu, J. McCoy, C. T. Chu, E. A. Burton, T. G. Hastings, J. T. Greenamyre, α-Synuclein binds to TOM20 and inhibits mitochondrial protein import in Parkinson's disease. *Sci. Transl. Med.* **8**, 342ra78 (2016).

Acknowledgments: We thank L. Demmer and A. Takhi for assistance with the experiments and assays; Y. Merkler for assistance with animal care and use requirements; personnel at the DZNE Light Microscope Facility, Image and Data Analysis Facility and Preclinical Center; and S. A. Jewell for her valuable comments on the manuscript. **Funding:** This work was supported by grants from the EU Innovative Medicines Initiative (IMI 821522, PD-MitoQUANT) (to D.A.D.M.) and the EU Joint Programme-Neurodegenerative Disease Research (JPND 01ED2005B, GBA-PaCTS) (to D.A.D.M.). D.A.D.M. and A.U. were in part funded by Aligning Science Across Parkinson's (ASAP-000420) through the Michael J. Fox Foundation for Parkinson's Research (MJFF). For the purpose of open access, the author has applied a CC BY public copyright license to all author-accepted manuscripts (AAM) arising from this submission. **Author contributions:** Study design: M.H. and D.A.D.M. Surgical procedures and execution of experiments: M.H. and A.R. New methodologies: A.U. Other methodologies and assays: A.U., M.H., A.R., S.A.O., H.A., R.P.-C., B.J., M.K., and S.S.L.L. Data analysis: D.A.D.M., A.U., and M.H. Writing: D.A.D.M. Editing: M.H., A.U., A.R., S.A.O., H.A., B.J., M.K., S.S.L.L., and D.A.D.M. **Competing interests:** The authors declare that they have no competing interest. **Data and materials availability:** All data needed to evaluate the conclusions in the paper are present in the paper and/or the Supplementary Materials.

Submitted 29 October 2021
Accepted 15 July 2022
Published 31 August 2022
10.1126/sciadv.abn0356

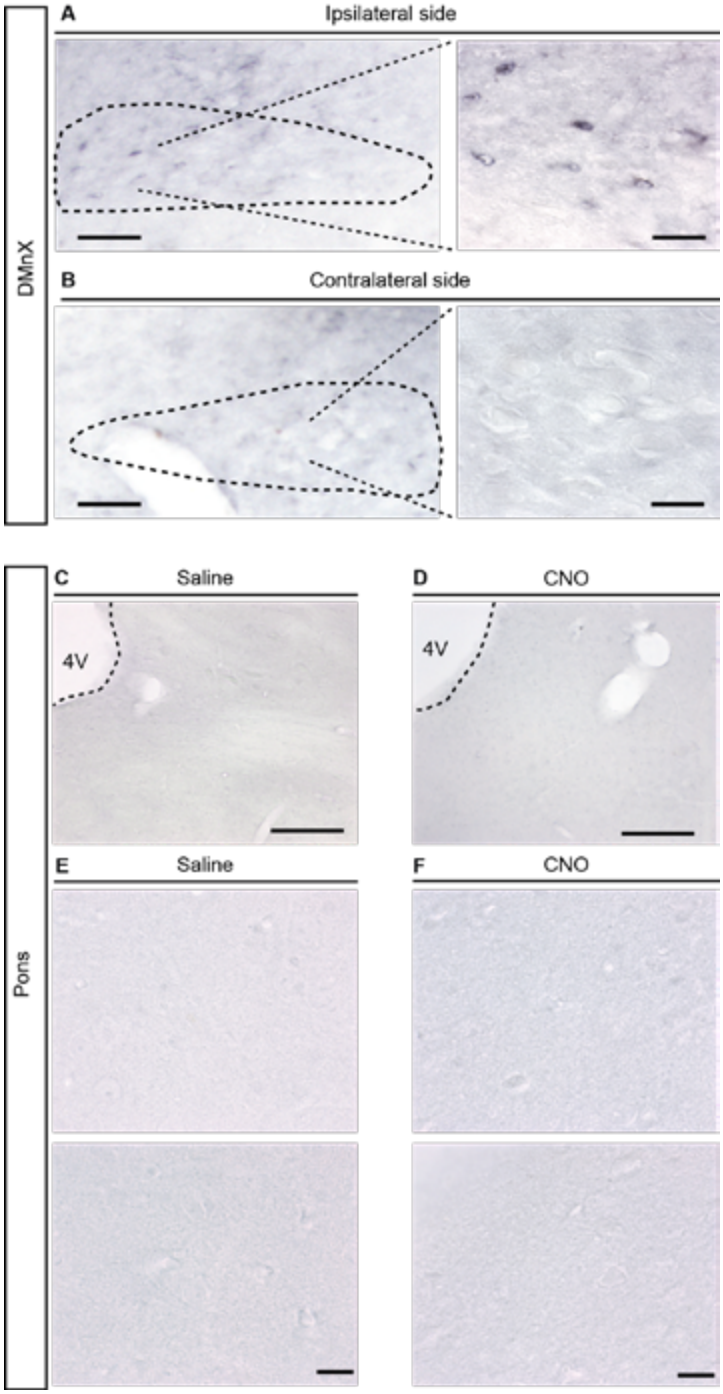
A
Ipsilateral side
DMnX
B
Contralateral side
C
Saline
D
CNO
4V
4V
Pons
E
Saline
F
CNO

Fig. S1. Selective detection of Cre-recombinase protein in the DMnX. (A-F) iR26-aS mice received an intravagal injection of Cre-AAVs together with hM3Dq-AAVs and were sacrificed five weeks later. They were also treated with daily intraperitoneal injections of either saline or CNO for two weeks prior to sacrifice. Tissue sections from the MO (A and B) and pons (C-F) were immunostained with anti-Cre and processed for brightfield microscopy. (**A** and **B**) Representative sections of the dorsal MO show the presence of immunoreactive neurons in the left (ipsilateral to the vagal AAV injection, A) but not the right (contralateral to the AAV injection, B) DMnX (delineated with dashed lines). Images were collected at low (left panels) and higher (right panels) magnification. Scale bars, 50 and 20 μm in the left and right panels, respectively. (**C-F**) Representative sections of the left pons at low (C and D) and higher (E and F) magnification from either saline- (C and E) or CNO- (D and F) treated mice show lack of Cre protein immunoreactivity. The 4th ventricle (4V) is delineated with dashed lines in C and D. Scale bars, 200 μm in C and D, and 20 μm in E and F.

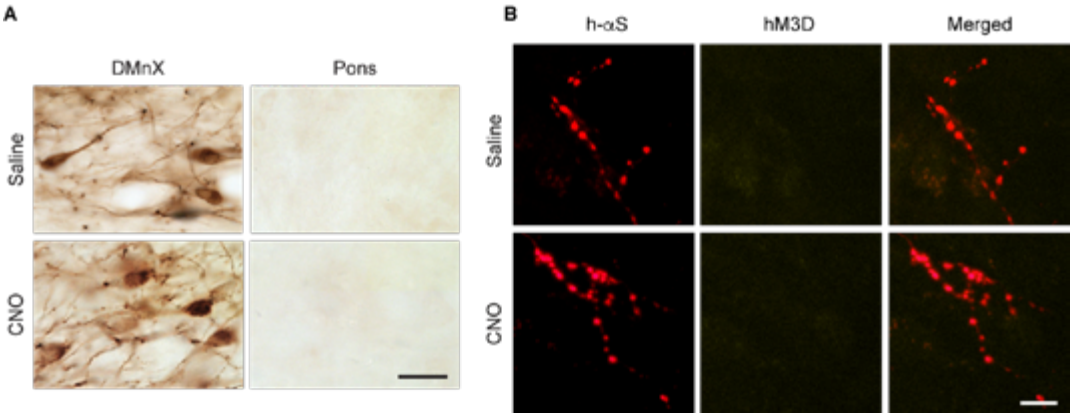

Fig. S2. Selective detection of mCherry-fused hM3D protein in the dorsal MO. (**A** and **B**) iR26-αS mice received an intravagal injection of Cre-AAVs together with hM3D^{fl}-AAVs and were sacrificed five weeks later. They were also treated with daily intraperitoneal injections of either saline or CNO for two weeks prior to sacrifice. (**A**) Tissue sections from the medulla oblongata and pons were immunostained with anti-RFP (for the detection of mCherry-tagged hM3D) and processed for brightfield microscopy. Images of representative sections show that robust protein expression characterized cell bodies and neurites in the DMnX, whereas pontine sections were devoid of immunoreactivity. Scale bar, 40 µm. (**B**) Tissue sections from the pons were double-labeled with anti-h-αS (red) and anti-RFP (yellow) and processed for confocal microscopy. Representative images show axons loaded with h-αS as a result of the spreading process. The same axons were devoid of RFP immunoreactivity, further confirming lack of medullary-to-pons transfer of the RFP protein. Scale bar, 10 µm.

Klinkenberg, M., Helwig, M., Pinto-Costa, R., Rollar, A., Rusconi, R., Di Monte, D.A., and **Ulusoy, A.** (2023). **Interneuronal in vivo transfer of synaptic proteins.** Cells 12, 569.

Objective: Neuron-to-neuron transfer of proteins may be a common underlying principle for neurodegeneration. Yet, very little is known about the identity and features of proteins that display the ability to spread between neurons. Are there common features that make these neurodegenerative disease-associated proteins prone to spread? Here we aimed to determine whether α-syn's spreading ability was shared by other proteins that are similar in structure, size or subcellular localization.

Methods and results: AAV vectors encoding for three synaptic proteins, namely β-synuclein (β-syn), vesicle-associated membrane protein 2 (VAMP2), or synaptosomal-associated protein of 25kDa (SNAP25) were injected into the vagus nerve of mice to induce their expression in the vagal nuclei. AAV-induced β-syn overexpression in the medulla oblongata, but not VAMP2 and SNAP25 was associated with detection and accumulation of the exogenous protein in more frontal brain regions suggesting that β-syn, but not VAMP2 or SNAP25, is capable of interneuronal transfer. A proximity ligase assay developed to detect aggregation of these proteins established that β-syn overexpression in the vagal nuclei is characterized by the accumulation of aggregated forms of the protein, contrary to VAMP2 and SNAP25 overexpression.

Conclusions: These data indicate that transfer and spreading of neuronal proteins are not mere consequences of enhanced protein expression or their subcellular localization but are likely mediated by unique structural properties that promote their aggregation.

cells

MDPI

Article

Interneuronal In Vivo Transfer of Synaptic Proteins

Michael Klinkenberg, Michael Helwig, Rita Pinto-Costa, Angela Rollar, Raffaella Rusconi, Donato A. Di Monte and Ayse Ulusoy *

German Center for Neurodegenerative Diseases (DZNE), 53127 Bonn, Germany
* Correspondence: ayse.ulusoy@dzne.de

Abstract: Neuron-to-neuron transfer of pathogenic α-synuclein species is a mechanism of likely relevance to Parkinson's disease development. Experimentally, interneuronal α-synuclein spreading from the low brainstem toward higher brain regions can be reproduced by the administration of AAV vectors encoding for α-synuclein into the mouse vagus nerve. The aim of this study was to determine whether α-synuclein's spreading ability is shared by other proteins. Given α-synuclein synaptic localization, experiments involved intravagal injections of AAVs encoding for other synaptic proteins, β-synuclein, VAMP2, or SNAP25. Administration of AAV-VAMP2 or AAV-SNAP25 caused robust transduction of either of the proteins in the dorsal medulla oblongata but was not followed by interneuronal VAMP2 or SNAP25 transfer and caudo-rostral spreading. In contrast, AAV-mediated β-synuclein overexpression triggered its spreading to more frontal brain regions. The aggregate formation was investigated as a potential mechanism involved in protein spreading, and consistent with this hypothesis, results showed that overexpression of β-synuclein, but not VAMP2 or SNAP25, in the dorsal medulla oblongata was associated with pronounced protein aggregation. Data indicate that interneuronal protein transfer is not a mere consequence of increased expression or synaptic localization. It is rather promoted by structural/functional characteristics of synuclein proteins that likely include their tendency to form aggregate species.

Keywords: protein spreading; oligomerization; animal models; Parkinson's disease; vagus nerve

Citation: Klinkenberg, M.; Helwig, M.; Pinto-Costa, R.; Rollar, A.; Rusconi, R.; Di Monte, D.A.; Ulusoy, A. Interneuronal In Vivo Transfer of Synaptic Proteins. *Cells* **2023**, *12*, 569. https://doi.org/10.3390/cells12040569

Academic Editors: Arianna Bellucci and Francesca Longhena

Received: 15 December 2022
Revised: 6 February 2023
Accepted: 8 February 2023
Published: 10 February 2023

1. Introduction

A significant feature of Parkinson's disease (PD) is the progressive accumulation of α-synuclein (α-syn)-containing inclusions in the brain and peripheral tissues [1,2]. Neuropathological studies and experimental evidence support the possibility that, in PD and PD models, α-syn pathology may spread from the site(s) of its initial accumulation to other interconnected sites following a stereotypical pattern [3,4]. Mechanisms of this spreading and its specificity to the α-syn protein remain relatively unclear, however. Investigations into specific features of α-syn that may contribute to its spreading could, therefore, provide critical clues on the molecular mechanisms underlying this phenomenon.

α-Syn is a natively unfolded protein enriched in pre-synaptic nerve terminals. Specific localization of α-syn in the synapse is mediated, at least in part, by its ability to bind to lipids (i.e., synaptic membranes) and pre-synaptic proteins [5,6]. From the pathological standpoint, findings of genetic studies indicate that changes in α-syn amino acid sequence due to missense mutations or increased α-syn expression caused by *SNCA* multiplication mutations trigger genetic forms of parkinsonism [7–16]. Interestingly, these disease-causing modifications are also associated with an increased propensity to aggregate and altered vesicular binding, suggesting that protein levels and amino acid sequence that affect α-syn's ability to aggregate or to bind to other molecules may play an important role in PD pathogenetic processes [6,17,18].

In the brain, pathological α-syn accumulation in the form of Lewy inclusions is not randomly distributed but targets specific neuronal populations. Cholinergic neurons in the dorsal motor nucleus of the vagus nerve (DMnX) represent one of the primary sites of

α-syn burden at the early stages of disease development [19]. As the disease progresses, the pathology often advances from this nucleus in the lower brainstem toward specific neuronal populations in more rostral brain regions [19,20]. The stereotypical pattern of this spreading supports the hypothesis that progressive pathology may arise from the interneuronal transfer of pathogenic α-syn species between anatomically connected brain regions. A variety of in vitro and in vivo experimental models have been developed and utilized to investigate this hypothesis [1,20,21]. For example, valuable clues on interneuronal α-syn spreading involving the DMnX have been obtained using an in vivo paradigm consisting of unilateral injection of adeno-associated viral vectors (AAVs) designed to express human α-syn (AAV-α-syn) into the mouse or rat vagus nerve [22–26]. This treatment first induces overexpression of human α-syn targeted to the dorsal medulla oblongata (dMO). It is then followed by neuron-to-neuron transfer and caudo-rostral advancement of human α-syn that progressively and stereotypically spreads towards pontine, midbrain, and forebrain regions [22,24,26,27]. Important findings obtained in this model include the demonstration that aggregated forms of α-syn and, in particular, oligomeric protein species, are likely to play an important role in neuron-to-neuron α-syn transfer [24].

A key question raised by the finding of overexpression-induced α-syn spreading concerns the specificity of this effect and the extent to which specific α-syn properties may underlie it. To address this question, experiments were carried out in animals that were intravagally injected with AAV vectors delivering green fluorescent protein DNA (AAV-GFP). Similar to the results after treatment with AAV-α-syn, these animals showed robust protein (GFP instead of human α-syn) expression in the dMO; this overexpression did not result, however, in caudo-rostral GFP spreading [22,24,26,27]. Lack of protein spreading in AAV-GFP-treated animals provided initial evidence suggesting that interneuronal spreading is not a mere consequence of protein overexpression. These experiments, however, did not thoroughly address the question of the specificity of the interneuronal α-syn transfer. It could be argued, for example, that GFP is a cytosolic (as compared to synaptic) protein almost double in size as compared to α-syn. Therefore, if the size and subcellular localization of a protein are important factors determining its neuron-to-neuron exchange, lack of GFP transfer would not itself rule out the possibility that the spreading properties of α-syn may be shared by other proteins.

The present study was designed to further investigate the specificity of overexpression-induced α-syn spreading. To achieve this goal, the spreading potential of proteins similar to α-syn in size, amino acid sequence, and subcellular localization (i.e., pre-synaptic) was assessed after induction of their overexpression in the mouse medulla oblongata. Experiments were also carried out to test the hypothesis that a relationship exists between interneuronal protein transfer and the formation of protein aggregates. The proteins investigated were β-syn, vesicle-associated membrane protein 2 (VAMP2), and synaptosomal-associated protein of 25kDa (SNAP25). β-Syn is a synuclein family protein with size and amino acid sequence very similar to α-syn. β-syn is not only expressed within the same neuronal populations in the brain but also shares with α-syn its synaptic localization [28]. VAMP2 and SNAP25 are key components of the soluble N-ethylmaleimide-sensitive fusion attachment protein receptor (SNARE) complex known to interact with α-syn in the synaptic compartment [29,30]. Results revealed marked differences in spreading capabilities among different proteins, supporting specific interneuronal mobility of synuclein proteins. This mobility could be mediated, at least in part, by the propensity of α- and β-syn to form aggregates within overexpressing neurons.

2. Materials and Methods

2.1. Viral Vectors

Serotype 6 recombinant AAVs were used for transgene expression of β-syn and human influenza hemagglutinin (HA)-tagged β-syn, VAMP2, SNAP25, and α-syn under the control of a human synapsin 1 promoter. All transgenes were human-derived and wild-type. Gene expression was enhanced using a woodchuck hepatitis virus posttran-

scriptional regulatory element (WPRE) and a polyA signal. AAV vector production, purification, concentration, and titration were performed by Vector Biolabs (Philadelphia, PA, USA). Vectors were diluted in phosphate-buffered saline solution to titers ranging between 3.5–5.0 $\times$ 10^{12} genome copies/mL in order to achieve similar transduction in vivo.

2.2. Animals and Surgical Procedures

Animal experiments were approved by the State Agency for Nature, Environment, and Consumer Protection in North-Rhine Westphalia, Germany. Experiments were conducted in female C57BL/6JRj mice (Janvier Labs, Le Genest-Saint-Isle, France) between 15 and 22 weeks of age. Animals were housed in individually ventilated cages in a specific-pathogen-free facility and kept on a 12-hour light/dark cycle with ad libitum access to food and water. To induce transgene expression, AAV vectors were injected into the left vagus nerve as previously described [24]. All surgical procedures were performed under isoflurane anesthesia and buprenorphine analgesia. A small incision was made at the midline of the neck, and the left vagus nerve was isolated. The AAV-containing solution (800 nL) was injected at a flow rate of 350 nL/min using a 35-gauge blunt steel needle fitted onto a 10 µL NanoFil syringe. Mice were sacrificed 6 weeks after the surgery with a lethal dose of sodium pentobarbital (i.p.) and perfused through the ascending aorta with 4% (*w*/*v*) paraformaldehyde. Brains were removed and immersed in 4% paraformaldehyde solution for 24 h before cryopreservation in 30% (*w*/*v*) sucrose.

2.3. Tissue Preparation and Immunohistochemistry

Coronal brain sections (35 µm) were generated using a freezing microtome. For bright-field microscopy, free-floating sections were quenched by incubation in a mixture of 3% H_2O_2 and 10% methanol in Tris-buffered saline (pH 7.6). Non-specific binding sites were blocked using 5% normal serum. Samples were kept overnight at room temperature in a solution containing the primary antibody: rabbit anti-β-syn (1:5000; ab6165, Abcam, Cambridge, UK), rabbit anti-HA (1:15,000; clone C29F4, Cell Signaling, Danvers, MA, USA), or rabbit anti-human α-syn (1:50,000; clone MJFR1, Abcam, Cambridge, UK). Sections were then rinsed and incubated in a biotinylated secondary antibody solution (1:200; Vector Laboratories, Newark, CA, USA). Following treatment with avidin–biotin–horseradish peroxidase complex (ABC Elite kit, Vector Laboratories, Newark, CA, USA), a color reaction was developed using a 3,3′-diaminobenzidine kit (Vector Laboratories, Newark, CA, USA). Sections were mounted on coated slides and coverslipped with Depex (Sigma-Aldrich, St. Louise, MO, USA). For fluorescent labeling, heat-induced epitope retrieval was carried out on free-floating medulla and pons sections with sodium citrate buffer (10 mM plus 0.05% Tween, pH 6.0) for 5 min at 95 °C. Samples were then blocked with 5% normal serum and incubated with rabbit anti-β-syn polyclonal antibody (1:1000; ab6165, Abcam, Cambridge, UK) and mouse anti-HA antibody (1:1000; clone HA-7, Sigma-Aldrich, St. Louise, MO, USA) overnight at 4 °C. Labeling was performed with anti-rabbit Dylight 488 and anti-mouse DyLight 594 (1:300; Vector Laboratories, Newark, CA, USA) antibodies. Sections were mounted on object slides and coverslipped with ProLong™ Gold Antifade Mountant (Invitrogen, Waltham, MA, USA).

2.4. In situ Proximity Ligation Assay (PLA)

Free-floating sections of the medulla oblongata were processed using Duolink (Sigma-Aldrich, St. Louise, MO, USA) according to the manufacturer's protocols as described previously [24–26]. HA and α-syn PLA probes were generated by linking the plus and minus oligonucleotides with primary antibodies anti-HA (clone C29F4, Cell Signaling) and anti-human α-syn (clone syn211, Millipore, Burlington, MA, USA) using a probemaker kit (Duolink, Sigma-Aldrich, Janvier Labs). HA/HA and α-syn/α-syn interactions were detected using a direct PLA method, which required incubating sections overnight in solutions containing the plus and minus PLA probes directly conjugated to the HA (1:250) or human α-syn–antibody (1:100; mouse-anti-Syn211, Millipore, Burlington, MA, USA).

Samples treated only with the plus probe served as negative controls. Following ligation and amplification, specific PLA signals were visualized using a brightfield detection kit (Duolink, Sigma-Aldrich, St. Louise, MO, USA). Sections were mounted on object slides and coverslipped using histomount mounting media (Life Technologies, Carlsbad, CA, USA).

2.5. RT-PCR

Brain tissue from 5 mice per treatment group was used to assess mRNA expression. Extraction of total RNA and analysis of mRNA expression by RT-PCR was carried out as previously described [24]. All viral vectors used in this study contained a WPRE sequence. Comparison of the expression levels of different transcripts, i.e., β-syn, VAMP2, and SNAP25, was therefore carried out by measuring WPRE mRNA levels. Target-specific primer pairs were generated for the WPRE (forward 5′ CAATTCCGTGGTGTTGTCGG and reverse 5′ CAAAGGGAGATCCGACTCGT) and the housekeeping gene hypoxanthine guanine phosphoribosyltransferase (Hprt) (forward: 5′ TCCTCCTCAGACCGCTTTT and reverse: 5′ CCTGGTTCATCATCGCTAATC. RT-PCR-amplified WPRE and Hprt products were run in prestained (Red safe, Intron Biotechnology, Seongnam-Si, Republic of Korea) agarose gels. Images were scanned with an InGenius3 imaging system, acquired with GeneSys software (v.1.5.7.0), and quantified using GeneTools analysis software (v.4.3.14.0, Syngene, Bangalore, India). The ratio of blank corrected raw volume values of WPRE and Hprt were calculated and expressed as WPRE/Hprt ratio.

2.6. Thioflavin-S Staining

Four mice from each experimental group were used for Thioflavin-S labeling. Medulla oblongata sections containing the DMnX were first stained with anti-HA and labeled using a secondary antibody conjugated with Dylight 594, as described above. Stained sections were mounted on glass slides and were incubated with 0.05% Thioflavin-S (Sigma-Aldrich, St. Louise, MO, USA) for 8 min, followed by sequential differentiation in 80–95–95% ethanol (3 min each). Sections were briefly rinsed in water, coverslipped with Prolong Gold antifade reagent (Thermo Fischer, Waltham, MA, USA), and the images were acquired on the same day.

2.7. Image Acquisition

Brightfield tile scan images of the dorsal medulla oblongata were acquired using an Observer.Z1 microscope (Carl Zeiss, Oberkochen, Germany) equipped with a motorized stage using a Plan-Apochromat 20×/0.8 M27 objective (Carl Zeiss, Oberkochen, Germany). Raw images were corrected for camera shading, and tiles were stitched with ZEN 2012 software (Blue edition, Carl Zeiss, Oberkochen, Germany). Confocal stack images were taken with a Plan-Apochromat 63×/1.4 oil objective on a Zeiss LSM800 and illustrated as maximum-intensity projection images. PLA images and high magnification brightfield stack images were generated on an Olympus BX53 widefield light microscope using a 10× Plan-Apochromat and 100×/1.40 UPlanSApo oil objective, respectively. Stack images were processed as minimum intensity projections with Stereoinvestigator® 10 software (MBF Biosciences, Williston, VT, USA). For image analysis purposes, sections assayed with PLA were scanned using an automated upright slide scanning microscope (AxioScan.Z, Carl Zeiss, Oberkochen, Germany).

2.8. Axonal Counts and Image Analysis

HA-immunoreactive axons were counted by a blinded investigator. $N \geq 7$ mice /group were used for these analyses. Sections were analyzed from caudal to rostral in the left hemisphere at pre-defined bregma coordinates in the pons (bregma −5.40 mm), the midbrain (bregma −4.60 mm), and the forebrain (bregma −1.70 mm) with an Axio Scope.A1 brightfield microscope (Carl Zeiss, Oberkochen, Germany) using EC Plan-Neofluar 40× oil objective. HA staining intensity, PLA signal intensity, and area occupied by the

PLA dots were assessed using Fiji (Image J, version 2.1.0/1.53c). Images collected from HA immunostained MO (n = 5 mice/group) and tissue sections processed from PLA ($n \geq 4$ mice/group) were converted to grayscale images and inverted. Background subtraction using a rolling ball radius of 50 pixels was applied. The left (injected side) dorsal vagal complex encompassing the DMnX, nucleus of tractus solitarius, and area postrema was delineated. HA staining intensity was then measured within this delineated area. For PLA image analyses, a fixed intensity threshold was set to automatically outline the PLA dots, and the PLA dots were analyzed using the "analyze particles" function of ImageJ (v.2.1.0/1.3Jc). The intensity of the PLA signal and the percent of area occupied by the PLA dots were measured for each animal.

2.9. Statistical Analyses

Prism 9 (v9.1.0, GraphPad Software, Boston, MA, USA) was used for all statistical analyses. Prior to using parametric tests, the normal distribution of the data was confirmed using the Shapiro–Wilk test for normality. A 2-tailed unpaired t-test was used to compare 2 groups, and a one-way ANOVA followed by Tukey's posthoc test was used to compare three groups. Data were expressed as mean ± standard error of the mean. p-Values less than 0.05 were considered statistically significant.

3. Results

3.1. Effects of β-syn Transduction

To assess whether size, amino acid sequence, and/or synaptic localization contribute to interneuronal protein transfer, we first assessed the spreading potential of a protein highly similar to α-syn, namely β-syn (Figure 1a). For these experiments, mice were treated using a paradigm capable of inducing targeted protein overexpression in the DMnX-containing dMO [22,24]. They received a unilateral injection of AAVs mediating human β-syn expression (AAV-β-syn) into the left vagus nerve and were kept for 6 weeks after surgery (Figure 1b). At this time point, brains were processed for histological assessment of β-syn in coronal sections of the medulla oblongata and pons that were stained with a β-syn antibody (Figure 1c–e). The purpose of these analyses was to detect levels of expression in the dMO and potential spreading (in the pons) of the exogenous protein, i.e., human β-syn. It is noteworthy that β-syn amino acid sequence is highly conserved and features 97% homology between humans and mice [31]. Therefore, antibodies against β-syn, including the reagent used for this study, are not species-specific and would react against both the human and murine protein. To circumvent this limitation, staining of our tissue sections was carried out using a relatively high antibody dilution that allowed us to reduce the basic immunoreactivity due to endogenous β-syn and to detect the effects of AAV-induced overexpression more distinctly. Targeted transduction was indicated by robust β-syn immunoreactivity in the dMO (Figure 1f).

The pattern of overexpression was consistent with the anatomical distribution of vagus-associated neurons and with the results of earlier studies that used the intravagal route of AAV administration for medullary protein overexpression [22,24]. In particular, AAV-mediated β-syn transduction affected cell bodies and neurites in the left DMnX (ipsilateral to the AAV injection) (Figure 1f,g); it was also evident within afferent vagal projections in the left and, to a lesser extent, right nucleus of the tractus solitarius and in the area postrema (Figure 1f,h). Next, coronal sections of the pons were immunostained for β-syn since the detection of β-syn-loaded axons in this brain region would indicate its interneuronal transfer [22,24]. Analyses revealed that strongly labeled axons were scattered throughout pontine sections in AAV-injected mice but not in control specimens from non-injected animals (Figure 1i,j). Taken together, these data suggested that, following its overexpression in the dMO, β-syn was able to spread toward more rostral brain regions and became accumulated within pontine axons. Important limitations of these analyses included the lack of specific detection of endogenous (mouse) vs. exogenous (human) β-syn that prevented a more refined characterization of protein overexpression in the dMO

and a clearer visualization and quantification of the spreading protein in pontine as well as more rostral brain regions.

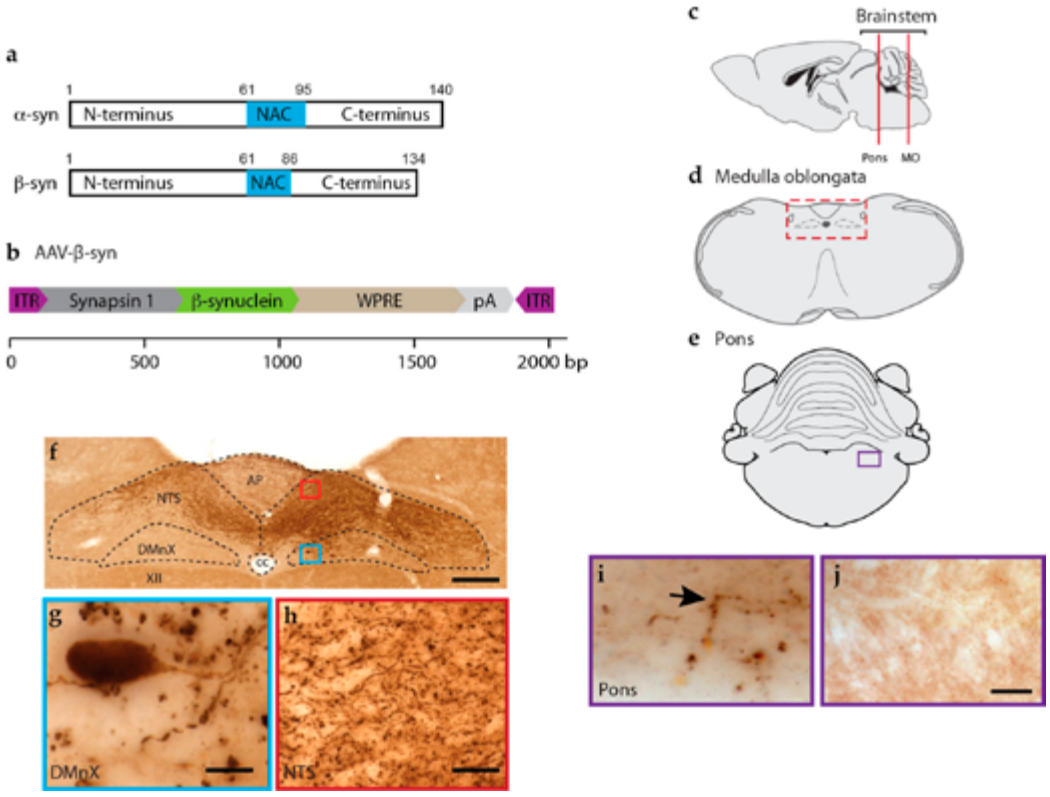

Figure 1. AAV-β-syn injections into the mouse vagus nerve induce increased expression of β-syn in the dMO and trigger its spreading to the pons. (**a**) Schematic illustration of α- and β-syn proteins displaying similarities in size and domain composition. (**b**) AAV-β-syn vector design illustrating the expression cassette flanking two ITRs. The scale displays the size (base pair, bp) of each genetic component. Mice received an injection of AAV-β-syn into the left vagus nerve. At 6 weeks post-surgery, coronal sections of the medulla oblongata and the pons were stained with a β-syn antibody. (**c**) Locations of the medulla oblongata and pontine coronal sections used for histological analyses are illustrated on a longitudinal plane. (**d**) Schematic image of a coronal section of the MO. The rectangular box (red) delineates an area of the dMO corresponding to the area shown in panel f. (**e**) Schematic image of a coronal section of the pons. The rectangular box (purple) delineates an area corresponding to the pontine area shown in panels i and j. (**f**–**h**) Representative image of the dMO showing β-syn immunoreactivity (**f**). Dotted lines in (f) delineate the borders between AP, NTS, DMnX, XII and cc. The blue and red boxes mark the locations of the areas shown at higher magnification in (**g**,**h**). These higher magnification images were acquired from the DMnX (**g**) and NTS (**h**) ipsilateral to the injection side. Scale bars: 200 µm (**f**) and 20 µm (**g**,**h**). (**i**) β-syn immunoreactivity in a representative pontine section displaying β-syn-filled axons (arrow). Scale bar: 10 µm. (**j**) β-syn immunoreactivity in a pontine section collected from an untreated naïve mouse. Scale bar: 10 µm. Abbreviations: XII: nucleus of the hypoglossal nerve; AP: area postrema; cc: central canal; dMO: dorsal medulla oblongata; DMnX: dorsal motor nucleus of the vagus nerve; ITR: inverted terminal repeat; NAC: non-amyloid component; NTS: nucleus tractus solitarius; pA: polyA; WPRE: woodchuck hepatitis virus posttranscriptional regulatory element.

3.2. Overexpression and Spreading of HA-Tagged α-syn

To overcome the technical issue described above, new AAVs were generated that encoded α-syn with an HA tag at its C-terminal end (AAV-β-syn-HA) (Figure 2a). Mice received a single injection of this AAV-β-syn-HA into the left vagus nerve, and 6 weeks later, their brains were processed for histological assessment. For the first set of analyses, coronal tissue sections of the medulla oblongata were immunostained using antibodies raised to detect β-syn or HA. Microscopic images of β-syn immunoreactivity were similar in samples from mice injected with AAV-β-syn-HA as compared to animals treated with AAV-β-syn (cf. Figures 1f and 2b); they showed increased labeling of dMO neurons on a relatively high background staining (Figure 2b). This background staining was abolished when specimens from AAV-β-syn-HA-injected mice were labeled with anti-HA, allowing a clear, unambiguous detection of transgenic human β-syn within vagus-associated dMO neurons (Figure 2c). Next, medullary sections from AAV-β-syn-HA-injected mice were double-labeled with anti-β-syn and anti-HA and processed for immunofluorescence. Results showed consistent co-localization, thus confirming a precise detection of β-syn using the HA antibody (Figure 2d). In particular, double-labeled neuronal cell bodies were evident in the DMnX, indicating neuronal transduction and overexpression (Figure 2d, higher magnification). Anti-β-syn and anti-HA were also used to double-label pontine sections and assess this tissue for the presence of extra-medullary human β-syn. Distinct, co-labeled axons were detected as a result of this analysis, pointing to a caudo-rostral (medullary-to-pontine) spreading of the "entire" (human β-syn plus HA) exogenous protein (Figure 2e).

Having demonstrated the suitability of staining with anti-HA as a means to detect exogenous β-syn in AAV-β-syn-HA-injected mice, a detailed evaluation of protein spreading was performed in coronal sections throughout the brain of these animals that were stained with anti-HA and analyzed with brightfield microscopy. Enlarged, dystrophic axons containing β-syn were observed in all sections of the pons, midbrain, and forebrain that were collected at predefined Bregma coordinates (Figure 2f). Consistent with the results of earlier reports, spreading predominantly affected the side of the brain ipsilateral to the AAV injection and occupied preferential sites; these sites included the locus coeruleus in the pons, the reticular formation (but not the substantia nigra) in the midbrain, and the central nucleus of the amygdala in the basal forebrain [22–24,26,32,33]. For quantification purposes, the number of HA-immunoreactive axons was counted and found to be higher in sections closer to the medulla oblongata, i.e., in the pons, and progressively lower in other more rostral brain regions (Figure 2g). The number of axons containing exogenous β-syn was consistently 60–70% lower on the contralateral as compared to the ipsilateral side of the brain. In particular, when bilateral counts were carried out in the pons of 5 AAV-injected mice, the number of β-syn-labeled axons was found to be 32.6 $\pm$ 6.1 and 87.6 $\pm$ 12.6 contralaterally and ipsilaterally, respectively.

3.3. Lack of Interneuronal Spreading of VAMP2 and SNAP25

The next set of experiments was designed to test the spreading potential of VAMP2 and SNAP25, two proteins that share their synaptic localization with α- and β-syn. To induce overexpression, mice were injected intravagally with AAVs encoding HA-tagged proteins, namely VAMP2-HA and SNAP25-HA (Figure 3a). The rationale for overexpressing tagged proteins was twofold. First, this strategy was chosen in order to improve the detection of the transduced protein, as indicated by the results of experiments using tagged β-syn (see above). Secondly, overexpression of tagged proteins allowed us to standardize our comparative analyses since the same antibody (anti-HA) could be used for quantification of protein spreading after transduction with β-syn, VAMP2, or SNAP25.

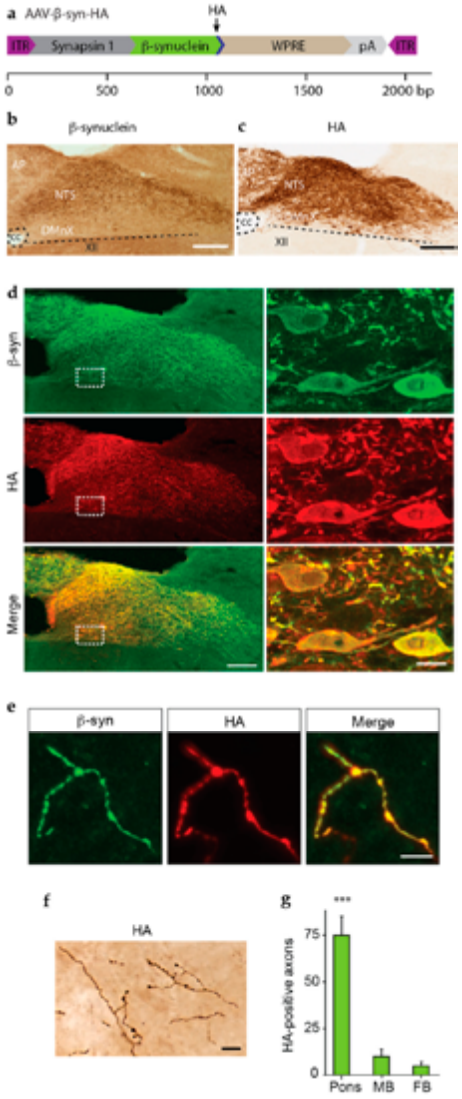

Figure 2. HA tagging allows sensitive and specific detection of β-syn protein. (**a**) Vector design of AAV-β-syn-HA. The scale bar displays the size (base pair, bp) of each genetic component. (**b**–**g**) Mice received an injection of AAV-β-syn-HA into the left vagus nerve and were sacrificed 6 weeks post-surgery. Brain tissue was processed for histological analyses. (**b** and **c**) Coronal sections of the medulla oblongata were immunostained with an antibody against β-syn (**b**) or HA (**c**). (**d**) β-syn (green) and HA (red) double immunolabeling in coronal sections of the dMO visualized by confocal microscopy. Panels on the right show transduced neuronal cell bodies in the DMnX at high magnification. Scale bars: 100 µm (low magnification) and 10 µm (higher magnification). (**e**,**f**) Coronal sections of the pons were either double-labeled with anti-β-syn (green) and anti-HA (red) and imaged with confocal microscopy (**e**) or stained with anti-HA and processed for brightfield microscopy (**f**). Scale bars: 10 µm (**e**) and 5 µm (**f**). (**g**) Counts of HA-positive axons in predefined coronal sections of the pons, MB, and FB. $F_{2,21} = 38.56$, *** $p < 0.0005$. Abbreviations: XII: nucleus of the hypoglossal nerve; AP: area postrema; cc: central canal; DMnX: dorsal motor nucleus of the vagus nerve; ITR: inverted terminal repeat; NTS: nucleus tractus solitarius; pA: polyA; WPRE: woodchuck hepatitis virus posttranscriptional regulatory element.

Cells **2023**, *12*, 569

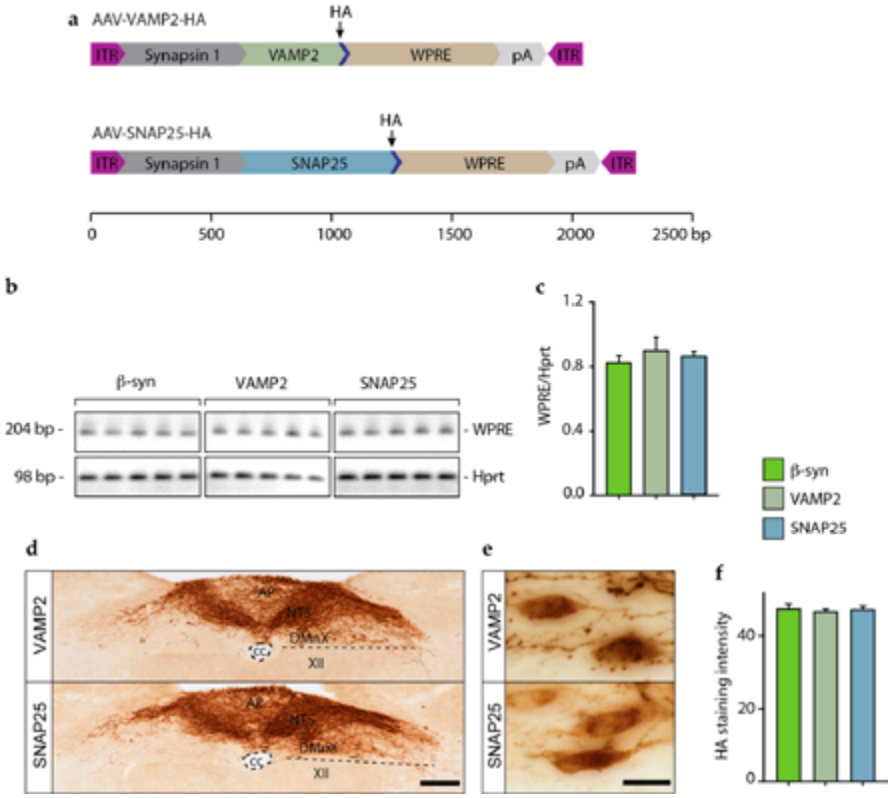

Figure 3. AAV-induced expression of β-syn, VAMP2, and SNAP25 in the dMO. Mice received an intravagal injection of AAV-β-syn-HA, AAV-VAMP2-HA, or AAV-SNAP25-HA and were sacrificed 6 weeks after surgery. (**a**) Vector design of AAV-VAMP2-HA and AAV-SNAP25-HA. The scale bar displays the size (base pair, bp) of each genetic component. (**b**,**c**) Tissue samples of the dMO ipsilateral to the injection site were collected from mice treated with AAV-β-syn-HA, AAV-VAMP2-HA, or AAV-SNAP25-HA (n = 5/group). RT-PCR was performed to detect WPRE and the housekeeping gene Hprt. Specific bands were detected at 204 (WPRE) and 98 (Hprt) bp (**b**). Densitometric measurements of WPRE and Hprt band intensities were plotted as WPRE to Hprt ratio. ANOVA, $F_{2,12} = 0.46$, $p = 0.64$ (**b**). (**d**,**e**) Representative images show medulla oblongata sections from mice injected with AAV-VAMP2-HA or AAV-SNAP25-HA that were stained with anti-HA (**d**). High magnification images show robust VAMP2 or SNAP25 expression within cell bodies of the DMnX (**e**). Scale bars: 200 μm (**d**) and 20 μm (**e**). (**f**) Intensity of HA labeling (arbitrary units) in the dMO ipsilateral to the side of AAV injection ANOVA, $F_{2,12} = 0.23$, $p = 0.80$. Abbreviations: XII: nucleus of the hypoglossal nerve; AP: area postrema; cc: central canal; DMnX: dorsal motor nucleus of the vagus nerve; ITR: inverted terminal repeat; NTS: nucleus tractus solitarius; pA: polyA; WPRE: woodchuck hepatitis virus posttranscriptional regulatory element.

Mice were sacrificed, and brains were collected and sectioned at 6 weeks after treatment with AAV-VAMP2-HA or AAV-SNAP25-HA. To verify and compare gene expression, tissue specimens of the left (ipsilateral to the AAV injection side) dMO were collected from mice injected with AAV-VAMP2-HA or AAV-SNAP25-HA as well as from animals treated with AAV-β-syn-HA. They were then processed for RT-PCR and assayed for the presence of WPRE (an enhancer element contained in all our vector constructs) and Hprt (used as a housekeeping gene) sequences. A 204 bp WPRE band and a 98 bp Hprt band

were present in all samples from AAV-injected animals (Figure 3b). Semi-quantification of band intensities revealed similar levels of WPRE mRNA, indicating that comparable transduction was achieved with each of the three different vectors (Figure 3c). HA immunohistochemistry on medullary tissue sections from mice treated with AAV-VAMP2-HA or AAV-SNAP25-HA showed clear and robust expression of both transgenes in the dMO (Figure 3d). The expression pattern of VAMP-2-HA or SNAP25-HA was similar to the pattern of overexpression of β-syn-HA previously described in animals treated with AAV-β-syn-HA (cf. Figures 2c and 3d); it included a robust protein accumulation within neuronal cell bodies in the left DMnX (Figure 3e). HA staining intensity was also comparable in the left dMO of mice injected with AAV-VAMP2-HA, AAV-SNAP25-HA, or AAV-β-syn-HA, further confirming that similar transduction and overexpression levels were achieved after treatment with three different vectors (Figure 3f).

Protein spreading was assessed and quantified by counting the number of HA-immunolabeled axons in predefined sections of the pons, midbrain, and forebrain. All brain sections from mice injected with AAV-VAMP2-HA were consistently devoid of HA immunoreactivity, whereas only a few very scant HA-labeled axons were seen in pontine (but not midbrain or forebrain) sections from SNAP25-HA-expressing animals. A comparison of these data with findings that were obtained after β-syn-HA overexpression revealed clear differences and indicated that, among these three synaptic proteins (VAMP2, SNAP25, and β-syn), only β-syn possessed overt neuron-to-neuron spreading capability (Table 1).

Table 1. Counts of HA-positive axons in predefined sections of the pons, midbrain, and forebrain.

		Mean Number of HA-Immunoreactive Axons		
Treatment	**Number of Samples**	**Pons ($F_{2,20}$ = 50.24)**	**MB ($F_{2,20}$ = 6.57)**	**FB ($F_{2,20}$ = 5.64)**
AAV-β-syn-HA	8	75 ± 10 ***	10 ± 4 *	5 ± 2 *
AAV-VAMP2-HA	8	0	0	0
AAV-SNAP25-HA	7	3±1	0	0

ANOVA followed by Tukey posthoc test. *** = $p < 0.0001$ when compared with AAV-VAMP2-HA and SNAP25-HA groups; * = $p < 0.05$ when compared with AAV-VAMP2-HA and SNAP25-HA groups.

3.4. Detection and Assessment of Aggregation of HA-Tagged Proteins

Results of earlier reports investigating the spreading properties of α-syn suggest that the formation of protein aggregates could promote interneuronal protein transfer [24,34–37]. In particular, soluble oligomeric species, which were detected by a proximity ligation assay (α-syn/α-syn PLA), were proposed as possible mediators of human α-syn transfer after its AAV-induced overexpression in the mouse dMO [24–26]. Based on these earlier data, a set of experiments was designed here to test the hypothesis that differences in spreading among synaptic proteins may be due, at least in part, to their different ability to form aggregate species.

To detect and compare aggregate formation after AAV-induced overexpression of HA-tagged proteins, a new PLA was developed; the assay was designed to recognize HA molecules in close proximity as markers of protein assembly. An important initial step in the development and validation of this HA/HA PLA was to carry out an experiment in mice that were injected intravagally with AAV vectors encoding for HA-tagged human α-syn (AAV-α-syn-HA) (Figure 4a). Since overexpression-induced aggregation of human α-syn has already been demonstrated using α-syn/α-syn PLA [24], the aim of these experiments was to analyze samples using either α-syn/α-syn or HA/HA PLAs and to determine if the two assays yielded comparable results. In mice injected with AAV-α-syn-HA and sacrificed 6 weeks later, robust protein overexpression was seen in the dMO after staining with an antibody raised against human α-syn; a similar pattern and intensity of immunostaining were observed in tissue sections labeled anti-HA (Figure 4b). Medullary sections from AAV-α-syn-HA-treated animals were then processed for α-syn/α-syn or HA/HA PLA. Results

Cells **2023**, *12*, 569

using the two complementary (negative and positive) α-syn/α-syn or HA/HA PLA probes showed clear labeling in vagus-associated medullary neurons, including cells in the DMnX (Figure 4c). The specificity of this labeling was confirmed by its absence in control samples that were processed without the negative PLA probe (Figure 4c). Further semi-quantitative assessment of PLA reactions was carried out by measuring PLA signal intensity and by calculating the dMO area occupied by the PLA signal. Comparative analyses indicated that similar signal intensities and similar areas of signal distribution characterized samples that were processed either with α-syn/α-syn or HA/HA PLA (Figure 4d). Data therefore demonstrated the suitability and effectiveness of HA/HA PLA as a technique capable of detecting the aggregation of HA-tagged proteins.

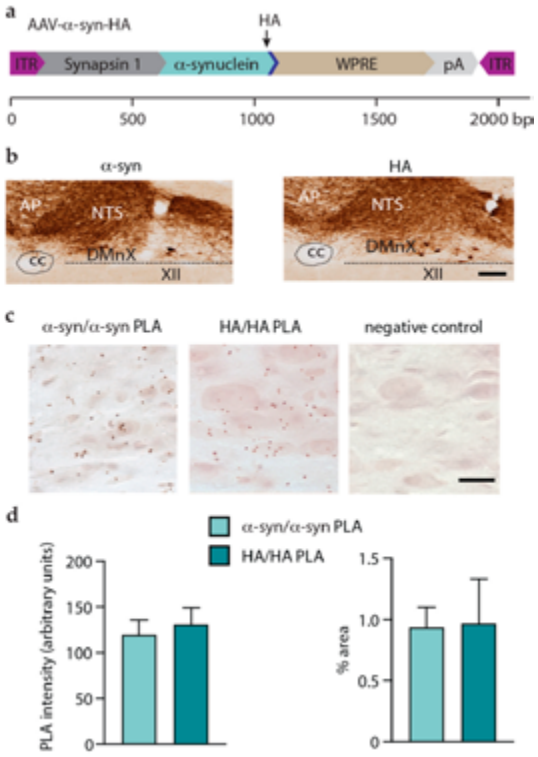

Figure 4. AAV-induced expression and aggregation of α-syn in the dMO. Mice received an injection of AAV-α-syn-HA into the left vagus nerve and were sacrificed 6 weeks after surgery. (**a**) Vector design of AAV-α-syn-HA. The scale bar displays the size (base pair, bp) of each genetic component. (**b**) Representative images of coronal sections of the medulla oblongata that were stained either with an antibody specific to human α-syn or with anti-HA. Scale bar: 100 µm. (**c**) Coronal sections of the medulla oblongata were processed for either α-syn/α-syn or HA/HA PLA. Representative images show specific PLA labeling (reddish brown) in the DMnX. No labeling was instead detected in negative control sections in which one of the HA/HA PLA probes was omitted. Scale bar: 10 µm. (**d**) Image analyses were carried out in the left (ipsilateral to AAV injections) dMO and measured the intensity of the PLA signal (left panel) and the percentage of the area occupied by this signal (right panel). Unpaired *t*-test, $t_4 = 0.48$, $p = 0.90$ (left panel) and $t_4 = 0.08$, $p = 0.32$ (right panel). Abbreviations: XII: nucleus of the hypoglossal nerve; AP: area postrema; cc: central canal; DMnX: dorsal motor nucleus of the vagus nerve; ITR: inverted terminal repeat; NTS: nucleus tractus solitarius; pA: polyA; WPRE: woodchuck hepatitis virus posttranscriptional regulatory element.

HA/HA PLA was then used to investigate protein assembly in mice injected with AAV-β-syn-HA, AAV-VAMP2-HA, or AAV-SNAP25-HA. Analyses indicated clear differences between the first vs. the other two groups of animals. Specific PLA signals were indeed detected in animals overexpressing β-syn-HA, whereas medullary sections from mice overexpressing VAMP2- or SNAP25-HA were consistently devoid of labeling (Figure 5a,b). Further evidence of β-syn-HA aggregation was obtained from the analysis of medullary sections from AAV-β-syn-HA-injected mice stained with Thioflavin-S, a fluorescent dye that binds to amyloid structures. As shown in Figure 5c, Thioflavin-S labeling was detected within DMnX cell bodies and neurites that overexpressed β-syn-HA and were therefore co-stained with anti-HA. Consistent with the results of HA/HA PLA analyses, medullary sections from mice treated with AAV-VAMP2-HA or AAV-SNAP25-HA were devoid of Thioflavin/HA co-localization (Figure 5c). These data revealed the ability of β-syn, but not VAMP2 or SNAP25, to form aggregate species after its overexpression within vagus-associated neurons in the dMO. Together with the results on overexpression-induced protein spreading, these findings also support a relationship between the formation of protein aggregates and interneuronal β-syn transfer.

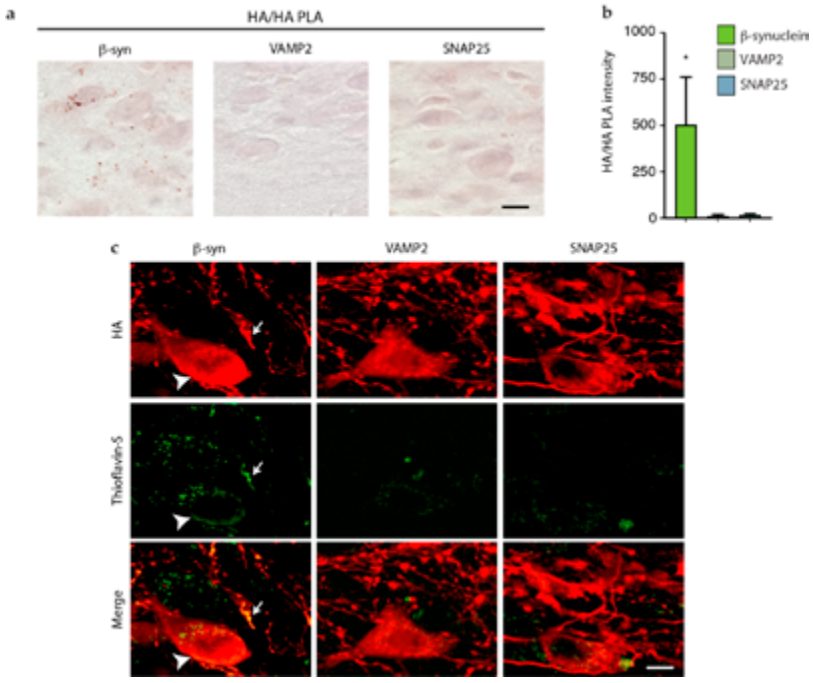

Figure 5. Aggregation of β-syn but not VAMP2 and SNAP25 in dMO. Mice received an injection of AAV-β-syn-HA, AAV-VAMP2-HA, or AAV-SNAP25-HA into the left vagus nerve and were sacrificed 6 weeks after surgery. Coronal sections of the medulla oblongata were processed for HA/HA PLA and HA/Thioflavin-S co-staining. (**a**) Representative images show specific PLA labeling (reddish brown) only in the DMnX of mice treated with AAV-β-syn-HA. Scale bar: 10 µm. (**b**) Image analyses were carried out in the left (ipsilateral to AAV injections) dMO and measured the intensity of the PLA signal. Data are expressed as arbitrary units. ANOVA, $F_{2,11} = 4.79$, * $p < 0.05$. (**c**) Representative images show Thioflavin-S labeling (green) within HA-immunoreactive neurites (arrow) and cell bodies (arrowhead) in the DMnX of mice treated with AAV-β-syn-HA but not AAV-VAMP2-HA or AAV-SNAP25-HA. Scale bar: 10 µm.

4. Discussion

The intravagal route of administration of viral vectors carrying specific coding DNA sequences has been successfully used to induce targeted protein overexpression in the dMO [22–27]. Earlier work has also demonstrated that, through this paradigm, AAV transduction and protein overexpression should remain confined within vagus-associated neurons. This anatomical restriction was evaded, however, when animals were treated intravagally with AAVs delivering human α-syn DNA. In these animals, the detection of human α-syn first in the pons and then in more rostral brain regions indicated a neuron-to-neuron transfer of the exogenous protein that resulted in its progressive spreading throughout the brain [22–27]. Caudo-rostral human α-syn advancement followed a stereotypical pattern and affected brain regions in the pons, midbrain, and forebrain that are anatomically connected to the dMO. The substantia nigra was not among these regions, probably because of its weak direct connections to the DMnX [22,38]. The present study aimed at investigating the interneuronal mobility of proteins other than human α-syn, addressing important questions: Is overexpression in the dMO sufficient to trigger protein spreading? Are synaptic proteins particularly prone to neuron-to-neuron transfer? In addition, do specific protein conformations confer greater protein mobility?

An initial key component of the study was to develop and validate tools and experimental paradigms most suitable to address these questions. The first technical obstacle to overcome related to the fact that basic endogenous protein expression prevented an accurate assessment, quantification, and comparison of the overexpression and potential spreading of the three proteins tested in this study, namely β-syn, VAMP2, or SNAP25. This limitation was successfully overcome by designing and using viral vectors that encoded β-syn, VAMP2, or SNAP25 with an HA tag at their C-terminal ends. Intravagal injections of these vectors induced expression of the tagged proteins that could all (β-syn-, VAMP2- or SNAP25-HA) be readily detected using the same HA antibody. Results of these experiments revealed similar levels of AAV-induced transduction and similar patterns of β-syn-HA, VAMP2-HA, or SNAP25-HA protein overexpression in the dMO. Quite in contrast, analyses of pontine, midbrain, and forebrain sections for the detection of extra-medullary proteins showed marked differences between mice transduced with AAV-β-syn-HA vs. animals injected with either AAV-VAMP2-HA or AAV-SNAP25-HA. In particular, a significant number of β-syn-HA-containing axons was observed in the pons, midbrain, and forebrain of AAV-β-syn-HA-treated animals, whereas transduction with AAV-VAMP2-HA or AAV-SNAP25-HA resulted in negligible or no detection of the corresponding protein in sections rostral to the medulla oblongata. It is noteworthy that cleavage and degradation of the HA tag, which have been reported by earlier investigations [39], might have hampered our assessment of protein overexpression (in the dMO) and protein spreading (in regions rostral to the medulla oblongata) using HA immunoreactivity. HA cleavage and clearance cannot be completely ruled out under our experimental conditions. Nonetheless, our findings do unequivocally indicate accumulation of β-syn-HA in the dMO and caudo-rostral spreading of β-syn-HA since co-labeling analyses consistently detected co-localization of HA and β-syn immunoreactivities.

Our results indicate that overexpression of a protein in the dMO does not necessarily trigger its interneuronal transfer. Similarly, protein size may not be a key factor in determining interneuronal transfer since two proteins with similar molecular weight, namely VAMP2 (13 kDa) and β-syn (14 kDa), displayed very different spreading abilities. Data also suggest that localization within neuronal synapses is not directly linked to protein transfer and is not sufficient to predict the spreading potential of a protein. Indeed, overexpression of α- and β-syn triggered their caudo-rostral spreading, whereas overexpression of VAMP2 or SNAP25, two other synaptic proteins, did not result in their detection and accumulation in brain regions rostral to the medulla oblongata. These marked differences in spreading ability may reflect important features of these synaptic proteins, such as their relative solubility (synucleins) and their ability to stably interact with synaptic membranes (VAMP2 or SNAP25), that could facilitate or impede their spreading potential. Further studies

are warranted to address this hypothesis. On the other hand, taken together, our current findings support the conclusion that similarities in amino acid protein sequence between α- and β-syn are likely responsible for their interneuronal mobility and, ultimately, their ability to spread between interconnected brain regions. Sequence and structural similarities between the two synucleins could underlie shared properties, such as their ability to form aggregates (see below), directly relevant to their spreading behavior.

Results of previous studies support the conclusion that interneuronal α-syn transfer is promoted by the formation of aggregated forms of the protein [24,34–36]. This effect may be related to the ability of aggregated α-syn to interact specifically with proteins involved in the exchange of small molecules between cells [36]. Amino acid sequences can play an important role in determining the ability of proteins to form aggregates. We therefore hypothesized that, due to its similarity to α-syn, β-syn may also aggregate after its overexpression within medullary neurons; this aggregation may then underlie β-syn's property to pass from neuron to neuron. As a corollary to this hypothesis, no significant aggregation would be expected to occur after overexpression of VAMP2 or SNAP25 since both these proteins were shown not to spread outside the dMO. Several conformation-specific antibodies are available to detect α-syn aggregates and have been used to distinguish between monomeric and aggregated forms of the protein [40–43]. No such in situ tools exist for assessing β-syn, VAMP2, or SNAP25 aggregates, and for this reason, another technical challenge of this study was to develop analytical assays capable of detecting β-syn, VAMP2, and SNAP25 assemblies. To achieve this goal, a new in situ PLA was established. PLA is a sensitive detection method that utilizes single-stranded oligonucleotides coupled with antibodies. Quite importantly, earlier studies have validated and used specific PLAs for detecting aggregated α-syn [24,44,45] as well as aggregated forms of other pathogenic proteins [46,47] in tissue from humans and animal models. Previous studies focusing on α-syn aggregation used a human-specific α-syn antibody and verified that this PLA method specifically detected aggregated rather than monomeric α-syn; results of these earlier investigations also indicated that the α-syn/α-syn PLA preferentially recognized oligomeric α-syn species [24,44,45]. Our current strategy was to develop, validate and use a PLA assay targeting the HA tags of α-syn-, β-syn-, VAMP2-, or SNAP25-HA proteins. In the dMO of mice overexpressing human α-syn-HA, this HA/HA PLA generated a specific signal that was comparable in intensity and distribution to the labeling obtained by processing the same tissues with α-syn/α-syn PLA. Following these validation experiments, HA/HA PLA was used to assess medullary sections from animals injected with AAV-β-syn-HA, AAV-VAMP2-HA, or AAV-SNAP25-HA. Results revealed a strong signal in the dMO of mice overexpressing β-syn-HA, whereas medullary tissues from mice overexpressing VAMP2-HA or SNAP25-HA were completely devoid of HA/HA PLA labeling. Further analyses using the fluorescent dye Thioflavin-S confirmed the accumulation of amyloid fibrils in specimens from animals treated with AAV-β-syn-HA but not AAV-VAMP2-HA or AAV-SNAP25-HA. Taken together, these results demonstrated the overexpression-induced formation of β-syn aggregates. They also indicated that spreading occurred only under conditions associated with protein (α- or β-syn) assembly, thus supporting a relationship between aggregation and interneuronal protein transfer.

Our current evidence showing aggregation and spreading of β-syn raises a few important considerations. Previous studies investigating the toxicity and pathogenicity of β-syn have reported findings that are apparently conflicting. Some studies concluded that β-syn, unlike α-syn, has a low propensity to aggregate and induce pathology and, in fact, may even possess protective properties and inhibit α-syn aggregation [48–55]. Other investigations reported that when overexpressed within nigral dopaminergic neurons, β-syn forms proteinase K-resistant aggregates and induces nigral neurodegeneration in rodents [56–58]. A likely explanation for these inconsistent data is that, while β-syn may not itself be an aggregation-prone protein, its assembly may be triggered by external factors. In support of this conclusion, earlier work showed that β-syn is capable of aggregating

and becoming neurotoxic under a variety of conditions that include oxidative stress, presence of dopamine, and exposure to environmental toxins, metals, glycosaminoglycans, or macromolecular-crowding agents [57–59]. Based on these earlier findings, it is reasonable to infer that, in our present model of AAV-mediated β-syn overexpression, one or more of these factors could underlie protein aggregation and interneuronal protein transfer. For example, in mice with overexpression of α-syn in the dMO, an intriguing relationship has recently been reported between α-syn overexpression, oxidative stress, protein aggregation, and spreading [26]. Further studies are warranted to assess whether a similar relationship exists as a result of increased β-syn load. Results of these future studies could not only underscore the important role of oxidative stress in the development of proteinopathies but could also elucidate important mechanisms that may underlie β-syn pathogenicity.

Author Contributions: Conceptualization, M.K., D.A.D.M. and A.U.; experiments, M.K., R.P.-C., M.H., A.R., R.R. and A.U.; data analysis, M.K., R.P.-C., D.A.D.M. and A.U.; writing—review and editing, M.K., R.P.-C., D.A.D.M. and A.U. All authors have read and agreed to the published version of the manuscript.

Funding: This research was funded by the EU Joint Programme-Neurodegenerative Disease Research (JPND 01ED2005B, GBA-PaCTS).

Institutional Review Board Statement: The study was conducted in accordance with the Declaration of Helsinki and approved by the State Agency for Nature, Environment, and Consumer Protection in North-Rhine Westphalia, Germany (84-02.04.2013.A137 and 81-02.04.2017.A384).

Informed Consent Statement: Not applicable.

Data Availability Statement: All data are available in the main text.

Acknowledgments: Authors thank Laura Demmer, Anushka Takhi, and Shirley S. Lee for assistance with the experiments; personnel at the DZNE Light Microscope Facility and Preclinical Center; and Deniz Kirik (Lund University) for providing the β-synuclein plasmid. This work was supported by the EU Joint Programme-Neurodegenerative Disease Research (JPND 01ED2005B, GBA-PaCTS).

Conflicts of Interest: The authors declare no conflict of interest.

References

1. Jucker, M.; Walker, L.C. Propagation and spread of pathogenic protein assemblies in neurodegenerative diseases. *Nat. Neurosci.* **2018**, *21*, 1341–1349. [CrossRef] [PubMed]
2. Spillantini, M.G.; Schmidt, M.L.; Lee, V.M.; Trojanowski, J.Q.; Jakes, R.; Goedert, M. Alpha-synuclein in Lewy bodies. *Nature* **1997**, *388*, 839–840. [CrossRef] [PubMed]
3. Braak, H.; Braak, E. Neuropathological stageing of Alzheimer-related changes. *Acta Neuropathol.* **1991**, *82*, 239–259. [CrossRef]
4. Braak, H.; de Vos, R.A.; Bohl, J.; Del Tredici, K. Gastric alpha-synuclein immunoreactive inclusions in Meissner's and Auerbach's plexuses in cases staged for Parkinson's disease-related brain pathology. *Neurosci. Lett.* **2006**, *396*, 67–72. [CrossRef]
5. Maroteaux, L.; Campanelli, J.T.; Scheller, R.H. Synuclein: A neuron-specific protein localized to the nucleus and presynaptic nerve terminal. *J. Neurosci.* **1988**, *8*, 2804–2815. [CrossRef] [PubMed]
6. Burre, J.; Sharma, M.; Sudhof, T.C. Cell biology and pathophysiology of alpha-synuclein. *Cold Spring Harb. Perspect. Med.* **2018**, *8*, a024091. [CrossRef]
7. Polymeropoulos, M.H.; Lavedan, C.; Leroy, E.; Ide, S.E.; Dehejia, A.; Dutra, A.; Pike, B.; Root, H.; Rubenstein, J.; Boyer, R.; et al. Mutation in the alpha-synuclein gene identified in families with Parkinson's disease. *Science* **1997**, *276*, 2045–2047. [CrossRef] [PubMed]
8. Kruger, R.; Kuhn, W.; Muller, T.; Woitalla, D.; Graeber, M.; Kosel, S.; Przuntek, H.; Epplen, J.T.; Schols, L.; Riess, O. Ala30Pro mutation in the gene encoding alpha-synuclein in Parkinson's disease. *Nat. Genet.* **1998**, *18*, 106–108. [CrossRef]
9. Zarranz, J.J.; Alegre, J.; Gomez-Esteban, J.C.; Lezcano, E.; Ros, R.; Ampuero, I.; Vidal, L.; Hoenicka, J.; Rodriguez, O.; Atares, B.; et al. The new mutation, E46K, of alpha-synuclein causes Parkinson and Lewy body dementia. *Ann. Neurol.* **2004**, *55*, 164–173. [CrossRef]
10. Proukakis, C.; Dudzik, C.G.; Brier, T.; MacKay, D.S.; Cooper, J.M.; Millhauser, G.L.; Houlden, H.; Schapira, A.H. A novel alpha-synuclein missense mutation in Parkinson disease. *Neurology* **2013**, *80*, 1062–1064. [CrossRef]
11. Pasanen, P.; Myllykangas, L.; Siitonen, M.; Raunio, A.; Kaakkola, S.; Lyytinen, J.; Tienari, P.J.; Poyhonen, M.; Paetau, A. Novel alpha-synuclein mutation A53E associated with atypical multiple system atrophy and Parkinson's disease-type pathology. *Neurobiol. Aging* **2014**, *35*, 2180.e1–2180.e5. [CrossRef] [PubMed]

12. Singleton, A.B.; Farrer, M.; Johnson, J.; Singleton, A.; Hague, S.; Kachergus, J.; Hulihan, M.; Peuralinna, T.; Dutra, A.; Nussbaum, R.; et al. alpha-Synuclein locus triplication causes Parkinson's disease. *Science* **2003**, *302*, 841. [CrossRef]
13. Ibanez, P.; Bonnet, A.M.; Debarges, B.; Lohmann, E.; Tison, F.; Pollak, P.; Agid, Y.; Durr, A.; Brice, A. Causal relation between alpha-synuclein gene duplication and familial Parkinson's disease. *Lancet* **2004**, *364*, 1169–1171. [CrossRef]
14. Chiba-Falek, O.; Nussbaum, R.L. Effect of allelic variation at the NACP-Rep1 repeat upstream of the alpha-synuclein gene (SNCA) on transcription in a cell culture luciferase reporter system. *Hum. Mol. Genet.* **2001**, *10*, 3101–3109. [CrossRef] [PubMed]
15. Farrer, M.; Maraganore, D.M.; Lockhart, P.; Singleton, A.; Lesnick, T.G.; de Andrade, M.; West, A.; de Silva, R.; Hardy, J.; Hernandez, D. alpha-Synuclein gene haplotypes are associated with Parkinson's disease. *Hum Mol Genet.* **2001**, *10*, 1847–1851. [CrossRef] [PubMed]
16. Maraganore, D.M.; de Andrade, M.; Elbaz, A.; Farrer, M.J.; Ioannidis, J.P.; Kruger, R.; Rocca, W.A.; Schneider, N.K.; Lesnick, T.G.; Lincoln, S.J.; et al. Collaborative analysis of alpha-synuclein gene promoter variability and Parkinson disease. *JAMA* **2006**, *296*, 661–670. [CrossRef]
17. Fortin, D.L.; Troyer, M.D.; Nakamura, K.; Kubo, S.; Anthony, M.D.; Edwards, R.H. Lipid rafts mediate the synaptic localization of alpha-synuclein. *J. Neurosci.* **2004**, *24*, 6715–6723. [CrossRef]
18. Stockl, M.; Fischer, P.; Wanker, E.; Herrmann, A. Alpha-synuclein selectively binds to anionic phospholipids embedded in liquid-disordered domains. *J. Mol. Biol.* **2008**, *375*, 1394–1404. [CrossRef]
19. Braak, H.; Del Tredici, K.; Rub, U.; de Vos, R.A.; Jansen Steur, E.N.; Braak, E. Staging of brain pathology related to sporadic Parkinson's disease. *Neurobiol. Aging* **2003**, *24*, 197–211. [CrossRef]
20. Goedert, M.; Spillantini, M.G.; Del Tredici, K.; Braak, H. 100 years of Lewy pathology. *Nat. Rev. Neurol.* **2013**, *9*, 13–24. [CrossRef]
21. Henderson, M.X.; Henrich, M.T.; Geibl, F.F.; Oertel, W.H.; Brundin, P.; Surmeier, D.J. The roles of connectivity and neuronal phenotype in determining the pattern of alpha-synuclein pathology in Parkinson's disease. *Neurobiol. Dis.* **2022**, *168*, 105687. [CrossRef] [PubMed]
22. Ulusoy, A.; Rusconi, R.; Perez-Revuelta, B.I.; Musgrove, R.E.; Helwig, M.; Winzen-Reichert, B.; Di Monte, D.A. Caudo-rostral brain spreading of alpha-synuclein through vagal connections. *EMBO Mol. Med.* **2013**, *5*, 1119–1127. [CrossRef] [PubMed]
23. Ulusoy, A.; Musgrove, R.E.; Rusconi, R.; Klinkenberg, M.; Helwig, M.; Schneider, A.; Di Monte, D.A. Neuron-to-neuron alpha-synuclein propagation in vivo is independent of neuronal injury. *Acta Neuropathol. Commun.* **2015**, *3*, 13. [CrossRef] [PubMed]
24. Helwig, M.; Klinkenberg, M.; Rusconi, R.; Musgrove, R.E.; Majbour, N.K.; El-Agnaf, O.M.; Ulusoy, A.; Di Monte, D.A. Brain propagation of transduced alpha-synuclein involves non-fibrillar protein species and is enhanced in alpha-synuclein null mice. *Brain* **2016**, *139*, 856–870. [CrossRef] [PubMed]
25. Helwig, M.; Ulusoy, A.; Rollar, A.; O'Sullivan, S.A.; Lee, S.S.L.; Aboutalebi, H.; Pinto-Costa, R.; Jevans, B.; Klinkenberg, M.; Di Monte, D.A. Neuronal hyperactivity-induced oxidant stress promotes in vivo alpha-synuclein brain spreading. *Sci. Adv.* **2022**, *8*, eabn0356. [CrossRef] [PubMed]
26. Musgrove, R.E.; Helwig, M.; Bae, E.J.; Aboutalebi, H.; Lee, S.J.; Ulusoy, A.; Di Monte, D.A. Oxidative stress in vagal neurons promotes parkinsonian pathology and intercellular alpha-synuclein transfer. *J. Clin. Invest.* **2019**, *129*, 3738–3753. [CrossRef]
27. Rusconi, R.; Ulusoy, A.; Aboutalebi, H.; Di Monte, D.A. Long-lasting pathological consequences of overexpression-induced alpha-synuclein spreading in the rat brain. *Aging Cell* **2018**, *17*, e12727. [CrossRef]
28. Jakes, R.; Spillantini, M.G.; Goedert, M. Identification of two distinct synucleins from human brain. *FEBS Lett.* **1994**, *345*, 27–32. [CrossRef]
29. Burre, J.; Sharma, M.; Tsetsenis, T.; Buchman, V.; Etherton, M.R.; Sudhof, T.C. Alpha-synuclein promotes SNARE-complex assembly in vivo and in vitro. *Science* **2010**, *329*, 1663–1667. [CrossRef]
30. Sudhof, T.C.; Rothman, J.E. Membrane fusion: Grappling with SNARE and SM proteins. *Science* **2009**, *323*, 474–477. [CrossRef]
31. Vigneswara, V.; Cass, S.; Wayne, D.; Bolt, E.L.; Ray, D.E.; Carter, W.G. Molecular ageing of alpha- and Beta-synucleins: Protein damage and repair mechanisms. *PLoS ONE* **2013**, *8*, e61442. [CrossRef] [PubMed]
32. van der Kooy, D.; Koda, L.Y.; McGinty, J.F.; Gerfen, C.R.; Bloom, F.E. The organization of projections from the cortex, amygdala, and hypothalamus to the nucleus of the solitary tract in rat. *J. Comp. Neurol.* **1984**, *224*, 1–24. [CrossRef] [PubMed]
33. Ter Horst, G.J.; Toes, G.J.; Van Willigen, J.D. Locus coeruleus projections to the dorsal motor vagus nucleus in the rat. *Neuroscience* **1991**, *45*, 153–160. [CrossRef]
34. Kim, C.; Ho, D.H.; Suk, J.E.; You, S.; Michael, S.; Kang, J.; Joong Lee, S.; Masliah, E.; Hwang, D.; Lee, H.J.; et al. Neuron-released oligomeric alpha-synuclein is an endogenous agonist of TLR2 for paracrine activation of microglia. *Nat. Commun.* **2013**, *4*, 1562. [CrossRef] [PubMed]
35. Danzer, K.M.; Kranich, L.R.; Ruf, W.P.; Cagsal-Getkin, O.; Winslow, A.R.; Zhu, L.; Vanderburg, C.R.; McLean, P.J. Exosomal cell-to-cell transmission of alpha synuclein oligomers. *Mol. Neurodegener.* **2012**, *7*, 42. [CrossRef] [PubMed]
36. Reyes, J.F.; Sackmann, C.; Hoffmann, A.; Svenningsson, P.; Winkler, J.; Ingelsson, M.; Hallbeck, M. Binding of alpha-synuclein oligomers to Cx32 facilitates protein uptake and transfer in neurons and oligodendrocytes. *Acta Neuropathol.* **2019**, *138*, 23–47. [CrossRef] [PubMed]
37. Elfarrash, S.; Jensen, N.M.; Ferreira, N.; Betzer, C.; Thevathasan, J.V.; Diekmann, R.; Adel, M.; Omar, N.M.; Boraie, M.Z.; Gad, S.; et al. Organotypic slice culture model demonstrates inter-neuronal spreading of alpha-synuclein aggregates. *Acta Neuropathol. Commun.* **2019**, *7*, 213. [CrossRef]

38. Pinto-Costa, R.; Harbachova, E.; La Vitola, P.; Di Monte, D.A. Overexpression-induced alpha-synuclein brain spreading. *Neurotherapeutics* **2022**, 1–14. [CrossRef]
39. Schembri, L.; Dalibart, R.; Tomasello, F.; Legembre, P.; Ichas, F.; De Giorgi, F. The HA tag is cleaved and loses immunoreactivity during apoptosis. *Nat. Methods* **2007**, *4*, 107–108. [CrossRef]
40. Kovacs, G.G.; Wagner, U.; Dumont, B.; Pikkarainen, M.; Osman, A.A.; Streichenberger, N.; Leisser, I.; Verchere, J.; Baron, T.; Alafuzoff, I.; et al. An antibody with high reactivity for disease-associated alpha-synuclein reveals extensive brain pathology. *Acta Neuropathol.* **2012**, *124*, 37–50. [CrossRef]
41. Vaikath, N.N.; Majbour, N.K.; Paleologou, K.E.; Ardah, M.T.; van Dam, E.; van de Berg, W.D.; Forrest, S.L.; Parkkinen, L.; Gai, W.P.; Hattori, N.; et al. Generation and characterization of novel conformation-specific monoclonal antibodies for alpha-synuclein pathology. *Neurobiol. Dis.* **2015**, *79*, 81–99. [CrossRef]
42. Covell, D.J.; Robinson, J.L.; Akhtar, R.S.; Grossman, M.; Weintraub, D.; Bucklin, H.M.; Pitkin, R.M.; Riddle, D.; Yousef, A.; Trojanowski, J.Q.; et al. Novel conformation-selective alpha-synuclein antibodies raised against different in vitro fibril forms show distinct patterns of Lewy pathology in Parkinson's disease. *Neuropathol. Appl. Neurobiol.* **2017**, *43*, 604–620. [CrossRef]
43. Kumar, S.T.; Jagannath, S.; Francois, C.; Vanderstichele, H.; Stoops, E.; Lashuel, H.A. How specific are the conformation-specific alpha-synuclein antibodies? Characterization and validation of 16 alpha-synuclein conformation-specific antibodies using well-characterized preparations of alpha-synuclein monomers, fibrils and oligomers with distinct structures and morphology. *Neurobiol. Dis.* **2020**, *146*, 105086. [PubMed]
44. Mazzetti, S.; Basellini, M.J.; Ferri, V.; Cassani, E.; Cereda, E.; Paolini, M.; Calogero, A.M.; Bolliri, C.; De Leonardis, M.; Sacilotto, G.; et al. alpha-Synuclein oligomers in skin biopsy of idiopathic and monozygotic twin patients with Parkinson's disease. *Brain* **2020**, *143*, 920–931. [CrossRef] [PubMed]
45. Roberts, R.F.; Wade-Martins, R.; Alegre-Abarrategui, J. Direct visualization of alpha-synuclein oligomers reveals previously undetected pathology in Parkinson's disease brain. *Brain* **2015**, *138*, 1642–1657. [CrossRef] [PubMed]
46. Kamali-Moghaddam, M.; Pettersson, F.E.; Wu, D.; Englund, H.; Darmanis, S.; Lord, A.; Tavoosidana, G.; Sehlin, D.; Gustafsdottir, S.; Nilsson, L.N.; et al. Sensitive detection of Abeta protofibrils by proximity ligation—relevance for Alzheimer's disease. *BMC Neurosci.* **2010**, *11*, 124. [CrossRef] [PubMed]
47. Bengoa-Vergniory, N.; Velentza-Almpani, E.; Silva, A.M.; Scott, C.; Vargas-Caballero, M.; Sastre, M.; Wade-Martins, R.; Alegre-Abarrategui, J. Tau-proximity ligation assay reveals extensive previously undetected pathology prior to neurofibrillary tangles in preclinical Alzheimer's disease. *Acta Neuropathol. Commun.* **2021**, *9*, 18. [CrossRef]
48. Biere, A.L.; Wood, S.J.; Wypych, J.; Steavenson, S.; Jiang, Y.; Anafi, D.; Jacobsen, F.W.; Jarosinski, M.A.; Wu, G.M.; Louis, J.C.; et al. Parkinson's disease-associated alpha-synuclein is more fibrillogenic than beta- and gamma-synuclein and cannot cross-seed its homologs. *J. Biol. Chem.* **2000**, *275*, 34574–34579. [CrossRef]
49. Brown, J.W.; Buell, A.K.; Michaels, T.C.; Meisl, G.; Carozza, J.; Flagmeier, P.; Vendruscolo, M.; Knowles, T.P.; Dobson, C.M.; Galvagnion, C. Beta-synuclein suppresses both the initiation and amplification steps of alpha-synuclein aggregation via competitive binding to surfaces. *Sci.Rep.* **2016**, *6*, 36010. [CrossRef]
50. Giasson, B.I.; Murray, I.V.; Trojanowski, J.Q.; Lee, V.M. A hydrophobic stretch of 12 amino acid residues in the middle of alpha-synuclein is essential for filament assembly. *J. Biol. Chem.* **2001**, *276*, 2380–2386. [CrossRef]
51. Hayashi, J.; Carver, J.A. Beta-synuclein: An enigmatic protein with diverse functionality. *Biomolecules* **2022**, *12*, 142. [CrossRef] [PubMed]
52. Jain, M.K.; Singh, P.; Roy, S.; Bhat, R. Comparative analysis of the conformation, aggregation, interaction, and fibril morphologies of human alpha-, beta-, and gamma-synuclein proteins. *Biochemistry* **2018**, *57*, 3830–3848. [CrossRef] [PubMed]
53. Leitao, A.; Bhumkar, A.; Hunter, D.J.B.; Gambin, Y.; Sierecki, E. Unveiling a selective mechanism for the inhibition of alpha-synuclein aggregation by beta-synuclein. *Int. J. Mol. Sci.* **2018**, *19*, 334. [CrossRef] [PubMed]
54. Uversky, V.N.; Li, J.; Souillac, P.; Millett, I.S.; Doniach, S.; Jakes, R.; Goedert, M.; Fink, A.L. Biophysical properties of the synucleins and their propensities to fibrillate: Inhibition of alpha-synuclein assembly by beta- and gamma-synucleins. *J. Biol. Chem.* **2002**, *277*, 11970–11978. [CrossRef]
55. Zibaee, S.; Fraser, G.; Jakes, R.; Owen, D.; Serpell, L.C.; Crowther, R.A.; Goedert, M. Human beta-synuclein rendered fibrillogenic by designed mutations. *J. Biol. Chem.* **2010**, *285*, 38555–38567. [CrossRef]
56. Raina, A.; Leite, K.; Guerin, S.; Mahajani, S.U.; Chakrabarti, K.S.; Voll, D.; Becker, S.; Griesinger, C.; Bahr, M.; Kugler, S. Dopamine promotes the neurodegenerative potential of beta-synuclein. *J. Neurochem.* **2021**, *156*, 674–691. [CrossRef]
57. Taschenberger, G.; Toloe, J.; Tereshchenko, J.; Akerboom, J.; Wales, P.; Benz, R.; Becker, S.; Outeiro, T.F.; Looger, L.L.; Bahr, M.; et al. Beta-synuclein aggregates and induces neurodegeneration in dopaminergic neurons. *Ann. Neurol.* **2013**, *74*, 109–118. [CrossRef]
58. Landeck, N.; Buck, K.; Kirik, D. Toxic effects of human and rodent variants of alpha-synuclein in vivo. *Eur. J. Neurosci.* **2017**, *45*, 536–547. [CrossRef]
59. Yamin, G.; Munishkina, L.A.; Karymov, M.A.; Lyubchenko, Y.L.; Uversky, V.N.; Fink, A.L. Forcing nonamyloidogenic beta-synuclein to fibrillate. *Biochemistry* **2005**, *44*, 9096–9107. [CrossRef]

4-GENERAL DISCUSSION

A significant characteristic feature of neurodegenerative diseases is the progressive accumulation of aggregation-prone proteins, such as α-syn, Aβ, tau, TDP-43, and huntingtin (htt) (Jucker and Walker, 2018; Spillantini et al., 1997). Neuropathological studies have identified that the development and progression of proteinopathy in these diseases are dynamic, i.e., it progresses and spreads from the initiation site to other brain regions in a stereotypical pattern (Braak et al., 2003b; Brettschneider et al., 2015; Thal et al., 2002). However, we know very little about the factors that play a role in this process.

To address the knowledge gap, we first developed an animal model that effectively replicates the caudo-rostral spreading of α-syn and then elucidated mechanisms and pathways involved in this phenomenon. The caudo-rostral spreading model is generated by injecting AAV vectors into the vagus nerve, a site of translational relevance to PD, to induce α-syn expression. The model is characterized by specific α-syn expression in the vagus nerve connected nuclei and terminals (aka., vagal complex). With time, it features interneuronal α-syn spreading from the donor neurons of the vagal complex towards recipient neurons in the frontal brain regions. This model offers several advantages in reproducing PD pathology. First, it generates relatively physiological levels of α-syn expression. A 3-fold increase in the dorsal medulla oblongata tissue in α-syn mRNA levels was observed as compared to endogenous levels of α-syn (Ulusoy et al., 2013). It is important to note that, although this tissue level mRNA measurement does not reflect the fold-change within a transduced neuron, the fine dissection of the region of interest ensures that the level of overexpression is not much overestimated. Helwig et al., (2022) (Paper VII) further attempted to control the interneuronal α-syn levels by inducing its expression using conditional α-syn expressing mice and successfully reproducing interneuronal α-syn spreading. This mouse line used an endogenous Rosa 26 promoter and allowed a physiological level of the transgene expression. Taken together, inducing mild to moderate increase of α-syn expression in the vagal complex is sufficient to promote its spreading.

Another significant merit of the vagal model is that it faithfully reproduces the entire process of neuron-to-neuron transfer of α-syn, including neuronal release and uptake. The fact that the expression and the spreading were induced by a AAV-mediated gene transfer allowed α-syn to be (1) expressed within the neurons, (2) go through post-translational modifications, (3) be released from the donor neuron, and (4) be taken up by the recipient neurons. Altogether this sequence of biological events allowed us to reproduce molecular mechanisms involved in cell-to-cell α-syn transfer. Finally, the model features mild but clear spreading to frontal brain regions allowing the detection of subtle changes. This feature makes this model ideal for therapeutic interventions. However, a limitation of this model is the absence of α-syn accumulation in the substantia nigra and the lack of DAergic neurodegeneration. Therefore, modeling behavioral and functional aspects associated with nigral pathology and DAergic neurodegeneration of PD is not possible using this specific model.

The "vagal model" has been instrumental in deepening our understanding of the mechanisms responsible for interneuronal α-syn transfer. Our findings indicate that the spreading process depends not on cell death and the subsequent release of α-syn from the dying neurons but on active biological path-

ways (Ulusoy et al., 2015). Indeed, neurodegeneration reduced caudo-rostral spreading of α-syn (Rusconi et al., 2018; Ulusoy et al., 2015). The spreading phenomenon also triggered long-lasting alterations, not only within the vagal complex targeted by the viral-vector-mediated α-syn transduction but also in brain regions situated anterior to the medulla oblongata, which were impacted by the spread of α-syn. These changes were characterized by significant neurodegeneration and inflammation, including cell death, astrogliosis, and microgliosis, and they progressed independently of α-syn spreading (Rusconi et al., 2018). These findings hold notable implications not just for comprehending the enduring effects of caudo-rostral α-syn propagation but also for elucidating the involvement of cell networks (both neuronal and neuron-glia networks) implicated in PD. While this habilitation thesis did not investigate the role of neuronal circuitry and neuron-glia networks, future studies should explore this aspect of interneuronal α-syn spreading and its functional consequences in both the brain and peripheral regions.

Several studies used in this habilitation thesis have documented and validated the correlation between increased spreading and oligomer formation (Helwig et al., 2016; Helwig et al., 2022; Klinkenberg et al., 2023; Musgrove et al., 2019). In addition to the correlation between increased spreading and oligomer formation, it is noteworthy that recipient neurons were found not to contain fibrillar α-syn (Helwig et al., 2016). These findings suggest that while the aggregation process (specifically oligomerization) of α-syn is associated with spreading, the occurrence of neuron-to-neuron α-syn transfer does not necessarily rely on fibrillar forms or templating. It is likely that the templating and seeding of endogenous α-syn represent subsequent pathological events. This insight provides valuable information regarding the sequential progression of α-syn pathology and its relationship to spreading mechanisms.

A principal finding of these work demonstrated that oxidative stress plays a crucial role in interneuronal α-syn spreading. Specifically, we observed the formation of an oxidative modification of α-syn protein. Both in vivo and in vitro observations suggested that nitrated α-syn are more likely to be transferred between neurons (Musgrove et al., 2019). We also investigated conditions that can increase oxidative stress in the DMX neurons and found that neuronal activity is one such condition. Increased neuronal activity leads to heightened oxidative stress, particularly mitochondrial oxidative stress, resulting in the aggregation and nitration of α-syn, ultimately leading to increased spreading. In summary, our experiments yielded valuable insights into the mechanisms underlying α-syn propagation, emphasizing the importance of oxidative stress and neuronal activity in driving this process. These findings have several therapeutic implications and implicated possible targets for interventions at early stages of PD, such as targeting oxidative stress and reducing nitration of α-syn.

Could targeting oxidative stress serve as a disease-modifying treatment for PD? The involvement of oxidative stress in the pathogenesis of PD has long been recognized, leading to numerous experimental and clinical studies attempting to intervene in ROS formation as a means to counteract PD pathology and disease symptoms (Chang and Chen, 2020). However, like many other trials investigating disease-modifying treatments for PD, these endeavors have not yielded conclusive evidence for beneficial effects in PD patients. Two major factors contribute to these failures: 1) the lack of animal models with high predictive value (Van Den Berge and Ulusoy, 2022), and 2) issues related to clinical design, including patient selection and endpoint measures of symptoms (Lo et al., 2022; Mari and Mestre, 2022).

Prior to clinical trials, the most commonly used preclinical models for PD aim to replicate the degeneration of nigrostriatal neurons, typically achieved through toxin models such as MPTP or 6-OHDA (Van Den Berge and Ulusoy, 2022). While these models serve various purposes, such as testing dopamine replacement therapies or dyskinesia treatments, they often induce severe pathology in the nigrostriatal system and are based on a single biological trigger, such as inhibition of mitochondrial complex 1. It is important to note that these models do not fully replicate the essential pathological feature of α-syn aggregation and propagation, which is a critical hallmark, potential biomarker, and a target for future clinical trial designs. The introduction of novel PD pathology models, such as the PFF injection model, AAV-mediated α-syn overexpression model, and the vagal model discussed in this habilitation thesis (Van Den Berge and Ulusoy, 2022), holds great promise for enhancing the translational value of preclinical models. However, it is crucial to recognize that no single model, including the PFF injection or the vagus model, can fully reproduce the entire spectrum of pathology and symptoms observed in PD. Therefore, it is essential to utilize a combination of these preclinical models before proceeding to clinical trials, as they can complement each other and enhance predictive value by capturing different aspects and mechanisms of α-syn pathology.

The second issue that can be attributed to the cause of failed clinical trials are related to clinical trial design. These trials often recruited late stage PD patients, where nigral neurodegeneration has been mostly completed (Kordower et al., 2013). This is partly due to the limited availability of diagnostic tools for early-stage detection of the disease. Another common reason for failure of PD disease-modification trials is the lack of end-points that could sensitively detect disease progression (Mari and Mestre, 2022). The current standard of disease scoring is the Movement Disorder Society's Unified Parkinson's Disease Rating Scale (MDS-UPDRS) shows a marked floor effect, reliability concerns, and reduced sensitivity in capturing early PD progression (Regnault et al., 2019). Recent advancements have focused on enhancing end-points, improving our ability to identify high-risk patients such as GBA mutation carriers or those with REM sleep behavior disorder, and introducing novel biomarker developments and advanced neuroimaging techniques (Lo et al., 2022; Mari and Mestre, 2022; Mitchell et al., 2021; Siderowf et al., 2023). These developments have placed us in a favorable position where the existing unmet conditions can now be addressed.

In conclusion, our development of an animal model replicating the caudo-rostral spreading of α-syn has provided valuable insights into the mechanisms of interneuronal α-syn transfer. This model, with its physiological α-syn levels and faithful replication of neuron-to-neuron transfer, has allowed us to study important biological pathways involved in α-syn propagation. We have identified oxidative stress, nitration and aberrant neuronal activity as causes of α-syn propagation and potential therapeutic targets for developing novel disease modifying treatments for PD. With recent advancements in biomarker development, imaging techniques, and patient identification/stratification, we are now better positioned to address these unmet conditions and pave the way for effective interventions and disease-modifying therapies in PD.

5- SUMMARY

Parkinson's disease is a neurodegenerative movement disorder characterized by the degeneration of dopamine-producing neurons in the substantia nigra pars compacta. Despite current therapies providing symptomatic relief, there is still no cure or treatment option available to slow disease progression. A key pathological feature of PD is the formation of protein aggregates called Lewy bodies, predominantly composed of α-synuclein. Although the disease is characterized by the loss of neurons in a particular brain region, i.e., substantia nigra pars compacta, α-synuclein pathology is widespread. The pathology is present in several brain regions but also in peripheral organs, particularly in the gut. Mounting evidence suggests that α-synuclein pathology spreads predictably in various brain regions, with the vagus nerve identified as a potential route for α-synuclein propagation from the peripheral organs to the brain. The exact molecular mechanisms underlying this propagation are not known. This thesis addresses the knowledge gap regarding the spreading of α-synuclein pathology. Experimental animal models are employed to replicate interneuronal α-synuclein spreading and to investigate hypotheses related to cell death, oxidative stress, aggregation, and neuronal activity. By utilizing these models, the experiments conducted as part of this thesis aim to uncover the mechanisms underlying α-synuclein propagation and shed light on the factors influencing its spread. Findings from these experiments have provided valuable insights into PD pathogenesis. The results suggest that interneuronal α-synuclein spreading is associated with aggregate formation, oxidative stress, and increased neuronal activity, providing evidence for the contribution of these processes to disease progression. Furthermore, the study highlighted the importance of nitrated and oligomeric forms of the protein in the propagation of pathology, demonstrating the potential role of these species for further spreading. These findings significantly contribute to our understanding of PD and provide insights into potential therapeutic targets for disease-modifying treatments. By elucidating the mechanisms of α-synuclein propagation, this thesis lays the foundation for future studies aimed at developing novel interventions to halt or slow the progression of Parkinson's disease. Ultimately, these efforts may lead to the development of more effective treatment strategies that target the disease's underlying pathology.

6-BESCHREIBUNG DER BEITRÄGE IN DEN ORIGINALARBEITEN

Diese Habilitationsschrift wurde auf der Grundlage von acht Originalarbeiten verfasst, an denen auch andere Autoren beteiligt waren. Ich bin der einzige Erstautor von drei dieser Originalmanuskripte (Ulusoy et al., 2013, 2015 und 2017), in denen ich der Hauptverantwortliche für die Durchführung der Experimente war. Dazu gehören alle chirurgischen Eingriffe, die meisten histologischen Färbungen, Mikroskopie und Bewertungen (einschließlich Quantifizierung der Ausbreitung und Stereologie), die Erstellung aller Abbildungen und das Verfassen des Manuskripts zusammen mit dem letzten Autor. Wichtig ist, dass ich die Technik der Vagus-Chirurgie und die Methode zur Quantifizierung der Ausbreitung entwickelt habe, die in mehreren anderen Studien verwendet wurde, einschließlich, aber nicht beschränkt auf die Studien in dieser Arbeit. Eine wichtige Anmerkung und Anerkennung, die erwähnt werden muss, ist der Beitrag von Dr. Phillips. Er hat alle immunhistochemischen Färbungen der Magenwand in dem in Ulusoy et al. (2017) veröffentlichten Manuskript durchgeführt. In Klinkenberg et al. (2023) bin ich der alleinige Letztautor, wobei ich mit Dr. Klinkenberg bei der Planung und Durchführung der Experimente und der Vorbereitung des Manuskripts zusammengearbeitet habe. Ich habe auch alle Proximity Ligation Assay Experimente für diese Studie durchgeführt, die in zwei Hauptabbildungen des Manuskripts resultierten. In Helwig et al., 2022, bin ich der zweite gemeinsame Autor (Helwig et al., 2022). In diesem Manuskript leistete Dr. Helwig einen wesentlichen Beitrag zur Konzeption der Experimente, führte den Großteil der Operationen durch und analysierte die Ausbreitung. Neben meinem konzeptionellen Beitrag führte ich alle PLA-Experimente und deren Quantifizierungen durch, führte immunhistochemische Analysen durch, analysierte und überwachte sie und bereitete die Abbildungen für die endgültige Veröffentlichung vor. Zusammen mit dem letzten Autor des Manuskripts (Dr. Di Monte) habe ich wesentlich zur endgültigen Fassung des schriftlichen Manuskripts beigetragen. Bei allen anderen Manuskripten, bei denen ich entweder der zweiterste oder zweitletzte Autor bin (Helwig, 2016-vorletzter Autor; Rusconi et al., 2018-zweiter Autor; Musgrove et al., 2019-vorletzter Autor) Ich habe maßgeblich an der Konzeption der Studien, der Erstellung der Abbildungen und dem Verfassen des Manuskripts mitgewirkt. In Helwig et al. (2016) habe ich Dr. Helwig bei der Etablierung des Vagusinjektionsmodells bei Mäusen betreut. Ich habe neue Techniken in das Labor eingeführt: Ich habe Proximity Ligation Assays entwickelt und etabliert und bestätigungsspezifische Antikörperfärbungen zum Nachweis oligomerer und fibrillärer Formen von a-syn eingeführt. Bei Rusconi et al. (2018) führte ich alle chirurgischen Eingriffe durch und beaufsichtigte Dr. Rusconi bei der Quantifizierung der Transduktion und Ausbreitung. Außerdem habe ich Dr. Aboutalebi bei der Bewertung des Mikroglia-Phänotyps und der Stereologie im Locus coeruleus beaufsichtigt. Ich habe stereologische Quantifizierungen in der DMX und in der zentralen Amygdala durchgeführt. In Musgrove et al. (2019) führte Dr. Musgrove Paraquat-Behandlungen und stereologische Quantifizierungen im DMX durch und etablierte die DHE-Behandlung zum Nachweis von oxidativem Stress in situ innerhalb der cholinergen Neuronen. Ich habe den Fluoreszenznachweis von PLA etabliert, PLA-Assays durchgeführt und quantifiziert sowie Bildanalysen durchgeführt. Ich habe Dr. Aboutalebi bei der Etablierung von PLA und der quantitativen Bildanalyse an ko-kultivierten BiFC-Zellen betreut.

7-REFERENCES

Abounit, S., Bousset, L., Loria, F., Zhu, S., de Chaumont, F., Pieri, L., Olivo-Marin, J.C., Melki, R., and Zurzolo, C. (2016). Tunneling nanotubes spread fibrillar alpha-synuclein by intercellular trafficking of lysosomes. EMBO J 35, 2120-2138.

Ahlskog, J.E., and Muenter, M.D. (2001). Frequency of levodopa-related dyskinesias and motor fluctuations as estimated from the cumulative literature. Mov Disord 16, 448-458.

Alafuzoff, I., Ince, P.G., Arzberger, T., Al-Sarraj, S., Bell, J., Bodi, I., Bogdanovic, N., Bugiani, O., Ferrer, I., Gelpi, E., et al. (2009). Staging/typing of Lewy body related alpha-synuclein pathology: a study of the BrainNet Europe Consortium. Acta Neuropathol 117, 635-652.

Attems, J., and Jellinger, K.A. (2008). The dorsal motor nucleus of the vagus is not an obligatory trigger site of Parkinson's disease. Neuropathol Appl Neurobiol 34, 466-467.

Aulic, S., Le, T.T., Moda, F., Abounit, S., Corvaglia, S., Casalis, L., Gustincich, S., Zurzolo, C., Tagliavini, F., and Legname, G. (2014). Defined alpha-synuclein prion-like molecular assemblies spreading in cell culture. BMC Neurosci 15, 69.

Beach, T.G., Adler, C.H., Sue, L.I., Vedders, L., Lue, L., White Iii, C.L., Akiyama, H., Caviness, J.N., Shill, H.A., Sabbagh, M.N., et al. (2010). Multi-organ distribution of phosphorylated alpha-synuclein histopathology in subjects with Lewy body disorders. Acta Neuropathol 119, 689-702.

Borghammer, P. (2018). How does parkinson's disease begin? Perspectives on neuroanatomical pathways, prions, and histology. Mov Disord 33, 48-57.

Braak, H., Del Tredici, K., Rub, U., de Vos, R.A., Jansen Steur, E.N., and Braak, E. (2003a). Staging of brain pathology related to sporadic Parkinson's disease. Neurobiol Aging 24, 197-211.

Braak, H., Rub, U., Gai, W.P., and Del Tredici, K. (2003b). Idiopathic Parkinson's disease: possible routes by which vulnerable neuronal types may be subject to neuroinvasion by an unknown pathogen. Journal of neural transmission 110, 517-536.

Brettschneider, J., Del Tredici, K., Lee, V.M., and Trojanowski, J.Q. (2015). Spreading of pathology in neurodegenerative diseases: a focus on human studies. Nat Rev Neurosci 16, 109-120.

Burre, J., Sharma, M., and Sudhof, T.C. (2018). Cell Biology and Pathophysiology of alpha-Synuclein. Cold Spring Harb Perspect Med 8.

Chang, K.H., and Chen, C.M. (2020). The Role of Oxidative Stress in Parkinson's Disease. Antioxidants (Basel) 9.

Cheon, S.M., Ha, M.S., Park, M.J., and Kim, J.W. (2008). Nonmotor symptoms of Parkinson's disease: prevalence and awareness of patients and families. Parkinsonism Relat Disord 14, 286-290.

Chiang, H.L., and Lin, C.H. (2019). Altered Gut Microbiome and Intestinal Pathology in Parkinson's Disease. J Mov Disord 12, 67-83.

Chiba-Falek, O., and Nussbaum, R.L. (2001). Effect of allelic variation at the NACP-Rep1 repeat upstream of the alpha-synuclein gene (SNCA) on transcription in a cell culture luciferase reporter system. Hum Mol Genet 10, 3101-3109.

Danzer, K.M., Haasen, D., Karow, A.R., Moussaud, S., Habeck, M., Giese, A., Kretzschmar, H., Hengerer, B., and Kostka, M. (2007). Different species of alpha-synuclein oligomers induce calcium influx and seeding. J Neurosci 27, 9220-9232.

Danzer, K.M., Krebs, S.K., Wolff, M., Birk, G., and Hengerer, B. (2009). Seeding induced by alpha-synuclein oligomers provides evidence for spreading of alpha-synuclein pathology. J Neurochem 111, 192-203.

Delenclos, M., Trendafilova, T., Mahesh, D., Baine, A.M., Moussaud, S., Yan, I.K., Patel, T., and McLean, P.J. (2017). Investigation of Endocytic Pathways for the Internalization of Exosome-Associated Oligomeric Alpha-Synuclein. Front Neurosci 11, 172.

Donadio, V., Incensi, A., Piccinini, C., Cortelli, P., Giannoccaro, M.P., Baruzzi, A., and Liguori, R. (2016). Skin nerve misfolded alpha-synuclein in pure autonomic failure and Parkinson disease. Ann Neurol 79, 306-316.

Emmanouilidou, E., Elenis, D., Papasilekas, T., Stranjalis, G., Gerozissis, K., Ioannou, P.C., and Vekrellis, K. (2011). Assessment of alpha-synuclein secretion in mouse and human brain parenchyma. PLoS One 6, e22225.

Ferreira, N., Goncalves, N.P., Jan, A., Jensen, N.M., van der Laan, A., Mohseni, S., Vaegter, C.B., and Jensen, P.H. (2021). Trans-synaptic spreading of alpha-synuclein pathology through sensory afferents leads to sensory nerve degeneration and neuropathic pain. Acta Neuropathol Commun 9, 31.

Fortin, D.L., Troyer, M.D., Nakamura, K., Kubo, S., Anthony, M.D., and Edwards, R.H. (2004). Lipid rafts mediate the synaptic localization of alpha-synuclein. J Neurosci 24, 6715-6723.

Freundt, E.C., Maynard, N., Clancy, E.K., Roy, S., Bousset, L., Sourigues, Y., Covert, M., Melki, R., Kirkegaard, K., and Brahic, M. (2012). Neuron-to-neuron transmission of alpha-synuclein fibrils through axonal transport. Ann Neurol 72, 517-524.

Gajdusek, D.C., Gibbs, C.J., Jr., Asher, D.M., Brown, P., Diwan, A., Hoffman, P., Nemo, G., Rohwer, R., and White, L. (1977). Precautions in medical care of, and in handling materials from, patients with transmissible virus dementia (Creutzfeldt-Jakob disease). N Engl J Med 297, 1253-1258.

Gelpi, E., Navarro-Otano, J., Tolosa, E., Gaig, C., Compta, Y., Rey, M.J., Marti, M.J., Hernandez, I., Valldeoriola, F., Rene, R., et al. (2014). Multiple organ involvement by alpha-synuclein pathology in Lewy body disorders. Mov Disord 29, 1010-1018.

Halliday, G., Hely, M., Reid, W., and Morris, J. (2008). The progression of pathology in longitudinally followed patients with Parkinson's disease. Acta Neuropathol 115, 409-415.

Hansen, C., Angot, E., Bergstrom, A.L., Steiner, J.A., Pieri, L., Paul, G., Outeiro, T.F., Melki, R., Kallunki, P., Fog, K., et al. (2011). alpha-Synuclein propagates from mouse brain to grafted dopaminergic neurons and seeds aggregation in cultured human cells. J Clin Invest 121, 715-725.

Helwig, M., Klinkenberg, M., Rusconi, R., Musgrove, R.E., Majbour, N.K., El-Agnaf, O.M., Ulusoy, A., and Di Monte, D.A. (2016). Brain propagation of transduced alpha-synuclein involves non-fibrillar protein species and is enhanced in alpha-synuclein null mice. Brain 139, 856-870.

Helwig, M., Ulusoy, A., Rollar, A., O'Sullivan, S.A., Lee, S.S.L., Aboutalebi, H., Pinto-Costa, R., Jevans, B., Klinkenberg, M., and Di Monte, D.A. (2022). Neuronal hyperactivity-induced oxidant stress promotes in vivo alpha-synuclein brain spreading. Sci Adv 8, eabn0356.

Holmqvist, S., Chutna, O., Bousset, L., Aldrin-Kirk, P., Li, W., Bjorklund, T., Wang, Z.Y., Roybon, L., Melki, R., and Li, J.Y. (2014). Direct evidence of Parkinson pathology spread from the gastrointestinal tract to the brain in rats. Acta Neuropathol 128, 805-820.

Horsager, J., Andersen, K.B., Knudsen, K., Skjaerbaek, C., Fedorova, T.D., Okkels, N., Schaeffer, E., Bonkat, S.K., Geday, J., Otto, M., et al. (2020). Brain-first versus body-first Parkinson's disease: a multimodal imaging case-control study. Brain 143, 3077-3088.

Ibanez, P., Bonnet, A.M., Debarges, B., Lohmann, E., Tison, F., Pollak, P., Agid, Y., Durr, A., and Brice, A. (2004). Causal relation between alpha-synuclein gene duplication and familial Parkinson's disease. Lancet 364, 1169-1171.

Jang, A., Lee, H.J., Suk, J.E., Jung, J.W., Kim, K.P., and Lee, S.J. (2010). Non-classical exocytosis of alpha-synuclein is sensitive to folding states and promoted under stress conditions. J Neurochem 113, 1263-1274.

Jucker, M., and Walker, L.C. (2018). Propagation and spread of pathogenic protein assemblies in neurodegenerative diseases. Nat Neurosci 21, 1341-1349.

Kim, C., Ho, D.H., Suk, J.E., You, S., Michael, S., Kang, J., Joong Lee, S., Masliah, E., Hwang, D., Lee, H.J., et al. (2013). Neuron-released oligomeric alpha-synuclein is an endogenous agonist of TLR2 for paracrine activation of microglia. Nat Commun 4, 1562.

Klinkenberg, M., Helwig, M., Pinto-Costa, R., Rollar, A., Rusconi, R., Di Monte, D.A., and Ulusoy, A. (2023). Interneuronal In Vivo Transfer of Synaptic Proteins. Cells 12, 569.

Kordower, J.H., and Brundin, P. (2009). Lewy body pathology in long-term fetal nigral transplants: is Parkinson's disease transmitted from one neural system to another? Neuropsychopharmacology 34, 254.

Kordower, J.H., Chu, Y., Hauser, R.A., Freeman, T.B., and Olanow, C.W. (2008). Lewy body-like pathology in

long-term embryonic nigral transplants in Parkinson's disease. Nat Med 14, 504-506.

Kordower, J.H., Olanow, C.W., Dodiya, H.B., Chu, Y., Beach, T.G., Adler, C.H., Halliday, G.M., and Bartus, R.T. (2013). Disease duration and the integrity of the nigrostriatal system in Parkinson's disease. Brain 136, 2419-2431.

Kovacs, G.G., Breydo, L., Green, R., Kis, V., Puska, G., Lorincz, P., Perju-Dumbrava, L., Giera, R., Pirker, W., Lutz, M., et al. (2014). Intracellular processing of disease-associated alpha-synuclein in the human brain suggests prion-like cell-to-cell spread. Neurobiol Dis 69, 76-92.

Kruger, R., Kuhn, W., Muller, T., Woitalla, D., Graeber, M., Kosel, S., Przuntek, H., Epplen, J.T., Schols, L., and Riess, O. (1998). Ala30Pro mutation in the gene encoding alpha-synuclein in Parkinson's disease. Nat Genet 18, 106-108.

Lee, H.J., Suk, J.E., Patrick, C., Bae, E.J., Cho, J.H., Rho, S., Hwang, D., Masliah, E., and Lee, S.J. (2010). Direct transfer of alpha-synuclein from neuron to astroglia causes inflammatory responses in synucleinopathies. J Biol Chem 285, 9262-9272.

Lewy, F. (1912). Paralysis agitans. Part I: Pathologische Anatomie, Vol III.

Li, J.Y., Englund, E., Holton, J.L., Soulet, D., Hagell, P., Lees, A.J., Lashley, T., Quinn, N.P., Rehncrona, S., Bjorklund, A., et al. (2008). Lewy bodies in grafted neurons in subjects with Parkinson's disease suggest host-to-graft disease propagation. Nat Med 14, 501-503.

Lo, C., Arora, S., Lawton, M., Barber, T., Quinnell, T., Dennis, G.J., Ben-Shlomo, Y., and Hu, M.T. (2022). A composite clinical motor score as a comprehensive and sensitive outcome measure for Parkinson's disease. J Neurol Neurosurg Psychiatry 93, 617-624.

Luk, K.C., Kehm, V., Carroll, J., Zhang, B., O'Brien, P., Trojanowski, J.Q., and Lee, V.M. (2012a). Pathological alpha-synuclein transmission initiates Parkinson-like neurodegeneration in nontransgenic mice. Science 338, 949-953.

Luk, K.C., Kehm, V.M., Zhang, B., O'Brien, P., Trojanowski, J.Q., and Lee, V.M. (2012b). Intracerebral inoculation of pathological alpha-synuclein initiates a rapidly progressive neurodegenerative alpha-synucleinopathy in mice. J Exp Med 209, 975-986.

Luk, K.C., Song, C., O'Brien, P., Stieber, A., Branch, J.R., Brunden, K.R., Trojanowski, J.Q., and Lee, V.M. (2009). Exogenous alpha-synuclein fibrils seed the formation of Lewy body-like intracellular inclusions in cultured cells. Proc Natl Acad Sci U S A 106, 20051-20056.

Manglani, M., Rua, R., Hendricksen, A., Braunschweig, D., Gao, Q., Tan, W., Houser, B., McGavern, D.B., and Oh, K. (2019). Method to quantify cytokines and chemokines in mouse brain tissue using Bio-Plex multiplex immunoassays. Methods 158, 22-26.

Mao, X., Ou, M.T., Karuppagounder, S.S., Kam, T.I., Yin, X., Xiong, Y., Ge, P., Umanah, G.E., Brahmachari, S., Shin, J.H., et al. (2016). Pathological alpha-synuclein transmission initiated by binding lymphocyte-

activation gene 3. Science 353.

Maraganore, D.M., de Andrade, M., Elbaz, A., Farrer, M.J., Ioannidis, J.P., Kruger, R., Rocca, W.A., Schneider, N.K., Lesnick, T.G., Lincoln, S.J., et al. (2006). Collaborative analysis of alpha-synuclein gene promoter variability and Parkinson disease. JAMA 296, 661-670.

Mari, Z., and Mestre, T.A. (2022). The Disease Modification Conundrum in Parkinson's Disease: Failures and Hopes. Front Aging Neurosci 14, 810860.

Maroteaux, L., Campanelli, J.T., and Scheller, R.H. (1988). Synuclein: a neuron-specific protein localized to the nucleus and presynaptic nerve terminal. J Neurosci 8, 2804-2815.

Masuda-Suzukake, M., Nonaka, T., Hosokawa, M., Oikawa, T., Arai, T., Akiyama, H., Mann, D.M., and Hasegawa, M. (2013). Prion-like spreading of pathological alpha-synuclein in brain. Brain 136, 1128-1138.

Mhyre, T.R., Boyd, J.T., Hamill, R.W., and Maguire-Zeiss, K.A. (2012). Parkinson's disease. Subcell Biochem 65, 389-455.

Mitchell, T., Lehericy, S., Chiu, S.Y., Strafella, A.P., Stoessl, A.J., and Vaillancourt, D.E. (2021). Emerging Neuroimaging Biomarkers Across Disease Stage in Parkinson Disease: A Review. JAMA Neurol 78, 1262-1272.

Mu, L., Sobotka, S., Chen, J., Su, H., Sanders, I., Adler, C.H., Shill, H.A., Caviness, J.N., Samanta, J.E., Beach, T.G., et al. (2013). Alpha-synuclein pathology and axonal degeneration of the peripheral motor nerves innervating pharyngeal muscles in Parkinson disease. J Neuropathol Exp Neurol 72, 119-129.

Musgrove, R.E., Helwig, M., Bae, E.J., Aboutalebi, H., Lee, S.J., Ulusoy, A., and Di Monte, D.A. (2019). Oxidative stress in vagal neurons promotes parkinsonian pathology and intercellular alpha-synuclein transfer. J Clin Invest 129, 3738-3753.

Orimo, S., Uchihara, T., Nakamura, A., Mori, F., Kakita, A., Wakabayashi, K., and Takahashi, H. (2008). Axonal alpha-synuclein aggregates herald centripetal degeneration of cardiac sympathetic nerve in Parkinson's disease. Brain 131, 642-650.

Palma, J.A., and Kaufmann, H. (2020). Orthostatic Hypotension in Parkinson Disease. Clin Geriatr Med 36, 53-67.

Parkkinen, L., Pirttila, T., and Alafuzoff, I. (2008). Applicability of current staging/categorization of alpha-synuclein pathology and their clinical relevance. Acta Neuropathol 115, 399-407.

Pasanen, P., Myllykangas, L., Siitonen, M., Raunio, A., Kaakkola, S., Lyytinen, J., Tienari, P.J., Poyhonen, M., and Paetau, A. (2014). Novel alpha-synuclein mutation A53E associated with atypical multiple system atrophy and Parkinson's disease-type pathology. Neurobiol Aging 35, 2180 e2181-2185.

Patterson, J.R., Duffy, M.F., Kemp, C.J., Howe, J.W., Collier, T.J., Stoll, A.C., Miller, K.M., Patel, P., Levine, N., Moore, D.J., et al. (2019). Time course and magnitude of alpha-synuclein inclusion formation and nigrostriatal degeneration in the rat model of synucleinopathy triggered by intrastriatal alpha-synu-

clein preformed fibrils. Neurobiol Dis 130, 104525.

Paumier, K.L., Luk, K.C., Manfredsson, F.P., Kanaan, N.M., Lipton, J.W., Collier, T.J., Steece-Collier, K., Kemp, C.J., Celano, S., Schulz, E., et al. (2015). Intrastriatal injection of pre-formed mouse alpha-synuclein fibrils into rats triggers alpha-synuclein pathology and bilateral nigrostriatal degeneration. Neurobiol Dis 82, 185-199.

Pavlov, V.A., and Tracey, K.J. (2012). The vagus nerve and the inflammatory reflex--linking immunity and metabolism. Nat Rev Endocrinol 8, 743-754.

Polymenidou, M., and Cleveland, D.W. (2012). Prion-like spread of protein aggregates in neurodegeneration. J Exp Med 209, 889-893.

Polymeropoulos, M.H., Lavedan, C., Leroy, E., Ide, S.E., Dehejia, A., Dutra, A., Pike, B., Root, H., Rubenstein, J., Boyer, R., et al. (1997). Mutation in the alpha-synuclein gene identified in families with Parkinson's disease. Science 276, 2045-2047.

Proukakis, C., Dudzik, C.G., Brier, T., MacKay, D.S., Cooper, J.M., Millhauser, G.L., Houlden, H., and Schapira, A.H. (2013). A novel alpha-synuclein missense mutation in Parkinson disease. Neurology 80, 1062-1064.

Prusiner, S.B. (1984). Some speculations about prions, amyloid, and Alzheimer's disease. N Engl J Med 310, 661-663.

Prusiner, S.B. (2013). Biology and genetics of prions causing neurodegeneration. Annu Rev Genet 47, 601-623.

Raunio, A., Kaivola, K., Tuimala, J., Kero, M., Oinas, M., Polvikoski, T., Paetau, A., Tienari, P.J., and Myllykangas, L. (2019). Lewy-related pathology exhibits two anatomically and genetically distinct progression patterns: a population-based study of Finns aged 85. Acta Neuropathol 138, 771-782.

Regnault, A., Boroojerdi, B., Meunier, J., Bani, M., Morel, T., and Cano, S. (2019). Does the MDS-UPDRS provide the precision to assess progression in early Parkinson's disease? Learnings from the Parkinson's progression marker initiative cohort. J Neurol 266, 1927-1936.

Roth, B.L. (2016). DREADDs for Neuroscientists. Neuron 89, 683-694.

Rusconi, R., Ulusoy, A., Aboutalebi, H., and Di Monte, D.A. (2018). Long-lasting pathological consequences of overexpression-induced alpha-synuclein spreading in the rat brain. Aging Cell 17:e12727.

Scheiblich, H., Dansokho, C., Mercan, D., Schmidt, S.V., Bousset, L., Wischhof, L., Eikens, F., Odainic, A., Spitzer, J., Griep, A., et al. (2021). Microglia jointly degrade fibrillar alpha-synuclein cargo by distribution through tunneling nanotubes. Cell 184, 5089-5106 e5021.

Schildknecht, S., Gerding, H.R., Karreman, C., Drescher, M., Lashuel, H.A., Outeiro, T.F., Di Monte, D.A., and Leist, M. (2013). Oxidative and nitrative alpha-synuclein modifications and proteostatic stress: implications for disease mechanisms and interventions in synucleinopathies. J Neurochem 125, 491-511.

Shimozawa, A., Ono, M., Takahara, D., Tarutani, A., Imura, S., Masuda-Suzukake, M., Higuchi, M., Yanai, K., Hisanaga, S.I., and Hasegawa, M. (2017). Propagation of pathological alpha-synuclein in marmoset brain. Acta Neuropathol Commun 5, 12.

Siderowf, A., Concha-Marambio, L., Lafontant, D.E., Farris, C.M., Ma, Y., Urenia, P.A., Nguyen, H., Alcalay, R.N., Chahine, L.M., Foroud, T., et al. (2023). Assessment of heterogeneity among participants in the Parkinson's Progression Markers Initiative cohort using alpha-synuclein seed amplification: a cross-sectional study. Lancet Neurol 22, 407-417.

Singleton, A.B., Farrer, M., Johnson, J., Singleton, A., Hague, S., Kachergus, J., Hulihan, M., Peuralinna, T., Dutra, A., Nussbaum, R., et al. (2003). alpha-Synuclein locus triplication causes Parkinson's disease. Science 302, 841.

Spillantini, M.G., Schmidt, M.L., Lee, V.M., Trojanowski, J.Q., Jakes, R., and Goedert, M. (1997). Alpha-synuclein in Lewy bodies. Nature 388, 839-840.

Stockl, M., Fischer, P., Wanker, E., and Herrmann, A. (2008). Alpha-synuclein selectively binds to anionic phospholipids embedded in liquid-disordered domains. J Mol Biol 375, 1394-1404.

Stokholm, M.G., Danielsen, E.H., Hamilton-Dutoit, S.J., and Borghammer, P. (2016). Pathological alpha-synuclein in gastrointestinal tissues from prodromal Parkinson disease patients. Ann Neurol 79, 940-949.

Surmeier, D.J., Schumacker, P.T., Guzman, J.D., Ilijic, E., Yang, B., and Zampese, E. (2017). Calcium and Parkinson's disease. Biochem Biophys Res Commun 483, 1013-1019.

Svensson, E., Horvath-Puho, E., Thomsen, R.W., Djurhuus, J.C., Pedersen, L., Borghammer, P., and Sorensen, H.T. (2015). Vagotomy and subsequent risk of Parkinson's disease. Ann Neurol 78, 522-529.

Thal, D.R., Rub, U., Orantes, M., and Braak, H. (2002). Phases of A beta-deposition in the human brain and its relevance for the development of AD. Neurology 58, 1791-1800.

Titova, N., Padmakumar, C., Lewis, S.J.G., and Chaudhuri, K.R. (2017). Parkinson's: a syndrome rather than a disease? Journal of neural transmission 124, 907-914.

Tretiakoff, C. (1919). Contribution a l'étude de l'anatomie pathologique du Locus Niger de Soemmering avec quelques déductions relative à la pathogénie des troubles du tonus muscularaire et de la maladie de Parkinson. . In These de Paris No 293.

Ulusoy, A., Musgrove, R.E., Rusconi, R., Klinkenberg, M., Helwig, M., Schneider, A., and Di Monte, D.A. (2015). Neuron-to-neuron alpha-synuclein propagation in vivo is independent of neuronal injury. Acta Neuropathol Commun 3, 13.

Ulusoy, A., Rusconi, R., Perez-Revuelta, B.I., Musgrove, R.E., Helwig, M., Winzen-Reichert, B., and Di Monte, D.A. (2013). Caudo-rostral brain spreading of alpha-synuclein through vagal connections. EMBO Mol Med 5, 1119-1127.

Van Den Berge, N., Ferreira, N., Gram, H., Mikkelsen, T.W., Alstrup, A.K.O., Casadei, N., Tsung-Pin, P., Riess, O., Nyengaard, J.R., Tamguney, G., et al. (2019). Evidence for bidirectional and trans-synaptic parasympathetic and sympathetic propagation of alpha-synuclein in rats. Acta Neuropathol 138, 535-550.

Van Den Berge, N., and Ulusoy, A. (2022). Animal models of brain-first and body-first Parkinson's disease. Neurobiol Dis 163, 105599.

Volpicelli-Daley, L.A., Luk, K.C., Patel, T.P., Tanik, S.A., Riddle, D.M., Stieber, A., Meaney, D.F., Trojanowski, J.Q., and Lee, V.M. (2011). Exogenous alpha-synuclein fibrils induce Lewy body pathology leading to synaptic dysfunction and neuron death. Neuron 72, 57-71.

Wu, Q., Shaikh, M.A., Meymand, E.S., Zhang, B., Luk, K.C., Trojanowski, J.Q., and Lee, V.M. (2020). Neuronal activity modulates alpha-synuclein aggregation and spreading in organotypic brain slice cultures and in vivo. Acta Neuropathol 140, 831-849.

Yamada, K., and Iwatsubo, T. (2018). Extracellular alpha-synuclein levels are regulated by neuronal activity. Mol Neurodegener 13, 9.

Zarranz, J.J., Alegre, J., Gomez-Esteban, J.C., Lezcano, E., Ros, R., Ampuero, I., Vidal, L., Hoenicka, J., Rodriguez, O., Atares, B., et al. (2004). The new mutation, E46K, of alpha-synuclein causes Parkinson and Lewy body dementia. Ann Neurol 55, 164-173.

8-ACKNOWLEDGEMENTS

Some hardships and interruptions are often left unmentioned in the acknowledgments of scientific manuscripts. Therefore, I would like to take this opportunity to express my gratitude to all my colleagues for their behind-the-scenes support. First and foremost, I am deeply grateful to my supervisor, Dino, for being an invaluable mentor throughout my scientific career. This thesis and the experiments conducted would not have had such depth without your support. Thank you for providing me with the opportunity to work in such a wonderful environment and for sharing your enthusiasm. Additionally, I would like to extend my gratitude to my subject representative, Christian, for his invaluable support and mentorship during my habilitation process, as this thesis would not have come to fruition without his contribution.

To my dear colleagues with whom I have worked during my time at the DZNE, we have built a laboratory from scratch when the DZNE was still in its early stages. From orders and quotations to technical specifications, I extend my heartfelt thanks to Anna, the purchasing department, the lab management, and the technical infrastructure for their hard work. Special thanks to my wonderful colleagues and friends, Blanca, for her enthusiasm and support, and Raffaella, for her amazing skills and patience. I will miss our time in and out of the lab. A big thanks to Michael H. for always bringing cheer, even during the darkest moments of experimental failures. Your humor made my long surgery sessions much more enjoyable. My dear Michael K., thank you for your diligence and unwavering commitment. These early works would not have been completed without Franziska's incredible speed in cutting rat brains. Our group meetings and scientific discussions would not have been as fruitful without Ruth's critical thinking. Many thanks to Laura, who started as a trainee, became a technician, and then became the behind-the-scenes organizer of our lab. She has overcome challenges and grown into an excellent technician with amazing management skills.

I would like to acknowledge all my colleagues working in the Di Monte team, whose assistance was invaluable during the challenging times of moving from the CAESAR building to the new DZNE building in Venusberg. And to the people of the post-move era... Helia, my extremely modest colleague who has inspired me in so many ways to achieve my goals. Your hard work and dedication deserve praise, and your high-quality stereology work has made a significant contribution to the published and upcoming work. To my current colleagues at the DZNE who played direct or indirect roles in this thesis: our wonderful technicians Shirley, Anushka, Camila, Zoe, and soon-to-be technician Lea. Thank you so much for your technical support and companionship. To my co-workers/students Eugenia, Pietro, Sinead, Rita, Eva, Carmen, and Joana, it has been a great pleasure working with all of you. I wish you all the best in your future careers. Angela, who started as a technician and then became a PhD student in our lab and is now the person who knows everything about the lab. Thank you for the surgeries, virus orders, organization, and the time you have spent ensuring the smooth operation of the lab. Thank you Eun-Jin for the powerful ELISA assays and setting up the in vitro BiFC system. A special acknowledgment for a vital scientific contribution goes to the person behind the beautiful images of the stomach wall and vagal projections: Bob Phillips.

Throughout the course of this thesis, several individuals have been involved in handling the ethical permits for animal experimentation and genetic engineering work. Those familiar with such work understand the amount of effort that goes into paperwork and reporting. Thank you, Anna, Blanca, Michael H., and Michael K., for your work on genetic engineering safety, and many thanks to Bettina and Yvonne for handling all the S1/S2 genetic engineering, animal protocols, and medical drug documentation. Thank you Sinead, Rita and Eugenia for taking over some of these responsibilities. Thank you, Kerstin, Almana, and Debbie, for the administrative support, arranging our trips, meetings and accomodations. And thank you to all the animal facility employees for excellent communication, handling, and support in our preclinical work. Ireen and Hans, for their unwavering support with the microscopes and introducing us to new equipment. Finally, a special thank you to Nàdia for proofreading the thesis.

I would also like to express my gratitude to my family and Carlos for their unwavering support throughout this time. Thank you Carlos, for enduring all my stressful moments and sharing my best moments in life. My sisters Elif and Hazal for being there for me and making me feel safe and supported. Berna for being such a sweet person that one can rely on. Thank you, Dad, to whom I dedicate this thesis, for always being there for me and encouraging my personal growth.

9-CV AYSE ULUSOY, PhD

Staff Scientist

German Center for Neurodegenerative Diseases (DZNE)

Venusberg-Campus 1, Building 99, 53127, Bonn

0176 70376829

ayse.ulusoy@dzne.de

EDUCATION

PhD.	**Lund University**
2005-2010	Faculty of Medicine, Department of Experimental Medical Science
Lund, Sweden	No grading system
	Thesis Title: "Modeling pathophysiological aspects of Parkinson's disease: Manipulating dopamine handling and α-synuclein expression in the nigrostriatal pathway using viral vectors" Advisors: Deniz Kirik and Anders Bjorklund, Opponent: Piers Emson
MSc.	**Hacettepe University**
2000-2002	Institute of Pure and Applied Science
Ankara, Turkey	GPA: 4.00/4.00
	Thesis Title: "Measurement of in vitro phagocytic activity using functional group carrying monodisperse poly(glycidyl methacrylate) microspheres in rat blood" Advisor: M. Ali Onur
BSc.	**Hacettepe University**
1996-2000	Faculty of Science Department of Biology
Ankara, Turkey	GPA: 3.15/4.00 ranked within the first 5 at the Department of Biology

POSITIONS

Tenured Scientist (Career Track), (2017-) Bonn, Germany	German Centre for Neurodegenerative Diseases (DZNE)
Postdoctoral Researcher, (2010-2017) Bonn, Germany	German Centre for Neurodegenerative Diseases (DZNE) **Mentor: Donato A. Di Monte**
Staff Researcher, (2010) Lund, Sweden	Lund University, Faculty of Medicine Department of Experimental Medical Science **Advisor: Deniz Kirik**
PhD Student, (2005-2010) Lund, Sweden	Lund University, Faculty of Medicine **Advisors: Deniz Kirik and Anders Bjorklund**
Marie Curie Research Fellow, (2004-2007) Lund, Sweden	Lund University, Faculty of Medicine **Advisors: Deniz Kirik and Anders Bjorklund**
Research & Teaching Assistant, (2000-2004) Ankara, Turkey	Hacettepe University, Faculty of Science Department of Biology **Advisor: M. Ali Onur**

OTHER INTERNATIONAL RESEARCH EXPERIENCES AND COLLABORATIONS

2018-2019 **Department of Neurology, University Hospital Zurich**

- Collaboration to establish sleep recordings in animal models of α-synuclein pathology at the laboratory of Daniela Noain and Christian Baumann

2017-2018 **Center for Applied Medical Research, Pamplona, Spain**

- Collaboration to establish sample preparation and transportation for single cell transcriptomic analysis from non-human primates at the laboratory of José Luis Lanciego

2015-2016 **Erasmus Medical Center, Rotterdam, The Netherlands**

- Several visits as a guest researcher to perform stereotaxic injection of viral vectors and preformed fibrils in transferrin receptor 2 knockout mice as part of our collaborative Michael J Fox Foundation grant with Pier Giorgio Mastroberardino

2009 **Instituto de Investigaciones Biomédicas "Alberto Sols" CSIC-UAM, Madrid, Spain**

- One week laboratory visit as a guest researcher to train and perform stereotaxic injections and establish/design post-mortem brain analysis in nrf2 knockout mice as part of our collaborative Michael J Fox Foundation grant with Antonio Cuadrado

2007 **Department of Biomedicine, Aarhus University, Aarhus, Denmark**

- Several visits to Poul Henning Jensen Laboratory to establish proteasome activity assay from brain tissue as part of our collaborative research funded by Nordic Center of Excellence and Lundbeck

AWARDS AND GRANTS

Aligning Science Across Parkinson's (ASAP) Grant (Key Personnel)

"The genome-microbiome axis in the cause of Parkinson disease: Mechanistic insights and therapeutic implications from experimental models and a genetically stratified patient population", 2021-2024

DZNE Innovation to Application (I2A) Award (PI)

"Induction of slow-wave sleep as a novel strategy to interfere with Parkinson's disease pathology and progression", 2019

Innovative Medicines Initiative 2 (IMI2) PD-MitoQuant (Co-applicant)

"A quantitative approach towards the characterisation of mitochondrial dysfunction in Parkinson's disease", 2019-2022

Margarita and Julia Köhler Stiften (Awardee)

"Parkinson's disease and Lewy Body Demetia Research", 2018

Blanche A. Paul Foundation Research Grant (Co-PI)

"Mechanisms of α-Synuclein Spreading and Pathology", 2013-2016

AWARDS AND GRANTS (CONTINUES)

Council for the Lindau Nobel Laureate Meeting
Qualification to participate in the 64th Lindau Nobel Laureate Meeting (Physiology or Medicine), Lindau, Germany 2014

DZNE - Travel Award
Neuroscience School of Advanced Studies "Synucleinopathies" Course, San Quirico, Italy 2012

Federation of European Neuroscience Societies
Travel Award, FENS Meeting, Amsterdam, The Netherlands 2010

Westlings Minnesfond
Travel Award, Society for Neuroscience Meeting, Chicago, USA 2010

Lund University, Faculty of Medicine - Travel Award
Society for Neuroscience Meeting, San Diego, USA 2007

Marie Curie Early Stage Training Fellowship
PhD Fellowship, European Union, 2004-2007

Hacettepe University Research Group Award
Ankara, Turkey, 2001

PROFESSIONAL ACTIVITIES

MEMBERSHIP

- Society for Neuroscience (2007-present)
- International Basal Ganglia Society (2019-present)

EDITOR

- Frontiers in Molecular Neuroscience (Associate Editor)
- npj Parkinson's Disease (Editorial Board member)

GRANT REVIEWER

- Parkinson's UK
- Cure Parkinson's Trust

CONSULTANT

- Muna Therapeutics

AD-HOC REVIEWER

- Acta Neuropathologica
- Acta Neuropathologica Communications
- Aging Cell
- Brain
- Brain Research
- Cell Death and Disease
- Cellular and Molecular Neurobiology
- Cell and Tissue Research
- European Journal of Neuroscience
- Experimental Neurology
- Frontiers in Neurology
- Frontiers in Molecular Neurocience
- Journal of Endocrinology
- Journal of Neurochemistry
- Journal of Neuroscience Methods
- Nature Communications
- Neurobiology of Disease
- Neurochemistry International
- Neuropathology and Applied Neurobiology
- Neurotoxicity Research

COMMITTEES

- Lund University, Department of Experimental Medicine PhD Student Council Member 2005-2008
- Marie Curie "Nervous System Repair" Steering Committee for organizing workshops 2005-2006

10-ERKLÄRUNG

Hiermit bestätige ich, dass ich die Richtlinien zur guten wissenschaftlichen Praxis der Universität Bonn, laut Habilitations-Ordnung, zur Kenntnis genommen habe und ich versichere, dass ich sie beim Verfassen der Habilitationsschrift beachtet habe. Insbesondere versichere ich, dass ich alle in der Habilitationsschrift benutzten Quellen und Hilfsmittel angegeben habe und und die Thesis eigenständig und ohne fremde Hilfe abgefasst habe.

Bonn, 30.05.2023